Technische Universität Kaiserslautern

Fachbereich Mathematik
Felix–Klein–Zentrum
AG Differential–Algebraische Systeme

Vom Fachbereich Mathematik der Technischen Universität Kaiserslautern
zur Verleihung des akademischen Grades
Doktor der Naturwissenschaften *(Doctor rerum naturalium, Dr. rer. nat.)*
genehmigte Dissertation.

Periodic homogenization and FFT-based methods for resolving microstructures of linear magneto-elastic problems

Felix Dietrich

1. Reviewer Prof. Dr. Bernd Simeon
Fachbereich Mathematik
Technische Universität Kaiserslautern

2. Reviewer Prof. Dr. Gerhard Starke
Fakultät für Mathematik
Universität Duisburg–Essen

Date of defense: July 30, 2021

- D 386 -

Felix Dietrich

Periodic homogenization
and FFT-based methods
for resolving microstructures
of linear magneto-elastic problems

Vom Fachbereich Mathematik der Technischen Universität Kaiserslautern
zur Verleihung des akademischen Grades
Doktor der Naturwissenschaften *(Doctor rerum naturalium, Dr. rer. nat.)*
genehmigte Dissertation. , Date of defense: July 30, 2021
Reviewers: Prof. Dr. Bernd Simeon and Prof. Dr. Gerhard Starke

Technische Universität Kaiserslautern
AG Differential–Algebraische Systeme
Felix–Klein–Zentrum
Fachbereich Mathematik
Paul–Ehrlich–Straße 31
67663 Kaiserslautern

Abstract

In this thesis one considers the periodic homogenization of a linearly coupled magneto-elastic model problem and focuses on the derivation of spectral methods to solve the obtained unit cell problem afterwards. In the beginning, the equations of linear elasticity and magnetism are presented together with the physical quantities used within. After specifying the model assumptions, the system of partial differential equations is rewritten in a weak form for which the existence and uniqueness of solutions is discussed. The model problem then undergoes a homogenization process where the original problem is approximated by a substitute problem with a repeating micro-structural geometry that was generated from a representative volume element (RVE). The following separation of scales, which can be achieved either by an asymptotic expansion or through a two-scale limit process, yields the homogenized problem on the macroscopic scale and the periodic unit cell problem. The latter is further analyzed using Fourier series, leading to periodic Lippmann–Schwinger type equations allowing for the development of matrix-free solvers. It is shown that, while it is possible to craft a scheme for the coupled problem from the purely elastic and magnetic Lippmann–Schwinger equations alone without much additional effort, a more general setting is provided when deriving a Lippmann–Schwinger equation for the coupled system directly. These numerical approaches are then validated with some analytically solvable test problems, before their performance is tested against each other for some more complex examples.

Zusammenfassung

Die vorliegende Dissertation fokussiert sich auf die periodische Homogenisierung eines linear gekoppelten magneto-elastischen Modellproblems, sowie die Herleitung spektraler Methoden für das dabei entstehende Zellenproblem. Zu Beginn werden die Gleichung der linearen Elastizität und des Magnetismus, sowie die dabei auftretenden physikalischen Größen vorgestellt. Nachdem die Annahmen für das Modellproblem konkretisiert wurden, wird das System von partiellen Differentialgleichungen in eine schwache Form überführt, für die anschließend die Existenz und Eindeutigkeit einer Lösung gezeigt wird. Das Modellproblem unterläuft daraufhin einen Homogenisierungsprozess, in dem es zunächst durch ein von einem RVE erzeugten Ersatzproblem mit sich wiederholender Mikrostruktur angenähert wird. Durch die darauf folgende Skalenteilung, die entweder durch Ansetzen einer asymptotischen Folge oder durch einen Zwei-Skalen–Grenzprozess erreicht werden kann, erhält man das homogenisierte Problem auf der makroskopischen Skala und das periodische Zellenproblem. Letzteres wird mittels Fourierreihen weiter betrachtet, um schließlich periodische Lippmann–Schwinger Gleichungen zu erhalten, welche den Entwurf Matrix-freier Löser erlauben. Es wird gezeigt, dass es zwar möglich ist aus den einzelnen Lippmann–Schwinger Gleichungen der rein elastischen und rein magnetischen Probleme ein numerisches Vorgehen ohne nennenswerten Mehraufwand zusammenzusetzen, die direkte Herleitung einer neuen Lippmann–Schwinger Gleichung für das gekoppelte System jedoch eine wesentlich allgemeinere Methodik liefert. Die numerischen Methoden werden abschließend zunächst an analytisch lösbaren Testproblemen validiert und anschließend gegeneinander in komplexeren Beispielen auf ihre Performance getestet.

Acknowledgments

On the next two pages I would like to take some time to give my thanks to all the people that helped and accompanied me throughout my time as a PhD student.

First, I want to sincerely thank my supervisor Bernd Simeon, not only for guiding me in my research, giving me the freedom to do things my own way and putting his trust in me when he offered me a position in his working group but also for simply being an understanding and kind human being that listens patiently to his students' problems and worries, is willing to support their decisions as much as possible and always treats others fairly as an equal.

Next, I wish to express my gratitude towards the two of my former colleagues that initially welcomed me in Prof. Simeon's working group and who strongly influenced the direction my research would eventually take. One being Dennis Merkert who I have to regard as kind of a second supervisor in my first years as a PhD student where he helped me to get started, shared his knowledge about the duties of a scientific employee with me and brought me in contact with the overarching themes of periodic homogenization and the spectral schemes used within in the first place. The other one is Mané Harutyunyan who always brightened the mood at work with her positive charisma but also knew when it was time to give others a push out of their comfort zone. Thanks to her efforts I was able to slowly but steadily get through some motivational lows and also found at a struggling point in my research a new connecting point in her works on magnetostrictive materials. Without these two people the contents of this thesis would simply not exist.

But of course I could not forget my former and current working group members that made this time an interesting and lively experience. Clarissa Arioli and Alexander Shamanskiy started around the same time as I did and we were able to share our ups and downs, our successes and our failures, our energetic highs and our dragging lows on our paths towards the title of doctor. Steffen Plunder who, despite being in this working group only for a short period of time, brought a fresh wind, new ideas and a burning passion for mathematics with him that helped to strengthen the exchange between working group members. Michael Gfrerer whose engineering roots allowed for new perspectives on problems at hand and often initiated worthwhile discussions in which we reflected on certain methodologies together. And then there are Jeremias Arf and Rozan Rosandi, making up the next generation of working group members, who reminded me where I started myself and whom I wish I would have been able to spend more time with if it were not for very extraordinary global events happening at the time this thesis is nearing its end.

I also wish to mention the insights offered to me by the Fraunhofer ITWM at the start of my PhD. In this context, I especially want to give a quick shoutout to Heiko Andrä, Matthias Kabel and Matti Schneider for providing me with helpful feedback during the beginning stages.

Getting a bit more personal now, these acknowledgments would be by no means complete if I were not to mention my best friend Kilian Werner who at the time of writing these pages is a PhD student in computer sciences himself. Without his friendship, the countless hours of time spend together and the numerous occasions on which he had to take on the role of my personal psychotherapist as I like to call it, I would have probably lost my mind at some point. Kilian, I can not thank you enough for sticking with me for all these years, encouraging me time and time again and overall just being the best friend I could wish for. I would like to thank my friends Markus Werner and Swenja Steiner as well, since they also take a big part in making my life a little less stressful and much more enjoyable. Together with Kilian, you all are like a second family to me.

Finally, speaking about families, I wish to thank my parents Peter and Bettina Dietrich from the bottom of my heart for always being there for me. You may not even understand what I am doing here or what this thesis is about but that is just all the more reason for me to appreciate and thank you for still always trying your best, giving me your unconditional support and love, helping me with all my struggles and listening to me when I needed to give vent to my emotions. I love you.

Symbols

d	dimension
$\tilde{d}$	dimension of corresponding Mandel notation
$\underline{\cdot}$	non-Mandel variants of quantities
$\widehat{\cdot}$	DFT of quantity
$\cdot_N$	discretized data
$\mathbf{u}$	displacement field
$\mathbf{v}$	mechanical perturbation / test function
$\boldsymbol{\varepsilon}$	mechanical strain (Mandel notation)
$\boldsymbol{\sigma}$	mechanical stress (Mandel notation)
$\mathbf{C}$	stiffness tensor (Mandel notation)
ψ	magnetic potential
ϕ	magnetic perturbation / test function
$\mathbf{H}$	magnetic field
$\mathbf{B}$	magnetic induction
$\boldsymbol{\mu}$	permeability tensor
$\mathbf{e}$	coupling tensor (Mandel notation)
$\mathbf{f}^{\mathrm{mech}}$	mechanical volume force density
$\mathrm{f}^{\mathrm{mag}}$	magnetic free charges
$\gamma_{\mathbf{C}}$, $\gamma_{\boldsymbol{\mu}}$	ellipticity constants
κ	scale ratio
$\mathbf{z}_i^{\mathrm{mech}}$, $\mathbf{z}_j^{\mathrm{mag}}$	unit vectors in $\mathbb{R}^{\tilde{d}}$ and $\mathbb{R}^d$
ω_i^{mech}, $\varrho_i^{\mathrm{mech}}$	correctors of the i-th mechanical corrector problem
ω_j^{mag}, ϱ_j^{mag}	correctors of the j-th magnetic corrector problem
τ^{mech}, τ^{mag}	inner forces
$\mathbf{g}^{\mathrm{mech}}$, $\mathbf{g}^{\mathrm{mag}}$	outer forces
$\mathbf{C}^0$, $\boldsymbol{\mu}^0$, $\mathbf{e}^0$	reference tensors
$\boldsymbol{\Gamma}^{\boldsymbol{\varepsilon}}_{\tau^{\mathrm{mech}}}$, $\boldsymbol{\Gamma}^{\mathbf{H}}_{\tau^{\mathrm{mag}}}$, ...	Green operators

Contents

1 Introduction

The name ‘composite material’ generally refers to any kind of material that consists of a combination of at least two separate constituents or phases [37]. This terminology typically includes steel-reinforced concrete, mixtures of different metals and laminated timber but it can even be used for certain types of sponges or foams where air can be considered as its own constituent. The ultimate goal when designing a new composite is to obtain a material with properties different from its constituents, often even surpassing the behavior of each individual phase. This might include for example elastic, magnetic, electrical or thermal properties that one wishes to enhance or to amplify which can then be used to an advantage in a variety of occupational fields such as civil engineering [7], aerospace applications [78] or biomedicine [98]. Due to the sheer number of different use cases, possible combinations of phases and near endless geometrical arrangement patterns, the design and analysis of such composites has remained a central research topic in material sciences over decades.

When aiming for a certain material behavior however, it would not be practical nor profitable to experiment with actual specimen for each composition until the desired effect is obtained. Instead, fast and efficient simulations are required to run tests in advance. The following example may give a better understanding of the main challenge that designers and researchers are then confronted with. The objective would be the design of an airplane wing out of several metal phases with the goal to reduce its weight while also ensuring its stability at high speeds and reducing corrosion through rain, wind, and low temperatures. If one wishes to simulate such an object that measures several dozens of meters in size, it is impossible to rely on the data available for the constituents involved, as these could only be captured in a meaningful way on a much smaller scale which would therefore require an unreasonably fine resolution for numerical methods. Ideally, one needs to know how the composite acts on a macroscopic level without having to look each time at the smaller geometrical features within. In other words, what is actually a highly heterogeneous mixture of separate phases, whose properties can be measured beforehand or are already known, should be replaced in these large scale simulations with a homogeneous material that mimics the behavior of the more complex composite [6]. This thought stands at the center of any homogenization procedure which can be separated into a localization step, where the underlying micro-structure is analyzed within a unit cell at certain points and replaced by a substitute, and the homogenization step, in which this substitute is then used for computations on a larger scale [22, 103].

Over the years, different homogenization techniques as well as different methods on how to solve the localization and homogenization problems have been developed [38], including classical finite element methods on both scales [102] or the usage of level sets and extended finite elements on image data [70]. One of the most popular methods for periodic homogenization, where the localized problem consists of solving an elliptic equation or system with periodic boundary conditions, is a spectral solution scheme introduced in the context of linear elasticity over 25 years ago by french researchers Moulinec and Suquet [87, 88]. By applying a multi-dimensional FFT to the equation, it is rewritten as an integral Lippmann–Schwinger-type equation that can be solved iteratively. This method which was later labeled as the Basic Scheme has several advantages specifically tailored to the problem at hand. Not only does the FFT implicitly incorporates the boundary conditions in a straight-forward manner but also allows to work directly on pixel- or voxel-based image data without the need to set up

a mesh as it would be the case in traditional FEM. Furthermore, apart from the FFT itself, which is a highly optimized routine at this point, all operations are performed for each pixel or voxel individually, giving way to parallelized computations. Therefore, the Basic Scheme provides a fast and efficient, matrix-free solver for the unit cell problem.

Due to its popularity, the Basic Scheme has steadily improved and extended since its introduction. A wide but surely not complete selection of its different developments shall be given here. The Basic Scheme was validated to work for classical Eshelby-type inclusion problems [4] and proven to converge not only for smooth but also rough material coefficients [100]. Since the Basic Scheme is originally formulated with the strain as the main variable, the reconstruction of the displacement field out of its solution has been researched [18] as well as a formulation that is directly based on the displacement field [74]. Augmented Lagrangian methods and Uzawa's algorithm were initially suggested to handle composites with larger phase contrasts [82]. Other reformulations and improvements include an accelerated formulation to improve the convergence speed [34], the usage of Krylov subspace methods [58, 121], a variational framework [19], computations on a staggered grid [101] and modifications of the involved Green operators [118]. Polarization-based schemes [84, 116] which define yet another quantity as the main variable and certain preconditioners [64] have been shown to improve the convergence speed even further, although the choice of numerical parameters plays a critical role here. The concept of FFT-based solvers was adapted to treat non-linearities [41, 117] and porous media [106] and has been successfully applied to elasto-viscoplasticity [32], hypoelastic plasticity [76] and polycrystalline materials [89] among others. More complex simulations of damage progression [35, 105] have been performed as well as full two-scale FE–FFT simulations [44, 60], some focusing on the introduction of a consistent macroscopic tangent operator to compute the effective material tensors [43]. Looking beyond the initial setting and ideas for which these methods were developed, FFT-based solvers for problems with non-periodic boundary conditions [39] or algorithms build around the Lippmann–Schwinger equation that operate purely in the real-space domain [120] were also brought up. To open up new applications and increase numerical precision, some people proposed an extension from uniform loadings to strain gradient loadings [40] or arbitrary higher-order terms [28, 29, 108], whereas others attempted to reduce occurring Gibbs phenomena through the usage of composite voxels at interfaces [59], by generalizing the existing methods to translation invariant spaces of anisotropic lattices [11, 81] or smoothing the obtained solution with periodic splines [85]. The computational cost of the schemes were further reduced by model order reduction techniques such as a sparse sampling approach [61] or low rank tensor approximations [111]. Several implementations for FFT-based homogenization have been designed and optimized [47, 95] and even been transferred in concept to GPUs [63].

In this theses, it is explained how the basic concepts of periodic and computational homogenization are then applied to linearly coupled systems at the example of a magneto-elastic model problem [49, 50]. Magneto-elastic effects such as piezomagnetism or (linearized) magnetostriction [20, 72] can once again be enhanced and exploited through cleverly designed composite materials [52, 67, 71] to then be used in the development of sensor and actuator technology [66, 91]. The problem is mainly analyzed from a mathematical point of view and focuses on the additional challenges and differences of coupled systems compared to single equations while keeping the following overarching goals of the thesis in mind. For once, the thesis should serve as an in-depth guideline on how the localized cell problem is derived starting from a macroscopic set of equations with highly oscillating coefficients. Additionally, it aims at formalizing the therein involved homogenization procedure within a mathematical framework. Lastly, it wants to derive numerically meaningful FFT-based schemes for coupled problems by building on top of the Basic Scheme in different ways and wishes to study their differences and commonalities.

The thesis is structured as follows. In Chap. 2 some notations are introduced and the most important function spaces are repeated. The basics of Fourier series and the Discrete Fourier Transform are given there as well. The coupled magneto-elastic model problem is introduced in Chap. 3 after going over the fundamental physical concepts of elasticity and magnetism. Existence and uniqueness of the solution for the weak formulation are studied. Afterwards, the goal and advantages of periodic homogenization for composite materials are explained in Chap. 4. The homogenization is first achieved through an asymptotic expansion approach before mathematically backing it up with a formal two-scale limit process. The resulting homogenized and cell problems are stated here, the latter one being studied in more detail in the following Chap. 5 by transforming it to the frequency domain to obtain periodic equations of Lippmann–Schwinger type. It is reviewed in detail how the Basic Scheme is build around these algebraic expressions for purely elastic or magnetic problems and how this knowledge can be used to come up with different schemes for the coupled system. The so derived methods are first validated in Chap. 6 with a simple analytically solvable test case before they are tested with more realistic and complex 2D and 3D geometries. Lastly, a summary of the contents will be given again in Chap. 7 together with a short outlook on possible extensions for future research.

2 Preliminaries

Before diving into the main contents of this thesis, an overview of the used notations and most commonly used mathematical concepts such as important function spaces and the basics of Fourier analysis will be given in this section. For more details on these subjects please refer for example to [113, 115].

2.1 Numbers, Vectors, Matrices and Co.

The following notations hold true throughout the remainder of this thesis unless explicitly stated otherwise.

Natural numbers are defined as the set $\mathbb{N} \coloneqq \{1, 2, 3, \dots\}$. The number zero gets included explicitly by the notation $\mathbb{N}_0$. Letters $\mathbb{Z}, \mathbb{Q}, \mathbb{R}$ and $\mathbb{C}$ denote the integers, rational numbers, real numbers and complex numbers, respectively. A $+/-$-superscript in connection with $\mathbb{Q}$ or $\mathbb{R}$ denotes only the positive/negative elements of the corresponding set. In these cases the number zero can again be explicitly added with a 0-subscript.

For better distinction, the mathematical constants e and i which denote Euler's number and the imaginary unit are set upright. The symbol δ_{ij} denotes the Kronecker delta defined as $\delta_{ij} \coloneqq 1$ if $i = j$ and $\delta_{ij} \coloneqq 0$ otherwise.

Scalar values $a \in \mathbb{C}$ are denoted by small, (column) vectors $\mathbf{a} \in \mathbb{C}^d$ by bold, matrices $\mathbf{A} \in \mathbb{C}^{d\times d}$ by bold capital, third-order tensors $\mathbb{A} \in \mathbb{C}^{d\times d\times d}$ by blackboard bold capital and fourth-order tensors $\mathcal{A} \in \mathbb{C}^{d\times d\times\times d}$ by calligraphic capital letters. The small letter $d \in \mathbb{N}$ is exclusively used to denote the (spatial) dimension; in most applications $d \in \{2, 3\}$. The letters f, g and h are reserved for scalar-valued functions, their bold counterparts $\mathbf{f}, \mathbf{g}$ and $\mathbf{h}$ for vector- or tensor-valued ones, respectively.

Entries of quantities $\mathbf{a}, \mathbf{A}, \mathbb{A}$ or $\mathcal{A}$ are denoted with small subscripts as $\mathbf{a}_i, \mathbf{A}_{ij}, \mathbb{A}_{ijk}$ and $\mathcal{A}_{ijkl}$ with i, j, k, l each being in an appropriate index set. For two vectors $\mathbf{a}, \mathbf{b} \in \mathbb{C}^d$ the Euclidian inner product is defined as

$$\langle \mathbf{a}, \mathbf{b} \rangle_{\mathbb{C}^d} \coloneqq \langle \mathbf{a}, \mathbf{b} \rangle \coloneqq \overline{\mathbf{a}^{\mathrm{T}}} \cdot \mathbf{b} \coloneqq \sum_{i=1}^{d} \overline{\mathbf{a}}_i \mathbf{b}_i \tag{2.1}$$

with $\overline{\cdot}$ being the (componentwise) complex conjugate and $\cdot^{\mathrm{T}}$ indicating the transpose of a quantity. The absolute value of a scalar is denoted with $|\cdot|$ while the Euclidian norm of a vector $\mathbf{a} \in \mathbb{C}^d$ is defined as

$$\|\mathbf{a}\|_{\mathbb{C}^d} \coloneqq \|\mathbf{a}\| \coloneqq \sqrt{\langle \mathbf{a}, \mathbf{a} \rangle}\,. \tag{2.2}$$

The corresponding matrix norm for a matrix $\mathbf{A} \in \mathbb{C}^{d\times d}$ is given as

$$\|\mathbf{A}\|_{\mathbb{C}^{d\times d}} \coloneqq \|\mathbf{A}\| \coloneqq \max_{\substack{\mathbf{v}\in\mathbb{C}^d \\ \mathbf{v}\neq\mathbf{0}}} \frac{\|\mathbf{A}\mathbf{v}\|}{\|\mathbf{v}\|}\,. \tag{2.3}$$

A third-order tensor can either be applied to a vector resulting in a matrix with entries

$$(\mathbb{A} \cdot \mathbf{a})_{ij} \coloneqq \sum_{k=1}^{d} \mathbb{A}_{ijk}\, \mathbf{a}_k \,, \quad i,j = 1,\dots,d \,, \tag{2.4}$$

or to a matrix yielding a vector with

$$(\mathbb{A} : \mathbf{A})_i \coloneqq \sum_{k,l=1}^{d} \mathbb{A}_{ikl}\, \mathbf{A}_{kl} \,, \quad i = 1,\dots,d \,, \tag{2.5}$$

where the double dot indicates the summation over two indices. Similarly, a fourth-order tensor $\mathcal{A} \in \mathbb{C}^{d\times d\times d\times d}$ can be applied to a second-order tensor (i.e. a matrix) $\mathbf{A} \in \mathbb{C}^{d\times d}$ with the resulting entries being defined as

$$(\mathcal{A} : \mathbf{A})_{ij} \coloneqq \sum_{k,l=1}^{d} \mathcal{A}_{ijkl}\, \mathbf{A}_{kl} \,, \quad i,j = 1,\dots,d \,. \tag{2.6}$$

2.2 Banach Spaces

For sequences $(x_k)_{k\in\mathbb{N}} \in \mathbb{C}^{\mathbb{N}}$ one defines the p-norm $\|\cdot\|_p$ as

$$\left\|(x_k)_{k\in\mathbb{N}}\right\|_p \coloneqq \left(\sum_{k=1}^{\infty} |x_k|^p\right)^{\frac{1}{p}} \tag{2.7}$$

for $1 \le p < \infty$ and

$$\left\|(x_k)_{k\in\mathbb{N}}\right\|_p \coloneqq \sup_{k\in\mathbb{N}} |x_k| \tag{2.8}$$

for $p = \infty$. The corresponding sequence spaces

$$\ell^p \coloneqq \left\{(x)_{k\in\mathbb{N}} \in \mathbb{C}^{\mathbb{N}} \,:\, \left\|(x_k)_{k\in\mathbb{N}}\right\|_p < \infty\right\} \tag{2.9}$$

are then Banach spaces with respect to this norm. In the case $p = 2$, it is furthermore a Hilbert space with the norm being induced by the inner product

$$\left\langle (x_k)_{k\in\mathbb{N}}, (y_k)_{k\in\mathbb{N}} \right\rangle_{\ell^2} \coloneqq \sum_{k=1}^{\infty} x_k \overline{y_k} \,, \quad (x_k)_{k\in\mathbb{N}}, (y_k)_{k\in\mathbb{N}} \in \ell^2 \,. \tag{2.10}$$

These definitions also carry over to other countable index sets instead of $\mathbb{N}$. For $1 \le p < q \le \infty$ one has the inclusion $\ell^p \subset \ell^q$.

Similar spaces can be introduced for functions. Let Ω be a non-empty measurable set and $f : \Omega \to \mathbb{C}$ a function. The p-seminorm of a function is then defined as the Lebesgue integral

$$\|f\|_p \coloneqq \left(\int_\Omega |f(x)|^p \,\mathrm{d}\, x\right)^{\frac{1}{p}} \tag{2.11}$$

for $1 \le p < \infty$ and

$$\|f\|_p \coloneqq \operatorname*{ess\,sup}_{x\in\Omega} |f(x)| \tag{2.12}$$

for $p = \infty$. One then defines the function spaces

$$\mathcal{L}^p(\Omega, \mathbb{C}) \coloneqq \left\{f : \Omega \to \mathbb{C} \,:\, \|f\|_p < \infty\right\} \tag{2.13}$$

and by excluding the subspace

$$\mathcal{N} \coloneqq \left\{f : \Omega \to \mathbb{C} \,:\, \|f\|_p = 0\right\} \tag{2.14}$$

of functions that are equal to zero almost everywhere one obtains the Banach spaces

$$L^p \coloneqq \mathcal{L}^p / \mathcal{N} \,, \tag{2.15}$$

where $\|\cdot\|_{L^p} \coloneqq \|\cdot\|_p$ is now an actual norm. In the case $p = 2$ this leads again to a Hilbert space with the inner product

$$\langle f, g \rangle_{L^2} \coloneqq \int_\Omega f(x)\overline{g(x)} \, \mathrm{d}\, x \,, \quad f, g \in L^2(\Omega, \mathbb{C}) \,. \tag{2.16}$$

For vector- or tensor-valued functions $\mathbf{f}$ and $\mathbf{g}$ with the same dimensions the above definitions are extended to

$$\|\mathbf{f}\|_{L^p} \coloneqq \left(\int_\Omega \sum_{i \in \mathcal{I}} |\mathbf{f}_i(x)|^p \, \mathrm{d}\, \mathbf{x} \right)^{\frac{1}{p}} \qquad \text{and} \qquad \langle \mathbf{f}, \mathbf{g} \rangle_{L^2} \coloneqq \int_\Omega \sum_{i \in \mathcal{I}} \mathbf{f}_i(x)\overline{\mathbf{g}_i(x)} \, \mathrm{d}\, \mathbf{x} \tag{2.17}$$

for $1 \leq p < \infty$; $\mathcal{I}$ being an appropriate index set over all components. For $p = \infty$ the essential supremum is taken over all components instead. If the dimension is clear from context, the dependency on $\mathbb{C}^d$ might be dropped, i.e. $L^p(\Omega)$ is written instead of $L^p(\Omega, \mathbb{C}^d)$. For $1 \leq p < q \leq \infty$ one has the inclusion $L^q(\Omega) \subset L^p(\Omega)$, contrary to the sequence spaces introduced before.

Now let $\Omega \subset \mathbb{R}^n$ be open and $\mathbf{f} : \Omega \to \mathbb{R}^m$. The function is called partially differentiable with respect to the i-th component at point $\mathbf{x}$ if the partial derivative

$$\frac{\partial \mathbf{f}}{\partial \mathbf{x}_i}(\mathbf{x}) \coloneqq \lim_{h \to 0} \frac{\mathbf{f}(\mathbf{x}_1, \ldots, \mathbf{x}_i + h, \ldots, \mathbf{x}_n) - \mathbf{f}(\mathbf{x}_1, \ldots, \mathbf{x}_i, \ldots, \mathbf{x}_n)}{h} \tag{2.18}$$

exists and is finite. The function is furthermore called partially differentiable at $\mathbf{x}$ if all partial derivatives at that point exist and partially differentiable if it is partially differentiable at every point $\mathbf{x} \in \Omega$. If additionally all partial derivatives are continuous on Ω, the function is called totally differentiable and for each point $\mathbf{x}_0$ its Jacobi matrix

$$\mathbf{J}_\mathbf{f}(\mathbf{x}) \coloneqq \left(\frac{\partial \mathbf{f}_i}{\partial \mathbf{x}_j}(\mathbf{x}) \right)_{\substack{i=1,\ldots,m \\ j=1,\ldots,n}} \tag{2.19}$$

fulfills the linear approximation

$$\lim_{\mathbf{x} \to \mathbf{x}_0} \frac{\|\mathbf{f}(\mathbf{x}) - \mathbf{f}(\mathbf{x}_0) - \mathbf{J}_\mathbf{f}(\mathbf{x}_0)(\mathbf{x} - \mathbf{x}_0)\|}{\|\mathbf{x} - \mathbf{x}_0\|} = 0 \,. \tag{2.20}$$

In the special case $m = 1$, the transposed vector

$$\nabla \mathbf{f}(\mathbf{x}) \coloneqq \operatorname{grad} \mathbf{f}(\mathbf{x}) \coloneqq \left(\frac{\partial \mathbf{f}}{\partial \mathbf{x}_i}(\mathbf{x}) \right)_{i=1,\ldots,n} \tag{2.21}$$

is also referred to as the gradient of $\mathbf{f}$. While the notation with the operator ∇ is actually exclusively used for gradients, within this thesis it can also denote the Jacobi matrix of arbitrary functions $\mathbf{f} : \Omega \to \mathbb{R}^m$. With multi-indices $\alpha = (\alpha_1, \ldots, \alpha_n) \in \mathbb{N}_0^n$ where one sets $|\alpha| \coloneqq \sum_{i=1}^n \alpha_i$, higher-order derivatives are defined by

$$\mathrm{D}^\alpha \mathbf{f} \coloneqq \frac{\partial^{|\alpha|} \mathbf{f}}{\partial \mathbf{x}_1^{\alpha_1} \cdots \partial \mathbf{x}_n^{\alpha_n}} \,, \tag{2.22}$$

i.e. differentiating with respect to each variable α_i times. It is assumed here that all partial derivatives are continuous, thus Schwarz's theorem holding true. For $k \in \mathbb{N}_0 \cup \{\infty\}$ the set of k times continuously differentiable functions on the set Ω that map to $\mathbb{R}^m$ is defined as

$$\mathcal{C}^k(\Omega, \mathbb{R}^m) \coloneqq \{\mathbf{f} : \Omega \to \mathbb{R}^m \;:\; \mathrm{D}^\alpha \mathbf{f} \text{ exists and is continuous } \forall \alpha \in \mathbb{N}_0^n \text{ with } |\alpha| \leq k\} \,. \tag{2.23}$$

For $k = 0$ the superscript can also be omitted. In the case of functions that are defined on a closed set, one requires for the derivatives to exist on the interior of Ω and to be continuously continuable on

Ω. All of the above definitions apply for complex-valued functions analogously. Derivatives of scalar functions can also be denoted with an according number of prime symbols or a roman superscript in parentheses. The dependency on $\mathbb{R}^m$ or $\mathbb{C}^m$ might be dropped again if the context is clear.

For vector fields $\mathbf{f} : \Omega \to \mathbb{C}^n$ one defines the divergence

$$\operatorname{div} \mathbf{f} \coloneqq \nabla \cdot \mathbf{f} \coloneqq \sum_{i=1}^{n} \frac{\partial \mathbf{f}_i}{\partial \mathbf{x}_i} \,. \tag{2.24}$$

For functions $\mathbf{g} : \Omega \to \mathbb{C}^{n \times n}$ this definition is extended to the vector field $\operatorname{div} \mathbf{g} : \Omega \to \mathbb{C}^n$ which is obtained by applying the regular divergence operator column-wise. In the case $n = 3$, one also defines the rotation

$$\operatorname{rot} \mathbf{f} \coloneqq \nabla \times \mathbf{f} \coloneqq \left(\frac{\partial \mathbf{f}_3}{\partial \mathbf{x}_2} - \frac{\partial \mathbf{f}_2}{\partial \mathbf{x}_3} \,,\, \frac{\partial \mathbf{f}_1}{\partial \mathbf{x}_3} - \frac{\partial \mathbf{f}_3}{\partial \mathbf{x}_1} \,,\, \frac{\partial \mathbf{f}_2}{\partial \mathbf{x}_1} - \frac{\partial \mathbf{f}_1}{\partial \mathbf{x}_2} \right)^{\mathrm{T}} \,. \tag{2.25}$$

A function $\mathbf{f} \in L^1(\Omega, \mathbb{R}^m)$ is said to have a weak α-derivative $\mathrm{D}^\alpha \mathbf{f}$, if there exists a measurable function $\mathbf{g} \in L^1(\Omega, \mathbb{R}^m)$, such that

$$\int_\Omega \mathbf{f}(\mathbf{x}) \, \mathrm{D}^\alpha \mathbf{h}(\mathbf{x}) \, \mathrm{d}\mathbf{x} = (-1)^{|\alpha|} \int_\Omega \mathbf{g}(\mathbf{x}) \, \mathbf{h}(\mathbf{x}) \, \mathrm{d}\mathbf{x} \,, \quad \forall \mathbf{h} \in C_0^\infty(\Omega, \mathbb{R}^m) \tag{2.26}$$

where the 0-subscript denotes compact support on Ω. If the statement holds true, one sets $\mathrm{D}^\alpha \mathbf{f} \coloneqq \mathbf{g}$. By introducing the norms

$$\|\mathbf{f}\|_{k,p} \coloneqq \left(\sum_{\substack{\alpha \in \mathbb{N}_0^n \\ |\alpha| \le k}} \|\mathrm{D}^\alpha \mathbf{f}\|_{L^p}^p \right)^{\frac{1}{p}} \tag{2.27}$$

for $k \in \mathbb{N}_0, 1 \le p < \infty$ and

$$\|\mathbf{f}\|_{k,p} \coloneqq \max_{\substack{\alpha \in \mathbb{N}_0^n \\ |\alpha| \le k}} \|\mathrm{D}^\alpha \mathbf{f}\|_{L^\infty} \tag{2.28}$$

for $k \in \mathbb{N}_0, p = \infty$, one defines the Sobolev spaces of weakly differentiable functions

$$W^{k,p}(\Omega) \coloneqq W^{k,p}(\Omega, \mathbb{R}^m) \coloneqq \left\{ \mathbf{f} \in L^p(\Omega, \mathbb{R}^m) \,:\, \|\mathbf{f}\|_{k,p} < \infty \right\} \,. \tag{2.29}$$

For the special case $p = 2$, the Sobolev space $H^k(\Omega) \coloneqq W^{k,2}(\Omega)$ is additionally a Hilbert space with the inner product

$$\langle \mathbf{f}, \mathbf{g} \rangle_{H^k} \coloneqq \sum_{\substack{\alpha \in \mathbb{N}_0^n \\ |\alpha| \le k}} \langle \mathrm{D}^\alpha \mathbf{f}, \, \mathrm{D}^\alpha \mathbf{g} \rangle_{L^2} \,, \quad \mathbf{f}, \mathbf{g} \in H^k(\Omega) \,. \tag{2.30}$$

In this case the notation $\|\cdot\|_{H^k} \coloneqq \|\cdot\|_{k,2}$ is also used for the norm instead. All the previously defined differential operators carry over to weak derivatives as well.

2.3 Fourier Series

Let $\mathbb{T}^d \coloneqq \mathbb{R}^d / \mathbb{Z}^d \cong \left[-\frac{1}{2}, \frac{1}{2}\right)^d$ denote the d-dimensional torus of length one; usually represented by the given interval. For a function $f \in L^1(\mathbb{T}^d, \mathbb{C})$ one can define the Fourier coefficients

$$c_{\mathbf{k}}(f) \coloneqq \int_{\mathbb{T}^d} f(\mathbf{x}) \, \mathrm{e}^{-2\pi \mathrm{i} \langle \mathbf{k}, \mathbf{x} \rangle} \, \mathrm{d}\mathbf{x} \tag{2.31}$$

for $\mathbf{k} \in \mathbb{Z}^d$. If f has a (weak) derivative $f' \in L^1\left(\mathbb{T}^d\right)^d$, its Fourier coefficients $c_{\mathbf{k}}\left(f'\right) \in \mathbb{C}^d$ can be computed directly as

$$c_{\mathbf{k}}\left(f'\right) \coloneqq 2\pi \mathrm{i}\, \mathbf{k} c_{\mathbf{k}}\left(f\right) \ . \tag{2.32}$$

Furthermore, the functions $\mathrm{e}^{2\pi \mathrm{i}\langle \mathbf{k}, \cdot \rangle} : \mathbb{T}^d \to \mathbb{C}$ form an orthonormal Schauder basis of $L^2\left(\mathbb{T}^d, \mathbb{C}\right)$, allowing to represent each function $f \in L^2\left(\mathbb{T}^d, \mathbb{C}\right)$ by its Fourier series

$$f\left(\mathbf{x}\right) = \sum_{\mathbf{k} \in \mathbb{Z}^d} c_{\mathbf{k}}\left(f\right) \mathrm{e}^{2\pi \mathrm{i}\langle \mathbf{k}, \mathbf{x} \rangle} \ . \tag{2.33}$$

The equality here is meant in the L^2-sense. Additionally, for $f, g \in L^2\left(\mathbb{T}^d\right)$, Parseval's equation

$$\langle f, g \rangle_{L^2} = \left\langle \left(c_{\mathbf{k}}\left(f\right)\right)_{\mathbf{k} \in \mathbb{Z}^d}, \left(c_{\mathbf{k}}\left(g\right)\right)_{\mathbf{k} \in \mathbb{Z}^d} \right\rangle_{\ell^2} \tag{2.34}$$

holds true.

To mimic the Fourier series in a discrete setting, one introduces the Discrete Fourier Transform or DFT $\mathcal{F} : \mathbb{C}^N \to \mathbb{C}^N$, where one defines $\hat{\mathbf{f}} \coloneqq \mathcal{F}\left(\mathbf{f}\right)$ for $\mathbf{f} \in \mathbb{C}^N$. When talking about the DFT, it is common and preferred to index vectors from zero to $N-1$ and the notation $\mathbf{f}\left(k\right) \coloneqq \mathbf{f}_{k+1}$ will be used instead to facilitate the readability. Thus, the DFT is given by

$$\hat{\mathbf{f}}\left(k\right) \coloneqq \sum_{j=0}^{N-1} \mathbf{f}\left(j\right) \mathrm{e}^{-2\pi \mathrm{i}\, jk/N} \ , \quad k = 0, \ldots, N-1 \ , \tag{2.35}$$

and the inverse mapping called inverse Fourier transform or IDFT follows as

$$\mathbf{f}\left(j\right) \coloneqq \frac{1}{N} \sum_{k=0}^{N-1} \hat{\mathbf{f}}\left(k\right) \mathrm{e}^{2\pi \mathrm{i}\, jk/N} \ , \quad j = 0, \ldots, N-1 \ . \tag{2.36}$$

The DFT and IDFT can analogously be defined for higher dimensions.

3 Derivation of a Magneto-Mechanical Model Problem

This chapter presents the model problem of a linearly coupled magneto-elastic system which will be analyzed throughout the remainder of this thesis. Albeit being a simple model to begin with, the mathematical theory used in the upcoming chapters already proves to be rich and combines a variety of different research fields.

First, the basic concepts of linear elasticity and magnetism will be given in Sec. 3.1 after introducing the reader to some helpful notations for the therein presented quantities. With these at hand the strong and weak forms of the model problem are derived in Sec. 3.2. The existence and uniqueness of its solution are studied afterwards in Sec. 3.3.

3.1 Physical Background and Quantities

While the physical theory of elasticity [30, 65, 99] or magnetism [24, 55] goes way beyond the scope of this theses, the basic notions and concepts present in the model problem are collected in this section.

3.1.1 Notational Aspects of Symmetric Tensors

Several of the following physical or mathematical quantities are tensors of higher rank featuring certain symmetry patterns in their entries. Different notations were introduced in the past to simplify the complexity of such expressions exploiting this property. This is commonly achieved by reducing the dimensionality of these expressions in representing them with equivalent tensors of lower rank, thus allowing for example to write a symmetric matrix as a single column vector instead.

One of these notations is the *Kelvin-Mandel notation* or simply *Mandel notation* [77] which will be used throughout this thesis. This way, most of the calculations can be done in a well-known matrix–vector setting. In the context of linear elasticity there exist other commonly used possibilities such as the *Voigt notation* [110] or the *Nye notation* [92]. However, contrary to these two where the notation and some multipliers within are dependent on the formula, the Mandel notation can be generally defined for symmetric tensors leading to a consistent alternative of writing down corresponding relations.

All notations follow the idea to traverse two- or three-dimensional symmetric matrices in a prescribed order, thus referring to their elements with a unique single index. Entries appearing more than once are multiplied with certain factors to reflect their symmetric entries as well. This idea is then extended

to tensors of rank three or four. The ordering used in the Mandel (and also Voigt) notation is given in Table 3.1 and visualized in Fig. 3.1.

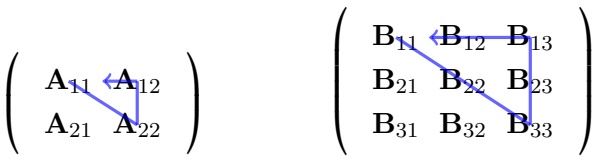

Fig. 3.1: For the Mandel notation the main diagonal of the matrix is traversed first before moving upwards in the column. In the three-dimensional case one additionally moves back to the start along the first row.

dimension	$d=2$			$d=3$					
original index	11	22	12=21	11	22	33	23=32	13=31	12=21
transformed index	1	2	3	1	2	3	4	5	6

Tab. 3.1: Indexing for Mandel notation

The following definition collects all necessary information for the Mandel notation in two or three dimensions in a formal way.

Definition 3.1.1 (Mandel notation)**.** *For* $\mathbb{K} \in \{\mathbb{R}, \mathbb{C}\}$ *and* $d \in \{2,3\}$ *define*

$$\mathbb{K}^{d\times d}_{\mathrm{sym}} \coloneqq \left\{ \mathbf{A} \in \mathbb{K}^{d\times d} \,:\, \mathbf{A}_{ij} = \mathbf{A}_{ji}\,,\ \forall i,j \in \{1,\dots,d\} \right\}, \tag{3.1}$$

$$\mathbb{K}^{d\times d\times d}_{\mathrm{sym}} \coloneqq \left\{ \mathbb{A} \in \mathbb{K}^{d\times d\times d} \,:\, \mathbb{A}_{ijk} = \mathbb{A}_{jik}\,,\ \forall i,j,k \in \{1,\dots,d\} \right\}, \tag{3.2}$$

$$\mathbb{K}^{d\times d\times d\times d}_{\mathrm{sym}} \coloneqq \left\{ \mathcal{A} \in \mathbb{K}^{d\times d\times d\times d} \,:\, \mathcal{A}_{ijkl} = \mathcal{A}_{jikl} = \mathcal{A}_{ijlk}\,,\ \forall i,j,k,l \in \{1,\dots,d\} \right\}, \tag{3.3}$$

as the spaces of (minor) symmetric d*-dimensional tensors of rank two, three and four respectively. Define furthermore* $\tilde{d} \coloneqq d\,(d+1)\,/2$*. Then the corresponding* Mandel transforms *or* Mandel notations *are defined as the mappings*

$$\mathcal{M}^d_2 \,:\, \mathbb{K}^{d\times d}_{\mathrm{sym}} \to \mathbb{K}^{\tilde{d}}\,,\ \mathbf{A} \mapsto \mathcal{M}^d_2(\mathbf{A})\,, \tag{3.4}$$

$$\mathcal{M}^d_3 \,:\, \mathbb{K}^{d\times d\times d}_{\mathrm{sym}} \to \mathbb{K}^{\tilde{d}\times d}\,,\ \mathbb{A} \mapsto \mathcal{M}^d_3(\mathbb{A})\,, \tag{3.5}$$

$$\mathcal{M}^d_4 \,:\, \mathbb{K}^{d\times d\times d\times d}_{\mathrm{sym}} \to \mathbb{K}^{\tilde{d}\times\tilde{d}}\,,\ \mathcal{A} \mapsto \mathcal{M}^d_4(\mathcal{A})\,. \tag{3.6}$$

In the case $d = 2$ *the resulting transforms are given by*

$$\mathcal{M}^2_2(\mathbf{A}) \coloneqq \begin{pmatrix} \mathbf{A}_{11} & \mathbf{A}_{22} & \sqrt{2}\,\mathbf{A}_{12} \end{pmatrix}^{\mathrm{T}}, \tag{3.7}$$

$$\mathcal{M}^2_3(\mathbb{A}) \coloneqq \begin{pmatrix} \mathbb{A}_{111} & \mathbb{A}_{221} & \sqrt{2}\,\mathbb{A}_{121} \\ \mathbb{A}_{112} & \mathbb{A}_{222} & \sqrt{2}\,\mathbb{A}_{122} \end{pmatrix}^{\mathrm{T}}, \tag{3.8}$$

$$\mathcal{M}^2_4(\mathcal{A}) \coloneqq \begin{pmatrix} \mathcal{A}_{1111} & \mathcal{A}_{1122} & \sqrt{2}\,\mathcal{A}_{1112} \\ \mathcal{A}_{2211} & \mathcal{A}_{2222} & \sqrt{2}\,\mathcal{A}_{2212} \\ \sqrt{2}\,\mathcal{A}_{1211} & \sqrt{2}\,\mathcal{A}_{1222} & 2\,\mathcal{A}_{1212} \end{pmatrix}. \tag{3.9}$$

In the case $d = 3$ the resulting transforms are given by

$$\mathcal{M}_2^3(\mathbf{A}) \coloneqq \begin{pmatrix} \mathbf{A}_{11} & \mathbf{A}_{22} & \mathbf{A}_{33} & \sqrt{2}\,\mathbf{A}_{23} & \sqrt{2}\,\mathbf{A}_{13} & \sqrt{2}\,\mathbf{A}_{12} \end{pmatrix}^{\mathrm{T}}, \tag{3.10}$$

$$\mathcal{M}_3^3(\mathbb{A}) \coloneqq \begin{pmatrix} \mathbb{A}_{111} & \mathbb{A}_{221} & \mathbb{A}_{331} & \sqrt{2}\,\mathbb{A}_{231} & \sqrt{2}\,\mathbb{A}_{131} & \sqrt{2}\,\mathbb{A}_{121} \\ \mathbb{A}_{112} & \mathbb{A}_{222} & \mathbb{A}_{332} & \sqrt{2}\,\mathbb{A}_{232} & \sqrt{2}\,\mathbb{A}_{132} & \sqrt{2}\,\mathbb{A}_{122} \\ \mathbb{A}_{113} & \mathbb{A}_{223} & \mathbb{A}_{333} & \sqrt{2}\,\mathbb{A}_{233} & \sqrt{2}\,\mathbb{A}_{133} & \sqrt{2}\,\mathbb{A}_{123} \end{pmatrix}^{\mathrm{T}}, \tag{3.11}$$

$$\mathcal{M}_4^3(\mathcal{A}) \coloneqq \begin{pmatrix} \mathcal{A}_{1111} & \mathcal{A}_{1122} & \mathcal{A}_{1133} & \sqrt{2}\,\mathcal{A}_{1123} & \sqrt{2}\,\mathcal{A}_{1113} & \sqrt{2}\,\mathcal{A}_{1112} \\ \mathcal{A}_{2211} & \mathcal{A}_{2222} & \mathcal{A}_{2233} & \sqrt{2}\,\mathcal{A}_{2223} & \sqrt{2}\,\mathcal{A}_{2213} & \sqrt{2}\,\mathcal{A}_{2212} \\ \mathcal{A}_{3311} & \mathcal{A}_{3322} & \mathcal{A}_{3333} & \sqrt{2}\,\mathcal{A}_{3323} & \sqrt{2}\,\mathcal{A}_{3313} & \sqrt{2}\,\mathcal{A}_{3312} \\ \sqrt{2}\,\mathcal{A}_{2311} & \sqrt{2}\,\mathcal{A}_{2322} & \sqrt{2}\,\mathcal{A}_{2333} & 2\,\mathcal{A}_{2323} & 2\,\mathcal{A}_{2313} & 2\,\mathcal{A}_{2312} \\ \sqrt{2}\,\mathcal{A}_{1311} & \sqrt{2}\,\mathcal{A}_{1322} & \sqrt{2}\,\mathcal{A}_{1333} & 2\,\mathcal{A}_{1323} & 2\,\mathcal{A}_{1313} & 2\,\mathcal{A}_{1312} \\ \sqrt{2}\,\mathcal{A}_{1211} & \sqrt{2}\,\mathcal{A}_{1222} & \sqrt{2}\,\mathcal{A}_{1233} & 2\,\mathcal{A}_{1223} & 2\,\mathcal{A}_{1213} & 2\,\mathcal{A}_{1212} \end{pmatrix}. \tag{3.12}$$

The following convention is used for the remainder of this thesis: whenever a quantity which will be mostly used in its corresponding Mandel notation is introduced, the unaltered quantity will be presented first and denoted with an underlined specifier, whereas its afterwards defined plain symbol shall refer to its Mandel notation. It is hoped that in this way the readability of equations is ensured while the option to access the unaltered quantity is still given.

3.1.2 Basics of Elasticity

Elastic deformation of a physical body refers to its mechanical behavior in a stress field which is usually induced by an outer force. While plastic or viscous deformations describe irreversible processes, the effects of an elastic deformation are reversed when the body is no longer exposed to the stress field.

To define any kind of deformation one first needs to choose a *reference state* for the body of interest. Let the body be described as a subset $\Omega \subset \mathbb{R}^d$ in a local coordinate system with d denoting the spatial dimensions (usually $d = 3$, sometimes planar settings are also used). The reference state is given by a mapping $\mathbf{f}_{\mathrm{ref}} : \Omega \to \mathbb{R}^d$ that links every particle $\mathbf{x}$ of the object to a position $\mathbf{f}_{\mathrm{ref}}(\mathbf{x})$ in the physical domain. The choice of a reference state is arbitrary in general but in most cases it is assumed to be a body's configuration when no outer forces are present. Since a quasi-static approach is used in this work, the time-dependent evolution of the deformation is not taken into account and only its final configuration is looked at. This final state of the object after deformation can be described by a similar map $\mathbf{f}_{\mathrm{end}} : \Omega \to \mathbb{R}^d$. The difference between the reference state and the final state of a body's particle can now be defined as the *displacement field* $\mathbf{u}$ given as

$$\mathbf{u} : \Omega \to \mathbb{R}^d, \quad \mathbf{u}(\mathbf{x}) \coloneqq \mathbf{f}_{\mathrm{end}}(\mathbf{x}) - \mathbf{f}_{\mathrm{ref}}(\mathbf{x}). \tag{3.13}$$

The connection between the displacement and an object's different states is visualized in Fig. 3.2.

A quantity measuring the displacement of any point in relation to the overall displacement is given by a *strain field*. For example, while an object may have been moved over a great distance, thus its particles having a large deformation assigned to them, their strain is equal to zero as long as the object is not experiencing additional rotations, shearing or pressure at its new location. As a ratio of lengths the strain field is dimensionless. There exist different strain measurements in continuum mechanics,

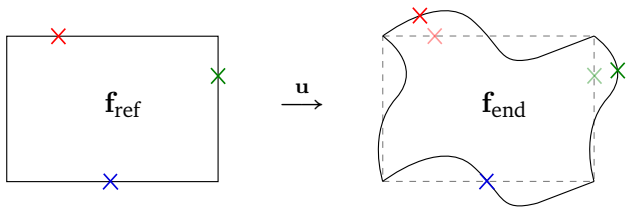

Fig. 3.2: A body in its reference state (left) is deformed to its altered final state (right). The new position of the body's points within the coordinate system differs by the displacement assigned to them. The blue point therefore would have a displacement equal to the zero vector.

one of them being the *Green–Lagrangian strain tensor* or *Green–St.-Venant strain tensor* used in finite strain theory that is defined as

$$\underline{\mathbf{E}}(\mathbf{u}) : \Omega \to \mathbb{R}^{d\times d}_{\text{sym}}, \quad \underline{\mathbf{E}}(\mathbf{u}(\mathbf{x})) \coloneqq \frac{1}{2}\left(\nabla \mathbf{u}(\mathbf{x}) + (\nabla \mathbf{u}(\mathbf{x}))^{\mathrm{T}} + \nabla \mathbf{u}(\mathbf{x}) \cdot (\nabla \mathbf{u}(\mathbf{x}))^{\mathrm{T}}\right), \tag{3.14}$$

where

$$\left(\nabla \mathbf{u}(\mathbf{x}) \cdot (\nabla \mathbf{u}(\mathbf{x}))^{\mathrm{T}}\right)_{ij} \coloneqq \sum_{k=1}^{d} \frac{\partial u_k}{\partial x_i}(\mathbf{x}) \frac{\partial u_k}{\partial x_j}(\mathbf{x}), \quad i,j = 1,\dots,d. \tag{3.15}$$

For the *theory of small displacements* which is applicable to many materials used in industrial projects such as concrete, steel or other minerals, one linearizes the strain tensor which yields the *Cauchy strain tensor*

$$\underline{\boldsymbol{\varepsilon}}(\mathbf{u}) : \Omega \to \mathbb{R}^{d\times d}_{\text{sym}}, \quad \underline{\boldsymbol{\varepsilon}}(\mathbf{u}(\mathbf{x})) \coloneqq \frac{1}{2}\left(\nabla \mathbf{u}(\mathbf{x}) + (\nabla \mathbf{u}(\mathbf{x}))^{\mathrm{T}}\right). \tag{3.16}$$

As explained before in Subsect. 3.1.1, the notation $\boldsymbol{\varepsilon}(\mathbf{u}) \coloneqq \mathcal{M}_2^d \circ \underline{\boldsymbol{\varepsilon}}(\mathbf{u})$ shall from now on refer to its Mandel notation.

Another quantity resulting from the difference in particle's displacement is the *stress field* which measures the internal forces acting between neighboring particles in a deformed state relative to the surface of their contact area. Therefore, stress fields are measured in *pascal* [Pa] as a special form of pressure. As with the strain tensor, multiple descriptions of stress tensors have been introduced for the finite strain theory, the *Piola–Kirchhoff stress tensors* and the *Biot stress tensor* being relevant examples. In the case of infinitesimal strain theory the *Cauchy stress tensor* is frequently used. In the regular three-dimensional case it is defined as

$$\underline{\boldsymbol{\sigma}} : \Omega \to \mathbb{R}^{3\times 3}_{\text{sym}}, \quad \underline{\boldsymbol{\sigma}}(\mathbf{x}) \coloneqq \begin{pmatrix} \underline{\boldsymbol{\sigma}}_{11}(\mathbf{x}) & \underline{\boldsymbol{\sigma}}_{12}(\mathbf{x}) & \underline{\boldsymbol{\sigma}}_{13}(\mathbf{x}) \\ \underline{\boldsymbol{\sigma}}_{21}(\mathbf{x}) & \underline{\boldsymbol{\sigma}}_{22}(\mathbf{x}) & \underline{\boldsymbol{\sigma}}_{23}(\mathbf{x}) \\ \underline{\boldsymbol{\sigma}}_{31}(\mathbf{x}) & \underline{\boldsymbol{\sigma}}_{32}(\mathbf{x}) & \underline{\boldsymbol{\sigma}}_{33}(\mathbf{x}) \end{pmatrix}, \tag{3.17}$$

with $\boldsymbol{\sigma} \coloneqq \mathcal{M}_2^3 \circ \underline{\boldsymbol{\sigma}}$ again denoting the corresponding Mandel notation. In the planar case for $d = 2$, the definitions follow analogously. Each column of the stress tensor refers to one of the spatial axes and collects the stresses of interest as a vector. The entries are divided into two categories. The ones on the main diagonal are referred to as the *orthogonal normal stresses* describing effects normal to the surface perpendicular to that column's direction. The remaining entries are *orthogonal shear stresses* corresponding to tangentially applied forces. The correct indexing of the stress tensor is depicted in Fig. 3.3.

In a continuous elastic material, strains and stresses are related to each other by *Hooke's law*

$$\underline{\boldsymbol{\sigma}}(\mathbf{x}) = \underline{\mathbf{C}}(\mathbf{x}) : \underline{\boldsymbol{\varepsilon}}(\mathbf{x}), \tag{3.18}$$

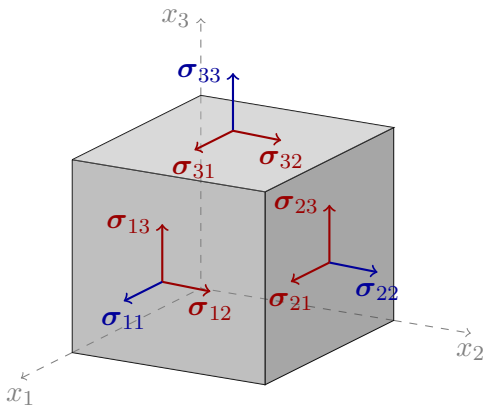

Fig. 3.3: Depiction of normal stresses (blue) and shear stresses (red) in three dimensions.

where $\underline{\mathbf{C}}(\mathbf{x})$ denotes the forth-order *stiffness* or *elasticity tensor* at point $\mathbf{x}$ given by

$$\underline{\mathbf{C}} : \Omega \to \mathbb{R}^{d\times d\times d\times d}_{\text{sym}} \ . \tag{3.19}$$

As with the strain and stress fields before, the notation $\mathbf{C} \coloneqq \mathcal{M}_4^d \circ \underline{\mathbf{C}}$ refers to the Mandel transform. It should be noted at this point that Hooke's law is equivalently written in this alternate notation as a simple matrix–vector–product $\boldsymbol{\sigma}(\mathbf{x}) = \mathbf{C}(\mathbf{x})\,\boldsymbol{\varepsilon}(\mathbf{x})$.

While the total number of entries for a stiffness tensor in three dimensions is 81, the number of different entries is actually far less due to its symmetric properties. Additionally to the *minor symmetries* given in (3.3) linked to the symmetric strain and stress tensors, the derivation of this relation from an energy density functional reveals the additional *major symmetries* which allow to switch the first and last two indices pairwise. This results in the Mandel transform being a symmetric matrix as well. All in all, the relations

$$\underline{\mathbf{C}}_{ijkl} = \underline{\mathbf{C}}_{jikl} = \underline{\mathbf{C}}_{ijlk} = \underline{\mathbf{C}}_{klij} \ , \quad i,j,k,l = 1,\dots,d \tag{3.20}$$

hold true, thus reducing the number of independent entries to 21.

According to their elastic behavior, materials can be classified into different categories. For example, *orthotropic materials* display different properties along three orthogonal planes of symmetry and for *transversely isotropic materials* there exists an axis normal to a plane that can be considered isotropic. Another important class which is used in this thesis is that of homogeneous *isotropic materials* whose properties do not depend on the spatial directions. In this case the entries of the stiffness tensor can be expressed through only two *elastic moduli*, material-dependent parameters that define a material's elastic properties in different situations. A conversion chart between different moduli is given in Table 3.2 and while any pairing could be used to define an isotropic material, the following two combinations are frequently found in the literature.

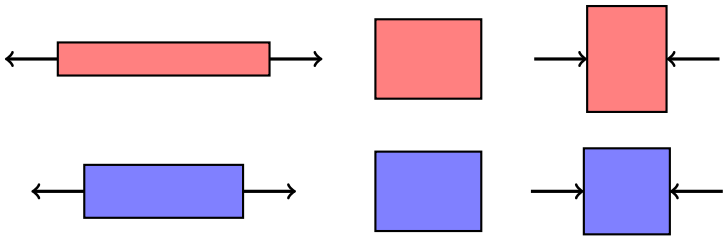

Fig. 3.4: When the same forces are applied, a body with low Young's modulus (red) is softer and more stretchy compared to a stiff one with high modulus (blue).

The first one consists of *Young's modulus* E and Poisson's ratio ν where the former measures the effects of uniaxial deformations as shown in Fig. 3.4 and the latter expresses the ratio of transverse and axial strains. In three dimensions the stiffness can then be written as

$$\mathbf{C} = \frac{E}{(1+\nu)(1-2\nu)} \begin{pmatrix} 1-\nu & \nu & \nu & 0 & 0 & 0 \\ \nu & 1-\nu & \nu & 0 & 0 & 0 \\ \nu & \nu & 1-\nu & 0 & 0 & 0 \\ 0 & 0 & 0 & 1-2\nu & 0 & 0 \\ 0 & 0 & 0 & 0 & 1-2\nu & 0 \\ 0 & 0 & 0 & 0 & 0 & 1-2\nu \end{pmatrix}. \tag{3.21}$$

Naturally, Young's modulus has a positive value with negative values only appearing in composites called *metamaterials*. Poisson's ratio is mostly positive as well, although a few cases of materials with a negative ratio exist. These are referred to as *auxetic materials*.

	Bulk modulus $K =$	Young's modulus $E =$	1st Lamé modulus $\lambda =$	Shear modulus $\mu =$	Poisson's ratio $\nu =$	P-wave modulus $M =$
(K, E)	—	—	$\frac{3K(3K-E)}{9K-E}$	$\frac{3KE}{9K-E}$	$\frac{3K-E}{6K}$	$\frac{3K(3K+E)}{9K-E}$
(K, λ)	—	$\frac{9K(K-\lambda)}{3K-\lambda}$	—	$\frac{3(K-\lambda)}{2}$	$\frac{\lambda}{3K-\lambda}$	$3K-2\lambda$
(K, μ)	—	$\frac{9K\mu}{3K+\mu}$	$K-\frac{2\mu}{3}$	—	$\frac{3K-2\mu}{2(3K+\mu)}$	$K+\frac{4\mu}{3}$
(K, ν)	—	$3K(1-2\nu)$	$\frac{3K\nu}{1+\nu}$	$\frac{3K(1-2\nu)}{2(1+\nu)}$	—	$\frac{3K(1-\nu)}{1+\nu}$
(K, M)	—	$\frac{9K(M-K)}{3K+M}$	$\frac{3K-M}{2}$	$\frac{3(M-K)}{4}$	$\frac{3K-M}{3K+M}$	—
$(E, \lambda)^{1)}$	$\frac{E+3\lambda+R}{6}$	—	—	$\frac{E-3\lambda+R}{4}$	$\frac{2\lambda}{E+\lambda+R}$	$\frac{E-\lambda+R}{2}$
(E, μ)	$\frac{E\mu}{3(3\mu-E)}$	—	$\frac{\mu(E-2\mu)}{3\mu-E}$	—	$\frac{E}{2\mu}-1$	$\frac{\mu(4\mu-E)}{3\mu-E}$
(E, ν)	$\frac{E}{3(1-2\nu)}$	—	$\frac{E\nu}{(1+\nu)(1-2\nu)}$	$\frac{E}{2(1+\nu)}$	—	$\frac{E(1-\nu)}{(1+\nu)(1-2\nu)}$
$(E, M)^{2)}$	$\frac{3M-E+S}{6}$	—	$\frac{M-E+S}{4}$	$\frac{3M+E-S}{8}$	$\frac{E-M+S}{4M}$	—
(λ, μ)	$\lambda+\frac{2\mu}{3}$	$\frac{\mu(3\lambda+2\mu)}{\lambda+\mu}$	—	—	$\frac{\lambda}{2(\lambda+\mu)}$	$\lambda+2\mu$
(λ, ν)	$\frac{\lambda(1+\nu)}{3\nu}$	$\frac{\lambda(1+\nu)(1-2\nu)}{\nu}$	—	$\frac{\lambda(1-2\nu)}{2\nu}$	—	$\frac{\lambda(1-\nu)}{\nu}$
(λ, M)	$\frac{M+2\lambda}{3}$	$\frac{(M-\lambda)(M+2\lambda)}{M+\lambda}$	—	$\frac{M-\lambda}{2}$	$\frac{\lambda}{M+\lambda}$	—
(μ, ν)	$\frac{2\mu(1+\nu)}{3(1-2\nu)}$	$2\mu(1+\nu)$	$\frac{2\mu\nu}{1-2\nu}$	—	—	$\frac{2\mu(1-\nu)}{1-2\nu}$
(μ, M)	$M-\frac{4\mu}{3}$	$\frac{\mu(3M-4\mu)}{M-\mu}$	$M-2\mu$	—	$\frac{M-2\mu}{2M-2\mu}$	—
(ν, M)	$\frac{M(1+\nu)}{3(1-\nu)}$	$\frac{M(1+\nu)(1-2\nu)}{1-\nu}$	$\frac{M\nu}{1-\nu}$	$\frac{M(1-2\nu)}{2(1-\nu)}$	—	—

1) $R = \sqrt{E^2+9\lambda^2+2E\lambda}$, 2) $S = \pm\sqrt{E^2+9M^2-10EM}$

Tab. 3.2: Conversion chart for elastic moduli

The second common pairing is given by the *Lamé parameters* λ and μ named after mathematician Gabriel Lamé. The second Lamé coefficient is also known as *shear modulus*. In terms of these parameters the elasticity tensor can also be written as

$$\mathbf{C} = \begin{pmatrix} \lambda+2\mu & \lambda & \lambda & 0 & 0 & 0 \\ \lambda & \lambda+2\mu & \lambda & 0 & 0 & 0 \\ \lambda & \lambda & \lambda+2\mu & 0 & 0 & 0 \\ 0 & 0 & 0 & 2\mu & 0 & 0 \\ 0 & 0 & 0 & 0 & 2\mu & 0 \\ 0 & 0 & 0 & 0 & 0 & 2\mu \end{pmatrix} . \tag{3.22}$$

While Lamé's first parameter can rarely attain negative values, the shear modulus always has to be a positive quantity. All previously discussed moduli are normally given in pascal, except for Poisson's ratio which is a dimensionless quantity.

For the two-dimensional case of isotropic materials, there exist two important versions of Hooke's law used in practice to reduce the complexity of actual three-dimensional objects. The first one is the *plane strain* setting which is used if one of the material's dimensional lengths is significantly larger than the other two. The stiffness tensor is then naturally reduced to

$$\mathbf{C} = \frac{E}{(1+\nu)(1-2\nu)} \begin{pmatrix} 1-\nu & \nu & 0 \\ \nu & 1-\nu & 0 \\ 0 & 0 & 1-2\nu \end{pmatrix} = \begin{pmatrix} \lambda+2\mu & \lambda & 0 \\ \lambda & \lambda+2\mu & 0 \\ 0 & 0 & 2\mu \end{pmatrix} , \tag{3.23}$$

with the parameters as introduced before. The second setting is that of *plane stress* where now one of the material's dimensional lengths is negligibly small in relation, making this setting the preferred choice for flat, thin objects. Under plane stress conditions, the Mandel notation of the stiffness tensor has the entries

$$\mathbf{C} = \frac{E}{(1-\nu^2)} \begin{pmatrix} 1 & \nu & 0 \\ \nu & 1 & 0 \\ 0 & 0 & 1-\nu \end{pmatrix} =: \begin{pmatrix} \tilde{\lambda}+2\tilde{\mu} & \tilde{\lambda} & 0 \\ \tilde{\lambda} & \tilde{\lambda}+2\tilde{\mu} & 0 \\ 0 & 0 & 2\tilde{\mu} \end{pmatrix} , \tag{3.24}$$

where E and ν once again refer to Young's modulus and Poisson's ratio but $\tilde{\lambda}$ and $\tilde{\mu}$ are not to be confused with the otherwise used Lamé parameters as they would follow a different conversion formula. Even so, when talking about and working with stiffness tensors within this thesis, the above definition of $\tilde{\lambda}$ and $\tilde{\mu}$ allows to consider the plane stress setting simultaneously with the plane strain setting or the classic three-dimensional case as they all share the same mathematical structure. Therefore, it is usually not explicitly differentiated between 'real' and 'fake' Lamé parameter pairs from now on.

3.1.3 Basics of Magnetism

Magnetic phenomena are by nature strongly coupled to electric ones, both together forming the overarching field of electromagnetism. The mathematical foundation for this subject is given by a set of partial differential equations known as the *Maxwell equations*, named after physicist James Clerk Maxwell [80].

One of these equations is *Ampère's circuital law*

$$\nabla \times \mathbf{H} = \mathbf{J}_\mathrm{f} + \frac{\partial \mathbf{D}}{\partial t} , \tag{3.25}$$

where $\mathbf{H}$ denotes the *magnetic field*, $\mathbf{J}_\mathrm{f}$ symbolizes the *free electric current density* and $\mathbf{D}$ refers to the *electric displacement field*. In the quasi-static case presented in this thesis where no free currents are assumed, (3.25) can be simplified to

$$\nabla \times \mathbf{H} = 0 \,, \tag{3.26}$$

allowing for the introduction of a *magnetic scalar potential*

$$\psi : \Omega \to \mathbb{R} \,. \tag{3.27}$$

By analogy with the electric potential in electrostatics, the magnetic potential is chosen so that the magnetic field corresponds to its negative gradient, therefore

$$\mathbf{H}(\psi) : \Omega \to \mathbb{R}^d \,, \quad \mathbf{H}(\psi(\mathbf{x})) = -\nabla \psi(\mathbf{x}) \,. \tag{3.28}$$

In physics, referring to the magnetic field without further information can be quite misleading, since there exist two strongly related but different quantities with this name. Additionally to the $\mathbf{H}$-field above, it could also mean the $\mathbf{B}$-field given by a function

$$\mathbf{B} : \Omega \to \mathbb{R}^d \,, \quad \mathbf{B}(\mathbf{x}) \coloneqq (\mathbf{B}_1(\mathbf{x}), \ldots, \mathbf{B}_d(\mathbf{x}))^\mathrm{T} \,. \tag{3.29}$$

Both, $\mathbf{B}$- and $\mathbf{H}$-field measure the strength and influence of magnetic effects. To avoid confusion in this work the term *magnetic field* shall always be understood as the $\mathbf{H}$-field, whereas the $\mathbf{B}$-field will be called *magnetic induction*. The corresponding SI units are *ampere per meter* $[\mathrm{A\,m^{-1}}]$ for $\mathbf{H}$ and *tesla* $[\mathrm{T}]$ for $\mathbf{B}$. Other alternative names exist in the literature.

Sometimes the magnetic field is considered to be just an auxiliary field, since it does not incorporate certain material dependent effects yet in contrast to the magnetic induction.The difference between both fields is captured by a vector field $\mathbf{M}$ called the *magnetization* or *magnetic polarization* of a material that describes the density of magnetic moments within a body. It connects the $\mathbf{B}$- and $\mathbf{H}$-field via the equation

$$\mathbf{B} = \boldsymbol{\mu}_0 (\mathbf{H} + \mathbf{M}) \tag{3.30}$$

with $\boldsymbol{\mu}_0 \approx 4\pi * 10^{-7} \mathrm{H\,m^{-1}}$ being the *vacuum permeability* (also previously known as *magnetic constant*; however after a revision of the SI system in 2018 the quantity has to be specified experimentally [26]). The magnetization is proportional to the magnetic field such that

$$\mathbf{M} = \chi_m \mathbf{H} \,. \tag{3.31}$$

The dimensionless factor of proportionality χ_m is called the *magnetic susceptibility* and with it (3.30) can be rewritten as

$$\mathbf{B} = \boldsymbol{\mu}_0 (1 + \chi_m) \mathbf{H} \,, \tag{3.32}$$

leading to the definition of *relative permeability* and (total) *permeability*,

$$\boldsymbol{\mu}_r \coloneqq 1 + \chi_m \quad \text{and} \quad \boldsymbol{\mu} \coloneqq \boldsymbol{\mu}_0 \boldsymbol{\mu}_r \,. \tag{3.33}$$

Just like the susceptibility, the relative permeability is a dimensionless and material-dependent parameter describing its magnetic qualities in relation to the free space case. For magnetically isotropic substances it is given as a single scalar value whereas for anisotropic ones it takes the form of a second rank diagonal tensor. To combine both cases, the permeability in this work is generally defined as a map to the space of symmetric $d \times d$-matrices; for isotropic materials simply mapping to a multiple of the identity matrix. Permeabilities take positive values naturally, while negative ones are only reachable through metamaterials.

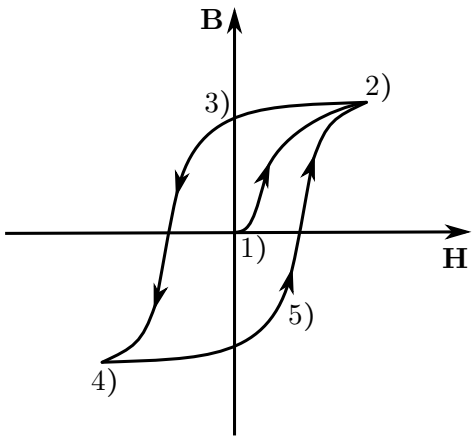

Fig. 3.5: Typical hysteresis curve for ferromagnetic materials: the material initially does not exhibit any inductive effects (1) until affected by an outer magnetic field to the point of saturation (2). When leaving the magnetic field afterwards, the material remains magnetized; this is called *remanence* (3). The same effect can be observed when exposing the material to a magnetic field of opposite polarization (4), creating the characteristic hysteresis loop (5).

elasticity		magnetism	
displacement	$\mathbf{u}(\mathbf{x})$	scalar potential	$\psi(\mathbf{x})$
stiffness	$\mathbf{C}(\mathbf{x})$	permeability	$\boldsymbol{\mu}(\mathbf{x})$
strain tensor	$\boldsymbol{\varepsilon}(\mathbf{u}(\mathbf{x})) = \nabla_{\mathrm{sym}}\mathbf{u}(\mathbf{x})$	magnetic field	$\mathbf{H}(\psi(\mathbf{x})) = -\nabla\psi(\mathbf{x})$
stress tensor	$\boldsymbol{\sigma}(\mathbf{x}) = \mathbf{C}(\mathbf{x})\boldsymbol{\varepsilon}(\mathbf{u}(\mathbf{x}))$	magnetic induction	$\mathbf{B}(\mathbf{x}) = \boldsymbol{\mu}(\mathbf{x})\mathbf{H}(\psi(\mathbf{x}))$

Tab. 3.3: Overview of important elastic and magnetic quantities and their analogies

It should be noted that the linear relation between magnetic field and induction given in (3.32) actually does not hold for ferromagnetic materials due to *hysteresis* effects [56]. Hysteresis describes the phenomenon in which a body's magnetic response does not only depend on the current exterior field it is positioned in but its previous history as well, resulting in a non-linear constitutive equation. A typical hysteresis curve is depicted in Fig. 3.5.

For the model problem used throughout this thesis, one should be aware of certain analogies between the elastic and the magnetic quantities. An overview of them is given in Table 3.3.

3.2 Strong and Weak Form of the Problem

The model presented within this thesis that will be used for further analysis in homogenization theory and spectral numerical methods is largely based on the work of Harutyunyan [49, 50]. Aside from smaller changes in its derivation, the model now allows for spatially non-constant material tensors and is extended to include volume forces and hypothetical magnetic monopoles as right-hand sides; more on that later. The following assumptions are made:

- only small deformations are considered
- no hysteresis is taken into account

- elastic and magnetic effects are linearly coupled
- the system is closed — no energy is lost or gained
- a quasi-static approach is used allowing for a time independent problem

In accordance with the third item one introduces the coupling tensor

$$\underline{\mathbf{e}} : \Omega \to \mathbb{R}^{d\times d\times d}_{\mathrm{sym}} \tag{3.34}$$

mapping onto the space of rank three tensors with the symmetries defined in (3.2). Its Mandel notation is given by $\mathbf{e} \coloneqq \mathcal{M}_3^d \circ \underline{\mathbf{e}}$. From now on the spatial dependence of all previously introduced quantities on $\mathbf{x}$ will be omitted to shorten equations and to ease the readability.

Let $\Omega \subset \mathbb{R}^d$ be a bounded domain with (piecewise) Lipschitz-continuous boundary $\partial\Omega$. Additionally, let the functional domain of all relevant quantities be extended to $\bar{\Omega}$. To prescribe boundary conditions one defines

$$\Lambda_{\mathrm{D}}^{\mathrm{mech}}, \Lambda_{\mathrm{N}}^{\mathrm{mech}} \subset \partial\Omega\,, \quad \text{s.t.} \quad \Lambda_{\mathrm{D}}^{\mathrm{mech}} \cap \Lambda_{\mathrm{N}}^{\mathrm{mech}} = \varnothing\,, \quad \overline{\Lambda_{\mathrm{D}}^{\mathrm{mech}}} \cup \overline{\Lambda_{\mathrm{N}}^{\mathrm{mech}}} = \partial\Omega\,, \tag{3.35}$$

$$\Lambda_{\mathrm{D}}^{\mathrm{mag}}, \Lambda_{\mathrm{N}}^{\mathrm{mag}} \subset \partial\Omega\,, \quad \text{s.t.} \quad \Lambda_{\mathrm{D}}^{\mathrm{mag}} \cap \Lambda_{\mathrm{N}}^{\mathrm{mag}} = \varnothing\,, \quad \overline{\Lambda_{\mathrm{D}}^{\mathrm{mag}}} \cup \overline{\Lambda_{\mathrm{N}}^{\mathrm{mag}}} = \partial\Omega\,, \tag{3.36}$$

for the mechanical and magnetic quantities separately. One assumes *homogeneous Dirichlet boundary conditions*

$$\mathbf{u}\big|_{\Lambda_{\mathrm{D}}^{\mathrm{mech}}} \equiv 0 \qquad \text{and} \qquad \psi\big|_{\Lambda_{\mathrm{D}}^{\mathrm{mag}}} \equiv 0 \tag{3.37}$$

and furthermore *Neumann boundary conditions*

$$\langle \boldsymbol{\sigma}, \mathbf{n}\rangle_{\mathcal{M}}\big|_{\Lambda_{\mathrm{N}}^{\mathrm{mech}}} \equiv \tilde{\boldsymbol{\sigma}} \qquad \text{and} \qquad \langle \mathbf{B}, \mathbf{n}\rangle\big|_{\Lambda_{\mathrm{N}}^{\mathrm{mag}}} \equiv -\tilde{\mathbf{B}} \tag{3.38}$$

where $\mathbf{n}$ denotes the outer normal vector and $\tilde{\boldsymbol{\sigma}} : \Lambda_{\mathrm{N}}^{\mathrm{mech}} \to \mathbb{R}^d$ as well as $\tilde{\mathbf{B}} : \Lambda_{\mathrm{N}}^{\mathrm{mag}} \to \mathbb{R}$ are prescribed surface stresses and (fictitious) magnetic charges respectively. The inner product between $\boldsymbol{\sigma}$ and $\mathbf{n}$ is to be understood as the matrix–vector product $\langle \boldsymbol{\sigma}, \mathbf{n}\rangle_{\mathcal{M}} \coloneqq \underline{\boldsymbol{\sigma}}\mathbf{n}$ as indicated by the $\mathcal{M}$-subscript.

The linearly coupled *constitutive equations* read

$$\left.\begin{aligned} \boldsymbol{\sigma}(\mathbf{u},\psi) &= \mathbf{C}\,\boldsymbol{\varepsilon}(\mathbf{u}) - \mathbf{e}\,\mathbf{H}(\psi) \\ \mathbf{B}(\mathbf{u},\psi) &= \mathbf{e}^{\mathrm{T}}\,\boldsymbol{\varepsilon}(\mathbf{u}) + \boldsymbol{\mu}\,\mathbf{H}(\psi) \end{aligned}\right\} \forall\, \mathbf{x} \in \Omega \tag{3.39}$$

where the stress and the induction now each depend on both the displacement field and the scalar potential. In reality the material tensors $\mathbf{C}$ and $\mathbf{H}$ would also change according to the alterations of mechanical and magnetic fields, greatly enhancing the complexity of the model. Since only small field changes with small influences on the materials behavior are considered, these tensors are here assumed to stay approximately constant in each point. To derive a set of partial differential equations, an energy minimization principle is applied to a *Lagrangian energy functional* of the magneto-elastic system. Let functions $\mathbf{f}^{\mathrm{mech}} : \Omega \to \mathbb{R}^d$ and $\mathrm{f}^{\mathrm{mag}} : \Omega \to \mathbb{R}$ assign a volume force density and magnetic free charges to the domain Ω. While no evidence for the existence of magnetic monopoles was found so far, the hypothetical concept has gained interest in particle theories such as the grand unified theory of Pati and Salam [97] and might be of future interest [25]. The Lagrangian can then be chosen as the difference between mechanical and magnetic energy

$$\mathcal{L}(\mathbf{u},\psi) \coloneqq W_{\mathrm{mech}}(\mathbf{u},\psi) - W_{\mathrm{mag}}(\mathbf{u},\psi) \tag{3.40}$$

with the energy terms consisting of the respective internal energies, externally opposing ones and surface terms, thus

$$W_{\mathrm{mech}}(\mathbf{u},\psi) = \frac{1}{2}\int_{\Omega} \langle \boldsymbol{\sigma}(\mathbf{u},\psi), \boldsymbol{\varepsilon}(\mathbf{u})\rangle \,\mathrm{d}\mathbf{x} - \int_{\Omega} \left\langle \mathbf{u}, \mathbf{f}^{\mathrm{mech}}\right\rangle \mathrm{d}\mathbf{x} - \int_{\Lambda_{\mathrm{N}}^{\mathrm{mech}}} \langle \mathbf{u}, \tilde{\boldsymbol{\sigma}}\rangle \,\mathrm{ds}\,, \tag{3.41}$$

$$W_{\mathrm{mag}}(\mathbf{u},\psi) = \frac{1}{2}\int_{\Omega} \langle \mathbf{H}(\psi), \mathbf{B}(\mathbf{u},\psi)\rangle \,\mathrm{d}\mathbf{x} - \int_{\Omega} \psi\, \mathrm{f}^{\mathrm{mag}} \,\mathrm{d}\mathbf{x} - \int_{\Lambda_{\mathrm{N}}^{\mathrm{mag}}} \psi\, \tilde{\mathbf{B}} \,\mathrm{ds}\,. \tag{3.42}$$

Remark. *At this point the attentive reader might wonder about the choice of signs in* (3.38)–(3.40)*. All of them stem from certain sign conventions in physics and might actually be chosen otherwise as long as they are consistently used afterwards. The minus sign for the magnetic surface charges in* (3.38) *ensures that positive values of* $\tilde{B}$ *relate to positive charges. As it will be seen later, the sign is derived naturally from the variational principle. The different signs in* (3.39) *are due to the choice of* $\boldsymbol{\varepsilon}$ *and* $\mathbf{H}$ *as the independent variables of the system, whereas the IEEE standard defines the constitutive equations with all positive signs for the choice of* σ *and* $\mathbf{H}$ *instead [53]. Finally, the Lagrangian* (3.40) *being not the sum but the difference of mechanical and magnetic energy is indicative of the energy–coenergy–principle for conservative systems [27, 79]. For further details on these conventions and some of the derivations, the interested reader is again referred to [49].*

The minimizer of (3.40) is found through a variational approach. Let $\mathbf{v} \in \mathcal{C}^1\left(\Omega, \mathbb{R}^d\right) \cap \mathcal{C}^0\left(\bar{\Omega}, \mathbb{R}^d\right)$ and $\phi \in \mathcal{C}^1(\Omega, \mathbb{R}) \cap \mathcal{C}^0\left(\bar{\Omega}, \mathbb{R}\right)$ be vector- and scalar-valued test functions with the same restrictions on the Dirichlet boundary given in (3.37). For parameters $\theta_{\mathbf{v}}, \theta_{\phi} \in \mathbb{R}$ one sets up the variational functional

$$J(\theta_{\mathbf{v}}, \theta_{\phi}) = W_{\mathrm{mech}}(\mathbf{u} + \theta_{\mathbf{v}}\,\mathbf{v}, \psi + \theta_{\phi}\,\phi) - W_{\mathrm{mag}}(\mathbf{u} + \theta_{\mathbf{v}}\,\mathbf{v}, \psi + \theta_{\phi}\,\phi) \tag{3.43}$$

and sets $\nabla J(0,0) = 0$. In full the functional reads

$$\begin{aligned} J(\theta_{\mathbf{v}}, \theta_{\phi}) \;=\; & \frac{1}{2}\int_{\Omega} \left(\boldsymbol{\varepsilon}(\mathbf{u}) + \theta_{\mathbf{v}}\,\boldsymbol{\varepsilon}(\mathbf{v})\right)^{\mathrm{T}} \left(\mathbf{C}\left(\boldsymbol{\varepsilon}(\mathbf{u}) + \theta_{\mathbf{v}}\,\boldsymbol{\varepsilon}(\mathbf{v})\right) - \mathbf{e}\left(\mathbf{H}(\psi) + \theta_{\phi}\,\mathbf{H}(\phi)\right)\right) \mathrm{d}\mathbf{x} \\ & - \frac{1}{2}\int_{\Omega} \left(\mathbf{H}(\psi) + \theta_{\phi}\,\mathbf{H}(\phi)\right)^{\mathrm{T}} \left(\mathbf{e}^{\mathrm{T}}\left(\boldsymbol{\varepsilon}(\mathbf{u}) + \theta_{\mathbf{v}}\,\boldsymbol{\varepsilon}(\mathbf{v})\right) + \boldsymbol{\mu}\left(\mathbf{H}(\psi) + \theta_{\phi}\,\mathbf{H}(\phi)\right)\right) \mathrm{d}\mathbf{x} \\ & - \int_{\Omega} \left\langle \mathbf{u} + \theta_{\mathbf{v}}\,\mathbf{v}, \mathbf{f}^{\mathrm{mech}}\right\rangle \mathrm{d}\mathbf{x} - \int_{\Lambda_{\mathrm{N}}^{\mathrm{mech}}} \langle \mathbf{u} + \theta_{\mathbf{v}}\,\mathbf{v}, \tilde{\boldsymbol{\sigma}}\rangle \,\mathrm{ds} \\ & + \int_{\Omega} (\psi + \theta_{\phi}\,\phi)\, \mathrm{f}^{\mathrm{mag}} \,\mathrm{d}\mathbf{x} + \int_{\Lambda_{\mathrm{N}}^{\mathrm{mag}}} (\psi + \theta_{\phi}\,\phi)\, \tilde{\mathbf{B}} \,\mathrm{ds} \end{aligned} \tag{3.44}$$

and its derivatives are computed as

$$\begin{aligned} \frac{\partial J}{\partial \theta_{\mathbf{v}}}(\theta_{\mathbf{v}}, \theta_{\phi}) \;=\; & \int_{\Omega} \left(\boldsymbol{\varepsilon}(\mathbf{v})\right)^{\mathrm{T}} \left(\mathbf{C}\left(\boldsymbol{\varepsilon}(\mathbf{u}) + \theta_{\mathbf{v}}\,\boldsymbol{\varepsilon}(\mathbf{v})\right) - \mathbf{e}\left(\mathbf{H}(\psi) + \theta_{\phi}\,\mathbf{H}(\phi)\right)\right) \mathrm{d}\mathbf{x} \\ & - \int_{\Omega} \left\langle \mathbf{v}, \mathbf{f}^{\mathrm{mech}}\right\rangle \mathrm{d}\mathbf{x} - \int_{\Lambda_{\mathrm{N}}^{\mathrm{mech}}} \langle \mathbf{v}, \tilde{\boldsymbol{\sigma}}\rangle \,\mathrm{ds} \end{aligned} \tag{3.45}$$

and

$$\begin{aligned} \frac{\partial J}{\partial \theta_{\phi}}(\theta_{\mathbf{v}}, \theta_{\phi}) \;=\; & -\int_{\Omega} \left(\mathbf{H}(\phi)\right)^{\mathrm{T}} \left(\mathbf{e}^{\mathrm{T}}\left(\boldsymbol{\varepsilon}(\mathbf{u}) + \theta_{\mathbf{v}}\,\boldsymbol{\varepsilon}(\mathbf{v})\right) + \boldsymbol{\mu}\left(\mathbf{H}(\psi) + \theta_{\phi}\,\mathbf{H}(\phi)\right)\right) \mathrm{d}\mathbf{x} \\ & + \int_{\Omega} \phi\, \mathrm{f}^{\mathrm{mag}} \,\mathrm{d}\mathbf{x} + \int_{\Lambda_{\mathrm{N}}^{\mathrm{mag}}} \phi\, \tilde{\mathbf{B}} \,\mathrm{ds} \end{aligned} \tag{3.46}$$

where the symmetry of the material tensors was taken into account. Evaluating these expressions for $\theta_{\mathbf{v}} = \theta_{\phi} = 0$, setting them equal to zero and integrating by parts yields

$$\begin{aligned} 0 &= \int_{\Omega} \mathbf{v}^{\mathrm{T}} \left(\mathbf{div} \left(\mathbf{C}\, \boldsymbol{\varepsilon}(\mathbf{u}) - \mathbf{e}\, \mathbf{H}(\psi) \right) + \mathbf{f}^{\mathrm{mech}} \right) \mathrm{d}\mathbf{x} \\ &\quad - \int_{\Lambda_{\mathrm{N}}^{\mathrm{mech}}} \mathbf{v}^{\mathrm{T}} \left(\langle \mathbf{C}\, \boldsymbol{\varepsilon}(\mathbf{u}) - \mathbf{e}\, \mathbf{H}(\psi), \mathbf{n} \rangle_{\mathcal{M}} - \tilde{\boldsymbol{\sigma}} \right) \mathrm{ds} \end{aligned} \tag{3.47}$$

for (3.45) where the boldface operator $\mathbf{div} \coloneqq \mathrm{div} \circ \left(\mathcal{M}_2^d \right)^{-1}$ is not to be confused with the regular divergence of a vector field but denotes the column-wise divergences of the underlying rank two tensor instead and

$$\begin{aligned} 0 &= \int_{\Omega} \phi \left(\mathrm{div} \left(\mathbf{e}^{\mathrm{T}}\, \boldsymbol{\varepsilon}(\mathbf{u}) + \boldsymbol{\mu}\, \mathbf{H}(\psi) \right) - \mathrm{f}^{\mathrm{mag}} \right) \mathrm{d}\mathbf{x} \\ &\quad - \int_{\Lambda_{\mathrm{N}}^{\mathrm{mag}}} \phi \left(\left\langle \mathbf{e}^{\mathrm{T}}\, \boldsymbol{\varepsilon}(\mathbf{u}) + \boldsymbol{\mu}\, \mathbf{H}(\psi), \mathbf{n} \right\rangle + \tilde{\mathbf{B}} \right) \mathrm{ds} \end{aligned} \tag{3.48}$$

for (3.46). The boundary integrals of (3.47) and (3.48) vanish due to the Neumann boundary conditions (3.38). Due to the fundamental lemma of calculus of variations (e.g. in [42, p. 9]), this leads to the strong form of the model problem.

Problem 1 (Strong form of magneto-elastic coupling)**.** *Let the domain and the material tensors be defined as before. Assume the material tensors to be sufficiently smooth. Find* $(\mathbf{u}, \psi) \in \left(\mathcal{C}^2\left(\Omega, \mathbb{R}^d\right) \cap \mathcal{C}^0\left(\bar{\Omega}, \mathbb{R}^d\right) \right) \times \left(\mathcal{C}^2(\Omega, \mathbb{R}) \cap \mathcal{C}^0\left(\bar{\Omega}, \mathbb{R}\right) \right)$ *such that*

$$\begin{aligned} \mathbf{div} \left(\mathbf{C}\, \boldsymbol{\varepsilon}(\mathbf{u}) - \mathbf{e}\, \mathbf{H}(\psi) \right) &= -\mathbf{f}^{\mathrm{mech}} && \text{in } \Omega\,, \\ \mathrm{div} \left(\mathbf{e}^{\mathrm{T}}\, \boldsymbol{\varepsilon}(\mathbf{u}) + \boldsymbol{\mu}\, \mathbf{H}(\psi) \right) &= \mathrm{f}^{\mathrm{mag}} && \text{in } \Omega\,, \end{aligned}$$

with Dirichlet boundary conditions

$$\mathbf{u}\big|_{\Lambda_{\mathrm{D}}^{\mathrm{mech}}} \equiv 0\,, \qquad \psi\big|_{\Lambda_{\mathrm{D}}^{\mathrm{mag}}} \equiv 0\,,$$

and Neumann boundary conditions

$$\begin{aligned} \langle \mathbf{C}\, \boldsymbol{\varepsilon}(\mathbf{u}) - \mathbf{e}\, \mathbf{H}(\psi), \mathbf{n} \rangle_{\mathcal{M}} \big|_{\Lambda_{\mathrm{N}}^{\mathrm{mech}}} &\equiv \tilde{\boldsymbol{\sigma}}\,, \\ \left\langle \mathbf{e}^{\mathrm{T}}\, \boldsymbol{\varepsilon}(\mathbf{u}) + \boldsymbol{\mu}\, \mathbf{H}(\psi), \mathbf{n} \right\rangle \big|_{\Lambda_{\mathrm{N}}^{\mathrm{mag}}} &\equiv -\tilde{\mathbf{B}}\,, \end{aligned}$$

being fulfilled.

The differential equations derived this way actually coincide with the *equation of motion* from Newtonian mechanics and *Gauss's law for magnetism* from the Maxwell equations as one would expect.

However, since the objects of interest considered here are composite materials, one can not expect the material tensors to be smooth enough to allow for strong solutions. Therefore, one has to resort to the *weak form* of the model problem which can be embedded into the *Lax–Milgram framework* for further analysis. To this end, define the Sobolev spaces

$$\mathcal{H}^1_{\mathrm{mech}} \coloneqq \left\{ \mathbf{u} \in \mathcal{H}^1\left(\Omega, \mathbb{R}^d\right) \,:\, \mathbf{u}\big|_{\Lambda_{\mathrm{D}}^{\mathrm{mech}}} \equiv 0 \right\}, \tag{3.49}$$

$$\mathcal{H}^1_{\mathrm{mag}} \coloneqq \left\{ \psi \in \mathcal{H}^1(\Omega, \mathbb{R}) \,:\, \psi\big|_{\Lambda_{\mathrm{D}}^{\mathrm{mag}}} \equiv 0 \right\} \tag{3.50}$$

where the restrictions on the boundary have to be understand in the sense of the *trace mapping theorem*. The theorem is repeated below as a reminder.

Theorem 3.2.1 (Trace mapping theorem; Proof in [12, p. 45 sq.]). *Let Ω be a bounded domain with piecewise continuous boundary $\partial\Omega$. Furthermore, it should fulfill a cone condition. Then there exists a unique linear and continuous mapping $\mathrm{tr} : \mathcal{H}^1(\Omega) \to L^2(\partial\Omega)$ such that $\mathrm{tr}(f) = f\big|_{\partial\Omega}$ for all $f \in \mathcal{C}^1(\bar{\Omega})$.*

The weak form can then be stated by defining the bilinear forms

$$a^{\mathrm{mech}} : \mathcal{H}^1_{\mathrm{mech}} \times \mathcal{H}^1_{\mathrm{mech}} \to \mathbb{R}\,, \qquad a^{\mathrm{mech}}(\mathbf{u},\mathbf{v}) = \int_\Omega (\boldsymbol{\varepsilon}(\mathbf{v}))^{\mathrm{T}}\, \mathbf{C}\, \boldsymbol{\varepsilon}(\mathbf{u})\ \mathrm{d}\mathbf{x}\,, \tag{3.51}$$

$$a^{\mathrm{mag}} : \mathcal{H}^1_{\mathrm{mag}} \times \mathcal{H}^1_{\mathrm{mag}} \to \mathbb{R}\,, \qquad a^{\mathrm{mag}}(\psi,\phi) = \int_\Omega (\mathbf{H}(\phi))^{\mathrm{T}}\, \boldsymbol{\mu}\, \mathbf{H}(\psi)\ \mathrm{d}\mathbf{x}\,, \tag{3.52}$$

$$a^{\mathrm{mix}} : \mathcal{H}^1_{\mathrm{mech}} \times \mathcal{H}^1_{\mathrm{mag}} \to \mathbb{R}\,, \qquad a^{\mathrm{mix}}(\mathbf{v},\phi) = \int_\Omega (\boldsymbol{\varepsilon}(\mathbf{v}))^{\mathrm{T}}\, \mathbf{e}\, \mathbf{H}(\phi)\ \mathrm{d}\mathbf{x} \tag{3.53}$$

and the linear functionals

$$l^{\mathrm{mech}} : \mathcal{H}^1_{\mathrm{mech}} \to \mathbb{R}\,, \qquad l^{\mathrm{mech}}(\mathbf{v}) = \int_\Omega \mathbf{v}^{\mathrm{T}}\, \mathbf{f}^{\mathrm{mech}}\ \mathrm{d}\mathbf{x} + \int_{\Lambda_{\mathrm{N}}^{\mathrm{mech}}} \mathbf{v}^{\mathrm{T}}\, \tilde{\boldsymbol{\sigma}}\ \mathrm{ds}\,, \tag{3.54}$$

$$l^{\mathrm{mag}} : \mathcal{H}^1_{\mathrm{mag}} \to \mathbb{R}\,, \qquad l^{\mathrm{mag}}(\phi) = \int_\Omega \phi\, \mathrm{f}^{\mathrm{mag}}\ \mathrm{d}\mathbf{x} + \int_{\Lambda_{\mathrm{N}}^{\mathrm{mag}}} \phi\, \tilde{\mathbf{B}}\ \mathrm{ds}\,. \tag{3.55}$$

Problem 2 (Weak form of magneto-elastic coupling). *Find $(\mathbf{u},\psi) \in \mathcal{H}^1_{\mathrm{mech}} \times \mathcal{H}^1_{\mathrm{mag}}$ such that using the notations from* (3.49)–(3.55) *the equations*

$$\begin{aligned} a^{\mathrm{mech}}(\mathbf{u},\mathbf{v}) - a^{\mathrm{mix}}(\mathbf{v},\psi) &= l^{\mathrm{mech}}(\mathbf{v}) \\ a^{\mathrm{mix}}(\mathbf{u},\phi) + a^{\mathrm{mag}}(\psi,\phi) &= l^{\mathrm{mag}}(\phi) \end{aligned}$$

are fulfilled for all pairs $(\mathbf{v},\phi) \in \mathcal{H}^1_{\mathrm{mech}} \times \mathcal{H}^1_{\mathrm{mag}}$.

In the upcoming discussion about the solution's existence and uniqueness of Problem 2, another formulation proves itself to be slightly more convenient. To this end set $\mathcal{H}^1_{\mathrm{mix}} := \mathcal{H}^1_{\mathrm{mech}} \times \mathcal{H}^1_{\mathrm{mag}}$. Note that $\mathcal{H}^1_{\mathrm{mix}}$ is again a Hilbert space with the inner product

$$\langle (\mathbf{u},\psi), (\mathbf{v},\phi) \rangle_{\mathcal{H}^1_{\mathrm{mix}}} := \langle \mathbf{u},\mathbf{v} \rangle_{\mathcal{H}^1} + \langle \psi,\phi \rangle_{\mathcal{H}^1} \tag{3.56}$$

and the induced norm

$$\|(\mathbf{u},\psi)\|_{\mathcal{H}^1_{\mathrm{mix}}} := \left(\|\mathbf{u}\|^2_{\mathcal{H}^1} + \|\psi\|^2_{\mathcal{H}^1} \right)^{1/2}\,. \tag{3.57}$$

This gives way to the combined bilinear form

$$a : \mathcal{H}^1_{\mathrm{mix}} \times \mathcal{H}^1_{\mathrm{mix}} \to \mathbb{R}\,, \quad a((\mathbf{u},\psi),(\mathbf{v},\phi)) = a^{\mathrm{mech}}(\mathbf{u},\mathbf{v}) - a^{\mathrm{mix}}(\mathbf{v},\psi) + a^{\mathrm{mix}}(\mathbf{u},\phi) + a^{\mathrm{mag}}(\psi,\phi) \tag{3.58}$$

and the combined linear functional

$$l : \mathcal{H}^1_{\mathrm{mix}} \to \mathbb{R}\,, \quad l(\mathbf{v},\phi) = l^{\mathrm{mech}}(\mathbf{v}) + l^{\mathrm{mag}}(\phi) \tag{3.59}$$

such that the single equation $a((\mathbf{u},\psi),(\mathbf{v},\phi)) = l(\mathbf{v},\phi)$ can be used instead in Problem 2.

3.3 Existence and Uniqueness of the Solution

As stated before the key to prove the existence as well as the uniqueness of the weak form's solution is given in form of the Lax–Milgram theorem further below. In preparation for that, some properties of bilinear forms are recalled here.

Definition 3.3.1. *Let $\mathcal{H}$ be a Hilbert space and let $a : \mathcal{H} \times \mathcal{H} \to \mathbb{R}$ be a bilinear form. One calls the bilinear form ...*

- *... symmetric, if $a(f,g) = a(g,f)$ for all $f, g \in \mathcal{H}$,*
- *... coercive, if $a(f,f) \geq \gamma \|f\|_{\mathcal{H}}^2$ for all $f \in \mathcal{H}$,*
- *... continuous, if $|a(f,g)| \leq C \|f\|_{\mathcal{H}} \|g\|_{\mathcal{H}}$ for all $f, g \in \mathcal{H}$,*

where $0 < \gamma \leq C < \infty$.

Theorem 3.3.2 (Lax–Milgram; Proof in [16, p. 62 sq.])**.** *Let $\mathcal{H}$ be a Hilbert space. Let $a : \mathcal{H} \times \mathcal{H} \to \mathbb{R}$ be a coercive and continuous bilinear form and let $l : \mathcal{H} \to \mathbb{R}$ be a continuous linear functional. Then there exists a unique element $f \in \mathcal{H}$ such that*

$$a(f,g) = l(g) \text{ for all } g \in \mathcal{H} \ .$$

Moreover, the estimate $\|f\|_{\mathcal{H}} \leq \frac{1}{\gamma} \|l\|_{\mathcal{H}'}$ holds true, where γ is the coercivity constant of the bilinear form and

$$\|\cdot\|_{\mathcal{H}'} \coloneqq \sup_{\substack{h \in \mathcal{H} \\ h \neq 0}} \frac{|l(h)|}{\|h\|_{\mathcal{H}}}$$

denotes the norm of the dual space of $\mathcal{H}$.

To meet the requirements for the Lax–Milgram theorem, a few additional assumptions have to be made. First, the material tensor mappings should be essentially bounded from above. Namely one has

$$\mathbf{C} \in L^\infty\left(\Omega, \mathbb{R}^{\tilde{d}\times\tilde{d}}_{\mathrm{sym}}\right) , \quad \mathbf{e} \in L^\infty\left(\Omega, \mathbb{R}^{\tilde{d}\times d}\right) , \quad \boldsymbol{\mu} \in L^\infty\left(\Omega, \mathbb{R}^{d\times d}_{\mathrm{sym}}\right) . \tag{3.60}$$

Second, the stiffness and permeability tensors have to fulfill an ellipticity condition, so that there exist $\gamma_{\mathbf{C}}, \gamma_{\boldsymbol{\mu}} > 0$ such that

$$\begin{aligned} \operatorname*{ess\,inf}_{\mathbf{x}\in\Omega} \left(\mathbf{a}^{\mathrm{T}} \mathbf{C}(\mathbf{x}) \mathbf{a}\right) &\geq \gamma_{\mathbf{C}} \|\mathbf{a}\|^2 \quad \text{for all } \mathbf{a} \in \mathbb{R}^{\tilde{d}} , \\ \operatorname*{ess\,inf}_{\mathbf{x}\in\Omega} \left(\mathbf{b}^{\mathrm{T}} \boldsymbol{\mu}(\mathbf{x}) \mathbf{b}\right) &\geq \gamma_{\boldsymbol{\mu}} \|\mathbf{b}\|^2 \quad \text{for all } \mathbf{b} \in \mathbb{R}^{d} . \end{aligned} \tag{3.61}$$

In practice, composite materials consist of a finite number of different phases. Their material tensors can therefore be modeled as piecewise constant functions, thus being of L^∞-type. Furthermore, evaluated stiffness and permeability tensors can be considered as not only symmetric but also positive definite quantities, since their eigenvalues are greater than zero, if parameters such as the Lamé constants are positive which is mostly the case for naturally arising substances as stated before in Subsects. 3.1.2 and 3.1.3. Then having an orthonormal basis of eigenvectors available, it is easy to check that (3.61) holds true in the case of such symmetric, positive definite, piecewise constant material tensors. To generalize for an infinite number of phases or the rare cases in which negative

parameters — and as a resulting consequence negative eigenvalues — might occur, it was decided here to state the necessary conditions (3.60) and (3.61) explicitly.

Additionally, the following paragraphs are restricted to the case of only Dirichlet boundary conditions which will already show all of the needed main techniques in this setting. Pure Neumann conditions or mixed boundary conditions use the same principles for the most part but differ in some details, further complicating the upcoming analysis. To read more about that topic, the interested reader is referred to [16, Chap. 5].

The next few pages will collect the necessary requirements for the Lax–Milgram theorem to hold true in form of three lemmas, each one with its own separate proof and therein applied theorems. Instead of sticking to the original system presented in Problem 2, the combined bilinear form a from (3.58) and the combined functional l from (3.59) simplify this process. The first property to be checked is the coercivity of the bilinear forms.

Lemma 3.3.3. *Let the stiffness and permeability tensors fulfill the ellipticity condition* (3.61)*. Then the bilinear forms* a^{mech} *and* a^{mag} *defined in* (3.51) *and* (3.52) *are coercive. Furthermore, the combined bilinear form* a *in* (3.58) *is then also coercive.*

The proof mainly revolves around two famous inequalities. The central estimate for a^{mech} is given by one of *Korn's inequalities*, while the *Poincaré inequality* takes care of a^{mag}.

Lemma 3.3.4 (Korn's inequality; Proof in [12, p. 295])**.** *Let* $\Omega \subset \mathbb{R}^3$ *be an open, bounded set with piecewise smooth boundary* $\partial\Omega$*. Also let* $\Lambda_{\mathrm{D}}^{\mathrm{mech}} \subset \partial\Omega$ *have a positive 2-dimensional measure. Then there exists a positive constant* $c \coloneqq c\left(\Omega, \Lambda_{\mathrm{D}}^{\mathrm{mech}}\right)$ *such that*

$$\int_{\Omega} \|\boldsymbol{\varepsilon}(\mathbf{v})\|^2 \, \mathrm{d}\mathbf{x} \geq c \|\mathbf{v}\|_{\mathcal{H}^1}^2 \text{ for all } \mathbf{v} \in \mathcal{H}_{\mathrm{mech}}^1 \ .$$

Theorem 3.3.5 (Poincaré inequality; Proof in [115, p. 246 sq.])**.** *Let* $\Omega \subset \mathbb{R}^d$ *be bounded. Then there exists a positive constant* $\tilde{c} \coloneqq \tilde{c}(\Omega)$ *such that*

$$\|f\|_{L^2} \leq \tilde{c} \|\nabla f\|_{L^2} \text{ for all } f \in \mathcal{H}_0^1(\Omega, \mathbb{R}) \coloneqq \left\{ f \in \mathcal{H}^1(\Omega, \mathbb{R}) \ : \ \mathrm{tr}(f) = 0 \right\} \ .$$

A direct corollary from Poincaré's inequality states an estimate for the $\mathcal{H}^1$-norm of f.

Corollary 3.3.6. *Let* $\Omega \subset \mathbb{R}^d$ *be bounded and let* $\tilde{c}$ *denote the constant from Theorem 3.3.5. Then*

$$\|\nabla f\|_{L^2}^2 \geq \frac{1}{1+\tilde{c}^2} \|f\|_{\mathcal{H}^1}^2 \text{ for all } f \in \mathcal{H}_0^1 \ .$$

Proof. Writing the $\mathcal{H}^1$-norm of f in terms of L^2-norms and applying Poincaré's inequality directly yields

$$\|f\|_{\mathcal{H}^1}^2 = \|f\|_{L^2}^2 + \|\nabla f\|_{L^2}^2 \leq \left(1+\tilde{c}^2\right) \|\nabla f\|_{L^2}^2 \ .$$

Division by the constant term gives the result. □

With these tools at hand, the proof for Lemma 3.3.3 can now be given.

Proof of 3.3.3. The coercivity of a^{mech} now follows directly from the stiffness tensor's ellipticity condition and Korn's inequality. For all $\mathbf{u} \in \mathcal{H}^1_{\mathrm{mech}}$ one has

$$a^{\mathrm{mech}}(\mathbf{u},\mathbf{u}) = \int_\Omega (\boldsymbol{\varepsilon}(\mathbf{u}))^{\mathrm{T}} \mathbf{C}\, \boldsymbol{\varepsilon}(\mathbf{u}) \,\mathrm{d}\mathbf{x} \geq \gamma_{\mathbf{C}} \int_\Omega \|\boldsymbol{\varepsilon}(\mathbf{u})\|^2 \,\mathrm{d}\mathbf{x} \geq c\gamma_{\mathbf{C}} \|\mathbf{u}\|^2_{\mathcal{H}^1} \ .$$

Similarly, the coercivity of a^{mag} is proven using the ellipticity condition on the permeability tensor and Corollary 3.3.6. More precisely, for all $\psi \in \mathcal{H}^1_{\mathrm{mag}}$ one has

$$a^{\mathrm{mag}}(\psi,\psi) = \int_\Omega (\mathbf{H}(\psi))^{\mathrm{T}} \boldsymbol{\mu}\, \mathbf{H}(\psi) \,\mathrm{d}\mathbf{x} \geq \gamma_{\boldsymbol{\mu}} \int_\Omega \|\mathbf{H}(\psi)\|^2 \,\mathrm{d}\mathbf{x} = \gamma_{\boldsymbol{\mu}} \|\nabla\psi\|^2_{L^2} \,\mathrm{d}\mathbf{x} \geq \frac{\gamma_{\boldsymbol{\mu}}}{1+\tilde{c}^2} \|\psi\|^2_{\mathcal{H}^1} \ .$$

The coercivity of the combined bilinear form then follows as well, since

$$\begin{aligned} a((\mathbf{u},\psi),(\mathbf{u},\psi)) &= a^{\mathrm{mech}}(\mathbf{u},\mathbf{u}) + a^{\mathrm{mag}}(\psi,\psi) \\ &\geq c\gamma_{\mathbf{C}} \|\mathbf{u}\|^2_{\mathcal{H}^1} + \frac{\gamma_{\boldsymbol{\mu}}}{1+\tilde{c}^2} \|\psi\|^2_{\mathcal{H}^1} \\ &\geq \min\left\{c\gamma_{\mathbf{C}}, \frac{\gamma_{\boldsymbol{\mu}}}{1+\tilde{c}^2}\right\} \left(\|\mathbf{u}\|^2_{\mathcal{H}^1} + \|\psi\|^2_{\mathcal{H}^1}\right) \\ &= \min\left\{c\gamma_{\mathbf{C}}, \frac{\gamma_{\boldsymbol{\mu}}}{1+\tilde{c}^2}\right\} \|(\mathbf{u},\psi)\|^2_{\mathcal{H}^1_{\mathrm{mix}}} \end{aligned}$$

holds true for all $(\mathbf{u},\psi) \in \mathcal{H}^1_{\mathrm{mix}}$. □

The second lemma leading up to the central statement of this section addresses the continuity of the bilinear forms.

Lemma 3.3.7. *Let the stiffness and permeability tensors be essentially bounded as stated in* (3.60)*. Then the bilinear forms $a^{\mathrm{mech}}, a^{\mathrm{mag}}$ and a^{mix} defined in* (3.51)–(3.53) *are continuous. Furthermore, the combined bilinear form a in* (3.58) *is then also continuous.*

Just as with the coercivity, the estimates are largely based on two known statements, both dating back to mathematician Otto Hölder. The first one being *Hölder's inequality* — a fundamental result in functional analysis.

Theorem 3.3.8 (Hölder's inequality; Proof in [115, p. 22])**.** *Let $1 \leq p \leq \infty$ and choose q such that $\frac{1}{p} + \frac{1}{q} = 1$ where the notational convention $\frac{1}{\infty} = 0$ is taken into account. Let (Ω, Σ, μ) be a measure space, $f \in L^p(\Omega)$ and $g \in L^q(\Omega)$. Then $fg \in L^1(\Omega)$ and $\|fg\|_{L^1} \leq \|f\|_{L^p} \|g\|_{L^q}$.*

Another crucial inequality concerns a generalized concept of means which is referred to as *Hölder or power means*.

Definition 3.3.9. *Let $p \in \mathbb{R} \setminus \{0\}$ and let $x_1, x_2, \ldots, x_n \geq 0$ be non-negative real numbers. The Hölder or power mean of these numbers with exponent p is then defined as*

$$M_p(x_1,\ldots,x_n) \coloneqq \left(\frac{1}{n}\sum_{i=1}^n x_i^p\right)^{\frac{1}{p}} \ .$$

Theorem 3.3.10 (Generalized mean inequality; Proof in [21, Chap. III])**.** *Let $p, q \in \mathbb{R} \setminus \{0\}$ with $p < q$ and let $x_1, x_2, \ldots, x_n \geq 0$ be non-negative real numbers. Then $M_p(x_1, \ldots, x_n) \leq M_q(x_1, \ldots, x_n)$.*

Corollary 3.3.11. *Let $x_1, x_2, \ldots, x_n \geq 0$ be non-negative real numbers. Then*

$$\sum_{i=1}^{n} \sqrt{x_i} \leq \sqrt{n} \sqrt{\sum_{i=1}^{n} x_i} \, .$$

Proof. The claim follows from Theorem 3.3.10 for $p = \frac{1}{2}$ and $q = 1$, since

$$\left(\frac{1}{n} \sum_{i=1}^{n} \sqrt{x_i} \right)^2 \leq \frac{1}{n} \sum_{i=1}^{n} x_i \quad \Leftrightarrow \quad \frac{1}{n} \sum_{i=1}^{n} \sqrt{x_i} \leq \frac{1}{\sqrt{n}} \sqrt{\sum_{i=1}^{n} x_i} \quad \Leftrightarrow \quad \sum_{i=1}^{n} \sqrt{x_i} \leq \sqrt{n} \sqrt{\sum_{i=1}^{n} x_i} \, .$$

□

To treat the elastic quantities correctly one also has to pose the question of how the strain tensor being the symmetric gradient of the displacement field compares to the classic gradient. This is answered in the following lemma.

Lemma 3.3.12. *Let $\mathbf{u} : \Omega \to \mathbb{R}^d$ be a (weakly) differentiable displacement field and let the strain operator be defined as before. Then $\|\boldsymbol{\varepsilon}(\mathbf{u})\|_{L^2} \leq \|\nabla \mathbf{u}\|_{L^2}$.*

Proof. The Euclidian norms of quantities in their original and their Mandel notation are the same. Therefore, going back to the strain's tensor notation one obtains

$$\begin{aligned}
\|\boldsymbol{\varepsilon}(\mathbf{u})\|_{L^2}^2 = \|\underline{\boldsymbol{\varepsilon}}(\mathbf{u})\|_{L^2}^2 &= \sum_{i,j=1}^{d} \int_{\Omega} \left| \underline{\boldsymbol{\varepsilon}}_{ij}(\mathbf{u}) \right|^2 \mathrm{d}\mathbf{x} \\
&= \sum_{i,j=1}^{d} \int_{\Omega} \frac{1}{4} \left(\frac{\partial u_i}{\partial x_j} + \frac{\partial u_j}{\partial x_i} \right)^2 \mathrm{d}\mathbf{x} \\
&= \sum_{i,j=1}^{d} \int_{\Omega} \frac{1}{4} \left(\left(\frac{\partial u_i}{\partial x_j} \right)^2 + 2 \frac{\partial u_i}{\partial x_j} \frac{\partial u_j}{\partial x_i} + \left(\frac{\partial u_j}{\partial x_i} \right)^2 \right) \mathrm{d}\mathbf{x} \, .
\end{aligned}$$

From the second binomial formula $0 \leq (a-b)^2 = a^2 - 2ab + b^2$, one can deduce that $2ab \leq a^2 + b^2$ for all real numbers, thus leading to

$$\begin{aligned}
\|\boldsymbol{\varepsilon}(\mathbf{u})\|_{L^2}^2 &= \sum_{i,j=1}^{d} \int_{\Omega} \frac{1}{4} \left(\left(\frac{\partial u_i}{\partial x_j} \right)^2 + 2 \frac{\partial u_i}{\partial x_j} \frac{\partial u_j}{\partial x_i} + \left(\frac{\partial u_j}{\partial x_i} \right)^2 \right) \mathrm{d}\mathbf{x} \\
&\leq \sum_{i,j=1}^{d} \int_{\Omega} \frac{1}{2} \left(\left(\frac{\partial u_i}{\partial x_j} \right)^2 + \left(\frac{\partial u_j}{\partial x_i} \right)^2 \right) \mathrm{d}\mathbf{x} \\
&= \sum_{i,j=1}^{d} \int_{\Omega} \left(\frac{\partial u_i}{\partial x_j} \right)^2 \mathrm{d}\mathbf{x} = \|\nabla \mathbf{u}\|_{L^2}^2 \, .
\end{aligned}$$

Taking the square root on both sides proves the claim. □

Theorem 3.3.8, Corollary 3.3.11 and Lemma 3.3.12 now provide everything to prove the continuity of the bilinear forms as stated in Lemma 3.3.7.

Proof of 3.3.7. Only the proof for a^{mech} will be given in detail here, since the ones for a^{mag} and a^{mix} follow the same steps. For a^{mech} and $\mathbf{u}, \mathbf{v} \in \mathcal{H}^1_{\mathrm{mech}}$ one derives

$$
\begin{aligned}
\left|a^{\mathrm{mech}}(\mathbf{u},\mathbf{v})\right| &= \left|\int_\Omega (\boldsymbol{\varepsilon}(\mathbf{u}))^{\mathrm{T}}\, \mathbf{C}\, \boldsymbol{\varepsilon}(\mathbf{u})\ \mathrm{d}\mathbf{x}\right| \\
&\leq \sum_{i,j=1}^{\tilde{d}} \int_\Omega \left|\boldsymbol{\varepsilon}_i(\mathbf{u})\, \mathbf{C}_{ij}\, \boldsymbol{\varepsilon}_j(\mathbf{v})\right| \mathrm{d}\mathbf{x} \\
&\overset{3.3.8}{\leq} \sum_{i,j=1}^{\tilde{d}} \|\mathbf{C}_{ij}\|_{L^\infty} \int_\Omega \left|\boldsymbol{\varepsilon}_i(\mathbf{u})\, \boldsymbol{\varepsilon}_j(\mathbf{v})\right| \mathrm{d}\mathbf{x} \\
&\overset{3.3.8}{\leq} \|\mathbf{C}\|_{L^\infty} \left(\sum_{i=1}^{\tilde{d}} \left(\int_\Omega |\boldsymbol{\varepsilon}_i(\mathbf{u})|^2\ \mathrm{d}\mathbf{x}\right)^{\frac{1}{2}}\right)\left(\sum_{j=1}^{\tilde{d}} \left(\int_\Omega |\boldsymbol{\varepsilon}_j(\mathbf{v})|^2\ \mathrm{d}\mathbf{x}\right)^{\frac{1}{2}}\right) \\
&\overset{3.3.11}{\leq} \tilde{d}\,\|\mathbf{C}\|_{L^\infty} \left(\int_\Omega \sum_{i=1}^{\tilde{d}} |\boldsymbol{\varepsilon}_i(\mathbf{u})|^2\ \mathrm{d}\mathbf{x}\right)^{\frac{1}{2}} \left(\int_\Omega \sum_{j=1}^{\tilde{d}} |\boldsymbol{\varepsilon}_j(\mathbf{v})|^2\ \mathrm{d}\mathbf{x}\right)^{\frac{1}{2}} \\
&= \tilde{d}\,\|\mathbf{C}\|_{L^\infty} \|\boldsymbol{\varepsilon}(\mathbf{u})\|_{L^2} \|\boldsymbol{\varepsilon}(\mathbf{v})\|_{L^2} \\
&\overset{3.3.12}{\leq} \tilde{d}\,\|\mathbf{C}\|_{L^\infty} \|\nabla \mathbf{u}\|_{L^2} \|\nabla \mathbf{v}\|_{L^2} \\
&\leq \tilde{d}\,\|\mathbf{C}\|_{L^\infty} \|\mathbf{u}\|_{\mathcal{H}^1} \|\mathbf{v}\|_{\mathcal{H}^1}
\end{aligned}
$$

Now let the continuity constants for the three bilinear forms be denoted accordingly by $C_{\mathrm{mech}}, C_{\mathrm{mag}}$ and C_{mix}. Define $C_{\max}$ to be the maximum out of these three constants. The continuity of the combined bilinear form then follows as well, since

$$
\begin{aligned}
\left|a((\mathbf{u},\psi),(\mathbf{v},\phi))\right| &= \left|a^{\mathrm{mech}}(\mathbf{u},\mathbf{v}) - a^{\mathrm{mix}}(\mathbf{v},\psi) + a^{\mathrm{mix}}(\mathbf{u},\phi) + a^{\mathrm{mag}}(\psi,\phi)\right| \\
&\leq \left|a^{\mathrm{mech}}(\mathbf{u},\mathbf{v})\right| + \left|a^{\mathrm{mix}}(\mathbf{v},\psi)\right| + \left|a^{\mathrm{mix}}(\mathbf{u},\phi)\right| + \left|a^{\mathrm{mag}}(\psi,\phi)\right| \\
&\leq C_{\max}\left(\|\mathbf{u}\|_{\mathcal{H}^1}\|\mathbf{v}\|_{\mathcal{H}^1} + \|\mathbf{v}\|_{\mathcal{H}^1}\|\psi\|_{\mathcal{H}^1} + \|\mathbf{u}\|_{\mathcal{H}^1}\|\phi\|_{\mathcal{H}^1} + \|\psi\|_{\mathcal{H}^1}\|\phi\|_{\mathcal{H}^1}\right) \\
&\leq C_{\max}\left(\|\mathbf{u}\|_{\mathcal{H}^1} + \|\psi\|_{\mathcal{H}^1}\right)\left(\|\mathbf{v}\|_{\mathcal{H}^1} + \|\phi\|_{\mathcal{H}^1}\right) \\
&\overset{3.3.11}{\leq} 2C_{\max}\left(\|\mathbf{u}\|^2_{\mathcal{H}^1} + \|\psi\|^2_{\mathcal{H}^1}\right)^{\frac{1}{2}}\left(\|\mathbf{v}\|^2_{\mathcal{H}^1} + \|\phi\|^2_{\mathcal{H}^1}\right)^{\frac{1}{2}} \\
&= 2C_{\max}\|(\mathbf{u},\psi)\|_{\mathcal{H}^1}\|(\mathbf{v},\phi)\|_{\mathcal{H}^1}\ .
\end{aligned}
$$

□

Finally, the continuity of the linear functionals is also ensured for a certain class of right-hand sides.

Lemma 3.3.13. *Let* $\mathbf{f}^{\mathrm{mech}} \in L^2(\Omega, \mathbb{R}^d)$ *and* $\mathrm{f}^{\mathrm{mag}} \in L^2(\Omega, \mathbb{R})$. *Additionally* $\Lambda_{\mathrm{N}}^{\mathrm{mech}} = \Lambda_{\mathrm{N}}^{\mathrm{mag}} = \varnothing$, *i.e. only Dirichlet boundary conditions are prescribed. Then the linear functionals* l^{mech} *and* l^{mag} *defined in* (3.54) *and* (3.55) *are continuous. Furthermore, the combined linear functional* l *in* (3.59) *is then also continuous.*

Proof. Since the right-hand sides are assumed to be L^2-functions, the claim can again be proven through Hölder's inequality. For l^{mag} the continuity then follows immediately, while Corollary 3.3.11 has to be applied again in the case of l^{mech}. The combined linear functional is treated similarly to the combined bilinear form in the previous proof which the reader is kindly referred to. □

Having checked all three conditions for the Lax–Milgram theorem, this leads to the final theorem of this section collecting the before presented lemmata.

Theorem 3.3.14. *Let* (3.60) *and* (3.61)*, as well as the prerequisites of Lemma 3.3.13 hold true. Then the weak form given in Problem 2 has a unique solution* $(\mathbf{u}, \psi) \in \mathcal{H}^1_{\mathrm{mix}}$.

Proof. Lemmata 3.3.3, 3.3.7 and 3.3.13 allow for the application of the Lax–Milgram theorem 3.3.2 with the Hilbert space $\mathcal{H} = \mathcal{H}^1_{\mathrm{mix}}$, thus proving the claim. □

Remark. *As it was proven, the classical methods presented here were sufficient to show the existence of a unique solution and provide a basis for upcoming related problems. Should one go one step further and examine the solution's dependency on the right-hand side data, it would turn out that while the dependency is continuous, thus Problem 2 being well-posed, the continuity constant's magnitude is too large to predict practical outcomes in the case of small disturbances. Another way is to interpret the weak form as a saddle point problem with a perturbation term. This analysis focuses around an inf-sup condition and yields better estimates in the end. Some properties and concepts of saddle point problems are explained for example in [17]. An extended theory of this approach in the context of magneto-elastic coupling together with stability estimates can be found in [49, Chap. 3]. On another note, more specific function spaces are often needed for numerical schemes such as Finite Element Methods that ensure divergence- or curl-free functions to mimic the physical conditions accordingly. This is most apparent for the magnetic laws of the Maxwell equations. Considerations from exterior calculus can lead to the development of fitting FE-methods within a generalized framework where one famous result is given by the so-called De Rham cohomology, connecting spaces like* $\mathcal{H}_{\mathrm{div}}(\Omega)$ *and* $\mathcal{H}_{\mathrm{curl}}(\Omega)$ *together which are difficult to grasp under normal means. More on the topic of exterior calculus can for example be found in [5] with some more applications given in [104].*

4 Periodic Homogenization of the Coupled Problem

The ultimate goal of this chapter is to derive a framework which allows the simplification of the magneto-elastic problem in the sense that the impact of the composite's micro-structural features and its underlying complex geometry can be analyzed separately from the macroscopic specimen at hand while still taking these effects into account. To this end, the ideas and concepts of periodic homogenization techniques are presented which provide a large fundamental theory to justify this procedure.

In Sect. 4.1 the general idea of homogenization is outlined and a few practically reasonable approximations are discussed. Despite not being perfectly mathematically sound, a first rather intuitive approach is then shown in Sect. 4.2 which already yields the central subproblems of the chapter which are extensively researched afterwards. To overcome the shortcomings of this method, the concept of two-scale convergence is introduced to the reader in Sect. 4.3 which validates the discussed problems belated.

4.1 The Idea of Homogenization

Homogenization in the mathematical sense can be used as a rather abstract and far-reaching term that can describe a multitude of different ideas, concepts and methods usually aiming at the unification of certain structures or quantities. It is predominantly used though to refer to a way of studying partial differential equations with highly oscillating coefficients — a problem class that stems for example from the studies of composite materials and is therefore inseparably connected to the physical topics of continuum and micromechanics. On the mathematical side, these studies give rise to multiscale models and multiple-scale analysis in hope of better understanding a system's behavior [9, 38, 54]. Due to the size of this research field, the specifics of homogenization in the context of the herein shown partial differential systems will be elaborated on in this chapter with references and further reading supplies mentioned at certain times. One reference the author wishes to mention specifically in advance is the collaborative work of Doina Cioranescu and Patrizia Donato [22] which served as an inspirational idol for this chapter and which will be referenced repeatedly, collecting many different homogenization approaches together with educating examples and applications. Another important guideline for this work is provided by the compact introduction to periodic homogenization given in [3].

As stated before, one wishes to distinguish between the overarching large-scale problem with the prescribed boundary conditions on one hand and the in comparison seemingly negligible geometrical structural effects on the other, effectively separating the problem into a macro- and a micro-scale. But in reality these two worlds are still connected and — contrary to the first impression one might have — the macroscopic properties of a metamaterial can change significantly, even if the microscopic structure may not have differed as much in relation. This circumstance poses the need for models and techniques that while allowing for this separation of scales also bridge the gap between the two in

such a way that the small-scale effects can take place on the macro-level. Such an approach greatly reduces the computational cost in numerical simulations, since very fine resolutions would be needed otherwise at all times to capture these features.

The general idea in mind is to substitute the highly heterogeneous composite material with a single artificial phase that exhibits the same behavioral properties outwards. This would divide the mathematical analysis into two parts. First, an appropriate substitute has to be defined with parameters depending on the number of constituents, their distribution and individual material parameters. After that, the new macroscopic boundary problem can be solved with standard methods without the need for extremely fine meshing algorithms. This methodology where the missing data for a macroscopic model is extracted from a microscopic one beforehand to fill in its constitutive equations is known as a *heterogeneous multiscale method* [114]. An overview of the process with the methods presented in this thesis is visualized in Fig. 4.1.

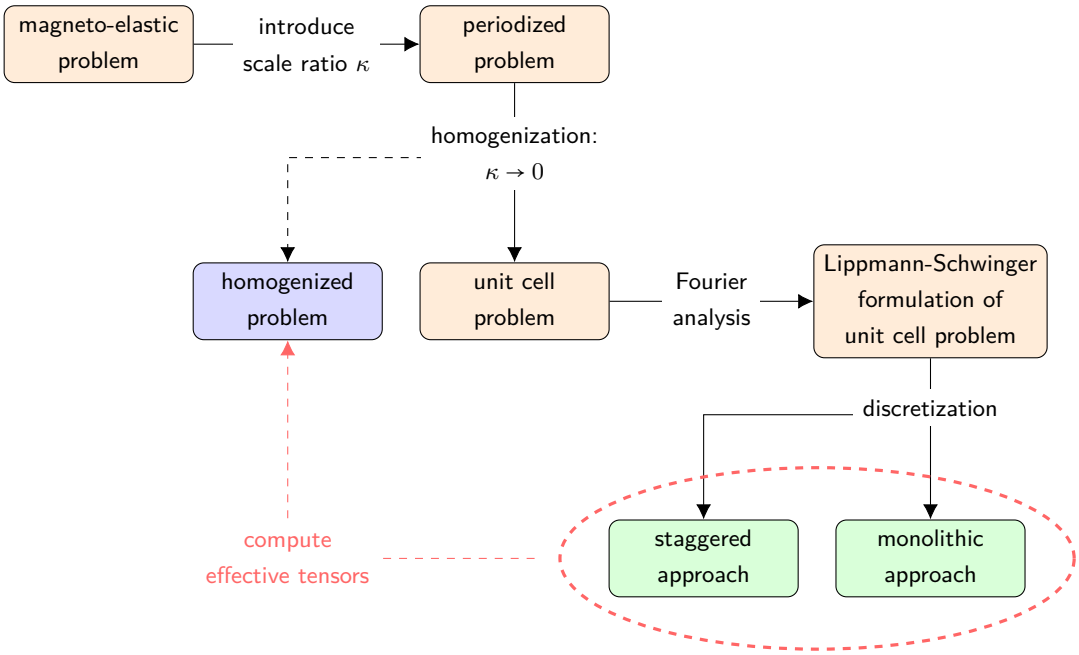

Fig. 4.1: The heterogeneous mutiscale method for the presented magneto-elastic system: after the original problem was substituted with a periodized one, the homogenization limit process leads to a homogenized and a unit cell problem. Solving the unit cell problem for example with Fourier-based methods allows for the computation of effective tensor quantities that can then be used to solve the homogenized problem.

To achieve the goal of finding an appropriate substitute, one can again proceed in two steps. Periodic homogenization — as the name suggests — can only be carried out on materials that display a periodic micro-structure, i.e. where the oscillating coefficients start to repeat themselves after a while. While this may be the case for layered materials such as laminates, fusing several phases into a new compound often involves statistical processes which do not allow for simple deterministic descriptions of metamaterials but instead result in the highly heterogeneous and complex setting we know of. Therefore, the first substitution step consists of trying to represent most of the material's geometrical features within only a small domain. The difficulty herein lies in balancing the supposedly small size against the necessary amount of structural information to accordingly represent the small scale at large. Such a small subdomain is called a *representative volume element* (RVE) or simply *unit cell*. An RVE is by no means uniquely identifiable, meaning there is no such thing as an optimal choice for it. In fact, the determination of a good RVE and its applicability opens up a research field on its own and is

the focal point of many works [31, 48, 96]. It is then assumed that the RVE is periodically continued in each spatial direction as it is seen in Fig. 4.2. To phrase it in a different way: instead of looking at the real specimen with its exact phase borders and inclusions, it is approximated by a repeating pattern that contains its core features. In the scope of this thesis, the chosen RVE is always of regular rectangular shape and will be mathematically modeled as the d-dimensional torus defined below.

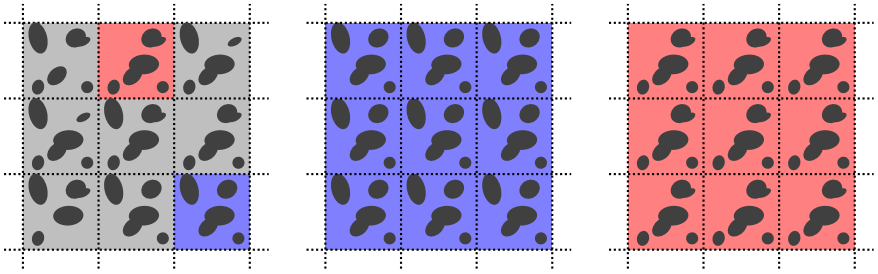

Fig. 4.2: **Left:** Micro-structure where indicated subcells already share similar geometrical features. **Middle:** A perfectly periodic substitute pattern obtained from choosing the blue cell as RVE. **Right:** Another possible substitute pattern if the red cell were chosen instead.

Definition 4.1.1. *The d-dimensional torus $\mathbb{T}^d$ is defined as the quotient space $\mathbb{T}^d := \mathbb{R}^d / \mathbb{Z}^d = (\mathbb{R} / \mathbb{Z})^d$.*

Although more general definitions are possible, the representation of the unit cell as a flat torus is sufficient within this context and even beneficial, since its metric is directly inherited this way.

Due to this first approximation, the material tensors are now supposedly defined on $\mathbb{T}^d$ instead of Ω throughout this chapter. Furthermore, the period of the micro-structure, i.e. the length of the chosen unit cell, will be denoted as κ. The adjusted model problem with Dirichlet boundary conditions now reads as follows.

Problem 3 (Magneto-elastic coupling with periodic coefficients)**.** *Let $\Omega \subset \mathbb{R}^d$ be a bounded domain with (piecewise) Lipschitz-continuous boundary $\partial\Omega$. Let furthermore the material tensors be essentially bounded and defined on the d-dimensional torus, i.e. $\mathbf{C} \in L^\infty\left(\mathbb{T}^d, \mathbb{R}^{\tilde{d}\times\tilde{d}}_{\mathrm{sym}}\right)$, $\mathbf{e} \in L^\infty\left(\mathbb{T}^d, \mathbb{R}^{\tilde{d}\times d}\right)$, $\boldsymbol{\mu} \in L^\infty\left(\mathbb{T}^d, \mathbb{R}^{d\times d}_{\mathrm{sym}}\right)$ and let the ellipticity conditions* (3.61) *hold true. Let functions $\mathbf{f}^{\mathrm{mech}} \in L^2\left(\Omega, \mathbb{R}^d\right)$ and $\mathrm{f}^{\mathrm{mag}} \in L^2\left(\Omega, \mathbb{R}\right)$ be given. Depending on a positive quantity κ, find a solution $(\mathbf{u}_\kappa, \psi_\kappa)$ such that*

$$\begin{aligned} \mathbf{div}\left(\mathbf{C}\left(\frac{\mathbf{x}}{\kappa}\right)\boldsymbol{\varepsilon}\left(\mathbf{u}_\kappa(\mathbf{x})\right) - \mathbf{e}\left(\frac{\mathbf{x}}{\kappa}\right)\mathbf{H}\left(\psi_\kappa(\mathbf{x})\right)\right) &= -\mathbf{f}^{\mathrm{mech}}(\mathbf{x}) \qquad \text{a.e. in } \Omega\,, \\ \mathrm{div}\left(\mathbf{e}^{\mathrm{T}}\left(\frac{\mathbf{x}}{\kappa}\right)\boldsymbol{\varepsilon}\left(\mathbf{u}_\kappa(\mathbf{x})\right) + \boldsymbol{\mu}\left(\frac{\mathbf{x}}{\kappa}\right)\mathbf{H}\left(\psi_\kappa(\mathbf{x})\right)\right) &= \mathrm{f}^{\mathrm{mag}}(\mathbf{x}) \qquad \text{a.e. in } \Omega\,, \end{aligned}$$

with Dirichlet boundary conditions

$$\mathbf{u}_\kappa\big|_{\partial\Omega} \equiv 0\,, \qquad \psi_\kappa\big|_{\partial\Omega} \equiv 0\,,$$

being fulfilled (in the sense of the trace mapping theorem 3.2.1).

It was established before that it stands to little reason to look for strong solutions in practical applications involving composites due to their discontinuous nature. Regardless, the strong notation as partial differential equations sometimes shortens or simplifies lengthy expressions and can still be used for further derivations. Therefore, the reader should understand strong forms that appear in the remainder of the thesis more as a form of notation that is associated with the according weak form

gained through the same procedure that was shown in Sect. 3.2. Keeping this in mind, $\mathcal{H}^1_{\text{mech}}$ and $\mathcal{H}^1_{\text{mag}}$ shall remain the appropriate spaces for practically reasonable solutions to Problem 3, even if it is not explicitly stated in its weak form.

The central subject of this chapter is now the second step in finding a substitute material which consists of a limit process in κ. One can think of this step as trying to force the different constituents to fuse together by reducing the shared space in a unit cell while simultaneously increasing the number of RVEs present within a certain area. This is of course just another approximation and at this point in time there is no way yet to tell whether or not this method will give reasonable results. But it is safe to assume that this model might only be applicable if the unit cell — or more precisely the microscopic features within — was relatively small compared to the overall probe. The idea of the limit process is visualized for different values of κ in Fig. 4.3.

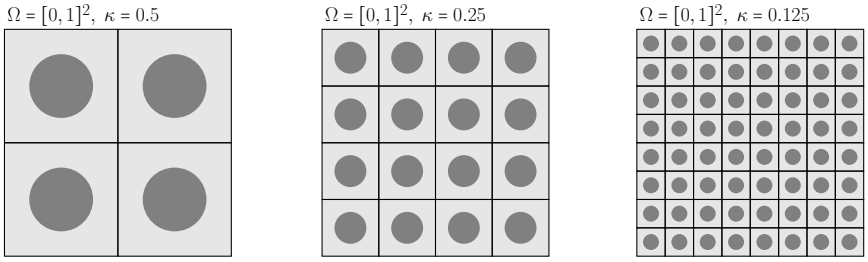

Fig. 4.3: Visualization of the influence of the scale ratio. As κ goes to zero, the number of subcells increases, but their individual size simultaneously becomes smaller. In the limit case the domain would consist of an infinite number of infinitesimally small subcells.

The analysis from Sect. 3.3 ensures the existence of unique solutions to Problem 3 as the proofs still hold true for the now periodic coefficients (with just a few changes to be made; more on that in the following). But the existence of a limit to these solutions as κ tends to zero is not ensured a priori. Thus the main question will be if the limits

$$\mathbf{u}_0 \coloneqq \lim_{\kappa \to 0} \mathbf{u}_\kappa \qquad \text{and} \qquad \psi_0 \coloneqq \lim_{\kappa \to 0} \psi_\kappa \tag{4.1}$$

even exist and, if they do, what meaning do they hold? Do these limits solve a related system that could be considered a homogenized version of Problem 3? The following sections will answer these issues.

4.2 The Asymptotic Expansion Approach

The first ansatz presented here is one of the first to ever originate from homogenization theory and probably the most intuitive one. It focuses on the concept of *asymptotic expansions* [33] to write the solution variables as a formal power series in the scale parameter κ. With functions $\mathbf{u}_{\kappa,i} : \Omega \times \mathbb{T}^d \to \mathbb{R}^d$ and $\psi_{\kappa,i} : \Omega \times \mathbb{T}^d \to \mathbb{R}$ for $i \in \mathbb{N}_0$ the formal expansion takes the form

$$\begin{aligned} \mathbf{u}_\kappa(\mathbf{x}) &= \mathbf{u}_{\kappa,0}\left(\mathbf{x}, \frac{\mathbf{x}}{\kappa}\right) + \kappa\, \mathbf{u}_{\kappa,1}\left(\mathbf{x}, \frac{\mathbf{x}}{\kappa}\right) + \kappa^2\, \mathbf{u}_{\kappa,2}\left(\mathbf{x}, \frac{\mathbf{x}}{\kappa}\right) + \kappa^3\, \mathbf{u}_{\kappa,3}\left(\mathbf{x}, \frac{\mathbf{x}}{\kappa}\right) + \dots, \\ \psi_\kappa(\mathbf{x}) &= \psi_{\kappa,0}\left(\mathbf{x}, \frac{\mathbf{x}}{\kappa}\right) + \kappa\, \psi_{\kappa,1}\left(\mathbf{x}, \frac{\mathbf{x}}{\kappa}\right) + \kappa^2\, \psi_{\kappa,2}\left(\mathbf{x}, \frac{\mathbf{x}}{\kappa}\right) + \kappa^3\, \psi_{\kappa,3}\left(\mathbf{x}, \frac{\mathbf{x}}{\kappa}\right) + \dots \end{aligned} \tag{4.2}$$

where an attempt at the separation of scales is started. The first argument $\mathbf{x}$ is the macroscopic variable living on the whole domain Ω whereas the second argument $\mathbf{y} \coloneqq \mathbf{x}/\kappa$ that is referred to as the microscopic variable is representative for the torus and rapidly oscillating changes.

Remark. *Obviously the two scales can not be considered independently, since* $\mathbf{y}$ *is just a scaled multiplicative of* $\mathbf{x}$*. Following the historical development of this method however, they will often be treated as already separate variables — a circumstance which calls for deeper mathematical investigation later on. Additionally, the existence of functions* $\mathbf{u}_{\kappa,i}$ *and* $\psi_{\kappa,i}$ *themselves as well as the actual convergence of the asymptotic expansion can not be guaranteed at all for right now. All of these shortcomings and mathematical inconsistencies will be taken care of in the following Sect. 4.3 where a proper theoretical foundation will be discussed. Although the asymptotic approach is lacking in some of these aspects, it already leads to important results which will reappear and be justified later on through this formalism. Due to its appeal in engineering fields, its historical importance and its rather easy albeit lengthy derivation, it was decided to discuss the expansion method first in this work.*

The expressions in (4.2) are then inserted into the model equations. To this end, a few definitions and notations have to be introduced in regards to the differential operators.

Definition 4.2.1. *For* $i \in \mathbb{N}_0$ *the total derivatives of functions* $\mathbf{u}_{\kappa,i} : \Omega \times \mathbb{T}^d \to \mathbb{R}^d$ *and* $\psi_{\kappa,i} : \Omega \times \mathbb{T}^d \to \mathbb{R}$ *with respect to the spatial variable* $\mathbf{x}$ *are calculated as*

$$\nabla \mathbf{u}_{\kappa,i} = \nabla_{\mathbf{x}} \mathbf{u}_{\kappa,i} + \frac{1}{\kappa} \nabla_{\mathbf{y}} \mathbf{u}_{\kappa,i} \qquad \text{and} \qquad \nabla \psi_{\kappa,i} = \nabla_{\mathbf{x}} \psi_{\kappa,i} + \frac{1}{\kappa} \nabla_{\mathbf{y}} \psi_{\kappa,i}$$

with operators $\nabla_{\mathbf{x}}$ *and* $\nabla_{\mathbf{y}}$ *denoting the derivatives with respect to the first and second argument respectively. Define furthermore the differential operators*

$$\underline{\varepsilon}_{\mathbf{x}}(\mathbf{u}_{\kappa,i}) = \frac{1}{2}\left(\nabla_{\mathbf{x}} \mathbf{u}_{\kappa,i} + (\nabla_{\mathbf{x}} \mathbf{u}_{\kappa,i})^{\mathrm{T}}\right) \qquad \text{and} \qquad \underline{\varepsilon}_{\mathbf{y}}(\mathbf{u}_{\kappa,i}) = \frac{1}{2}\left(\nabla_{\mathbf{y}} \mathbf{u}_{\kappa,i} + (\nabla_{\mathbf{y}} \mathbf{u}_{\kappa,i})^{\mathrm{T}}\right) ,$$

their corresponding Mandel transforms

$$\varepsilon_{\mathbf{x}}(\mathbf{u}_{\kappa,i}) = \mathcal{M}_2^d \circ \underline{\varepsilon}_{\mathbf{x}}(\mathbf{u}_{\kappa,i}) \qquad \text{and} \qquad \varepsilon_{\mathbf{y}}(\mathbf{u}_{\kappa,i}) = \mathcal{M}_2^d \circ \underline{\varepsilon}_{\mathbf{y}}(\mathbf{u}_{\kappa,i}) ,$$

as well as

$$\mathbf{H}_{\mathbf{x}}(\psi_{\kappa,i}) = -\nabla_{\mathbf{x}} \psi_{\kappa,i} \qquad \text{and} \qquad \mathbf{H}_{\mathbf{y}}(\psi_{\kappa,i}) = -\nabla_{\mathbf{y}} \psi_{\kappa,i} .$$

With this the series for the Cauchy strain and the magnetic field take the form

$$\begin{aligned} \varepsilon(\mathbf{u}_\kappa) &= \varepsilon_{\mathbf{x}}(\mathbf{u}_{\kappa,0}) + \kappa^{-1} \varepsilon_{\mathbf{y}}(\mathbf{u}_{\kappa,0}) + \kappa \varepsilon_{\mathbf{x}}(\mathbf{u}_{\kappa,1}) + \varepsilon_{\mathbf{y}}(\mathbf{u}_{\kappa,1}) + \dots , \\ \mathbf{H}(\psi_\kappa) &= \mathbf{H}_{\mathbf{x}}(\psi_{\kappa,0}) + \kappa^{-1} \mathbf{H}_{\mathbf{y}}(\psi_{\kappa,0}) + \kappa \mathbf{H}_{\mathbf{x}}(\psi_{\kappa,1}) + \mathbf{H}_{\mathbf{y}}(\psi_{\kappa,1}) + \dots \end{aligned} \tag{4.3}$$

which can then be put into the constitutive equations for the stress field and the magnetic induction. Applying the divergence operator in the last step and another splitting of the therein involved derivatives into $\mathbf{x}$ and $\mathbf{y}$ parts yields the equations

$$\begin{aligned} -\mathbf{f}^{\mathrm{mech}} &= \kappa^{-2} \mathbf{div}_{\mathbf{y}}\left(\mathbf{C}\varepsilon_{\mathbf{y}}(\mathbf{u}_{\kappa,0}) - \mathbf{e}\mathbf{H}_{\mathbf{y}}(\psi_{\kappa,0})\right) \\ &+ \kappa^{-1} \mathbf{div}_{\mathbf{x}}\left(\mathbf{C}\varepsilon_{\mathbf{y}}(\mathbf{u}_{\kappa,0}) - \mathbf{e}\mathbf{H}_{\mathbf{y}}(\psi_{\kappa,0})\right) \\ &+ \kappa^{-1} \mathbf{div}_{\mathbf{y}}\left(\mathbf{C}\varepsilon_{\mathbf{x}}(\mathbf{u}_{\kappa,0}) - \mathbf{e}\mathbf{H}_{\mathbf{x}}(\psi_{\kappa,0}) + \mathbf{C}\varepsilon_{\mathbf{y}}(\mathbf{u}_{\kappa,1}) - \mathbf{e}\mathbf{H}_{\mathbf{y}}(\psi_{\kappa,1})\right) \\ &+ \kappa^{0} \mathbf{div}_{\mathbf{x}}\left(\mathbf{C}\varepsilon_{\mathbf{x}}(\mathbf{u}_{\kappa,0}) - \mathbf{e}\mathbf{H}_{\mathbf{x}}(\psi_{\kappa,0}) + \mathbf{C}\varepsilon_{\mathbf{y}}(\mathbf{u}_{\kappa,1}) - \mathbf{e}\mathbf{H}_{\mathbf{y}}(\psi_{\kappa,1})\right) \\ &+ \kappa^{0} \mathbf{div}_{\mathbf{y}}\left(\mathbf{C}\varepsilon_{\mathbf{x}}(\mathbf{u}_{\kappa,1}) - \mathbf{e}\mathbf{H}_{\mathbf{x}}(\psi_{\kappa,1}) + \mathbf{C}\varepsilon_{\mathbf{y}}(\mathbf{u}_{\kappa,2}) - \mathbf{e}\mathbf{H}_{\mathbf{y}}(\psi_{\kappa,2})\right) \\ &+ \dots \end{aligned} \tag{4.4}$$

for the mechanical part and

$$\begin{aligned}
\mathrm{f}^{\mathrm{mag}} &= \kappa^{-2}\operatorname{div}_{\mathbf{y}}\left(\mathbf{e}^{\mathrm{T}}\,\boldsymbol{\varepsilon}_{\mathbf{y}}\left(\mathbf{u}_{\kappa,0}\right)+\boldsymbol{\mu}\,\mathbf{H}_{\mathbf{y}}\left(\psi_{\kappa,0}\right)\right)\\
&+ \kappa^{-1}\operatorname{div}_{\mathbf{x}}\left(\mathbf{e}^{\mathrm{T}}\,\boldsymbol{\varepsilon}_{\mathbf{y}}\left(\mathbf{u}_{\kappa,0}\right)+\boldsymbol{\mu}\,\mathbf{H}_{\mathbf{y}}\left(\psi_{\kappa,0}\right)\right)\\
&+ \kappa^{-1}\operatorname{div}_{\mathbf{y}}\left(\mathbf{e}^{\mathrm{T}}\,\boldsymbol{\varepsilon}_{\mathbf{x}}\left(\mathbf{u}_{\kappa,0}\right)+\boldsymbol{\mu}\,\mathbf{H}_{\mathbf{x}}\left(\psi_{\kappa,0}\right)+\mathbf{e}^{\mathrm{T}}\,\boldsymbol{\varepsilon}_{\mathbf{y}}\left(\mathbf{u}_{\kappa,1}\right)+\boldsymbol{\mu}\,\mathbf{H}_{\mathbf{y}}\left(\psi_{\kappa,1}\right)\right)\\
&+ \kappa^{0}\operatorname{div}_{\mathbf{x}}\left(\mathbf{e}^{\mathrm{T}}\,\boldsymbol{\varepsilon}_{\mathbf{x}}\left(\mathbf{u}_{\kappa,0}\right)+\boldsymbol{\mu}\,\mathbf{H}_{\mathbf{x}}\left(\psi_{\kappa,0}\right)+\mathbf{e}^{\mathrm{T}}\,\boldsymbol{\varepsilon}_{\mathbf{y}}\left(\mathbf{u}_{\kappa,1}\right)+\boldsymbol{\mu}\,\mathbf{H}_{\mathbf{y}}\left(\psi_{\kappa,1}\right)\right)\\
&+ \kappa^{0}\operatorname{div}_{\mathbf{y}}\left(\mathbf{e}^{\mathrm{T}}\,\boldsymbol{\varepsilon}_{\mathbf{x}}\left(\mathbf{u}_{\kappa,1}\right)+\boldsymbol{\mu}\,\mathbf{H}_{\mathbf{x}}\left(\psi_{\kappa,1}\right)+\mathbf{e}^{\mathrm{T}}\,\boldsymbol{\varepsilon}_{\mathbf{y}}\left(\mathbf{u}_{\kappa,2}\right)+\boldsymbol{\mu}\,\mathbf{H}_{\mathbf{y}}\left(\psi_{\kappa,2}\right)\right)\\
&+ \dots
\end{aligned} \tag{4.5}$$

for the magnetic part of the system. These equalities hold true, if all terms associated with a certain power of κ add up to zero each.

Remark. *One could try to argue that this conclusion is reached through multiplication with different powers of κ and then taking the limit for $\kappa \to 0$. But as stated in the remark before, the convergence of these expressions is not ensured in this setting, since the divergence terms need to be bounded for this argument which is not necessarily the case for L^{∞}-coefficients. It is also reminded here that due to the heavy restrictions for strong ones, one wishes to obtain weak solutions at the end instead and that all the differential operators used should be understood in a weak sense as well; see for example [22] for the definition of derivatives of general distributions. Moreover, important formulas such as the integration by parts are still valid for elements from $\mathcal{H}^1$ and will be used repeatedly in the upcoming derivations.*

Therefore, a system of subproblems has to be solved. The following definition helps to shorten the notation.

Definition 4.2.2. *Let $i \in \mathbb{N}_0$. For functions $\mathbf{u}_{\kappa,i} : \Omega \times \mathbb{T}^d \to \mathbb{R}^d$ and $\psi_{\kappa,i} : \Omega \times \mathbb{T}^d \to \mathbb{R}$ define the operators*

$$\begin{aligned}
\mathcal{P}^{\mathrm{mech}}_{-2}\left(\mathbf{u}_{\kappa,i},\psi_{\kappa,i}\right) &= \mathbf{div}_{\mathbf{y}}\left(\mathbf{C}\,\boldsymbol{\varepsilon}_{\mathbf{y}}\left(\mathbf{u}_{\kappa,i}\right)-\mathbf{e}\,\mathbf{H}_{\mathbf{y}}\left(\psi_{\kappa,i}\right)\right),\\
\mathcal{P}^{\mathrm{mech}}_{-1}\left(\mathbf{u}_{\kappa,i},\psi_{\kappa,i}\right) &= \mathbf{div}_{\mathbf{y}}\left(\mathbf{C}\,\boldsymbol{\varepsilon}_{\mathbf{x}}\left(\mathbf{u}_{\kappa,i}\right)-\mathbf{e}\,\mathbf{H}_{\mathbf{x}}\left(\psi_{\kappa,i}\right)\right)+\mathbf{div}_{\mathbf{x}}\left(\mathbf{C}\,\boldsymbol{\varepsilon}_{\mathbf{y}}\left(\mathbf{u}_{\kappa,i}\right)-\mathbf{e}\,\mathbf{H}_{\mathbf{y}}\left(\psi_{\kappa,i}\right)\right),\\
\mathcal{P}^{\mathrm{mech}}_{0}\left(\mathbf{u}_{\kappa,i},\psi_{\kappa,i}\right) &= \mathbf{div}_{\mathbf{x}}\left(\mathbf{C}\,\boldsymbol{\varepsilon}_{\mathbf{x}}\left(\mathbf{u}_{\kappa,i}\right)-\mathbf{e}\,\mathbf{H}_{\mathbf{x}}\left(\psi_{\kappa,i}\right)\right)
\end{aligned}$$

associated with the mechanical equation of the system and

$$\begin{aligned}
\mathcal{P}^{\mathrm{mag}}_{-2}\left(\mathbf{u}_{\kappa,i},\psi_{\kappa,i}\right) &= \operatorname{div}_{\mathbf{y}}\left(\mathbf{e}^{\mathrm{T}}\,\boldsymbol{\varepsilon}_{\mathbf{y}}\left(\mathbf{u}_{\kappa,i}\right)+\boldsymbol{\mu}\,\mathbf{H}_{\mathbf{y}}\left(\psi_{\kappa,i}\right)\right),\\
\mathcal{P}^{\mathrm{mag}}_{-1}\left(\mathbf{u}_{\kappa,i},\psi_{\kappa,i}\right) &= \operatorname{div}_{\mathbf{y}}\left(\mathbf{e}^{\mathrm{T}}\,\boldsymbol{\varepsilon}_{\mathbf{x}}\left(\mathbf{u}_{\kappa,i}\right)+\boldsymbol{\mu}\,\mathbf{H}_{\mathbf{x}}\left(\psi_{\kappa,i}\right)\right)+\operatorname{div}_{\mathbf{x}}\left(\mathbf{e}^{\mathrm{T}}\,\boldsymbol{\varepsilon}_{\mathbf{y}}\left(\mathbf{u}_{\kappa,i}\right)+\boldsymbol{\mu}\,\mathbf{H}_{\mathbf{y}}\left(\psi_{\kappa,i}\right)\right),\\
\mathcal{P}^{\mathrm{mag}}_{0}\left(\mathbf{u}_{\kappa,i},\psi_{\kappa,i}\right) &= \operatorname{div}_{\mathbf{x}}\left(\mathbf{e}^{\mathrm{T}}\,\boldsymbol{\varepsilon}_{\mathbf{x}}\left(\mathbf{u}_{\kappa,i}\right)+\boldsymbol{\mu}\,\mathbf{H}_{\mathbf{x}}\left(\psi_{\kappa,i}\right)\right)
\end{aligned}$$

associated with the magnetic part of the system.

Thus the hierarchical system can be compactly written down for $\diamond \in \{\mathrm{mech},\mathrm{mag}\}$ as

$$\begin{aligned}
&\mathcal{P}^{\diamond}_{-2}\left(\mathbf{u}_{\kappa,0},\psi_{\kappa,0}\right)=0\\
&\mathcal{P}^{\diamond}_{-2}\left(\mathbf{u}_{\kappa,1},\psi_{\kappa,1}\right)+\mathcal{P}^{\diamond}_{-1}\left(\mathbf{u}_{\kappa,0},\psi_{\kappa,0}\right)=0\\
&\mathcal{P}^{\diamond}_{-2}\left(\mathbf{u}_{\kappa,2},\psi_{\kappa,2}\right)+\mathcal{P}^{\diamond}_{-1}\left(\mathbf{u}_{\kappa,1},\psi_{\kappa,1}\right)+\mathcal{P}^{\diamond}_{0}\left(\mathbf{u}_{\kappa,0},\psi_{\kappa,0}\right)=\begin{cases}-\mathbf{f}^{\mathrm{mech}}, & \diamond=\mathrm{mech},\\ \mathrm{f}^{\mathrm{mag}}, & \diamond=\mathrm{mag},\end{cases}\\
&\vdots
\end{aligned} \tag{4.6}$$

with all remaining subproblems also consisting of all three operators but with right-hand sides equal to zero and the indices of the functions increased by one each. The advantage of this notation is that the

sum of the index of an operator together with the index of the functions in the argument directly refer to the corresponding power of κ in the series expansion. At the beginning, the subproblems grow more complex with increasing order as more terms get involved. Exploiting this initial staircase structure, one can attempt to solve (4.6) gradually.

Taking a look at the first problem associated with the factor κ^{-2} one has

$$\begin{aligned} \mathbf{div}_{\mathbf{y}}\left(\mathbf{C}\,\boldsymbol{\varepsilon}_{\mathbf{y}}\left(\mathbf{u}_{\kappa,0}\right) - \mathbf{e}\,\mathbf{H}_{\mathbf{y}}\left(\psi_{\kappa,0}\right)\right) &= 0\,, \\ \operatorname{div}_{\mathbf{y}}\left(\mathbf{e}^{\mathrm{T}}\,\boldsymbol{\varepsilon}_{\mathbf{y}}\left(\mathbf{u}_{\kappa,0}\right) + \boldsymbol{\mu}\,\mathbf{H}_{\mathbf{y}}\left(\psi_{\kappa,0}\right)\right) &= 0\,, \end{aligned} \tag{4.7}$$

a system with only y-derivatives that depends just on the terms $\mathbf{u}_{\kappa,0}$ and $\psi_{\kappa,0}$. Similarly to how weak forms are derived, the two equations are multiplied with $\mathbf{u}_{\kappa,0}$ or $\psi_{\kappa,0}$ respectively and then integrated over the torus $\mathbb{T}^d$. Both equations now take the form

$$\begin{aligned} \int_{\mathbb{T}^d} \left(\boldsymbol{\varepsilon}_{\mathbf{y}}\left(\mathbf{u}_{\kappa,0}\right)\right)^{\mathrm{T}} \mathbf{C}\,\boldsymbol{\varepsilon}_{\mathbf{y}}\left(\mathbf{u}_{\kappa},0\right) - \left(\boldsymbol{\varepsilon}_{\mathbf{y}}\left(\mathbf{u}_{\kappa,0}\right)\right)^{\mathrm{T}} \mathbf{e}\,\mathbf{H}_{\mathbf{y}}\left(\psi_{\kappa,0}\right)\,\mathrm{d}\,\mathbf{y} &= 0\,, \\ \int_{\mathbb{T}^d} \left(\mathbf{H}_{\mathbf{y}}\left(\psi_{\kappa,0}\right)\right)^{\mathrm{T}} \mathbf{e}^{\mathrm{T}}\,\boldsymbol{\varepsilon}_{\mathbf{y}}\left(\mathbf{u}_{\kappa,0}\right) + \left(\mathbf{H}_{\mathbf{y}}\left(\psi_{\kappa,0}\right)\right)^{\mathrm{T}} \boldsymbol{\mu}\,\mathbf{H}_{\mathbf{y}}\left(\psi_{\kappa,0}\right)\,\mathrm{d}\,\mathbf{y} &= 0 \end{aligned} \tag{4.8}$$

and summing them up yields

$$\begin{aligned} 0 &= \int_{\mathbb{T}^d} \left(\boldsymbol{\varepsilon}_{\mathbf{y}}\left(\mathbf{u}_{\kappa,0}\right)\right)^{\mathrm{T}} \mathbf{C}\,\boldsymbol{\varepsilon}_{\mathbf{y}}\left(\mathbf{u}_{\kappa,0}\right) + \left(\mathbf{H}_{\mathbf{y}}\left(\psi_{\kappa,0}\right)\right)^{\mathrm{T}} \boldsymbol{\mu}\,\mathbf{H}_{\mathbf{y}}\left(\psi_{\kappa,0}\right)\,\mathrm{d}\,\mathbf{y} \\ &\geq \int_{\mathbb{T}^d} \gamma_{\mathbf{C}} \left\|\boldsymbol{\varepsilon}_{\mathbf{y}}\left(\mathbf{u}_{\kappa,0}\right)\right\|^2 + \gamma_{\boldsymbol{\mu}} \left\|\mathbf{H}_{\mathbf{y}}\left(\psi_{\kappa,0}\right)\right\|^2\,\mathrm{d}\,\mathbf{y}\,, \end{aligned} \tag{4.9}$$

with $\gamma_{\mathbf{C}}$ and $\gamma_{\boldsymbol{\mu}}$ being the coercivity constants from (3.61). Thus, both norms and in conclusion both fields with respect to the $\mathbf{y}$ variable are equal to zero. Thus, one can deduce that $\mathbf{u}_{\kappa,0}$ and $\psi_{\kappa,0}$ only depend on $\mathbf{x}$. This is obvious for the magnetic scalar potential, since the magnetic field is just the negative gradient, but for the displacement field this statement is not as trivial. The symmetric gradient being equal to zero could still allow for a non-vanishing regular gradient and a dependency on $\mathbf{y}$. The idea is to split the displacement into two parts, one that depends only on $\mathbf{x}$ by definition and another one that can be shown to be equal to zero already. A promising choice is to define the mean value over one unit cell as

$$\mathbf{U}\left(\mathbf{x}\right) \coloneqq \int_{\mathbb{T}^d} \mathbf{u}_{\kappa,0}\left(\mathbf{x},\mathbf{y}\right)\,\mathrm{d}\,\mathbf{y} \tag{4.10}$$

and to take a look at the fluctuating part $\tilde{\mathbf{u}}_{\kappa,0} \coloneqq \mathbf{u}_{\kappa,0} - \mathbf{U}$. Due to the linearity of the strain operator and the mean value's independence from $\mathbf{y}$, one has

$$0 = \left\|\boldsymbol{\varepsilon}_{\mathbf{y}}\left(\mathbf{u}_{\kappa,0}\right)\right\| = \left\|\boldsymbol{\varepsilon}_{\mathbf{y}}\left(\tilde{\mathbf{u}}_{\kappa,0}\right) + \boldsymbol{\varepsilon}_{\mathbf{y}}\left(\mathbf{U}\right)\right\| = \left\|\boldsymbol{\varepsilon}_{\mathbf{y}}\left(\tilde{\mathbf{u}}_{\kappa,0}\right)\right\|\,. \tag{4.11}$$

Then $\mathbf{u}_{\kappa,0}$ being zero follows from a variant of Korn's inequality (3.3.4) for the periodic setting.

Lemma 4.2.3 (Korn's inequality for periodic functions; Proof in [94, p. 21 sq.])**.** *There exists a positive constant c, such that*

$$\int_{\mathbb{T}^d} \left\|\boldsymbol{\varepsilon}\left(\mathbf{v}\right)\right\|^2\,\mathrm{d}\,\mathbf{y} \geq c\left\|\mathbf{v}\right\|_{\mathcal{H}^1}^2 \text{ for all } \mathbf{v} \in \mathcal{H}^1\left(\mathbb{T}^d,\mathbb{R}^d\right) \text{ with } \int_{\mathbb{T}^d} \mathbf{v}\,\mathrm{d}\,\mathbf{y} = 0\,.$$

Assuming that $\tilde{\mathbf{u}}_{\kappa,0}\left(\mathbf{x},\cdot\right)$ is for each $\mathbf{x} \in \Omega$ in the Sobolev space $\mathcal{H}^1\left(\mathbb{T}^d,\mathbb{R}^d\right)$, one can estimate

$$0 = \int_{\mathbb{T}^d} \left\|\boldsymbol{\varepsilon}_{\mathbf{y}}\left(\tilde{\mathbf{u}}_{\kappa,0}\left(\mathbf{x},\cdot\right)\right)\right\|^2\,\mathrm{d}\,\mathbf{y} \geq c\left\|\tilde{\mathbf{u}}_{\kappa,0}\left(\mathbf{x},\cdot\right)\right\|_{\mathcal{H}^1}^2 \geq c\left\|\tilde{\mathbf{u}}_{\kappa,0}\left(\mathbf{x},\cdot\right)\right\|_{L^2}^2\,. \tag{4.12}$$

This shows that $\tilde{\mathbf{u}}_{\kappa,0} = 0$ in the L^2-sense and so $\mathbf{u}_{\kappa,0} = \mathbf{U}$ solely depends on $\mathbf{x}$.

Next, the equations associated with the factor κ^{-1} are

$$\begin{aligned} 0 &= \mathbf{div}_{\mathbf{x}}\left(\mathbf{C}\,\boldsymbol{\varepsilon}_{\mathbf{y}}\left(\mathbf{u}_{\kappa,0}\right) - \mathbf{e}\,\mathbf{H}_{\mathbf{y}}\left(\psi_{\kappa,0}\right)\right) \\ &+ \mathbf{div}_{\mathbf{y}}\left(\mathbf{C}\,\boldsymbol{\varepsilon}_{\mathbf{x}}\left(\mathbf{u}_{\kappa,0}\right) - \mathbf{e}\,\mathbf{H}_{\mathbf{x}}\left(\psi_{\kappa,0}\right) + \mathbf{C}\,\boldsymbol{\varepsilon}_{\mathbf{y}}\left(\mathbf{u}_{\kappa,1}\right) - \mathbf{e}\,\mathbf{H}_{\mathbf{y}}\left(\psi_{\kappa,1}\right)\right)\,, \\ 0 &= \mathrm{div}_{\mathbf{x}}\left(\mathbf{e}^{\mathrm{T}}\,\boldsymbol{\varepsilon}_{\mathbf{y}}\left(\mathbf{u}_{\kappa,0}\right) + \boldsymbol{\mu}\,\mathbf{H}_{\mathbf{y}}\left(\psi_{\kappa,0}\right)\right) \\ &+ \mathrm{div}_{\mathbf{y}}\left(\mathbf{e}^{\mathrm{T}}\,\boldsymbol{\varepsilon}_{\mathbf{x}}\left(\mathbf{u}_{\kappa,0}\right) + \boldsymbol{\mu}\,\mathbf{H}_{\mathbf{x}}\left(\psi_{\kappa,0}\right) + \mathbf{e}^{\mathrm{T}}\,\boldsymbol{\varepsilon}_{\mathbf{y}}\left(\mathbf{u}_{\kappa,1}\right) + \boldsymbol{\mu}\,\mathbf{H}_{\mathbf{y}}\left(\psi_{\kappa,1}\right)\right)\,. \end{aligned} \tag{4.13}$$

Due to $\boldsymbol{\varepsilon}_{\mathbf{y}}\left(\mathbf{u}_{\kappa,0}\right)$ and $\mathbf{H}_{\mathbf{y}}\left(\psi_{\kappa,0}\right)$ being equal to zero as seen from (4.9), these expressions can be simplified and rewritten as a system that will be referred to as the *cell problem*.

Problem 4 (Cell problem)**.** *Let the assumptions of Problem 3 hold true. Let furthermore the functions $\mathbf{u}_{\kappa,0} : \Omega \to \mathbb{R}^d$ and $\psi_{\kappa,0} : \Omega \to \mathbb{R}$ be given. The cell problem then consists of finding a solution $\left(\mathbf{u}_{\kappa,1}, \psi_{\kappa,1}\right)$ such that the equations*

$$\begin{aligned} \mathbf{div}_{\mathbf{y}}\left(\mathbf{C}\,\boldsymbol{\varepsilon}_{\mathbf{y}}\left(\mathbf{u}_{\kappa,1}\right) - \mathbf{e}\,\mathbf{H}_{\mathbf{y}}\left(\psi_{\kappa,1}\right)\right) &= -\mathbf{div}_{\mathbf{y}}\left(\mathbf{C}\,\boldsymbol{\varepsilon}_{\mathbf{x}}\left(\mathbf{u}_{\kappa,0}\right) - \mathbf{e}\,\mathbf{H}_{\mathbf{x}}\left(\psi_{\kappa,0}\right)\right)\,, \\ \mathrm{div}_{\mathbf{y}}\left(\mathbf{e}^{\mathrm{T}}\,\boldsymbol{\varepsilon}_{\mathbf{y}}\left(\mathbf{u}_{\kappa,1}\right) + \boldsymbol{\mu}\,\mathbf{H}_{\mathbf{y}}\left(\psi_{\kappa,1}\right)\right) &= -\mathrm{div}_{\mathbf{y}}\left(\mathbf{e}^{\mathrm{T}}\,\boldsymbol{\varepsilon}_{\mathbf{x}}\left(\mathbf{u}_{\kappa,0}\right) + \boldsymbol{\mu}\,\mathbf{H}_{\mathbf{x}}\left(\psi_{\kappa,0}\right)\right) \end{aligned}$$

are fulfilled a.e. on the torus $\mathbb{T}^d$.

Instead of solving for $\mathbf{u}_{\kappa,1}$ and $\psi_{\kappa,1}$ directly, one exchanges the $\mathbf{x}$-derivatives on the right-hand side of the cell problem for unit vectors of appropriate size and tries to solve these problem.

Definition 4.2.4. *For $i = 1, \ldots, \tilde{d}$ let the i-th unit vector in $\mathbb{R}^{\tilde{d}}$ be denoted as $\mathbf{z}_i^{\mathrm{mech}}$. Analogously for $j = 1, \ldots, d$ let the j-th unit vector in $\mathbb{R}^d$ be denoted as $\mathbf{z}_j^{\mathrm{mag}}$. The solutions ω_i^{mech} and $\varrho_i^{\mathrm{mech}}$ to the system*

$$\begin{aligned} \mathbf{div}_{\mathbf{y}}\left(\mathbf{C}\,\boldsymbol{\varepsilon}_{\mathbf{y}}\left(\omega_i^{\mathrm{mech}}\right) - \mathbf{e}\,\mathbf{H}_{\mathbf{y}}\left(\varrho_i^{\mathrm{mech}}\right)\right) &= -\mathbf{div}_{\mathbf{y}}\left(\mathbf{C}\,\mathbf{z}_i^{\mathrm{mech}}\right)\,, \\ \mathrm{div}_{\mathbf{y}}\left(\mathbf{e}^{\mathrm{T}}\,\boldsymbol{\varepsilon}_{\mathbf{y}}\left(\omega_i^{\mathrm{mech}}\right) + \boldsymbol{\mu}\,\mathbf{H}_{\mathbf{y}}\left(\varrho_i^{\mathrm{mech}}\right)\right) &= -\mathrm{div}_{\mathbf{y}}\left(\mathbf{e}^{\mathrm{T}}\,\mathbf{z}_i^{\mathrm{mech}}\right) \end{aligned}$$

as well as the solutions ω_j^{mag} and ϱ_j^{mag} to the system

$$\begin{aligned} \mathbf{div}_{\mathbf{y}}\left(\mathbf{C}\,\boldsymbol{\varepsilon}_{\mathbf{y}}\left(\omega_j^{\mathrm{mag}}\right) - \mathbf{e}\,\mathbf{H}_{\mathbf{y}}\left(\varrho_j^{\mathrm{mag}}\right)\right) &= -\mathbf{div}_{\mathbf{y}}\left(-\mathbf{e}\,\mathbf{z}_j^{\mathrm{mag}}\right)\,, \\ \mathrm{div}_{\mathbf{y}}\left(\mathbf{e}^{\mathrm{T}}\,\boldsymbol{\varepsilon}_{\mathbf{y}}\left(\omega_j^{\mathrm{mag}}\right) + \boldsymbol{\mu}\,\mathbf{H}_{\mathbf{y}}\left(\varrho_j^{\mathrm{mag}}\right)\right) &= -\mathrm{div}_{\mathbf{y}}\left(\boldsymbol{\mu}\,\mathbf{z}_j^{\mathrm{mag}}\right) \end{aligned}$$

are called correctors.

The advantage gained from this seemingly more complicated approach is another separation of variables. Since all derivatives and material tensors involved in the corrector problems are independent from $\mathbf{x}$, the correctors are only dependent on $\mathbf{y}$ themselves. Their existence and uniqueness is again guaranteed by the Lax–Milgram theorem (3.3.2) with the majority of the arguments from Sect. 3.3 remaining unchanged. The interesting question left open is the choice of a Hilbert space $\mathcal{H}$. Contrary to the Dirichlet boundary value problems seen before, the implicit periodic boundary conditions for the torus demand an additional constraint for the solutions to be unique. It is easy to notice that for any corrector pairs found another pair that differs up to an additive constant solves the same problem as well, since these constants vanish when the strain and magnetic field operators are applied. The appropriate solution space would therefore be

$$\mathcal{H} = \mathcal{H}^1\left(\mathbb{T}^d, \mathbb{R}^d\right) / \mathbb{R}^d \times \mathcal{H}^1\left(\mathbb{T}^d, \mathbb{R}\right) / \mathbb{R} \tag{4.14}$$

which is the product of two quotient spaces whose entries are considered equivalent to each other whenever their difference is a vector- or scalar-valued constant respectively. If one wishes to specify one representative specifically, a standardization constraint is usually put in place. The common choice in this case is to prescribe the quantities' mean value as zero which leads to the solution space

$$\mathcal{H} = \left\{ (\omega, \varrho) \in \mathcal{H}^1\left(\mathbb{T}^d, \mathbb{R}^d\right) \times \mathcal{H}^1\left(\mathbb{T}^d, \mathbb{R}\right) \,:\, \int_{\mathbb{T}^d} \omega\left(\mathbf{y}\right) \,\mathrm{d}\,\mathbf{y} = 0\,, \int_{\mathbb{T}^d} \varrho\left(\mathbf{y}\right) \,\mathrm{d}\,\mathbf{y} = 0 \right\}\,. \tag{4.15}$$

The original right-hand sides of Problem 4 can now be regained through a linear combination of these unit vectors with the coefficients being the components of $\boldsymbol{\varepsilon}_{\mathbf{x}}\left(\mathbf{u}_{\kappa,0}\right)$ and $\mathbf{H}_{\mathbf{x}}\left(\psi_{\kappa,0}\right)$. The solutions $\mathbf{u}_{\kappa,1}$ and $\psi_{\kappa,1}$ are then also obtained from this linear combination. It is important to note though that while the proof for existence and uniqueness follows the same steps as before in concept, a few inequalities were only valid for bounded domains with vanishing boundary conditions so far and have to be adapted for the new periodic setting on the torus. This mainly affects the estimates to show coercivity of the bilinear form. Namely, the periodic version of Korn's inequality given in Lemma 4.2.3 has to be used instead of Lemma 3.3.4 and one has to exchange the Poincaré inequality from Theorem 3.3.5 for its generalized version — the *Poincaré–Wirtinger inequality* which holds for any connected domain — given below.

Theorem 4.2.5 (Poincaré–Wirtinger inequality on $\mathbb{T}^d$; Proof in [69, p. 361])**.** *There exists a positive constant $\tilde{c}$ such that*

$$\left\| f - \int_{\mathbb{T}^d} f\left(\mathbf{y}\right) \,\mathrm{d}\,\mathbf{y} \right\|_{L^2} \leq \tilde{c}\, \|\nabla f\|_{L^2} \text{ for all } f \in \mathcal{H}^1\left(\mathbb{T}^d, \mathbb{R}\right)\,.$$

Since the solution spaces are considered as equivalence classes in the sense of (4.14), one can assume that without loss of generality the mean value of the solutions is equal to zero as explained before in (4.15), in which case Theorem 4.2.5 gives the same estimate as the regular Poincaré inequality without specifying any values on the boundary.

Theorem 4.2.6. *The cell problem (Problem 4) has a unique solution $\left(\mathbf{u}_{\kappa,1}, \psi_{\kappa,1}\right)$ in the sense of the correctors defined in 4.2.4 being considered as representatives of equivalence classes according to 4.14. For given functions $\mathbf{u}_{\kappa,0} : \Omega \to \mathbb{R}^d$ and $\psi_{\kappa,0} : \Omega \to \mathbb{R}$, the solutions can be written as*

$$\begin{aligned}
\mathbf{u}_{\kappa,1}\left(\mathbf{x},\mathbf{y}\right) &= \sum_{i=1}^{\tilde{d}} \left(\boldsymbol{\varepsilon}_{\mathbf{x}}\left(\mathbf{u}_{\kappa,0}\left(\mathbf{x}\right)\right)\right)_i \omega_i^{\mathrm{mech}}\left(\mathbf{y}\right) + \sum_{j=1}^{d} \left(\mathbf{H}_{\mathbf{x}}\left(\psi_{\kappa,0}\left(\mathbf{x}\right)\right)\right)_j \omega_j^{\mathrm{mag}}\left(\mathbf{y}\right)\,, \\
\psi_{\kappa,1}\left(\mathbf{x},\mathbf{y}\right) &= \sum_{i=1}^{\tilde{d}} \left(\boldsymbol{\varepsilon}_{\mathbf{x}}\left(\mathbf{u}_{\kappa,0}\left(\mathbf{x}\right)\right)\right)_i \varrho_i^{\mathrm{mech}}\left(\mathbf{y}\right) + \sum_{j=1}^{d} \left(\mathbf{H}_{\mathbf{x}}\left(\psi_{\kappa,0}\left(\mathbf{x}\right)\right)\right)_j \varrho_j^{\mathrm{mag}}\left(\mathbf{y}\right)\,.
\end{aligned}$$

Proof. Follows by the linearity of all operators and the existence and uniqueness of the correctors. □

Remark. *Although the fact $\boldsymbol{\varepsilon}_{\mathbf{y}}\left(\mathbf{u}_{\kappa,0}\right) = 0$ would have been enough for the simplification to the cell problem and the definition of the correctors, the reconstruction of $\mathbf{u}_{\kappa,1}$ and $\psi_{\kappa,1}$ is only possible because the $\mathbf{x}$-derivatives can be exchanged with the $\mathbf{y}$-divergence operators in the linear combinations. This is the reason why it was important to show further that $\mathbf{u}_{\kappa,0}$ and $\psi_{\kappa,0}$ themselves — and by extension $\boldsymbol{\varepsilon}_{\mathbf{x}}\left(\mathbf{u}_{\kappa,0}\right)$ and $\mathbf{H}_{\mathbf{x}}\left(\psi_{\kappa,0}\right)$ — do not depend on the microscopic variable $\mathbf{y}$. On a second note, Theorem 4.2.6 did not state the solution spaces for $\mathbf{u}_{\kappa,1}$ and $\psi_{\kappa,1}$ yet. This is due to the circumstance that while the functions' behavior with respect to the variable $\mathbf{y}$ is known through the correctors, its properties on the $\mathbf{x}$-variable*

are still unknown at this point. It seems reasonable to assume at least square-integrability in this regard. This will eventually turn out to be the case when investigating the homogenized problem and is again justified by the framework presented in Sect. 4.3.

Finally, the system for κ^0 is given as

$$\begin{aligned} -\mathbf{f}^{\mathrm{mech}} &= \mathbf{div}_{\mathbf{x}}\left(\mathbf{C}\,\boldsymbol{\varepsilon}_{\mathbf{x}}\left(\mathbf{u}_{\kappa,0}\right) - \mathbf{e}\,\mathbf{H}_{\mathbf{x}}\left(\psi_{\kappa,0}\right) + \mathbf{C}\,\boldsymbol{\varepsilon}_{\mathbf{y}}\left(\mathbf{u}_{\kappa,1}\right) - \mathbf{e}\,\mathbf{H}_{\mathbf{y}}\left(\psi_{\kappa,1}\right)\right) \\ &+ \mathbf{div}_{\mathbf{y}}\left(\mathbf{C}\,\boldsymbol{\varepsilon}_{\mathbf{x}}\left(\mathbf{u}_{\kappa,1}\right) - \mathbf{e}\,\mathbf{H}_{\mathbf{x}}\left(\psi_{\kappa,1}\right) + \mathbf{C}\,\boldsymbol{\varepsilon}_{\mathbf{y}}\left(\mathbf{u}_{\kappa,2}\right) - \mathbf{e}\,\mathbf{H}_{\mathbf{y}}\left(\psi_{\kappa,2}\right)\right)\,, \\ \mathrm{f}^{\mathrm{mag}} &= \mathrm{div}_{\mathbf{x}}\left(\mathbf{e}^{\mathrm{T}}\,\boldsymbol{\varepsilon}_{\mathbf{x}}\left(\mathbf{u}_{\kappa,0}\right) + \boldsymbol{\mu}\,\mathbf{H}_{\mathbf{x}}\left(\psi_{\kappa,0}\right) + \mathbf{e}^{\mathrm{T}}\,\boldsymbol{\varepsilon}_{\mathbf{y}}\left(\mathbf{u}_{\kappa,1}\right) + \boldsymbol{\mu}\,\mathbf{H}_{\mathbf{y}}\left(\psi_{\kappa,1}\right)\right) \\ &+ \mathrm{div}_{\mathbf{y}}\left(\mathbf{e}^{\mathrm{T}}\,\boldsymbol{\varepsilon}_{\mathbf{x}}\left(\mathbf{u}_{\kappa,1}\right) + \boldsymbol{\mu}\,\mathbf{H}_{\mathbf{x}}\left(\psi_{\kappa,1}\right) + \mathbf{e}^{\mathrm{T}}\,\boldsymbol{\varepsilon}_{\mathbf{y}}\left(\mathbf{u}_{\kappa,2}\right) + \boldsymbol{\mu}\,\mathbf{H}_{\mathbf{y}}\left(\psi_{\kappa,2}\right)\right)\,. \end{aligned} \tag{4.16}$$

Integrating over the unit cell $\mathbb{T}^d$ and applying the divergence theorem for the $\mathbf{y}$-divergence operators greatly reduces the complexity of these equations as the involved quantities being defined on $\mathbb{T}^d$ are periodic by nature and as such have different signs on opposing sides of the boundary resulting in their cancellation. Additionally, since the terms $\mathbf{f}^{\mathrm{mech}}$ and $\mathrm{f}^{\mathrm{mag}}$ only depend on $\mathbf{x}$, one has

$$\int_{\mathbb{T}^d} \mathbf{f}^{\mathrm{mech}}\,\mathrm{d}\,\mathbf{y} = \mathbf{f}^{\mathrm{mech}} \qquad \text{and} \qquad \int_{\mathbb{T}^d} \mathrm{f}^{\mathrm{mag}}\,\mathrm{d}\,\mathbf{y} = \mathrm{f}^{\mathrm{mag}} \tag{4.17}$$

as the volume of the unit cell is equal to one. The problem now reads in its simplified form as

$$\begin{aligned} \mathbf{div}_{\mathbf{x}} \int_{\mathbb{T}^d} \mathbf{C}\,\boldsymbol{\varepsilon}_{\mathbf{x}}\left(\mathbf{u}_{\kappa,0}\right) - \mathbf{e}\,\mathbf{H}_{\mathbf{x}}\left(\psi_{\kappa,0}\right) + \mathbf{C}\,\boldsymbol{\varepsilon}_{\mathbf{y}}\left(\mathbf{u}_{\kappa,1}\right) - \mathbf{e}\,\mathbf{H}_{\mathbf{y}}\left(\psi_{\kappa,1}\right)\,\mathrm{d}\,\mathbf{y} &= -\mathbf{f}^{\mathrm{mech}}\,, \\ \mathrm{div}_{\mathbf{x}} \int_{\mathbb{T}^d} \mathbf{e}^{\mathrm{T}}\,\boldsymbol{\varepsilon}_{\mathbf{x}}\left(\mathbf{u}_{\kappa,0}\right) + \boldsymbol{\mu}\,\mathbf{H}_{\mathbf{x}}\left(\psi_{\kappa,0}\right) + \mathbf{e}^{\mathrm{T}}\,\boldsymbol{\varepsilon}_{\mathbf{y}}\left(\mathbf{u}_{\kappa,1}\right) + \boldsymbol{\mu}\,\mathbf{H}_{\mathbf{y}}\left(\psi_{\kappa,1}\right)\,\mathrm{d}\,\mathbf{y} &= \mathrm{f}^{\mathrm{mag}}\,. \end{aligned} \tag{4.18}$$

These simplification steps allowed to get rid of $\mathbf{u}_{\kappa,2}$ and $\psi_{\kappa,2}$. Inserting now the formulas from Theorem 4.2.6 for $\mathbf{u}_{\kappa,1}$ and $\psi_{\kappa,1}$ into (4.18) yields a system only depending on the $\mathbf{x}$-variable. This system is called the *homogenized problem* for which the *homogenized* or *effective material tensors* are defined as integrals over the unit cell.

Problem 5 (Homogenized problem)**.** *Let the assumptions of Problem 3 hold true. Let furthermore the correctors being defined as in Definition 4.2.4. Define the effective stiffness tensor* $\mathbf{C}^{\mathrm{eff}} \in \mathbb{R}^{\tilde{d}\times\tilde{d}}$ *with entries*

$$\mathbf{C}^{\mathrm{eff}}_{mn} = \int_{\mathbb{T}^d} \mathbf{C}_{mn} + \sum_{k=1}^{\tilde{d}} \mathbf{C}_{mk}\left(\boldsymbol{\varepsilon}_{\mathbf{y}}\left(\omega_n^{\mathrm{mech}}\right)\right)_k - \sum_{l=1}^{d} \mathbf{e}_{ml}\left(\mathbf{H}_{\mathbf{y}}\left(\varrho_n^{\mathrm{mech}}\right)\right)_l\,\mathrm{d}\,\mathbf{y}\,,$$

the effective permeability tensor $\boldsymbol{\mu}^{\mathrm{eff}} \in \mathbb{R}^{d\times d}$ *with entries*

$$\boldsymbol{\mu}^{\mathrm{eff}}_{mn} = \int_{\mathbb{T}^d} \boldsymbol{\mu}_{mn} + \sum_{k=1}^{\tilde{d}} \mathbf{e}_{km}\left(\boldsymbol{\varepsilon}_{\mathbf{y}}\left(\omega_n^{\mathrm{mag}}\right)\right)_k + \sum_{l=1}^{d} \boldsymbol{\mu}_{ml}\left(\mathbf{H}_{\mathbf{y}}\left(\varrho_n^{\mathrm{mag}}\right)\right)_l\,\mathrm{d}\,\mathbf{y}\,,$$

and the effective coupling tensors $\mathbf{e}^{\mathrm{eff}} \in \mathbb{R}^{\tilde{d}\times d}$ *and* $\tilde{\mathbf{e}}^{\mathrm{eff}} \in \mathbb{R}^{d\times\tilde{d}}$ *with entries*

$$\mathbf{e}^{\mathrm{eff}}_{mn} = \int_{\mathbb{T}^d} \mathbf{e}_{mn} - \sum_{k=1}^{\tilde{d}} \mathbf{C}_{mk}\left(\boldsymbol{\varepsilon}_{\mathbf{y}}\left(\omega_n^{\mathrm{mag}}\right)\right)_k + \sum_{l=1}^{d} \mathbf{e}_{ml}\left(\mathbf{H}_{\mathbf{y}}\left(\varrho_n^{\mathrm{mag}}\right)\right)_l\,\mathrm{d}\,\mathbf{y}$$

and

$$\tilde{\mathbf{e}}^{\mathrm{eff}}_{mn} = \int_{\mathbb{T}^d} \mathbf{e}_{nm} + \sum_{k=1}^{\tilde{d}} \mathbf{e}_{km}\left(\boldsymbol{\varepsilon}_{\mathbf{y}}\left(\omega_n^{\mathrm{mech}}\right)\right)_k + \sum_{l=1}^{d} \boldsymbol{\mu}_{ml}\left(\mathbf{H}_{\mathbf{y}}\left(\varrho_n^{\mathrm{mech}}\right)\right)_l\,\mathrm{d}\,\mathbf{y}\,.$$

The homogenized problem then consists of finding a solution $\left(\mathbf{u}_{\kappa,0}, \psi_{\kappa,0}\right)$ *such that*

$$\begin{aligned} \mathbf{div}\left(\mathbf{C}^{\mathrm{eff}}\,\varepsilon_{\mathbf{x}}\left(\mathbf{u}_{\kappa,0}\right) - \mathbf{e}^{\mathrm{eff}}\,\mathbf{H}_{\mathbf{x}}\left(\psi_{\kappa,0}\right)\right) &= -\mathbf{f}^{\mathrm{mech}} \qquad \text{a.e. in } \Omega\,, \\ \mathrm{div}\left(\tilde{\mathbf{e}}^{\mathrm{eff}}\,\varepsilon_{\mathbf{x}}\left(\mathbf{u}_{\kappa,0}\right) + \boldsymbol{\mu}^{\mathrm{eff}}\,\mathbf{H}_{\mathbf{x}}\left(\psi_{\kappa,0}\right)\right) &= \mathrm{f}^{\mathrm{mag}} \qquad \text{a.e. in } \Omega \end{aligned}$$

with Dirichlet boundary conditions

$$\mathbf{u}_{\kappa,0}\big|_{\partial\Omega} \equiv 0\,, \qquad \psi_{\kappa,0}\big|_{\partial\Omega} \equiv 0$$

being fulfilled (in the sense of the trace mapping theorem 3.2.1).

The homogenized problem is obviously very similar in its structure to Problem 3 and an unique solution will once again be ensured by the theorem of Lax–Milgram 3.3.2. But a few questions have to be answered beforehand as the introduction of the effective tensors may lead to some issues. First, since all involved quantities are at least square-integrable the integrals for the effective tensors are well-defined thanks to Hölder's inequality (3.3.8). Moreover, as constants they fulfill the assumption to be essentially bounded in the Lax–Milgram analysis.

Another concern lies within the definition of the effective coupling tensors. The formulas given above are derived directly from inserting the linear combinations for $\mathbf{u}_{\kappa,1}$ and $\psi_{\kappa,1}$ from Theorem 4.2.6 and allow to exchange the regular coupling tensor $\mathbf{e}$ and its transpose within the magneto-elastic problem for $\mathbf{e}^{\mathrm{eff}}$ and $\tilde{\mathbf{e}}^{\mathrm{eff}}$. The fact that both equations of the system make use of the same coupling tensor played an important role in the definition of the combined linear and bilinear forms at the end of Sect. 3.2 and the successful proofs given afterwards. It is not clear for right now though, whether or not $\mathbf{e}^{\mathrm{eff}}$ and $\tilde{\mathbf{e}}^{\mathrm{eff}}$ expose the same kind of relation of being transposed to each other. The proof relies heavily on some equalities derived from the weak form of the cell problem.

Lemma 4.2.7. *Let all quantities be defined according to the cell problem (Problem 4) and the definition of the correctors (Definition 4.2.4).*

1. *For all* $\omega \in \mathcal{H}^1\left(\mathbb{T}^d, \mathbb{R}^d\right)/\mathbb{R}^d$ *and* $i = 1, \ldots, \tilde{d}$ *one has*

$$\int_{\mathbb{T}^d} \left(\varepsilon_{\mathbf{y}}\left(\omega\right)\right)^{\mathrm{T}} \mathbf{C}\left(\mathbf{z}_i^{\mathrm{mech}} + \varepsilon_{\mathbf{y}}\left(\omega_i^{\mathrm{mech}}\right)\right)\,\mathrm{d}\,\mathbf{y} = \int_{\mathbb{T}^d} \left(\varepsilon_{\mathbf{y}}\left(\omega\right)\right)^{\mathrm{T}} \mathbf{e}\,\mathbf{H}_{\mathbf{y}}\left(\varrho_i^{\mathrm{mech}}\right)\,\mathrm{d}\,\mathbf{y}\,.$$

2. *For all* $\varrho \in \mathcal{H}^1\left(\mathbb{T}^d, \mathbb{R}\right)/\mathbb{R}$ *and* $i = 1, \ldots, \tilde{d}$ *one has*

$$\int_{\mathbb{T}^d} \left(\mathbf{H}_{\mathbf{y}}\left(\varrho\right)\right)^{\mathrm{T}} \mathbf{e}^{\mathrm{T}}\left(\mathbf{z}_i^{\mathrm{mech}} + \varepsilon_{\mathbf{y}}\left(\omega_i^{\mathrm{mech}}\right)\right)\,\mathrm{d}\,\mathbf{y} = -\int_{\mathbb{T}^d} \left(\mathbf{H}_{\mathbf{y}}\left(\varrho\right)\right)^{\mathrm{T}} \boldsymbol{\mu}\,\mathbf{H}_{\mathbf{y}}\left(\varrho_i^{\mathrm{mech}}\right)\,\mathrm{d}\,\mathbf{y}\,.$$

3. *For all* $\omega \in \mathcal{H}^1\left(\mathbb{T}^d, \mathbb{R}^d\right)/\mathbb{R}^d$ *and* $j = 1, \ldots, d$ *one has*

$$\int_{\mathbb{T}^d} \left(\varepsilon_{\mathbf{y}}\left(\omega\right)\right)^{\mathrm{T}} \mathbf{e}\left(\mathbf{z}_j^{\mathrm{mag}} + \mathbf{H}_{\mathbf{y}}\left(\varrho_j^{\mathrm{mag}}\right)\right)\,\mathrm{d}\,\mathbf{y} = \int_{\mathbb{T}^d} \left(\varepsilon_{\mathbf{y}}\left(\omega\right)\right)^{\mathrm{T}} \mathbf{C}\,\varepsilon_{\mathbf{y}}\left(\omega_j^{\mathrm{mag}}\right)\,\mathrm{d}\,\mathbf{y}\,.$$

4. *For all* $\varrho \in \mathcal{H}^1\left(\mathbb{T}^d, \mathbb{R}\right)/\mathbb{R}$ *and* $j = 1, \ldots, d$ *one has*

$$\int_{\mathbb{T}^d} \left(\mathbf{H}_{\mathbf{y}}\left(\varrho\right)\right)^{\mathrm{T}} \boldsymbol{\mu}\left(\mathbf{z}_j^{\mathrm{mag}} + \mathbf{H}_{\mathbf{y}}\left(\varrho_j^{\mathrm{mag}}\right)\right)\,\mathrm{d}\,\mathbf{y} = -\int_{\mathbb{T}^d} \left(\mathbf{H}_{\mathbf{y}}\left(\varrho\right)\right)^{\mathrm{T}} \mathbf{e}^{\mathrm{T}}\,\varepsilon_{\mathbf{y}}\left(\omega_j^{\mathrm{mag}}\right)\,\mathrm{d}\,\mathbf{y}\,.$$

Proof. Let $\omega \in \mathcal{H}^1\left(\mathbb{T}^d, \mathbb{R}^d\right)/\mathbb{R}^d$ and $\varrho \in \mathcal{H}^1\left(\mathbb{T}^d, \mathbb{R}\right)/\mathbb{R}$ be arbitrary. Then multiplying the corrector problems from Definition 4.2.4 with these functions, integrating over the torus and partial integration yield the corresponding weak forms

$$\begin{aligned}
\int_{\mathbb{T}^d} \left(\boldsymbol{\varepsilon}_{\mathbf{y}}(\omega)\right)^{\mathrm{T}} \mathbf{C}\, \boldsymbol{\varepsilon}_{\mathbf{y}}\left(\omega_i^{\mathrm{mech}}\right) - \left(\boldsymbol{\varepsilon}_{\mathbf{y}}(\omega)\right)^{\mathrm{T}} \mathbf{e}\, \mathbf{H}_{\mathbf{y}}\left(\varrho_i^{\mathrm{mech}}\right) \,\mathrm{d}\mathbf{y} &= -\int_{\mathbb{T}^d} \left(\boldsymbol{\varepsilon}_{\mathbf{y}}(\omega)\right)^{\mathrm{T}} \mathbf{C}\, \mathbf{z}_i^{\mathrm{mech}} \,\mathrm{d}\mathbf{y}\,, \\
\int_{\mathbb{T}^d} \left(\mathbf{H}_{\mathbf{y}}(\varrho)\right)^{\mathrm{T}} \mathbf{e}^{\mathrm{T}}\, \boldsymbol{\varepsilon}_{\mathbf{y}}\left(\omega_i^{\mathrm{mech}}\right) + \left(\mathbf{H}_{\mathbf{y}}(\varrho)\right)^{\mathrm{T}} \boldsymbol{\mu}\, \mathbf{H}_{\mathbf{y}}\left(\varrho_i^{\mathrm{mech}}\right) \,\mathrm{d}\mathbf{y} &= -\int_{\mathbb{T}^d} \left(\mathbf{H}_{\mathbf{y}}(\varrho)\right)^{\mathrm{T}} \mathbf{e}^{\mathrm{T}}\, \mathbf{z}_i^{\mathrm{mech}} \,\mathrm{d}\mathbf{y}
\end{aligned}$$

for $i = 1, \ldots, \tilde{d}$ and

$$\begin{aligned}
\int_{\mathbb{T}^d} \left(\boldsymbol{\varepsilon}_{\mathbf{y}}(\omega)\right)^{\mathrm{T}} \mathbf{C}\, \boldsymbol{\varepsilon}_{\mathbf{y}}\left(\omega_j^{\mathrm{mag}}\right) - \left(\boldsymbol{\varepsilon}_{\mathbf{y}}(\omega)\right)^{\mathrm{T}} \mathbf{e}\, \mathbf{H}_{\mathbf{y}}\left(\varrho_j^{\mathrm{mag}}\right) \,\mathrm{d}\mathbf{y} &= \int_{\mathbb{T}^d} \left(\boldsymbol{\varepsilon}_{\mathbf{y}}(\omega)\right)^{\mathrm{T}} \mathbf{e}\, \mathbf{z}_j^{\mathrm{mag}} \,\mathrm{d}\mathbf{y}\,, \\
\int_{\mathbb{T}^d} \left(\mathbf{H}_{\mathbf{y}}(\varrho)\right)^{\mathrm{T}} \mathbf{e}^{\mathrm{T}}\, \boldsymbol{\varepsilon}_{\mathbf{y}}\left(\omega_j^{\mathrm{mag}}\right) + \left(\mathbf{H}_{\mathbf{y}}(\varrho)\right)^{\mathrm{T}} \boldsymbol{\mu}\, \mathbf{H}_{\mathbf{y}}\left(\varrho_j^{\mathrm{mag}}\right) \,\mathrm{d}\mathbf{y} &= -\int_{\mathbb{T}^d} \left(\mathbf{H}_{\mathbf{y}}(\varrho)\right)^{\mathrm{T}} \boldsymbol{\mu}\, \mathbf{z}_j^{\mathrm{mag}} \,\mathrm{d}\mathbf{y}
\end{aligned}$$

for $j = 1, \ldots, d$. Rearranging the terms leads to the desired equations. □

Lemma 4.2.8. *Let $\mathbf{e}^{\mathrm{eff}} \in \mathbb{R}^{\tilde{d}\times d}$ and $\tilde{\mathbf{e}}^{\mathrm{eff}} \in \mathbb{R}^{d\times\tilde{d}}$ denote the effective coupling tensors defined in Problem 5. Then the relation $\left(\mathbf{e}^{\mathrm{eff}}\right)^{\mathrm{T}} = \tilde{\mathbf{e}}^{\mathrm{eff}}$ holds true.*

Proof. It is sufficient to prove that all entries of the difference $\left(\mathbf{e}^{\mathrm{eff}}\right)^{\mathrm{T}} - \tilde{\mathbf{e}}^{\mathrm{eff}}$ are equal to zero. For $i = 1, \ldots, \tilde{d}$ and $j = 1, \ldots, d$ one has according to Problem 5 the form

$$\begin{aligned}
\left(\left(\mathbf{e}^{\mathrm{eff}}\right)^{\mathrm{T}} - \tilde{\mathbf{e}}^{\mathrm{eff}}\right)_{ji} &= \int_{\mathbb{T}^d} \mathbf{e}_{ij} - \sum_{k=1}^{\tilde{d}} \mathbf{C}_{ik} \left(\boldsymbol{\varepsilon}_{\mathbf{y}}\left(\omega_j^{\mathrm{mag}}\right)\right)_k + \sum_{l=1}^{d} \mathbf{e}_{il} \left(\mathbf{H}_{\mathbf{y}}\left(\varrho_j^{\mathrm{mag}}\right)\right)_l \,\mathrm{d}\mathbf{y} \\
&\quad - \int_{\mathbb{T}^d} \mathbf{e}_{ij} + \sum_{k=1}^{\tilde{d}} \mathbf{e}_{kj} \left(\boldsymbol{\varepsilon}_{\mathbf{y}}\left(\omega_i^{\mathrm{mech}}\right)\right)_k + \sum_{l=1}^{d} \boldsymbol{\mu}_{jl} \left(\mathbf{H}_{\mathbf{y}}\left(\varrho_i^{\mathrm{mech}}\right)\right)_l \,\mathrm{d}\mathbf{y}\,.
\end{aligned}$$

These lines can be rewritten using unit vectors. This gives

$$\begin{aligned}
\left(\left(\mathbf{e}^{\mathrm{eff}}\right)^{\mathrm{T}} - \tilde{\mathbf{e}}^{\mathrm{eff}}\right)_{ji} &= \int_{\mathbb{T}^d} \left(\mathbf{z}_i^{\mathrm{mech}}\right)^{\mathrm{T}} \mathbf{e} \left(\mathbf{z}_j^{\mathrm{mag}} + \mathbf{H}_{\mathbf{y}}\left(\varrho_j^{\mathrm{mag}}\right)\right) - \left(\mathbf{z}_i^{\mathrm{mech}}\right)^{\mathrm{T}} \mathbf{C}\, \boldsymbol{\varepsilon}_{\mathbf{y}}\left(\omega_j^{\mathrm{mag}}\right) \,\mathrm{d}\mathbf{y} \\
&\quad - \int_{\mathbb{T}^d} \left(\mathbf{z}_j^{\mathrm{mag}}\right)^{\mathrm{T}} \mathbf{e}^{\mathrm{T}} \left(\mathbf{z}_i^{\mathrm{mech}} + \boldsymbol{\varepsilon}_{\mathbf{y}}\left(\omega_i^{\mathrm{mech}}\right)\right) + \left(\mathbf{z}_j^{\mathrm{mag}}\right)^{\mathrm{T}} \boldsymbol{\mu}\, \mathbf{H}_{\mathbf{y}}\left(\varrho_i^{\mathrm{mech}}\right) \,\mathrm{d}\mathbf{y}\,.
\end{aligned}$$

Next, artificial zeros are created by adding the second and third formula from Lemma 4.2.7 with $\omega = \omega_i^{\mathrm{mech}}$ and $\varrho = \varrho_j^{\mathrm{mag}}$. One obtains

$$\begin{aligned}
\left(\left(\mathbf{e}^{\mathrm{eff}}\right)^{\mathrm{T}} - \tilde{\mathbf{e}}^{\mathrm{eff}}\right)_{ji} &= \int_{\mathbb{T}^d} \left(\mathbf{z}_i^{\mathrm{mech}} + \boldsymbol{\varepsilon}_{\mathbf{y}}\left(\omega_i^{\mathrm{mech}}\right)\right)^{\mathrm{T}} \mathbf{e} \left(\mathbf{z}_j^{\mathrm{mag}} + \mathbf{H}_{\mathbf{y}}\left(\varrho_j^{\mathrm{mag}}\right)\right) \,\mathrm{d}\mathbf{y} \\
&\quad - \int_{\mathbb{T}^d} \left(\mathbf{z}_i^{\mathrm{mech}} + \boldsymbol{\varepsilon}_{\mathbf{y}}\left(\omega_i^{\mathrm{mech}}\right)\right)^{\mathrm{T}} \mathbf{C}\, \boldsymbol{\varepsilon}_{\mathbf{y}}\left(\omega_j^{\mathrm{mag}}\right) \,\mathrm{d}\mathbf{y} \\
&\quad - \int_{\mathbb{T}^d} \left(\mathbf{z}_j^{\mathrm{mag}} + \mathbf{H}_{\mathbf{y}}\left(\varrho_j^{\mathrm{mag}}\right)\right)^{\mathrm{T}} \mathbf{e}^{\mathrm{T}} \left(\mathbf{z}_i^{\mathrm{mech}} + \varepsilon\left(\omega_i^{\mathrm{mech}}\right)\right) \,\mathrm{d}\mathbf{y} \\
&\quad - \int_{\mathbb{T}^d} \left(\mathbf{z}_j^{\mathrm{mag}} + \mathbf{H}_{\mathbf{y}}\left(\varrho_j^{\mathrm{mag}}\right)\right)^{\mathrm{T}} \boldsymbol{\mu}\, \mathbf{H}_{\mathbf{y}}\left(\varrho_i^{\mathrm{mech}}\right) \,\mathrm{d}\mathbf{y}
\end{aligned}$$

which after canceling some terms leaves

$$\begin{aligned}\left(\left(\mathbf{e}^{\mathrm{eff}}\right)^{\mathrm{T}} - \tilde{\mathbf{e}}^{\mathrm{eff}}\right)_{ji} &= \int_{\mathbb{T}^d} \left(\mathbf{z}_j^{\mathrm{mag}} + \mathbf{H}_{\mathbf{y}}\left(\varrho_j^{\mathrm{mag}}\right)\right)^{\mathrm{T}} \boldsymbol{\mu}\, \mathbf{H}_{\mathbf{y}}\left(\varrho_i^{\mathrm{mech}}\right) \,\mathrm{d}\mathbf{y} \\ &\quad - \int_{\mathbb{T}^d} \left(\mathbf{z}_i^{\mathrm{mech}} + \boldsymbol{\varepsilon}_{\mathbf{y}}\left(\omega_i^{\mathrm{mech}}\right)\right)^{\mathrm{T}} \mathbf{C}\, \boldsymbol{\varepsilon}_{\mathbf{y}}\left(\omega_j^{\mathrm{mag}}\right) \,\mathrm{d}\mathbf{y} \,.\end{aligned}$$

Applying now the first and fourth formula from Lemma 4.2.7 proves the claim as the final expression

$$\begin{aligned}\left(\left(\mathbf{e}^{\mathrm{eff}}\right)^{\mathrm{T}} - \tilde{\mathbf{e}}^{\mathrm{eff}}\right)_{ji} &= \int_{\mathbb{T}^d} \left(\boldsymbol{\varepsilon}_{\mathbf{y}}\left(\omega_j^{\mathrm{mag}}\right)\right)^{\mathrm{T}} \mathbf{e}\, \mathbf{H}_{\mathbf{y}}\left(\varrho_i^{\mathrm{mech}}\right) \,\mathrm{d}\mathbf{y} \\ &\quad - \int_{\mathbb{T}^d} \left(\mathbf{H}_{\mathbf{y}}\left(\varrho_i^{\mathrm{mech}}\right)\right)^{\mathrm{T}} \mathbf{e}^{\mathrm{T}}\, \boldsymbol{\varepsilon}_{\mathbf{y}}\left(\omega_j^{\mathrm{mag}}\right) \,\mathrm{d}\mathbf{y}\end{aligned}$$

vanishes. □

From now on the notation $\tilde{\mathbf{e}}^{\mathrm{eff}}$ will be dropped for this reason and $\left(\mathbf{e}^{\mathrm{eff}}\right)^{\mathrm{T}}$ will be used instead. Lastly, the effective stiffness and permeability tensors need to fulfill the ellipticity condition (3.61) for the bilinear forms to be coercive. Again with the help of Lemma 4.2.7, this property should follow from the ellipticity of the original tensors. To the author's great regret however, a complete proof for this statement is yet missing. Instead, only a proof idea will be laid out with the yet unproven parts explicitly mentioned as going through it.

Lemma 4.2.9. *Let $\mathbf{C}^{\mathrm{eff}} \in \mathbb{R}^{\tilde{d}\times\tilde{d}}$ and $\boldsymbol{\mu}^{\mathrm{eff}} \in \mathbb{R}^{d\times d}$ denote the effective stiffness and permeability tensors defined in Problem 5. Then both tensors fulfill the ellipticity condition 3.61, i.e. there exist constants $\gamma_{\mathbf{C}^{\mathrm{eff}}}, \gamma_{\boldsymbol{\mu}^{\mathrm{eff}}} > 0$, such that*

$$\begin{aligned}\mathbf{a}^{\mathrm{T}}\, \mathbf{C}^{\mathrm{eff}}\, \mathbf{a} &\geq \gamma_{\mathbf{C}^{\mathrm{eff}}} \|\mathbf{a}\|^2 \quad \text{for all } \mathbf{a} \in \mathbb{R}^{\tilde{d}}\,, \\ \mathbf{b}^{\mathrm{T}}\, \boldsymbol{\mu}^{\mathrm{eff}}\, \mathbf{b} &\geq \gamma_{\boldsymbol{\mu}^{\mathrm{eff}}} \|\mathbf{b}\|^2 \quad \text{for all } \mathbf{b} \in \mathbb{R}^{d}\,.\end{aligned}$$

Proof. (*incomplete*) To prove the claim one wishes to show that $\mathbf{C}^{\mathrm{eff}}$ is a symmetric, positive definite matrix. Starting with the definition of the entries of $\mathbf{C}^{\mathrm{eff}}$, one successively applies the first and second equation from Lemma 4.2.7 to obtain

$$\begin{aligned}\mathbf{C}^{\mathrm{eff}}_{mn} &= \int_{\mathbb{T}^d} \mathbf{C}_{mn} + \sum_{k=1}^{\tilde{d}} \mathbf{C}_{mk}\left(\boldsymbol{\varepsilon}_{\mathbf{y}}\left(\omega_n^{\mathrm{mech}}\right)\right)_k - \sum_{l=1}^{d} \mathbf{e}_{ml}\left(\mathbf{H}_{\mathbf{y}}\left(\varrho_n^{\mathrm{mech}}\right)\right)_l \,\mathrm{d}\mathbf{y} \\ &= \int_{\mathbb{T}^d} \left(\mathbf{z}_m^{\mathrm{mech}}\right)^{\mathrm{T}} \mathbf{C}\left(\mathbf{z}_n^{\mathrm{mech}} + \boldsymbol{\varepsilon}_{\mathbf{y}}\left(\omega_n^{\mathrm{mech}}\right)\right) \,\mathrm{d}\mathbf{y} - \int_{\mathbb{T}^d} \left(\mathbf{z}_m^{\mathrm{mech}}\right)^{\mathrm{T}} \mathbf{e}\, \mathbf{H}_{\mathbf{y}}\left(\varrho_n^{\mathrm{mech}}\right) \,\mathrm{d}\mathbf{y} \\ &= \int_{\mathbb{T}^d} \left(\mathbf{z}_m^{\mathrm{mech}} + \boldsymbol{\varepsilon}_{\mathbf{y}}\left(\omega_m^{\mathrm{mech}}\right)\right)^{\mathrm{T}} \mathbf{C}\left(\mathbf{z}_n^{\mathrm{mech}} + \boldsymbol{\varepsilon}_{\mathbf{y}}\left(\omega_n^{\mathrm{mech}}\right)\right) - \left(\mathbf{z}_m^{\mathrm{mech}} + \boldsymbol{\varepsilon}_{\mathbf{y}}\left(\omega_m^{\mathrm{mech}}\right)\right)^{\mathrm{T}} \mathbf{e}\, \mathbf{H}_{\mathbf{y}}\left(\varrho_n^{\mathrm{mech}}\right) \,\mathrm{d}\mathbf{y} \\ &= \int_{\mathbb{T}^d} \left(\mathbf{z}_m^{\mathrm{mech}} + \boldsymbol{\varepsilon}_{\mathbf{y}}\left(\omega_m^{\mathrm{mech}}\right)\right)^{\mathrm{T}} \mathbf{C}\left(\mathbf{z}_n^{\mathrm{mech}} + \boldsymbol{\varepsilon}_{\mathbf{y}}\left(\omega_n^{\mathrm{mech}}\right)\right) + \left(\mathbf{H}_{\mathbf{y}}\left(\varrho_m^{\mathrm{mech}}\right)\right)^{\mathrm{T}} \boldsymbol{\mu}\, \mathbf{H}_{\mathbf{y}}\left(\varrho_n^{\mathrm{mech}}\right) \,\mathrm{d}\mathbf{y}\end{aligned}$$

for all $m, n = 1, \ldots, \tilde{d}$. This shows that $\mathbf{C}^{\mathrm{eff}}$ is symmetric. Furthermore, for an arbitrary vector $\mathbf{a} \in \mathbb{R}^{\tilde{d}}$ with $\mathbf{a} \neq 0$ one has

$$\begin{aligned}\mathbf{a}^{\mathrm{T}}\, \mathbf{C}^{\mathrm{eff}}\, \mathbf{a} = \sum_{m,n=1}^{\tilde{d}} \mathbf{a}_m\, \mathbf{C}^{\mathrm{eff}}_{mn}\, \mathbf{a}_n &= \int_{\mathbb{T}^d} \left(\mathbf{a} + \sum_{m=1}^{\tilde{d}} \mathbf{a}_m\, \boldsymbol{\varepsilon}_{\mathbf{y}}\left(\omega_m^{\mathrm{mech}}\right)\right)^{\mathrm{T}} \mathbf{C}\left(\mathbf{a} + \sum_{n=1}^{\tilde{d}} \mathbf{a}_n\, \boldsymbol{\varepsilon}_{\mathbf{y}}\left(\omega_n^{\mathrm{mech}}\right)\right) \,\mathrm{d}\mathbf{y} \\ &\quad + \int_{\mathbb{T}^d} \left(\sum_{m=1}^{\tilde{d}} \mathbf{a}_m\, \mathbf{H}_{\mathbf{y}}\left(\varrho_m^{\mathrm{mech}}\right)\right)^{\mathrm{T}} \boldsymbol{\mu}\left(\sum_{n=1}^{\tilde{d}} \mathbf{a}_n\, \mathbf{H}_{\mathbf{y}}\left(\varrho_n^{\mathrm{mech}}\right)\right) \,\mathrm{d}\mathbf{y}\end{aligned}$$

which leads to the estimate

$$\mathbf{a}^{\mathrm{T}}\,\mathbf{C}^{\mathrm{eff}}\,\mathbf{a} \geq \gamma_{\mathbf{C}} \int\limits_{\mathbb{T}^d} \left\| \mathbf{a} + \sum_{m=1}^{\tilde{d}} \mathbf{a}_m\, \boldsymbol{\varepsilon}_{\mathbf{y}}\left(\omega_m^{\mathrm{mech}}\right) \right\|^2 \mathrm{d}\,\mathbf{y} + \gamma_{\boldsymbol{\mu}} \int\limits_{\mathbb{T}^d} \left\| \sum_{m=1}^{\tilde{d}} \mathbf{a}_m\, \mathbf{H}_{\mathbf{y}}\left(\varrho_m^{\mathrm{mech}}\right) \right\|^2 \mathrm{d}\,\mathbf{y}$$

where $\gamma_{\mathbf{C}}$ and $\gamma_{\boldsymbol{\mu}}$ are the ellipticity constants from $\mathbf{C}$ and $\boldsymbol{\mu}$. If one were now able to show that the two occurring norms never happen to simultaneously be equal to zero, it would follow that $\mathbf{C}^{\mathrm{eff}}$ is also positive definite and possesses only positive eigenvalues λ_i with $i = 1, \ldots, \tilde{d}$. Because $\mathbf{C}^{\mathrm{eff}}$ is a symmetric and real-valued matrix as shown above, the corresponding eigenvectors $\mathbf{o}_i$ would form an orthonormal basis of $\mathbb{R}^{\tilde{d}}$. With coefficients α_i let $\sum_{i=1}^{\tilde{d}} \alpha_i \mathbf{o}_i$ be the unique linear combination of the vector $\mathbf{a}$. Then the ellipticity condition would be fulfilled, since

$$\mathbf{a}^{\mathrm{T}}\,\mathbf{C}\,\mathbf{a} = \left(\sum_{i=1}^{\tilde{d}} \alpha_i \mathbf{o}_i\right)^{\mathrm{T}} \mathbf{C} \left(\sum_{j=1}^{\tilde{d}} \alpha_j \mathbf{o}_j\right) = \sum_{i=1}^{\tilde{d}} \lambda_i \alpha_i^2 \geq \min_i \{\lambda_i\} \sum_{i=1}^{\tilde{d}} \alpha_i^2 = \min_i \{\lambda_i\}\, \|\mathbf{a}\|^2 \ .$$

Similarly, using the third and fourth equation from Lemma 4.2.7, $\boldsymbol{\mu}^{\mathrm{eff}}$ takes the form

$$\begin{aligned}
\boldsymbol{\mu}_{mn}^{\mathrm{eff}} &= \int\limits_{\mathbb{T}^d} \boldsymbol{\mu}_{mn} + \sum_{k=1}^{\tilde{d}} \mathbf{e}_{km}\left(\boldsymbol{\varepsilon}_{\mathbf{y}}\left(\omega_n^{\mathrm{mag}}\right)\right)_k + \sum_{l=1}^{d} \boldsymbol{\mu}_{ml}\left(\mathbf{H}_{\mathbf{y}}\left(\varrho_n^{\mathrm{mag}}\right)\right)_l \,\mathrm{d}\,\mathbf{y} \\
&= \int\limits_{\mathbb{T}^d} \left(\mathbf{z}_m^{\mathrm{mag}}\right)^{\mathrm{T}} \boldsymbol{\mu}\left(\mathbf{z}_n^{\mathrm{mag}} + \mathbf{H}_{\mathbf{y}}\left(\varrho_n^{\mathrm{mag}}\right)\right) \mathrm{d}\,\mathbf{y} + \int\limits_{\mathbb{T}^d} \left(\mathbf{z}_m^{\mathrm{mag}}\right)^{\mathrm{T}} \mathbf{e}^{\mathrm{T}}\, \boldsymbol{\varepsilon}_{\mathbf{y}}\left(\omega_n^{\mathrm{mag}}\right) \mathrm{d}\,\mathbf{y} \\
&= \int\limits_{\mathbb{T}^d} \left(\mathbf{z}_m^{\mathrm{mag}} + \mathbf{H}_{\mathbf{y}}\left(\varrho_m^{\mathrm{mag}}\right)\right)^{\mathrm{T}} \boldsymbol{\mu}\left(\mathbf{z}_n^{\mathrm{mag}} + \mathbf{H}_{\mathbf{y}}\left(\varrho_n^{\mathrm{mag}}\right)\right) + \left(\mathbf{z}_m^{\mathrm{mag}} + \mathbf{H}_{\mathbf{y}}\left(\varrho_m^{\mathrm{mag}}\right)\right)^{\mathrm{T}} \mathbf{e}^{\mathrm{T}}\, \boldsymbol{\varepsilon}_{\mathbf{y}}\left(\omega_n^{\mathrm{mag}}\right) \mathrm{d}\,\mathbf{y} \\
&= \int\limits_{\mathbb{T}^d} \left(\mathbf{z}_m^{\mathrm{mag}} + \mathbf{H}_{\mathbf{y}}\left(\varrho_m^{\mathrm{mag}}\right)\right)^{\mathrm{T}} \boldsymbol{\mu}\left(\mathbf{z}_n^{\mathrm{mag}} + \mathbf{H}_{\mathbf{y}}\left(\varrho_n^{\mathrm{mag}}\right)\right) + \left(\boldsymbol{\varepsilon}_{\mathbf{y}}\left(\omega_n^{\mathrm{mag}}\right)\right)^{\mathrm{T}} \mathbf{C}\, \boldsymbol{\varepsilon}_{\mathbf{y}}\left(\omega_m^{\mathrm{mag}}\right) \mathrm{d}\,\mathbf{y}
\end{aligned}$$

for all $m, n = 1, \ldots, \tilde{d}$. For an arbitrary vector $\mathbf{b} \in \mathbb{R}^d$ with $\mathbf{b} \neq 0$ one has

$$\begin{aligned}
\mathbf{b}^{\mathrm{T}}\,\boldsymbol{\mu}^{\mathrm{eff}}\,\mathbf{b} = \sum_{m,n=1}^{d} \mathbf{b}_m\, \boldsymbol{\mu}_{mn}^{\mathrm{eff}}\, \mathbf{b}_n &= \int\limits_{\mathbb{T}^d} \left(\mathbf{b} + \sum_{m=1}^{d} \mathbf{b}_m\, \mathbf{H}_{\mathbf{y}}\left(\varrho_m^{\mathrm{mag}}\right)\right)^{\mathrm{T}} \boldsymbol{\mu} \left(\mathbf{b} + \sum_{n=1}^{d} \mathbf{b}_n\, \mathbf{H}_{\mathbf{y}}\left(\varrho_n^{\mathrm{mag}}\right)\right) \mathrm{d}\,\mathbf{y} \\
&\quad + \int\limits_{\mathbb{T}^d} \left(\sum_{m=1}^{d} \mathbf{b}_m\, \boldsymbol{\varepsilon}_{\mathbf{y}}\left(\omega_m^{\mathrm{mag}}\right)\right)^{\mathrm{T}} \mathbf{C} \left(\sum_{n=1}^{d} \mathbf{b}_n\, \boldsymbol{\varepsilon}_{\mathbf{y}}\left(\omega_n^{\mathrm{mag}}\right)\right) \mathrm{d}\,\mathbf{y} \ ,
\end{aligned}$$

which leads to the estimate

$$\mathbf{b}^{\mathrm{T}}\,\boldsymbol{\mu}^{\mathrm{eff}}\,\mathbf{b} \geq \gamma_{\boldsymbol{\mu}} \int\limits_{\mathbb{T}^d} \left\| \mathbf{b} + \sum_{m=1}^{d} \mathbf{b}_m\, \mathbf{H}_{\mathbf{y}}\left(\varrho_m^{\mathrm{mag}}\right) \right\|^2 \mathrm{d}\,\mathbf{y} + \gamma_{\mathbf{C}} \int\limits_{\mathbb{T}^d} \left\| \sum_{m=1}^{d} \mathbf{b}_m\, \boldsymbol{\varepsilon}_{\mathbf{y}}\left(\omega_m^{\mathrm{mag}}\right) \right\|^2 \mathrm{d}\,\mathbf{y} \ .$$

Again, if at least one the norms involved is different from zero, this would prove $\boldsymbol{\mu}^{\mathrm{eff}}$ to be a symmetric, positive definite matrix as well which would therefore fulfill the ellipticity condition due to the same arguments as for $\mathbf{C}^{\mathrm{eff}}$ before. □

The resulting existence and uniqueness statement is once again formally captured in its own theorem.

Theorem 4.2.10. *The homogenized problem (Problem 5) has a unique solution* $\left(\mathbf{u}_{\kappa,0}, \psi_{\kappa,0}\right) \in \mathcal{H}^1_{\mathrm{mix}}$.

Proof. Due to Lemma 4.2.8 and Lemma 4.2.9, the conditions for the Lax–Milgram theorem 3.3.2 are met. The problem furthermore only depends on the $\mathbf{x}$-variable explicitly. □

Remark. *The ideas and techniques used to define the effective quantities from the correctors or to prove the applicability of Lax–Milgram for the homogenized problem can also be transferred to other coupled problems of larger complexity which may also include electrical or thermal effects [1, 13, 68]. For simple structures such as laminates it is also possible to compute the effective tensor entries explicitly without having to approximate an integral.*

4.3 Two-Scale Convergence

The asymptotic expansion approach allowed the definition of two separate problems — the cell and the homogenized one — with their own spatial variables and domains. However, while the ultimate goal of finding a limit to Problem 3 for $\kappa \to 0$ was achieved through the solution of said homogenized problem which was indeed constructed with constant substitute materials, the derivation of the problem hierarchy does not appear to be mathematically sound. Moreover, the construction of the homogenized problem only follows after a chain of arguments long after the actual limit procedure. This appears rather inelegant as the limit process and the problem surrounding it which is supposed to link back to the original problem with periodic coefficients are derived one after the other. One would rather wish for the homogenized problem to emerge instantly as a result of the limit procedure.

To cope with these issues, the theoretical framework of *two-scale convergence* will be established. This concept was first introduced by Gabriel Nguetseng [90] and further developed by Grégoire Allaire [2]. It formally establishes a connection between the domain Ω and the torus and justifies the interpretation of $\mathbf{x}/\kappa$ as its own independent variable $\mathbf{y}$. To emphasize the differentiation between these two and to avoid confusion when integrating over Ω and $\mathbb{T}^d$ simultaneously, the arguments of most quantities will be written down explicitly in this section. Since the general idea of scale separation remains untouched, the resulting equations will coincide with Problems 4 and 5 and the afore presented analysis regarding existence and uniqueness carries over almost completely.

Definition 4.3.1. *Let $(f_\kappa)_{\kappa>0}$ be a sequence of functions in $L^2(\Omega)$.*
If there exists a function $f_0 \in L^2\left(\Omega \times \mathbb{T}^d\right)$ such that for all $g \in \mathcal{D}\left(\Omega, \mathcal{C}^\infty\left(\mathbb{T}^d\right)\right)$ the limit

$$\lim_{\kappa\to 0} \int_\Omega f_\kappa(\mathbf{x})\, g\left(\mathbf{x}, \frac{\mathbf{x}}{\kappa}\right) \mathrm{d}\mathbf{x} = \int_{\Omega\times\mathbb{T}^d} f_0(\mathbf{x},\mathbf{y})\, g(\mathbf{x},\mathbf{y}) \;\mathrm{d}\mathbf{x}\;\mathrm{d}\mathbf{y}$$

holds true, the sequence $(f_\kappa)_{\kappa>0}$ is two-scale convergent with the limit f_0 for $\kappa \to 0$. One then also writes $f_\kappa \twoheadrightarrow f_0$.

The space $\mathcal{D}\left(\Omega, \mathcal{C}^\infty\left(\mathbb{T}^d\right)\right)$ here denotes the set of all measurable functions g defined on $\Omega \times \mathbb{T}^d$ such that $g(\mathbf{x}, \cdot) \in \mathcal{C}^\infty\left(\mathbb{T}^d\right)$ for any $\mathbf{x} \in \Omega$ and such that the map $\mathbf{x} \mapsto g(\mathbf{x}, \cdot)$ is infinitely differentiable with a compact support in Ω. While two-scale convergence is sufficient enough for the herein discussed homogenization problems, the definition is easily extendable to the generalized concept of *n-scale convergence* [75, p. 29]. The central theorem for two-scale convergence in $\mathcal{H}^1$ ensures the existence of convergent subsequences and their limits, if the original sequence was bounded.

Theorem 4.3.2. *Let $(f_\kappa)_{\kappa>0}$ be a sequence bounded in $\mathcal{H}^1(\Omega)$. Then there exists a subsequence $(f_{\kappa_\ell})_{\ell\in\mathbb{N}}$, as well as functions $f_0 \in \mathcal{H}^1(\Omega)$ and $f_1 \in L^2\left(\Omega, \mathcal{H}^1\left(\mathbb{T}^d\right)/\mathbb{R}\right)$ such that*

$$\begin{aligned} f_{\kappa_\ell} &\twoheadrightarrow f_0\,, \\ \nabla f_{\kappa_\ell} &\twoheadrightarrow \nabla_{\mathbf{x}} f_0 + \nabla_{\mathbf{y}} f_1\,. \end{aligned}$$

Proof. It is known that a bounded sequence in a Hilbert space contains a weakly convergent subsequence; see for example [115, p. 247]. The remainder of the proof is then given in [22, p. 180 sq.]. □

The theorem above provides the starting point for the two-scale analysis of the coupled problem. Before going into the details however, one needs to know about two additional limits that are fulfilled for two-scale convergent series.

Lemma 4.3.3. *[Examples of admissible functions; Proof in [75, p. 11 sqq.]] Let $(f_\kappa)_{\kappa>0}$ be a sequence in $L^2(\Omega)$ which two-scales converges to $f_0 \in L^2\left(\Omega \times \mathbb{T}^d\right)$. If a function g was either in $L^2\left(\mathbb{T}^d, C(\Omega)\right)$ or of the form $g(\mathbf{x},\mathbf{y}) = g_1(\mathbf{x})\, g_2(\mathbf{y})$, with $g_1 \in L^2(\Omega)$ and $g_2 \in L^2\left(\mathbb{T}^d\right)$, one has*

$$\lim_{\kappa\to 0} \int_\Omega f_\kappa(\mathbf{x})\, g\left(\mathbf{x}, \frac{\mathbf{x}}{\kappa}\right) \mathrm{d}\mathbf{x} = \int_{\Omega\times\mathbb{T}^d} f_0(\mathbf{x},\mathbf{y})\, g(\mathbf{x},\mathbf{y}) \,\mathrm{d}\mathbf{x}\,\mathrm{d}\mathbf{y} \ .$$

Remark. *Lemma 4.3.3 can be seen as an extension of Definition 4.3.1 to a larger set of test functions. In fact, the two possibilities addressed here are only special cases of the more general concept of so-called admissible functions which the defining equation of two-scale convergence can be extended to [2, p. 1490]. A function g is considered to be admissible if*

$$\lim_{\kappa\to 0} \int_\Omega \left(g\left(\mathbf{x}, \frac{\mathbf{x}}{\kappa}\right)\right)^2 \mathrm{d}\mathbf{x} = \int_{\Omega\times\mathbb{T}^d} (g(\mathbf{x},\mathbf{y}))^2 \,\mathrm{d}\mathbf{x}\,\mathrm{d}\mathbf{y}$$

holds true. It is known that at least any functions that are continuous in one variable and measurable in the second one — also known as Carathéodory functions — fulfill this property, although a better characterization of the space of admissible functions remains unknown. More about admissible functions and some examples can be found in [2, 75].

To begin the two-scale analysis, the weak form of Problem 3 is recalled here. It consists of finding a pair of solutions $(\mathbf{u}_\kappa, \psi_\kappa) \in \mathcal{H}^1_{\mathrm{mix}} = \mathcal{H}^1_{\mathrm{mech}} \times \mathcal{H}^1_{\mathrm{mag}}$, such that

$$\begin{aligned}
\int_\Omega (\boldsymbol{\varepsilon}_{\mathbf{x}}(\mathbf{v}(\mathbf{x})))^{\mathrm{T}} \left(\mathbf{C}\left(\frac{\mathbf{x}}{\kappa}\right)\boldsymbol{\varepsilon}_{\mathbf{x}}(\mathbf{u}_\kappa(\mathbf{x})) - \mathbf{e}\left(\frac{\mathbf{x}}{\kappa}\right)\mathbf{H}_{\mathbf{x}}(\psi_\kappa(\mathbf{x}))\right) \mathrm{d}\mathbf{x} &= \int_\Omega (\mathbf{v}(\mathbf{x}))^{\mathrm{T}}\, \mathbf{f}^{\mathrm{mech}}(\mathbf{x})\, \mathrm{d}\mathbf{x}\,, \\
\int_\Omega (\mathbf{H}_{\mathbf{x}}(\phi(\mathbf{x})))^{\mathrm{T}} \left(\mathbf{e}^{\mathrm{T}}\left(\frac{\mathbf{x}}{\kappa}\right)\boldsymbol{\varepsilon}_{\mathbf{x}}(\mathbf{u}_\kappa(\mathbf{x})) + \boldsymbol{\mu}\left(\frac{\mathbf{x}}{\kappa}\right)\mathbf{H}_{\mathbf{x}}(\psi_\kappa(\mathbf{x}))\right) \mathrm{d}\mathbf{x} &= \int_\Omega \phi(\mathbf{x})\, \mathrm{f}^{\mathrm{mag}}(\mathbf{x})\, \mathrm{d}\mathbf{x}
\end{aligned}$$

are fulfilled for all pairs $(\mathbf{v}, \phi) \in \mathcal{H}^1_{\mathrm{mix}}$. From the Lax–Milgram theorem 3.3.2 one has the estimate

$$\|(\mathbf{u}_\kappa, \psi_\kappa)\|_{\mathcal{H}^1_{\mathrm{mix}}} \leq \frac{1}{\gamma}\, \|l\|_{(\mathcal{H}^1_{\mathrm{mix}})'} \ , \tag{4.19}$$

where l is the combined linear functional defined in (3.59) and γ is the coercivity constant of the corresponding bilinear form (3.58). Since the sequences are therefore bounded, one can extract subsequences according to Theorem 4.3.2 such that the displacement and the magnetic scalar potential each two-scale converge. A difference in notation between the original sequence and the subsequence will be left aside for better readability. However, one should keep in mind that the following findings

still have to be carried over to the whole sequence afterwards. There exist functions $\mathbf{u}_0 \in \mathcal{H}^1_{\text{mech}}$, $\psi_0 \in \mathcal{H}^1_{\text{mag}}, \mathbf{u}_1 \in L^2\left(\Omega, \mathcal{H}^1\left(\mathbb{T}^d, \mathbb{R}^d\right)/\mathbb{R}^d\right)$ and $\psi_1 \in L^2\left(\Omega, \mathcal{H}^1\left(\mathbb{T}^d, \mathbb{R}\right)/\mathbb{R}\right)$ such that

$$\begin{aligned} \mathbf{u}_\kappa &\twoheadrightarrow \mathbf{u}_0 \,, \\ \psi_\kappa &\twoheadrightarrow \psi_0 \,, \\ \boldsymbol{\varepsilon}\left(\mathbf{u}_\kappa\right) &\twoheadrightarrow \boldsymbol{\varepsilon}_{\mathbf{x}}\left(\mathbf{u}_0\right) + \boldsymbol{\varepsilon}_{\mathbf{y}}\left(\mathbf{u}_1\right) \,, \\ \mathbf{H}\left(\psi_\kappa\right) &\twoheadrightarrow \mathbf{H}_{\mathbf{x}}\left(\psi_0\right) + \mathbf{H}_{\mathbf{y}}\left(\psi_1\right) \,. \end{aligned} \tag{4.20}$$

To derive a variational two-scale formulation, the test functions $\mathbf{v}$ and ϕ are then chosen of the specific form

$$\begin{aligned} \mathbf{v}(\mathbf{x}) &= \mathbf{v}_0(\mathbf{x}) + \kappa\, \mathbf{v}_1\left(\mathbf{x}, \frac{\mathbf{x}}{\kappa}\right) \quad \text{with} \quad \mathbf{v}_0 \in \mathcal{D}\left(\Omega, \mathbb{R}^d\right), \mathbf{v}_1 \in \mathcal{D}\left(\Omega, \mathcal{C}^\infty\left(\mathbb{T}^d, \mathbb{R}^d\right)/\mathbb{R}^d\right) \,, \\ \phi(\mathbf{x}) &= \phi_0(\mathbf{x}) + \kappa\, \phi_1\left(\mathbf{x}, \frac{\mathbf{x}}{\kappa}\right) \quad \text{with} \quad \phi_0 \in \mathcal{D}(\Omega, \mathbb{R}), \phi_1 \in \mathcal{D}\left(\Omega, \mathcal{C}^\infty\left(\mathbb{T}^d, \mathbb{R}\right)/\mathbb{R}\right) \,. \end{aligned} \tag{4.21}$$

Computing the necessary derivatives as

$$\begin{aligned} \boldsymbol{\varepsilon}_{\mathbf{x}}\left(\mathbf{v}(\mathbf{x})\right) &= \boldsymbol{\varepsilon}_{\mathbf{x}}\left(\mathbf{v}_0(\mathbf{x})\right) + \kappa\, \boldsymbol{\varepsilon}_{\mathbf{x}}\left(\mathbf{v}_1\left(\mathbf{x}, \frac{\mathbf{x}}{\kappa}\right)\right) + \boldsymbol{\varepsilon}_{\mathbf{y}}\left(\mathbf{v}_1\left(\mathbf{x}, \frac{\mathbf{x}}{\kappa}\right)\right) \,, \\ \mathbf{H}_{\mathbf{x}}\left(\phi(\mathbf{x})\right) &= \mathbf{H}_{\mathbf{x}}\left(\phi_0(\mathbf{x})\right) + \kappa\, \mathbf{H}_{\mathbf{x}}\left(\phi_1\left(\mathbf{x}, \frac{\mathbf{x}}{\kappa}\right)\right) + \mathbf{H}_{\mathbf{y}}\left(\phi_1\left(\mathbf{x}, \frac{\mathbf{x}}{\kappa}\right)\right) \end{aligned} \tag{4.22}$$

leads to the weak forms

$$\begin{aligned} &\int_\Omega \left(\boldsymbol{\varepsilon}_{\mathbf{x}}\left(\mathbf{v}_0(\mathbf{x})\right) + \boldsymbol{\varepsilon}_{\mathbf{y}}\left(\mathbf{v}_1\left(\mathbf{x}, \frac{\mathbf{x}}{\kappa}\right)\right)\right)^{\mathrm{T}} \left(\mathbf{C}\left(\frac{\mathbf{x}}{\kappa}\right) \boldsymbol{\varepsilon}_{\mathbf{x}}\left(\mathbf{u}_\kappa(\mathbf{x})\right) - \mathbf{e}\left(\frac{\mathbf{x}}{\kappa}\right) \mathbf{H}_{\mathbf{x}}\left(\psi_\kappa(\mathbf{x})\right)\right) \mathrm{d}\mathbf{x} \\ + &\int_\Omega \left(\kappa\, \boldsymbol{\varepsilon}_{\mathbf{x}}\left(\mathbf{v}_1\left(\mathbf{x}, \frac{\mathbf{x}}{\kappa}\right)\right)\right)^{\mathrm{T}} \left(\mathbf{C}\left(\frac{\mathbf{x}}{\kappa}\right) \boldsymbol{\varepsilon}_{\mathbf{x}}\left(\mathbf{u}_\kappa(\mathbf{x})\right) - \mathbf{e}\left(\frac{\mathbf{x}}{\kappa}\right) \mathbf{H}_{\mathbf{x}}\left(\psi_\kappa(\mathbf{x})\right)\right) \mathrm{d}\mathbf{x} \\ = &\int_\Omega \left(\mathbf{v}_0(\mathbf{x}) + \kappa\, \mathbf{v}_1\left(\mathbf{x}, \frac{\mathbf{x}}{\kappa}\right)\right)^{\mathrm{T}} \mathbf{f}^{\text{mech}}(\mathbf{x}) \, \mathrm{d}\mathbf{x} \end{aligned} \tag{4.23}$$

and

$$\begin{aligned} &\int_\Omega \left(\mathbf{H}_{\mathbf{x}}\left(\phi_0(\mathbf{x})\right) + \mathbf{H}_{\mathbf{y}}\left(\phi_1\left(\mathbf{x}, \frac{\mathbf{x}}{\kappa}\right)\right)\right)^{\mathrm{T}} \left(\mathbf{e}^{\mathrm{T}}\left(\frac{\mathbf{x}}{\kappa}\right) \boldsymbol{\varepsilon}_{\mathbf{x}}\left(\mathbf{u}_\kappa(\mathbf{x})\right) + \boldsymbol{\mu}\left(\frac{\mathbf{x}}{\kappa}\right) \mathbf{H}_{\mathbf{x}}\left(\psi_\kappa(\mathbf{x})\right)\right) \mathrm{d}\mathbf{x} \\ + &\int_\Omega \left(\kappa\, \mathbf{H}_{\mathbf{x}}\left(\phi_1\left(\mathbf{x}, \frac{\mathbf{x}}{\kappa}\right)\right)\right)^{\mathrm{T}} \left(\mathbf{e}^{\mathrm{T}}\left(\frac{\mathbf{x}}{\kappa}\right) \boldsymbol{\varepsilon}_{\mathbf{x}}\left(\mathbf{u}_\kappa(\mathbf{x})\right) + \boldsymbol{\mu}\left(\frac{\mathbf{x}}{\kappa}\right) \mathbf{H}_{\mathbf{x}}\left(\psi_\kappa(\mathbf{x})\right)\right) \mathrm{d}\mathbf{x} \\ = &\int_\Omega \left(\phi_0(\mathbf{x}) + \kappa\, \phi_1\left(\mathbf{x}, \frac{\mathbf{x}}{\kappa}\right)\right) \mathrm{f}^{\text{mag}}(\mathbf{x}) \, \mathrm{d}\mathbf{x} \,. \end{aligned} \tag{4.24}$$

Now one wishes to take the limit for $\kappa \to 0$. A few of the terms in both equations vanish in this procedure. For once, since $\mathbf{f}^{\text{mech}}$ is assumed to be in $L^2 \subset L^1$ and $\mathbf{v}_1$ as a continuous function with compact support has to be essentially bounded, one can deduce with Hölder's inequality 3.3.8 that

$$\left| \lim_{\kappa \to 0} \int_\Omega \kappa \left(\mathbf{v}_1\left(\mathbf{x}, \frac{\mathbf{x}}{\kappa}\right)\right)^{\mathrm{T}} \mathbf{f}^{\text{mech}}(\mathbf{x}) \, \mathrm{d}\mathbf{x} \right| \leq \lim_{\kappa \to 0} \kappa \left\|\mathbf{v}_1\right\|_{L^\infty(\Omega \times \mathbb{T}^d)} \left\|\mathbf{f}^{\text{mech}}\right\|_{L^1(\Omega)} = 0 \,, \tag{4.25}$$

meaning that the integral itself also has to be equal to zero. Similarly, $\boldsymbol{\varepsilon}_{\mathbf{x}}(\mathbf{v}_1)$ also has to be essentially bounded and one can estimate on the left-hand side that

$$\begin{aligned} &\left| \lim_{\kappa \to 0} \int_\Omega \kappa\, \boldsymbol{\varepsilon}_{\mathbf{x}}\left(\mathbf{v}_1\left(\mathbf{x}, \frac{\mathbf{x}}{\kappa}\right)\right) \left(\mathbf{C}\left(\frac{\mathbf{x}}{\kappa}\right) \boldsymbol{\varepsilon}_{\mathbf{x}}\left(\mathbf{u}_\kappa(\mathbf{x})\right) - \mathbf{e}\left(\frac{\mathbf{x}}{\kappa}\right) \mathbf{H}_{\mathbf{x}}\left(\psi_\kappa(\mathbf{x})\right)\right) \mathrm{d}\mathbf{x} \right| \\ \leq &\lim_{\kappa \to 0} \kappa \tilde{d} \left\|\boldsymbol{\varepsilon}_{\mathbf{x}}(\mathbf{v}_1)\right\|_{L^\infty(\Omega \times \mathbb{T}^d)} \left(\left\|\mathbf{C}\right\|_{L^\infty(\Omega)} \left\|\boldsymbol{\varepsilon}_{\mathbf{x}}\left(\mathbf{u}_\kappa\right)\right\|_{L^1(\Omega)} + \left\|\mathbf{e}\right\|_{L^\infty(\Omega)} \left\|\mathbf{H}_{\mathbf{x}}\left(\psi_\kappa\right)\right\|_{L^1(\Omega)}\right) \\ = &\; 0 \,, \end{aligned} \tag{4.26}$$

since sequences $(\mathbf{u}_\kappa)_{\kappa>0}$ and $(\psi_\kappa)_{\kappa>0}$ were shown to be bounded in $\mathcal{H}^1$ and therefore the L^2- and by inclusion the L^1-norms of their (symmetric/negative) gradients are bounded as well. The same arguments carry over to the second equation analogously, so that the expressions (4.23) and (4.24) are reduced to

$$\begin{aligned}
&\lim_{\kappa\to 0}\int_\Omega \left(\varepsilon_{\mathbf{x}}\left(\mathbf{v}_0\left(\mathbf{x}\right)\right)+\varepsilon_{\mathbf{y}}\left(\mathbf{v}_1\left(\mathbf{x},\frac{\mathbf{x}}{\kappa}\right)\right)\right)^{\mathrm{T}}\left(\mathbf{C}\left(\frac{\mathbf{x}}{\kappa}\right)\varepsilon_{\mathbf{x}}\left(\mathbf{u}_\kappa\left(\mathbf{x}\right)\right)-\mathbf{e}\left(\frac{\mathbf{x}}{\kappa}\right)\mathbf{H}_{\mathbf{x}}\left(\psi_\kappa\left(\mathbf{x}\right)\right)\right)\mathrm{d}\mathbf{x}\\
&=\int_\Omega \left(\mathbf{v}_0\left(\mathbf{x}\right)\right)^{\mathrm{T}}\mathbf{f}^{\mathrm{mech}}\left(\mathbf{x}\right)\,\mathrm{d}\mathbf{x}\,,\\
&\lim_{\kappa\to 0}\int_\Omega \left(\mathbf{H}_{\mathbf{x}}\left(\phi_0\left(\mathbf{x}\right)\right)+\mathbf{H}_{\mathbf{y}}\left(\phi_1\left(\mathbf{x},\frac{\mathbf{x}}{\kappa}\right)\right)\right)^{\mathrm{T}}\left(\mathbf{e}^{\mathrm{T}}\left(\frac{\mathbf{x}}{\kappa}\right)\varepsilon_{\mathbf{x}}\left(\mathbf{u}_\kappa\left(\mathbf{x}\right)\right)+\boldsymbol{\mu}\left(\frac{\mathbf{x}}{\kappa}\right)\mathbf{H}_{\mathbf{x}}\left(\psi_\kappa\left(\mathbf{x}\right)\right)\right)\mathrm{d}\mathbf{x}\\
&=\int_\Omega \phi_0\left(\mathbf{x}\right)\mathrm{f}^{\mathrm{mag}}\left(\mathbf{x}\right)\,\mathrm{d}\mathbf{x}\,.
\end{aligned}\tag{4.27}$$

Looking at the first equation again, the maps

$$\begin{aligned}
g_1 &: \quad \Omega\times\mathbb{T}^d\to\mathbb{R}^{1\times\tilde{d}}\,,\ (\mathbf{x},\mathbf{y})\mapsto\left(\varepsilon_{\mathbf{x}}\left(\mathbf{v}_0\left(\mathbf{x}\right)\right)\right)^{\mathrm{T}}\mathbf{C}\left(\mathbf{y}\right)\\
g_2 &: \quad \Omega\times\mathbb{T}^d\to\mathbb{R}^{1\times d}\,,\ (\mathbf{x},\mathbf{y})\mapsto\left(\varepsilon_{\mathbf{x}}\left(\mathbf{v}_0\left(\mathbf{x}\right)\right)\right)^{\mathrm{T}}\mathbf{e}\left(\mathbf{y}\right)
\end{aligned}\tag{4.28}$$

both consist of the product of two L^2-functions who solely depend on only one variable each. On the other hand, the functions

$$\begin{aligned}
g_3 &: \quad \Omega\times\mathbb{T}^d\to\mathbb{R}^{1\times\tilde{d}}\,,\ (\mathbf{x},\mathbf{y})\mapsto\left(\varepsilon_{\mathbf{x}}\left(\mathbf{v}_1\left(\mathbf{x},\mathbf{y}\right)\right)\right)^{\mathrm{T}}\mathbf{C}\left(\mathbf{y}\right)\\
g_4 &: \quad \Omega\times\mathbb{T}^d\to\mathbb{R}^{1\times d}\,,\ (\mathbf{x},\mathbf{y})\mapsto\left(\varepsilon_{\mathbf{x}}\left(\mathbf{v}_1\left(\mathbf{x},\mathbf{y}\right)\right)\right)^{\mathrm{T}}\mathbf{e}\left(\mathbf{y}\right)
\end{aligned}\tag{4.29}$$

are square-measurable in $\mathbf{y}$ and continuous in $\mathbf{x}$ due to the choice of $\mathbf{v}_1$. Thus, since $\varepsilon\left(\mathbf{u}_\kappa\right)$ is known to two-scale converge to $\varepsilon_{\mathbf{x}}\left(\mathbf{u}_0\right)+\varepsilon_{\mathbf{y}}\left(\mathbf{u}_1\right)$ and $\mathbf{H}\left(\psi_\kappa\right)$ to $\mathbf{H}_{\mathbf{x}}\left(\psi_0\right)+\mathbf{H}_{\mathbf{y}}\left(\psi_1\right)$, Lemma 4.3.3 provides the limit

$$\begin{aligned}
&\int_{\Omega\times\mathbb{T}^d}\left(\varepsilon_{\mathbf{x}}\left(\mathbf{v}_0\left(\mathbf{x}\right)\right)+\varepsilon_{\mathbf{y}}\left(\mathbf{v}_1\left(\mathbf{x},\mathbf{y}\right)\right)\right)^{\mathrm{T}}\mathbf{C}\left(\mathbf{y}\right)\left(\varepsilon_{\mathbf{x}}\left(\mathbf{u}_0\left(\mathbf{x}\right)\right)+\varepsilon_{\mathbf{y}}\left(\mathbf{u}_1\left(\mathbf{x},\mathbf{y}\right)\right)\right)\,\mathrm{d}\mathbf{x}\,\mathrm{d}\mathbf{y}\\
-&\int_{\Omega\times\mathbb{T}^d}\left(\varepsilon_{\mathbf{x}}\left(\mathbf{v}_0\left(\mathbf{x}\right)\right)+\varepsilon_{\mathbf{y}}\left(\mathbf{v}_1\left(\mathbf{x},\mathbf{y}\right)\right)\right)^{\mathrm{T}}\mathbf{e}\left(\mathbf{y}\right)\left(\mathbf{H}_{\mathbf{x}}\left(\psi_0\left(\mathbf{x}\right)\right)+\mathbf{H}_{\mathbf{y}}\left(\psi_1\left(\mathbf{x},\mathbf{y}\right)\right)\right)\,\mathrm{d}\mathbf{x}\,\mathrm{d}\mathbf{y}\\
=&\int_\Omega\left(\mathbf{v}_0\left(\mathbf{x}\right)\right)^{\mathrm{T}}\mathbf{f}^{\mathrm{mech}}\left(\mathbf{x}\right)\,\mathrm{d}\mathbf{x}\,.
\end{aligned}\tag{4.30}$$

Analogously, the limit for the second equation reads

$$\begin{aligned}
&\int_{\Omega\times\mathbb{T}^d}\left(\mathbf{H}_{\mathbf{x}}\left(\psi_0\left(\mathbf{x}\right)\right)+\mathbf{H}_{\mathbf{y}}\left(\psi_1\left(\mathbf{x},\mathbf{y}\right)\right)\right)^{\mathrm{T}}\mathbf{e}^{\mathrm{T}}\left(\mathbf{y}\right)\left(\varepsilon_{\mathbf{x}}\left(\mathbf{u}_0\left(\mathbf{x}\right)\right)+\varepsilon_{\mathbf{y}}\left(\mathbf{u}_1\left(\mathbf{x},\mathbf{y}\right)\right)\right)\,\mathrm{d}\mathbf{x}\,\mathrm{d}\mathbf{y}\\
+&\int_{\Omega\times\mathbb{T}^d}\left(\mathbf{H}_{\mathbf{x}}\left(\psi_0\left(\mathbf{x}\right)\right)+\mathbf{H}_{\mathbf{y}}\left(\psi_1\left(\mathbf{x},\mathbf{y}\right)\right)\right)^{\mathrm{T}}\boldsymbol{\mu}\left(\mathbf{y}\right)\left(\mathbf{H}_{\mathbf{x}}\left(\psi_0\left(\mathbf{x}\right)\right)+\mathbf{H}_{\mathbf{y}}\left(\psi_1\left(\mathbf{x},\mathbf{y}\right)\right)\right)\,\mathrm{d}\mathbf{x}\,\mathrm{d}\mathbf{y}\\
=&\int_\Omega\phi_0\left(\mathbf{x}\right)\mathrm{f}^{\mathrm{mag}}\left(\mathbf{x}\right)\,\mathrm{d}\mathbf{x}\,.
\end{aligned}\tag{4.31}$$

Equations (4.30) and (4.31) essentially present the two-scale variational form. Until now, the test functions $\mathbf{v}$ and ϕ consisted only of infinitely differentiable ones but through an argument of density both equations also hold true for test functions chosen from the same space as the solutions, allowing again for a formulation in the more abstract framework of Hilbert spaces and bilinear forms.

Problem 6 (Two-scale variational formulation)**.** *Let the assumptions of Problem 3 hold true. In its combined form, the two-scale variational formulation consists of finding a quadruple*

$$\left(\mathbf{u}_0,\mathbf{u}_1,\psi_0,\psi_1\right)\in\mathcal{H}_{2S}:=\mathcal{H}^1_{\mathrm{mech}}\times L^2\left(\Omega,\mathcal{H}^1\left(\mathbb{T}^d,\mathbb{R}^d\right)/\mathbb{R}^d\right)\times\mathcal{H}^1_{\mathrm{mag}}\times L^2\left(\Omega,\mathcal{H}^1\left(\mathbb{T}^d,\mathbb{R}\right)/\mathbb{R}\right)$$

such that the equation obtained as the sum of (4.30) *and* (4.31) *is fulfilled for all test quadruples* $(\mathbf{v}_0, \mathbf{v}_1, \phi_0, \phi_1) \in \mathcal{H}_{2S}$.

Remember that $\mathcal{H}^1_{\text{mech}}$ and $\mathcal{H}^1_{\text{mag}}$ are equipped with the regular $\mathcal{H}^1$-norm and that function spaces $L^2(\Omega, Y)$ with a Banach space Y can be equipped with the norm

$$\|f\|_{L^2(\Omega,Y)} \coloneqq \left(\int_\Omega \|f(\mathbf{x}, \cdot)\|_Y^2 \, \mathrm{d}\mathbf{x} \right)^{\frac{1}{2}} . \tag{4.32}$$

Then the norm of the combined space $\mathcal{H}_{2S}$ follows naturally as

$$\|\mathbf{u}_0, \mathbf{u}_1, \psi_0, \psi_1\|_{\mathcal{H}_{2S}} \coloneqq \left(\|\mathbf{u}_0\|_{\mathcal{H}^1}^2 + \left(\int_\Omega \|\mathbf{u}_1(\mathbf{x}, \cdot)\|_{\mathcal{H}^1}^2 \, \mathrm{d}\mathbf{x} \right) + \|\psi_0\|_{\mathcal{H}^1}^2 + \left(\int_\Omega \|\psi_1(\mathbf{x}, \cdot)\|_{\mathcal{H}^1}^2 \, \mathrm{d}\mathbf{x} \right) \right)^{\frac{1}{2}} \tag{4.33}$$

and since all involved spaces are Hilbert spaces, it is clear that $\mathcal{H}_{2S}$ has to be one as well.

Theorem 4.3.4. *The two-scale variational formulation (Problem 6) has a unique solution in* $\mathcal{H}_{2S}$.

Proof. Let $\tilde{a}_1 \coloneqq \tilde{a}((\mathbf{v}_0, \mathbf{v}_1, \phi_0, \phi_1), (\mathbf{v}_0, \mathbf{v}_1, \phi_0, \phi_1))$ denote the combined bilinear form of this problem for an arbitrary quadruple $(\mathbf{v}_0, \mathbf{v}_1, \phi_0, \phi_1) \in \mathcal{H}_{2S}$. The coercivity and continuity of this bilinear form is obtained similarly to the bilinear form of (3.58) with only a few technical differences. One has

$$\begin{aligned} \tilde{a}_1 &= \int_{\Omega \times \mathbb{T}^d} (\boldsymbol{\varepsilon}_{\mathbf{x}}(\mathbf{v}_0(\mathbf{x})) + \boldsymbol{\varepsilon}_{\mathbf{y}}(\mathbf{v}_1(\mathbf{x}, \mathbf{y})))^{\mathrm{T}} \mathbf{C}(\mathbf{y}) (\boldsymbol{\varepsilon}_{\mathbf{x}}(\mathbf{v}_0(\mathbf{x})) + \boldsymbol{\varepsilon}_{\mathbf{y}}(\mathbf{v}_1(\mathbf{x}, \mathbf{y}))) \, \mathrm{d}\mathbf{x} \, \mathrm{d}\mathbf{y} \\ &+ \int_{\Omega \times \mathbb{T}^d} (\mathbf{H}_{\mathbf{x}}(\phi_0(\mathbf{x})) + \mathbf{H}_{\mathbf{y}}(\phi_1(\mathbf{x}, \mathbf{y})))^{\mathrm{T}} \boldsymbol{\mu}(\mathbf{y}) (\mathbf{H}_{\mathbf{x}}(\phi_0(\mathbf{x})) + \mathbf{H}_{\mathbf{y}}(\phi_1(\mathbf{x}, \mathbf{y}))) \, \mathrm{d}\mathbf{x} \, \mathrm{d}\mathbf{y} . \end{aligned}$$

Since $\mathbf{C}$ and $\boldsymbol{\mu}$ fulfill the ellipticity condition (3.61), the bilinear form can be estimated from below with

$$\tilde{a}_1 \geq \gamma_{\mathbf{C}} \|\boldsymbol{\varepsilon}_{\mathbf{x}}(\mathbf{v}_0) + \boldsymbol{\varepsilon}_{\mathbf{y}} \mathbf{v}_1\|_{L^2(\Omega \times \mathbb{T}^d)}^2 + \gamma_{\boldsymbol{\mu}} \|\mathbf{H}_{\mathbf{x}}(\phi_0) + \mathbf{H}_{\mathbf{y}} \phi_1\|_{L^2(\Omega \times \mathbb{T}^d)}^2$$

which is the same as

$$\begin{aligned} \tilde{a}_1 &= \gamma_{\mathbf{C}} \left(\|\boldsymbol{\varepsilon}_{\mathbf{x}}(\mathbf{v}_0)\|_{L^2(\Omega)}^2 + 2 \int_\Omega (\boldsymbol{\varepsilon}_{\mathbf{x}}(\mathbf{v}_0(\mathbf{x})))^{\mathrm{T}} \int_{\mathbb{T}^d} \boldsymbol{\varepsilon}_{\mathbf{y}}(\mathbf{v}_1(\mathbf{x}, \mathbf{y})) \, \mathrm{d}\mathbf{y} \, \mathrm{d}\mathbf{x} + \|\boldsymbol{\varepsilon}_{\mathbf{y}}(\mathbf{v}_1)\|_{L^2(\Omega \times \mathbb{T}^d)}^2 \right) \\ &+ \gamma_{\boldsymbol{\mu}} \left(\|\mathbf{H}_{\mathbf{x}}(\phi_0)\|_{L^2(\Omega)}^2 + 2 \int_\Omega (\mathbf{H}_{\mathbf{x}}(\phi_0(\mathbf{x})))^{\mathrm{T}} \int_{\mathbb{T}^d} \mathbf{H}_{\mathbf{y}}(\phi_1(\mathbf{x}, \mathbf{y})) \, \mathrm{d}\mathbf{y} \, \mathrm{d}\mathbf{x} + \|\mathbf{H}_{\mathbf{y}}(\phi_1)\|_{L^2(\Omega \times \mathbb{T}^d)}^2 \right) \end{aligned}$$

Due to the periodicity of $\boldsymbol{\varepsilon}_{\mathbf{y}}(\mathbf{v}_1)$ and $\mathbf{H}_{\mathbf{y}}(\phi_1)$, the two integral terms in the middle vanish after the application of the divergence theorem. The remaining terms are estimated as follows.

- Korn's inequality 3.3.4 provides a positive constant c_1, such that

$$\|\boldsymbol{\varepsilon}_{\mathbf{x}}(\mathbf{v}_0)\|_{L^2(\Omega)}^2 \geq c_1 \|\mathbf{v}_0\|_{\mathcal{H}^1}^2 .$$

- The periodic version of Korn's inequality 4.2.3 provides a positive constant c_2, such that

$$\|\boldsymbol{\varepsilon}_{\mathbf{y}}(\mathbf{v}_1)\|_{L^2(\Omega \times \mathbb{T}^d)}^2 \geq c_2 \left(\int_\Omega \|\mathbf{v}_1(\mathbf{x}, \cdot)\|_{\mathcal{H}^1}^2 \, \mathrm{d}\mathbf{x} \right) .$$

- Corollary 3.3.6 provides a positive constant $\tilde{c}_1$, such that

$$\|\mathbf{H}_{\mathbf{x}}(\phi_0)\|^2_{L^2(\Omega)} \geq \frac{1}{1+\tilde{c}_1^2} \|\phi_0\|^2_{\mathcal{H}^1} .$$

- Analogously, the Poincaré–Wirtinger inequality 4.2.5 provides a positive constant $\tilde{c}_2$, such that

$$\|\mathbf{H}_{\mathbf{y}}(\phi_1)\|^2_{L^2(\Omega\times\mathbb{T}^d)} \geq \frac{1}{1+\tilde{c}_2^2} \left(\int_\Omega \|\phi_1(\mathbf{x},\cdot)\|^2_{\mathcal{H}^1} \, \mathrm{d}\mathbf{x} \right) .$$

Then taking the maximum over all constants leaves exactly the squared $\mathcal{H}_{2S}$-norm on right-hand side, proving coercivity.

Continuity follows once more from the application of Hölder's inequality 3.3.8 and Corollary 3.3.11. Let now $\tilde{a}_2 \coloneqq \tilde{a}((\mathbf{u}_0,\mathbf{u}_1,\psi_0,\psi_1),(\mathbf{v}_0,\mathbf{v}_1,\phi_0,\phi_1))$ be used as abbreviation for the bilinear form with two different quadruples as arguments. Then

$$\begin{aligned}
|\tilde{a}_2| \quad &\leq \quad \tilde{d}\|\mathbf{C}\|_{L^\infty(\mathbb{T}^d)} \|\boldsymbol{\varepsilon}_{\mathbf{x}}(\mathbf{v}_0)+\boldsymbol{\varepsilon}_{\mathbf{y}}(\mathbf{v}_1)\|_{L^2(\Omega\times\mathbb{T}^d)} \|\boldsymbol{\varepsilon}_{\mathbf{x}}(\mathbf{u}_0)+\boldsymbol{\varepsilon}_{\mathbf{y}}(\mathbf{u}_1)\|_{L^2(\Omega\times\mathbb{T}^d)} \\
&+ \quad \sqrt{\tilde{d}d}\|\mathbf{e}\|_{L^\infty(\mathbb{T}^d)} \|\boldsymbol{\varepsilon}_{\mathbf{x}}(\mathbf{v}_0)+\boldsymbol{\varepsilon}_{\mathbf{y}}(\mathbf{v}_1)\|_{L^2(\Omega\times\mathbb{T}^d)} \|\mathbf{H}_{\mathbf{x}}(\psi_0)+\mathbf{H}_{\mathbf{y}}(\psi_1)\|_{L^2(\Omega\times\mathbb{T}^d)} \\
&+ \quad \sqrt{\tilde{d}d}\|\mathbf{e}\|_{L^\infty(\mathbb{T}^d)} \|\boldsymbol{\varepsilon}_{\mathbf{x}}(\mathbf{u}_0)+\boldsymbol{\varepsilon}_{\mathbf{y}}(\mathbf{u}_1)\|_{L^2(\Omega\times\mathbb{T}^d)} \|\mathbf{H}_{\mathbf{x}}(\phi_0)+\mathbf{H}_{\mathbf{y}}(\phi_1)\|_{L^2(\Omega\times\mathbb{T}^d)} \\
&+ \quad d\|\boldsymbol{\mu}\|_{L^\infty(\mathbb{T}^d)} \|\mathbf{H}_{\mathbf{x}}(\psi_0)+\mathbf{H}_{\mathbf{y}}(\psi_1)\|_{L^2(\Omega\times\mathbb{T}^d)} \|\mathbf{H}_{\mathbf{x}}(\phi_0)+\mathbf{H}_{\mathbf{y}}(\phi_1)\|_{L^2(\Omega\times\mathbb{T}^d)} .
\end{aligned}$$

Defining

$$C_{\max} \coloneqq \max\left\{ \tilde{d}\|\mathbf{C}\|_{L^\infty(\mathbb{T}^d)} , \sqrt{\tilde{d}d}\|\mathbf{e}\|_{L^\infty(\mathbb{T}^d)} , d\|\boldsymbol{\mu}\|_{L^\infty(\mathbb{T}^d)} \right\}$$

allows to simplify the expression as

$$\begin{aligned}
|\tilde{a}_2| \quad &\leq \quad C_{\max} \\
&\times \quad \left(\|\boldsymbol{\varepsilon}_{\mathbf{x}}(\mathbf{u}_0)+\boldsymbol{\varepsilon}_{\mathbf{y}}(\mathbf{u}_1)\|_{L^2(\Omega\times\mathbb{T}^d)} + \|\mathbf{H}_{\mathbf{x}}(\psi_0)+\mathbf{H}_{\mathbf{y}}(\psi_1)\|_{L^2(\Omega\times\mathbb{T}^d)} \right) \\
&\times \quad \left(\|\boldsymbol{\varepsilon}_{\mathbf{x}}(\mathbf{v}_0)+\boldsymbol{\varepsilon}_{\mathbf{y}}(\mathbf{v}_1)\|_{L^2(\Omega\times\mathbb{T}^d)} + \|\mathbf{H}_{\mathbf{x}}(\phi_0)+\mathbf{H}_{\mathbf{y}}(\phi_1)\|_{L^2(\Omega\times\mathbb{T}^d)} \right)
\end{aligned}$$

which can then be further estimated by the triangle inequality as

$$\begin{aligned}
|\tilde{a}_2| \quad &\leq \quad C_{\max} \\
&\times \quad \left(\|\boldsymbol{\varepsilon}_{\mathbf{x}}(\mathbf{u}_0)\|_{L^2(\Omega\times\mathbb{T}^d)} + \|\boldsymbol{\varepsilon}_{\mathbf{y}}(\mathbf{u}_1)\|_{L^2(\Omega\times\mathbb{T}^d)} + \|\mathbf{H}_{\mathbf{x}}(\psi_0)\|_{L^2(\Omega\times\mathbb{T}^d)} + \|\mathbf{H}_{\mathbf{y}}(\psi_1)\|_{L^2(\Omega\times\mathbb{T}^d)} \right) \\
&\times \quad \left(\|\boldsymbol{\varepsilon}_{\mathbf{x}}(\mathbf{v}_0)\|_{L^2(\Omega\times\mathbb{T}^d)} + \|\boldsymbol{\varepsilon}_{\mathbf{y}}(\mathbf{v}_1)\|_{L^2(\Omega\times\mathbb{T}^d)} + \|\mathbf{H}_{\mathbf{x}}(\phi_0)\|_{L^2(\Omega\times\mathbb{T}^d)} + \|\mathbf{H}_{\mathbf{y}}(\phi_1)\|_{L^2(\Omega\times\mathbb{T}^d)} \right) .
\end{aligned}$$

Then making use of Lemma 3.3.12, estimating the L^2-norms with the necessary $\mathcal{H}^1$-norms from above and applying Corollary 3.3.11 a second time yields the final estimate

$$|\tilde{a}_2| \leq 4C_{\max} \|(\mathbf{u}_0,\mathbf{u}_1,\psi_0,\psi_1)\|_{\mathcal{H}_{2S}} \|(\mathbf{v}_0,\mathbf{v}_1,\phi_0,\phi_1)\|_{\mathcal{H}_{2S}} .$$

The right-hand side was already shown before to be continuous, thus all conditions for the Lax–Milgram theorem 3.3.2 are met. □

Looking back at the derivation of the two-scale variational form, it was emphasized that there might only exist subsequences of $\mathbf{u}_\kappa$ and ψ_κ that two-scale converge to the defined limits. But since the quadruple is uniquely determined through the weak form for any chosen subsequence, one can conclude that in fact the entire series attains the two-scale limits stated in (4.20).

The only thing left to do is to link the two-scale variational form back to the cell and the homogenized problem. Choosing only test functions with $\mathbf{v}_0 = 0$ and $\phi_0 = 0$ one obtains

$$\begin{aligned}
0 &= \int_{\Omega\times\mathbb{T}^d} \left(\boldsymbol{\varepsilon}_{\mathbf{y}}\left(\mathbf{v}_1(\mathbf{x},\mathbf{y})\right)\right)^{\mathrm{T}} \mathbf{C}(\mathbf{y}) \left(\boldsymbol{\varepsilon}_{\mathbf{x}}\left(\mathbf{u}_0(\mathbf{x})\right) + \boldsymbol{\varepsilon}_{\mathbf{y}}\left(\mathbf{u}_1(\mathbf{x},\mathbf{y})\right)\right) \,\mathrm{d}\mathbf{x}\,\mathrm{d}\mathbf{y} \\
&\quad - \int_{\Omega\times\mathbb{T}^d} \left(\boldsymbol{\varepsilon}_{\mathbf{y}}\left(\mathbf{v}_1(\mathbf{x},\mathbf{y})\right)\right)^{\mathrm{T}} \mathbf{e}(\mathbf{y}) \left(\mathbf{H}_{\mathbf{x}}\left(\psi_0(\mathbf{x})\right) + \mathbf{H}_{\mathbf{y}}\left(\psi_1(\mathbf{x},\mathbf{y})\right)\right) \,\mathrm{d}\mathbf{x}\,\mathrm{d}\mathbf{y}\,, \\
0 &= \int_{\Omega\times\mathbb{T}^d} \left(\mathbf{H}_{\mathbf{y}}\left(\phi_1(\mathbf{x},\mathbf{y})\right)\right)^{\mathrm{T}} \mathbf{e}^{\mathrm{T}}(\mathbf{y}) \left(\boldsymbol{\varepsilon}_{\mathbf{x}}\left(\mathbf{u}_0(\mathbf{x})\right) + \boldsymbol{\varepsilon}_{\mathbf{y}}\left(\mathbf{u}_1(\mathbf{x},\mathbf{y})\right)\right) \,\mathrm{d}\mathbf{x}\,\mathrm{d}\mathbf{y} \\
&\quad + \int_{\Omega\times\mathbb{T}^d} \left(\mathbf{H}_{\mathbf{y}}\left(\phi_1(\mathbf{x},\mathbf{y})\right)\right)^{\mathrm{T}} \boldsymbol{\mu}(\mathbf{y}) \left(\mathbf{H}_{\mathbf{x}}\left(\psi_0(\mathbf{x})\right) + \mathbf{H}_{\mathbf{y}}\left(\psi_1(\mathbf{x},\mathbf{y})\right)\right) \,\mathrm{d}\mathbf{x}\,\mathrm{d}\mathbf{y}
\end{aligned}$$

which is just the weak form of the cell problem (Problem 4). Choosing test functions with $\mathbf{v}_1 = 0$ and $\phi_1 = 0$ instead leads to

$$\begin{aligned}
\int_{\Omega} \left(\mathbf{v}_0(\mathbf{x})\right)^{\mathrm{T}} \mathbf{f}^{\mathrm{mech}}(\mathbf{x}) \,\mathrm{d}\mathbf{x} &= \int_{\Omega\times\mathbb{T}^d} \left(\boldsymbol{\varepsilon}_{\mathbf{y}}\left(\mathbf{v}_0(\mathbf{x})\right)\right)^{\mathrm{T}} \mathbf{C}(\mathbf{y}) \left(\boldsymbol{\varepsilon}_{\mathbf{x}}\left(\mathbf{u}_0(\mathbf{x})\right) + \boldsymbol{\varepsilon}_{\mathbf{y}}\left(\mathbf{u}_1(\mathbf{x},\mathbf{y})\right)\right) \,\mathrm{d}\mathbf{x}\,\mathrm{d}\mathbf{y} \\
&\quad - \int_{\Omega\times\mathbb{T}^d} \left(\boldsymbol{\varepsilon}_{\mathbf{y}}\left(\mathbf{v}_0(\mathbf{x})\right)\right)^{\mathrm{T}} \mathbf{e}(\mathbf{y}) \left(\mathbf{H}_{\mathbf{x}}\left(\psi_0(\mathbf{x})\right) + \mathbf{H}_{\mathbf{y}}\left(\psi_1(\mathbf{x},\mathbf{y})\right)\right) \,\mathrm{d}\mathbf{x}\,\mathrm{d}\mathbf{y}\,, \\
\int_{\Omega} \phi_0(\mathbf{x})\, \mathrm{f}^{\mathrm{mag}}(\mathbf{x}) \,\mathrm{d}\mathbf{x} &= \int_{\Omega\times\mathbb{T}^d} \left(\mathbf{H}_{\mathbf{y}}\left(\phi_0(\mathbf{x})\right)\right)^{\mathrm{T}} \mathbf{e}^{\mathrm{T}}(\mathbf{y}) \left(\boldsymbol{\varepsilon}_{\mathbf{x}}\left(\mathbf{u}_0(\mathbf{x})\right) + \boldsymbol{\varepsilon}_{\mathbf{y}}\left(\mathbf{u}_1(\mathbf{x},\mathbf{y})\right)\right) \,\mathrm{d}\mathbf{x}\,\mathrm{d}\mathbf{y} \\
&\quad + \int_{\Omega\times\mathbb{T}^d} \left(\mathbf{H}_{\mathbf{y}}\left(\phi_0(\mathbf{x})\right)\right)^{\mathrm{T}} \boldsymbol{\mu}(\mathbf{y}) \left(\mathbf{H}_{\mathbf{x}}\left(\psi_0(\mathbf{x})\right) + \mathbf{H}_{\mathbf{y}}\left(\psi_1(\mathbf{x},\mathbf{y})\right)\right) \,\mathrm{d}\mathbf{x}\,\mathrm{d}\mathbf{y}
\end{aligned}$$

which together with the Dirichlet boundary conditions equals the weak form of the homogenized problem (Problem 5). The methods discussed previously to obtain the solutions to these problems remain unaffected and can be adopted now.

5 Reformulation of the Corrector Problems as Periodic Lippmann–Schwinger Equations

While both the unit cell and the homogenized problem are equally important to the homogenization of the original problem, the following chapters of this thesis will focus exclusively on the former one as its periodic nature allows for a slightly different methodology in the solution process.

Section 5.1 fits the unit cell problem into a generalized problem class and highlights the idea of a fitting methodology. In Sect. 5.2 it is attempted to derive a solution of the coupled system based on the already existing solution equations of the uncoupled problems, whereas Sect. 5.3 will make use of the established concepts to develop such a formula from scratch, resulting in a more general numerical scheme.

5.1 Setting and Methodology

As explained in the previous chapter, the unit cell problem itself can be seen as a linear combination of the more fundamental corrector problems presented in Definition 4.2.4. All of these problems share the common structure

$$\begin{aligned} \mathbf{div}_{\mathbf{y}} \left(\mathbf{C}\, \varepsilon_{\mathbf{y}} \left(\omega \right) - \mathbf{e}\, \mathbf{H}_{\mathbf{y}} \left(\varrho \right) \right) &= -\mathbf{g}^{\mathrm{mech}} \,, \\ \mathrm{div}_{\mathbf{y}} \left(\mathbf{e}^{\mathrm{T}}\, \varepsilon_{\mathbf{y}} \left(\omega \right) + \boldsymbol{\mu}\, \mathbf{H}_{\mathbf{y}} \left(\varrho \right) \right) &= -\mathbf{g}^{\mathrm{mag}} \end{aligned}$$

with right-hand side terms $\mathbf{g}^{\mathrm{mech}}$ and $\mathbf{g}^{\mathrm{mag}}$ being chosen accordingly. Since these terms are divergence operators themselves in the context of corrector problems, one might instead move all expressions to the left-hand side, obtaining the equivalent but differently structured system

$$\begin{aligned} \mathbf{div}_{\mathbf{y}} \left(\mathbf{C}\, \varepsilon_{\mathbf{y}} \left(\omega \right) - \mathbf{e}\, \mathbf{H}_{\mathbf{y}} \left(\varrho \right) + \tau^{\mathrm{mech}} \right) &= 0 \,, \\ \mathrm{div}_{\mathbf{y}} \left(\mathbf{e}^{\mathrm{T}}\, \varepsilon_{\mathbf{y}} \left(\omega \right) + \boldsymbol{\mu}\, \mathbf{H}_{\mathbf{y}} \left(\varrho \right) + \tau^{\mathrm{mag}} \right) &= 0 \,. \end{aligned}$$

While the initial motivation of this chapter should be to find a solution of the corrector problems specifically, it is preferred to keep things as general as possible. Based on both structural representations above, problems defined on the unit cell of the form

$$\begin{aligned} \mathbf{div}_{\mathbf{y}} \left(\mathbf{C}\, \varepsilon_{\mathbf{y}} \left(\omega \right) - \mathbf{e}\, \mathbf{H}_{\mathbf{y}} \left(\varrho \right) + \tau^{\mathrm{mech}} \right) + \mathbf{g}^{\mathrm{mech}} &= 0 \,, \\ \mathrm{div}_{\mathbf{y}} \left(\mathbf{e}^{\mathrm{T}}\, \varepsilon_{\mathbf{y}} \left(\omega \right) + \boldsymbol{\mu}\, \mathbf{H}_{\mathbf{y}} \left(\varrho \right) + \tau^{\mathrm{mag}} \right) + \mathbf{g}^{\mathrm{mag}} &= 0 \,, \end{aligned} \tag{5.1}$$

will be considered within this chapter. Additionally to the assumptions from Problem 3 being fulfilled, it is expected that the new terms are at least square-integrable functions. In detail, one requires $\tau^{\mathrm{mech}} \in L^2 \left(\mathbb{T}^d, \mathbb{R}^{\tilde{d}} \right), \tau^{\mathrm{mag}} \in L^2 \left(\mathbb{T}^d, \mathbb{R}^d \right), \mathbf{g}^{\mathrm{mech}} \in L^2 \left(\mathbb{T}^d, \mathbb{R}^d \right) / \mathbb{R}^d$ and $\mathbf{g}^{\mathrm{mag}} \in L^2 \left(\mathbb{T}^d, \mathbb{R} \right) / \mathbb{R}$. Also

from now on, the subscript y will be omitted in the gradient and divergence operators, since only one spatial variable will be present anyway.

As the implicit periodic boundary conditions of the unit cell sets the system (5.1) apart from many other partial differential equations arising in practical applications, it seems reasonable that one wants to exploit this circumstance. The most important tool to analyze periodic functions is the *Fourier series* of which some important properties were mentioned in Sect. 2.3. One of its greatest advantages when applied to differential equations is provided by the fact that derivatives can be expressed as a multiplication of each Fourier coefficient with the corresponding frequency. This makes it possible to translate the analytic system into purely algebraic expressions in the Fourier domain. This idea falls into the category of *spectral methods* which were largely developed and popularized by mathematician Steven Alan Orszag [45]. While these methods are strongly related to classical Finite Element Methods as both represent functions as linear combinations of basis vectors, they differ in the fact that the chosen basis in spectral methods leads to a global approach whereas standard FEM make use of a local ansatz.

In the mid-nineties french mathematicians Hervé Moulinec and Pierre Suquet proposed this FFT-based spectral method for the analysis of composites based on micro-structural images [87, 88]. Although the estimated errors might in this case turn out rather large locally due to the presence of Gibb's phenomenon [46] near phase boundaries, there are some clear advantages over FEM in this case. For one thing, their so-called *Basic Scheme* is directly applicable to digital image data gained through techniques like microtomography or scanning electron microscopy, working on pixel or voxel data as equidistant grids and avoiding additional meshing procedures. Furthermore, the algorithm consists only of operations that either can be performed for each data point or frequency independently, leading to prominent speed-up through parallelization in their implementation, or FFT-based operations that can be handled efficiently by existing software libraries such as the FFTW library by Matteo Frigo and Steven G. Johnson [36]. Additionally, as one is usually not interested in the solution of the unit cell problem for its own sake but to further calculate the effective tensors needed within the homogenized problem, the aforementioned high errors in a small set of data points turn out to be less problematic as they are smoothed out during integration. Therefore, the Basic Scheme offers an efficient, fast and rather easy to implement alternative to solve the unit cell problem. The scheme itself is centered around an algebraic expression derived in the Fourier domain which is referred to as *periodic Lippmann–Schwinger equation* or *pLS–equation* for short [62, 73]. It is derived by first solving an auxiliary problem with a constant stiffness tensor and leading the case of variable tensors back to this solution later.

5.2 Post-pLS Coupling

With algorithms such as the Basic Scheme already available for the uncoupled equations, one might first try to combine the separately derived pLS–equations of the mechanical and the magnetic problems back together in such a way that one obtains a valid pLS–equation for the coupled system [14]. This is what the title of this section refers to as *post-pLS coupling*. Before two of these recoupling strategies are presented, the derivation of the purely mechanical and magnetic pLS–equations are revised. This has several advantages. For one, the reader is able to follow and to understand the necessary steps to derive a pLS–equation without having to look up the referenced sources first. It also serves as preparation for the next section in which a pLS–equation for the coupled system is derived directly, as several ideas and quantities occurring within the separate analyses will reappear later.

Besides, while in most scientific works the pLS–equations of such elliptic problems is often derived from their strong form directly by using the differentiation properties of the Fourier series, this procedure is not mathematically sound as it would imply the existence of strong derivatives of our solution fields. As it was seen however in the previous chapter, in Problem 6 and Theorem 4.3.4 to be precise, these assumptions are too restrictive to guarantee the existence of unique solutions, since only weak derivatives may exist. Therefore, the pLS–equations are gained from the weak forms within this thesis, resulting in a slightly more sophisticated derivation but also revealing how the original approach from Moulinec and Suquet connects back to a Galerkin projection, an observation made before by Jaroslav Vondřejc [112].

5.2.1 The Mechanical Problem

As hinted at before, problems with non-constant material tensors, such as the stiffness tensor $\mathbf{C}$, are difficult to tackle from the start. Instead, it is a good idea to first take a look at cases where the material tensors are constant over the whole unit cell, as this situation offers a considerable simplification in which each frequency can be treated on its own.

Constant Case

Now assuming a constant stiffness tensor $\mathbf{C}^0 \in \mathbb{R}^{\tilde{d}\times\tilde{d}}$, the corresponding uncoupled mechanical equation would read

$$\mathbf{div}\left(\mathbf{C}^0\,\varepsilon(\omega) + \tau^{\mathrm{mech}}\right) + \mathbf{g}^{\mathrm{mech}} = 0$$

in its strong form or equivalently

$$\int_{\mathbb{T}^d} \left(\varepsilon(\mathbf{v})\right)^{\mathrm{T}} \left(\mathbf{C}^0\,\varepsilon(\omega) + \tau^{\mathrm{mech}}\right) - \mathbf{v}^{\mathrm{T}}\,\mathbf{g}^{\mathrm{mech}}\;\mathrm{d}\,\mathbf{y} = 0$$

in its weak form which has to hold true for all test functions $\mathbf{v} \in \mathcal{H}^1\left(\mathbb{T}^d, \mathbb{R}^d\right) / \mathbb{R}^d$. Remember that solutions for problems defined on the unit cell are only unique up to a constant and vanishing mean values are often prescribed in practice. The idea is now to express all quantities as a Fourier series and to choose the test function $\mathbf{v}$ as an element from the orthonormal Schauder basis introduced in Sect. 2.3 to obtain closed expressions for each Fourier coefficient independently.

To make good use of the basis functions $\mathrm{e}^{2\pi\,\mathrm{i}\langle\mathbf{k},\cdot\rangle}$ for these problems however, one has to think about some potential hindrances before. First, notice that the zero–frequency term determines a quantity's mean value and needs to get dropped in the Fourier series of $\omega, \mathbf{v}$ and $\mathbf{g}^{\mathrm{mech}}$ due to their uniqueness up to a constant; hence only frequency vectors $\mathbf{k} \in \mathbb{Z}^d_\star \coloneqq \mathbb{Z}^d \setminus \{0\}$ are considered. One can once again think of this as implicitly choosing representatives with mean values of zero within their respective equivalence classes. The Fourier series of τ^{mech} on the other hand still includes the zero–frequency term as it is a regular L^2-quantity. Even with this formal distinction though, it will turn out that this term does not actually play a role in forming the solution.

Another problem may seemingly lie within the fact that these exponential functions are generally complex-valued, whereas all quantities in the presented equations including the test functions in the weak form are only real-valued. There are two ways to solve this conundrum without straying away too far from the original idea. One possible solution might be to switch from the exponential form of the Fourier series to its equivalent sine–cosine form instead (see for example [113, p.2–10]). The basis functions in this version are given by real-valued functions $\sin(2\pi\,\langle\mathbf{k},\cdot\rangle)$ and $\cos(2\pi\,\langle\mathbf{k},\cdot\rangle)$ which

can then be used as test functions in place of the exponential ones. Alternatively, since the choice of real-valued functions up to this point is only a result of the physical origin behind these equations but nothing that impacted the mathematical analysis in any major way so far, it would be feasible to consider complex-valued quantities and test functions anyway. As this allows for a much more compact derivation of the pLS–equations, the thesis at hand will follow this approach instead. The real-valued setting could then be considered as a special case where results keep their validity and the solution field necessarily turns out to be a real-valued function as well. At that point in time, the choice of either $\mathbb{R}^d$ or $\mathbb{C}^d$ as the codomain will be nothing but a formal one in the Lax–Milgram setting.

Lastly, despite the set $\left\{ \mathrm{e}^{2\pi\,\mathrm{i}\langle \mathbf{k}, \cdot \rangle} \,:\, \mathbf{k} \in \mathbb{Z}^d_\star \right\}$ forming a Schauder basis of $L^2\left(\mathbb{T}^d, \mathbb{R}\right)/\mathbb{R}$ and all finite linear combinations being strongly differentiable, the same does not hold true for infinite expressions as there are square-integrable functions that are not even weakly differentiable, such as square or sawtooth waves. This means that the exponential functions can not be used as a Schauder basis for the Sobolev space $\mathcal{H}^1\left(\mathbb{T}^d, \mathbb{R}\right)/\mathbb{R}$ as well. This matter of fact might complicate or completely prevent the derivation of analytically exact solution formulas in theory but merely poses a problem from a numerical point of view, as one ultimately has to approximate the solution due to having only a limited number of discrete data points available in practice anyway. Therefore, albeit large parts of the upcoming computations still holding true for infinite Fourier series, working on the approximate versions of the problems at hand from the start seems reasonable. Cut off Fourier series — that means trigonometric polynomials — come as the natural choice to limit the number of Fourier coefficients manageable in a numerical scheme, depending on the number of discretized pixel or voxel data provided.

Definition 5.2.1. *For $m, n \in \mathbb{N}$ and $N \in \mathbb{N}^m$, with N being odd in each entry, define the set of feasible frequency vectors*

$$\mathbb{Z}_N \coloneqq \left\{ \mathbf{k} \in \mathbb{Z}^m_\star \,:\, |\mathbf{k}_p| \leq \frac{N_p}{2} \quad \text{for} \quad p = 1, \dots, m \right\}$$

and the set of feasible trigonometric polynomials

$$\Pi^n_N \coloneqq \left\{ \sum_{\mathbf{k} \in \mathbb{Z}_N} \alpha_{\mathbf{k}}\, \mathrm{e}^{2\pi\,\mathrm{i}\langle \mathbf{k}, \cdot \rangle} \,:\, \alpha_{\mathbf{k}} \in \mathbb{C}^n \right\} \subset \mathcal{H}^1\left(\mathbb{T}^d, \mathbb{R}^n\right)/\mathbb{R}^n \ .$$

In the above definition the vector N represents what will later be a *discretization vector* where the p-th entry equals the number of voxels along the p-th dimension. Only allowing for odd entries of N ensures that for each positive frequency its negative counterpart is also taken into account, which is especially important with respect to real-valued quantities. One should also pay attention to the different roles of m and n, as the former one denotes the dimensionality of the frequency vectors and as such of the unit cell, whereas the latter one refers to the dimensionality to the quantity expressed as a Fourier series.

Problem 7 (Mechanical auxiliary problem)**.** *For $N \in \mathbb{N}^d$, with N being odd in each entry, find $\omega \in \Pi^d_N$ such that*

$$\int_{\mathbb{T}^d} \left(\boldsymbol{\varepsilon}(\mathbf{v})\right)^{\mathrm{T}} \left(\mathbf{C}^0\, \boldsymbol{\varepsilon}(\omega) + \tau^{\mathrm{mech}} \right) - \mathbf{v}^{\mathrm{T}}\, \mathbf{g}^{\mathrm{mech}} \ \mathrm{d}\,\mathbf{y} = 0$$

holds true for all test functions $\mathbf{v} \in \Pi^d_N$.

The existence of a unique solution to this problem is ensured once again by the Lax–Milgram theorem. The proof follows the same steps as seen in previous iterations, now only restricted to a smaller Hilbert space.

Two remarks regarding notation will also be made here. For one, it should be mentioned that while the Mandel notation simplified the entire analysis so far, the original tensor notation which is referred to by underlining the affected variables is preferred in the upcoming derivations and definitions of what will be later called the *Green operators*. In hopes of shortening the notation and to avoid confusion on which indices are paired together during high-rank tensor operations, the *Einstein summation convention* will be used, implicitly summing up over repeating indices [8].

Second, the notation $\hat{f}(\mathbf{k})$ which was originally introduced in Sect. 2.3 exclusively for the discrete Fourier series of a function f will already be used during the upcoming operations in the Fourier domain, even though most of the derivations are actually performed with the Fourier coefficients $c_{\mathbf{k}}(f)$. One can justify this decision by arguing that the coefficients of a finite Fourier series can be computed exactly through a DFT, if the number of sample points was just chosen high enough. For the time being this should really be seen as a notational change only, allowing for better readability and preventing unintentional mix-ups with subscript indices, as it is important to keep in mind that the DFT and the Fourier coefficients of a function generally don't coincide and that some of the properties exploited in the following are only valid for the latter. The actual computation of a DFT and the accompanying treatment of the discrete input data in practice will be discussed in more detail later on.

With all these things in mind, choosing a test function $\mathbf{v}$ with entries

$$\mathbf{v}_j = \begin{cases} \mathrm{e}^{2\pi\,\mathrm{i}\langle -\mathbf{k},\mathbf{y}\rangle} & , \text{if } j = m \\ 0 & , \text{otherwise} \end{cases}$$

for some index $m \in \{1,\dots,d\}$ and a frequency vector $\mathbf{k} \in \mathbb{Z}_N$ and inserting Fourier series into the weak form yields

$$\begin{aligned} &\int_{\mathbb{T}^d} \left(-2\pi\,\mathrm{i}\,\mathbf{k}_n\,\mathrm{e}^{2\pi\,\mathrm{i}\langle -\mathbf{k},\mathbf{y}\rangle}\right)\left(\underline{\mathbf{C}}^0_{mnop}\left(\sum_{\mathbf{l}\in\mathbb{Z}_N} 2\pi\,\mathrm{i}\,\mathbf{l}_o\hat{\omega}_p(\mathbf{l})\,\mathrm{e}^{2\pi\,\mathrm{i}\langle\mathbf{l},\mathbf{y}\rangle}\right) + \left(\sum_{\mathbf{l}\in\mathbb{Z}^d} \hat{\underline{\varepsilon}}^{\mathrm{mech}}_{mn}(\mathbf{l})\,\mathrm{e}^{2\pi\,\mathrm{i}\langle\mathbf{l},\mathbf{y}\rangle}\right)\right)\mathrm{d}\,\mathbf{y} \\ = &\int_{\mathbb{T}^d} \mathrm{e}^{2\pi\,\mathrm{i}\langle -\mathbf{k},\mathbf{y}\rangle}\left(\sum_{\mathbf{l}\in\mathbb{Z}^d_\star} \hat{\mathbf{g}}^{\mathrm{mech}}_m(\mathbf{l})\,\mathrm{e}^{2\pi\,\mathrm{i}\langle\mathbf{l},\mathbf{y}\rangle}\right)\mathrm{d}\,\mathbf{y}\ . \end{aligned} \tag{5.2}$$

Although this expression might seem overly complex at first, most of the summands vanish thanks to the orthogonality property of the exponential basis functions. Precisely, given two frequency vectors $\alpha, \beta \in \mathbb{Z}^d$, one has

$$\int_{\mathbb{T}^d} \mathrm{e}^{2\pi\,\mathrm{i}\langle\alpha,\mathbf{y}\rangle}\,\mathrm{e}^{2\pi\,\mathrm{i}\langle\beta,\mathbf{y}\rangle}\,\mathrm{d}\,\mathbf{y} = \int_{\mathbb{T}^d} \mathrm{e}^{2\pi\,\mathrm{i}\langle\alpha+\beta,\mathbf{y}\rangle}\,\mathrm{d}\,\mathbf{y} = \begin{cases} 1 & , \text{if } \alpha = -\beta \\ 0 & , \text{otherwise} \end{cases}\ . \tag{5.3}$$

In case of (5.2) this means that only the summand for $\mathbf{l} = \mathbf{k}$ leads to non-vanishing integrals, resulting in the much simpler expression

$$4\pi^2\underline{\mathbf{C}}^0_{mnop}\mathbf{k}_n\mathbf{k}_o\hat{\omega}_p(\mathbf{k}) - 2\pi\,\mathrm{i}\,\mathbf{k}_n\hat{\underline{\varepsilon}}^{\mathrm{mech}}_{mn}(\mathbf{k}) = \hat{\mathbf{g}}^{\mathrm{mech}}_m(\mathbf{k})$$

or equivalently

$$\underline{\mathbf{C}}^0_{mnop}\mathbf{k}_n\mathbf{k}_o\hat{\omega}_p(\mathbf{k}) = \frac{\mathrm{i}}{2\pi}\mathbf{k}_n\hat{\underline{\varepsilon}}^{\mathrm{mech}}_{mn}(\mathbf{k}) + \frac{1}{4\pi^2}\hat{\mathbf{g}}^{\mathrm{mech}}_m(\mathbf{k})\ . \tag{5.4}$$

As (5.4) has to hold true for all $m \in \{1,\dots,d\}$, the $\mathbf{k}$-th Fourier coefficient $\hat{\omega}(\mathbf{k})$ can then be gained from a linear system with the *acoustic algebraic operator* $\mathbf{A}(\mathbf{k}) \in \mathbb{R}^{d\times d}$ whose entries are defined as

$$\left(\mathbf{A}(\mathbf{k})\right)_{mp} \coloneqq \underline{\mathbf{C}}^0_{mnop}\mathbf{k}_n\mathbf{k}_o\ , \quad m,p = 1,\dots,d\ . \tag{5.5}$$

Of course this statement only holds true, if the acoustic tensor proves to be invertible. Before answering this question in the following lemma, there are some more remarks about the notation to be made. Notice how the acoustic tensor is strongly dependent on the choice of the constant stiffness tensor $\underline{\mathbf{C}}^0$ but it was decided to omit a corresponding superscript denoting this connection in an attempt to reduce the number of total super- and subscripts. Additionally, whenever only a single frequency vector appears within a certain formula, the Fourier coefficients' dependence will from now on be left out as well. This is especially important to remember for the acoustic tensor, as it is defined for each frequency individually. With these newly established rules (5.4) would then be written as

$$\mathbf{A}_{mp}\hat{\omega}_p = \frac{\mathrm{i}}{2\pi}\mathbf{k}_n\hat{\underline{\tau}}^{\mathrm{mech}}_{mn} + \frac{1}{4\pi^2}\hat{\mathbf{g}}^{\mathrm{mech}}_m \qquad \text{for all } \mathbf{k} \in \mathbb{Z}_N \ . \tag{5.6}$$

Lemma 5.2.2. *The acoustic algebraic operator* $\mathbf{A}$ *defined in* (5.5) *is for all* $\mathbf{k} \in \mathbb{Z}_N$ *symmetric and positive definite, therefore invertible.*

Proof. The goal is to lead the claim back to the ellipticity condition (3.61) which should hold true for $\underline{\mathbf{C}}^0$. First, let $M \in \mathbb{R}^{d\times d}$ be an arbitrary matrix. Every such matrix can be uniquely decomposed into its symmetric part $M^{\mathrm{sym}} \coloneqq \frac{1}{2}\left(M + M^{\mathrm{T}}\right)$ and its skew-symmetric part $M^{\mathrm{asym}} \coloneqq \frac{1}{2}\left(M - M^{\mathrm{T}}\right)$. This gives

$$\begin{aligned} M^{\mathrm{T}} : \underline{\mathbf{C}}^0 : M &= \left(M^{\mathrm{sym}} + M^{\mathrm{asym}}\right)^{\mathrm{T}} : \underline{\mathbf{C}}^0 : \left(M^{\mathrm{sym}} + M^{\mathrm{asym}}\right) \\ &= M^{\mathrm{sym}}_{ji}\underline{\mathbf{C}}^0_{ijmn}M^{\mathrm{sym}}_{mn} + \underbrace{M^{\mathrm{sym}}_{ji}\underline{\mathbf{C}}^0_{ijmn}M^{\mathrm{asym}}_{mn} + M^{\mathrm{asym}}_{ji}\underline{\mathbf{C}}^0_{ijmn}M^{\mathrm{sym}}_{mn} + M^{\mathrm{asym}}_{ji}\underline{\mathbf{C}}^0_{ijmn}M^{\mathrm{asym}}_{mn}}_{=0} \\ &= \left(M^{\mathrm{sym}}\right)^{\mathrm{T}} : \underline{\mathbf{C}}^0 : M^{\mathrm{sym}} \ . \end{aligned}$$

The latter terms are all canceled out due to the skew-symmetry of M^{asym} and the minor symmetries of the stiffness tensor. For example, in the second expression every summand $M^{\mathrm{sym}}_{ji}\underline{\mathbf{C}}^0_{ijmn}M^{\mathrm{asym}}_{mn}$ would be canceled by the summand with flipped indices m and n, as $\underline{\mathbf{C}}^0_{ijnm} = \underline{\mathbf{C}}^0_{ijmn}$ but $M^{\mathrm{asym}}_{mn} = -M^{\mathrm{asym}}_{nm}$. Similar arguments hold true for the third and forth expression, only leaving the first one in the end. Since the remaining quantities are all symmetric, one can then transform the expression into its Mandel notation and apply the ellipticity condition, yielding

$$M^{\mathrm{T}} : \underline{\mathbf{C}}^0 : M = \left(M^{\mathrm{sym}}\right)^{\mathrm{T}} : \underline{\mathbf{C}}^0 : M^{\mathrm{sym}} \geq \gamma_{\mathbf{C}^0}\left\|\mathcal{M}_2^d(M^{\mathrm{sym}})\right\| \ .$$

Now choose $M = \mathbf{a}\mathbf{k}^{\mathrm{T}}$ for any vector $\mathbf{a} \in \mathbb{R}^d, \mathbf{a} \neq 0$ and $\mathbf{k} \in \mathbb{Z}_N$. Then $M^{\mathrm{sym}} \neq 0$, since $M = M^{\mathrm{asym}}$ otherwise and if that was the case, all diagonal entries $\mathbf{a}_i\mathbf{k}_i$ for $i = 1, \dots, d$ would have to be zero. Since both $\mathbf{a}$ and $\mathbf{k}$ were assumed to not be the zero vector, there has to be at least one index i_0 such that without loss of generality $\mathbf{a}_{i_0} = 0$ but $\mathbf{k}_{i_0} \neq 0$. This would mean that all entries $\mathbf{a}_{i_0}\mathbf{k}_j$ in the i_0-th row for $j = 1, \dots, d$ are also zero. Due to the skew-symmetry, this would imply that also all entries $\mathbf{a}_j\mathbf{k}_{i_0}$ in the i_0-th column for $j = 1, \dots, d$ have to be zero as well which could then only be possible, if $\mathbf{a}$ was the zero vector, contradicting the original assumption. Thus, one obtains with the estimate above for all frequency vectors $\mathbf{k} \in \mathbb{Z}_N$ that

$$\mathbf{a}^{\mathrm{T}}\mathbf{A}\mathbf{a} = \left(\mathbf{a}\mathbf{k}^{\mathrm{T}}\right)^{\mathrm{T}} : \underline{\mathbf{C}}^0 : \mathbf{a}\mathbf{k}^{\mathrm{T}} > 0, \qquad \forall \mathbf{a} \in \mathbb{R}^d, \mathbf{a} \neq 0 \ ,$$

proving positive definiteness of the acoustic tensor. Furthermore, $\mathbf{A}$ is symmetric due to the symmetry properties of the stiffness tensor detailed in (3.20). □

This lemma just provides the theoretical existence of the acoustic inverse, but for the algorithms developed later on it would be quite helpful and time-reducing, if the inverse could be computed

directly instead of first setting up $\mathbf{A}$ for each frequency and inverting it numerically afterwards. Such formulas can be set up for different types of stiffness tensors and while each one might have certain advantages in specific situations, the most common choice for $\underline{\mathbf{C}}^0$ is that of an artificial isotropic material, as it only needs two variables such as the Lamé parameters to be specified. For this reason, the important case of inverting the acoustic tensor of such an isotropic stiffness tensor will be presented explicitly.

Lemma 5.2.3. *If the stiffness tensor is isotropic of the form* $\underline{\mathbf{C}}^0_{mnop} = \lambda^0 \delta_{mn}\delta_{op} + \mu^0 \left(\delta_{mo}\delta_{np} + \delta_{mp}\delta_{no}\right)$ *where* λ^0 *and* μ^0 *denote the first and second Lamé parameter, the inverse of the acoustic tensor* $\mathbf{A}$ *for any non-zero frequency vector* $\mathbf{k}$ *is given by*

$$\mathbf{A}^{-1}_{mn} = \frac{1}{\mu^0 \|\mathbf{k}\|^2}\left(\delta_{mn} - \frac{\mathbf{k}_m \mathbf{k}_n}{\|\mathbf{k}\|^2}\frac{\lambda^0 + \mu^0}{\lambda^0 + 2\mu^0}\right) .$$

Proof. The acoustic tensor has the entries

$$\mathbf{A}_{no} = \underline{\mathbf{C}}^0_{nrso}\mathbf{k}_r\mathbf{k}_s = \left(\lambda^0 + \mu^0\right)\mathbf{k}_n\mathbf{k}_o + \delta_{no}\mu^0\|\mathbf{k}\|^2 .$$

Now simply check that the matrix product indeed yields the identity matrix.

$$\begin{aligned}
\mathbf{A}^{-1}_{mn}\mathbf{A}_{no} &= \frac{1}{\mu^0\|\mathbf{k}\|^2}\left(\delta_{mn} - \frac{\mathbf{k}_m\mathbf{k}_n}{\|\mathbf{k}\|^2}\frac{\lambda^0+\mu^0}{\lambda^0+2\mu^0}\right)\left(\left(\lambda^0+\mu^0\right)\mathbf{k}_n\mathbf{k}_o + \delta_{no}\mu^0\|\mathbf{k}\|^2\right) \\
&= \frac{1}{\mu^0\|\mathbf{k}\|^2}\left(\left(\lambda^0+\mu^0\right)\mathbf{k}_m\mathbf{k}_o + \delta_{om}\mu^0\|\mathbf{k}\|^2 - \mathbf{k}_m\mathbf{k}_o\frac{(\lambda^0+\mu^0)^2}{\lambda^0+2\mu^0} - \mathbf{k}_m\mathbf{k}_o\frac{\mu^0(\lambda^0+\mu^0)}{\lambda^0+2\mu^0}\right) \\
&= \frac{1}{\mu^0\|\mathbf{k}\|^2}\left(\delta_{om}\mu^0\|\mathbf{k}\|^2 + \left(\lambda^0+\mu^0\right)\mathbf{k}_m\mathbf{k}_o - \left(\lambda^0+\mu^0\right)\mathbf{k}_m\mathbf{k}_o\right) \\
&= \delta_{mo}
\end{aligned}$$

□

With these results at hand, it is now time to solve (5.6). One obtains

$$\hat{\omega}_m = \frac{\mathrm{i}}{2\pi}\mathbf{A}^{-1}_{mo}\mathbf{k}_p\hat{\underline{\tau}}^{\mathrm{mech}}_{op} + \frac{1}{4\pi^2}\mathbf{A}^{-1}_{mo}\hat{\mathbf{g}}^{\mathrm{mech}}_o \qquad \text{for all } \mathbf{k} \in \mathbb{Z}_N \ . \tag{5.7}$$

While this equation is again totally fine from a theoretical standpoint, the application of what can be defined as a tensor of rank three to $\hat{\underline{\tau}}^{\mathrm{mech}}$ is not quite as elegant as standard matrix–vector calculus. While some definitions like the one for the acoustic tensor can only be written down in tensor notation due to the lack of symmetries, one still wishes to exploit notations like the Mandel transform in the end for the greater computations. With (5.7) however, such a notation might not be as straightforward as one would hope.

To explain this further, $\hat{\underline{\tau}}^{\mathrm{mech}}_{op}$ is for example symmetric with respect to its indices o and p but the same symmetry can not be found in the operator $\mathbf{A}^{-1}_{mo}\mathbf{k}_p$ being applied to it. The only symmetry found within this operator would be between indices m and o instead. While this would still allow for both, the operator of rank three and the quantity it is applied to, to each have Mandel notations on their own — transforming them into a matrix and a vector respectively — it is not immediately possible to write down a coherent transformed expression that makes use of symmetries shared between the two.

This leads to a little trick when defining the Green operators. In a certain sense it does not really matter how these operators are defined as long as their actions on the corresponding quantity yield

the correct result. With this idea and the fact that $\underline{\hat{\tau}}^{\mathrm{mech}}$ is always required to be symmetric for the presented problems, one can take advantage of the equality

$$\begin{aligned}\mathbf{A}^{-1}_{mo}\mathbf{k}_p\underline{\hat{\tau}}^{\mathrm{mech}}_{op} &= \frac{1}{2}\left(\mathbf{A}^{-1}_{mo}\mathbf{k}_p\underline{\hat{\tau}}^{\mathrm{mech}}_{op} + \mathbf{A}^{-1}_{mp}\mathbf{k}_o\underline{\hat{\tau}}^{\mathrm{mech}}_{po}\right)\\ &= \frac{1}{2}\left(\mathbf{A}^{-1}_{mo}\mathbf{k}_p\underline{\hat{\tau}}^{\mathrm{mech}}_{op} + \mathbf{A}^{-1}_{mp}\mathbf{k}_o\underline{\hat{\tau}}^{\mathrm{mech}}_{op}\right)\\ &= \frac{1}{2}\left(\mathbf{A}^{-1}_{mo}\mathbf{k}_p + \mathbf{A}^{-1}_{mp}\mathbf{k}_o\right)\underline{\hat{\tau}}^{\mathrm{mech}}_{op}\,,\end{aligned} \tag{5.8}$$

effectively resulting in a symmetrized operator — now with respect to indices o and p — without changing the effect it has when applied to symmetric matrices.

Theorem 5.2.4. *For every $\mathbf{k} \in \mathbb{Z}_N$, the $\mathbf{k}$-th Fourier coefficient of the displacement field ω of Problem 7 can be computed in matrix–vector notation as*

$$\hat{\omega} = \hat{\Gamma}^{\omega}_{\tau^{\mathrm{mech}}}\hat{\tau}^{\mathrm{mech}} + \hat{\Gamma}^{\omega}_{\mathbf{g}^{\mathrm{mech}}}\hat{\mathbf{g}}^{\mathrm{mech}}$$

with the Green operators

$$\begin{aligned}\hat{\Gamma}^{\omega}_{\tau^{\mathrm{mech}}} &\in \mathbb{C}^{d\times\tilde{d}} \quad \textit{with} \quad \left(\underline{\hat{\Gamma}}^{\omega}_{\tau^{\mathrm{mech}}}\right)_{mop} = \frac{\mathrm{i}}{4\pi}\left(\mathbf{A}^{-1}_{mo}\mathbf{k}_p + \mathbf{A}^{-1}_{mp}\mathbf{k}_o\right)\,,\\ \hat{\Gamma}^{\omega}_{\mathbf{g}^{\mathrm{mech}}} &\in \mathbb{C}^{d\times d} \quad \textit{with} \quad \left(\hat{\Gamma}^{\omega}_{\mathbf{g}^{\mathrm{mech}}}\right)_{mo} = \frac{1}{4\pi^2}\mathbf{A}^{-1}_{mo}\end{aligned}$$

where the mechanical acoustic tensor $\mathbf{A}$ is defined according to (5.5).

Alternatively, Green operators with respect to the strain field $\boldsymbol{\varepsilon}_{\mathbf{y}}(\omega)$ can be defined after an additional application of the symmetric gradient. As it will be shown later on, it is favorable for the pLS–equations to be formulated with respect to the gradient fields, instead of the displacement or magnetic scalar potential directly. The theorem would then read as follows.

Theorem 5.2.5. *For every $\mathbf{k} \in \mathbb{Z}_N$, the $\mathbf{k}$-th Fourier coefficient of the strain field $\boldsymbol{\varepsilon}(\omega)$ of Problem 7 can be computed in matrix–vector notation as*

$$\hat{\boldsymbol{\varepsilon}}(\omega) = \hat{\Gamma}^{\boldsymbol{\varepsilon}}_{\tau^{\mathrm{mech}}}\hat{\tau}^{\mathrm{mech}} + \hat{\Gamma}^{\boldsymbol{\varepsilon}}_{\mathbf{g}^{\mathrm{mech}}}\hat{\mathbf{g}}^{\mathrm{mech}}$$

with the Green operators

$$\begin{aligned}\hat{\Gamma}^{\boldsymbol{\varepsilon}}_{\tau^{\mathrm{mech}}} &\in \mathbb{C}^{\tilde{d}\times\tilde{d}} \quad \textit{with} \quad \left(\underline{\hat{\Gamma}}^{\boldsymbol{\varepsilon}}_{\tau^{\mathrm{mech}}}\right)_{mnop} = -\frac{1}{4}\left(\mathbf{A}^{-1}_{mo}\mathbf{k}_n\mathbf{k}_p + \mathbf{A}^{-1}_{mp}\mathbf{k}_n\mathbf{k}_o + \mathbf{A}^{-1}_{no}\mathbf{k}_m\mathbf{k}_p + \mathbf{A}^{-1}_{np}\mathbf{k}_m\mathbf{k}_o\right)\,,\\ \hat{\Gamma}^{\boldsymbol{\varepsilon}}_{\mathbf{g}^{\mathrm{mech}}} &\in \mathbb{C}^{\tilde{d}\times d} \quad \textit{with} \quad \left(\underline{\hat{\Gamma}}^{\boldsymbol{\varepsilon}}_{\mathbf{g}^{\mathrm{mech}}}\right)_{mno} = \frac{\mathrm{i}}{4\pi}\left(\mathbf{A}^{-1}_{mo}\mathbf{k}_n + \mathbf{A}^{-1}_{no}\mathbf{k}_m\right)\end{aligned}$$

where the mechanical acoustic tensor $\mathbf{A}$ is defined according to (5.5).

Non-Constant Case

The question remains how one could solve the mechanical equation, if the stiffness tensor was not constant over the entire domain — which is usually the case in practical applications. With the ultimate goal of post-pLS coupling in mind, solving the mechanical equation

$$\mathbf{div}\left(\mathbf{C}\,\boldsymbol{\varepsilon}(\omega) - \mathbf{e}\,\mathbf{H}(\varrho) + \tau^{\mathrm{mech}}\right) + \mathbf{g}^{\mathrm{mech}} = 0$$

of system (5.1), which not only contains a now spatially dependent stiffness tensor $\mathbf{C}$ but also explicitly includes the coupling term $\mathbf{e}\,\mathbf{H}(\varrho)$, will be the next step to take.

The idea now is to again choose a constant reference tensor $\mathbf{C}^0 \in \mathbb{R}^{\tilde{d}\times\tilde{d}}$ fulfilling the usual ellipticity and boundedness requirements to lead the non-constant problem back to the constant case by artificially adding zero to the equation, so that it can be expanded into

$$\mathbf{div}\left(\mathbf{C}^0\,\varepsilon(\omega) + \left(\mathbf{C}-\mathbf{C}^0\right)\varepsilon(\omega) - \mathbf{e}\,\mathbf{H}(\varrho) + \tau^{\mathrm{mech}}\right) + \mathbf{g}^{\mathrm{mech}} = 0\,.$$

Then setting

$$\tau^{\mathrm{mech}}_{\mathrm{new}} \coloneqq \left(\mathbf{C}-\mathbf{C}^0\right)\varepsilon(\omega) - \mathbf{e}\,\mathbf{H}(\varrho) + \tau^{\mathrm{mech}} \in L^2\left(\mathbb{T}^d, \mathbb{R}^{\tilde{d}}\right)$$

leads to

$$\mathbf{div}\left(\mathbf{C}^0\,\varepsilon(\omega) + \tau^{\mathrm{mech}}_{\mathrm{new}}\right) + \mathbf{g}^{\mathrm{mech}} = 0\,,$$

the exact type of equation whose solution was given by Theorem 5.2.4 or 5.2.5. Going along with the second option, this yields in the Fourier domain for each frequency vector $\mathbf{k} \in \mathbb{Z}_N$ the expression

$$\begin{aligned}\hat{\varepsilon}(\omega) &= \hat{\Gamma}^{\varepsilon}_{\tau^{\mathrm{mech}}}\hat{\tau}^{\mathrm{mech}}_{\mathrm{new}} + \hat{\Gamma}^{\varepsilon}_{\mathbf{g}^{\mathrm{mech}}}\hat{\mathbf{g}}^{\mathrm{mech}} \\ &= \hat{\Gamma}^{\varepsilon}_{\tau^{\mathrm{mech}}}\left(\widehat{\left(\mathbf{C}-\mathbf{C}^0\right)\varepsilon(\omega)} - \widehat{\mathbf{e}\,\mathbf{H}(\varrho)} + \hat{\tau}^{\mathrm{mech}}\right) + \hat{\Gamma}^{\varepsilon}_{\mathbf{g}^{\mathrm{mech}}}\hat{\mathbf{g}}^{\mathrm{mech}}\,. \end{aligned} \tag{5.9}$$

At this point one is faced with two new obstacles. For one, adding an artificial zero earlier may have allowed for Theorem 5.2.5 to be applied but by gathering all the remaining terms in $\tau^{\mathrm{mech}}_{\mathrm{new}}$, the solution field $\varepsilon(\omega)$ now appears on both sides within the equation, making at least a reordering of terms necessary. This connects to the second difficulty where one does not simply has to multiply Fourier coefficients in (5.9) but instead computes the coefficients of products, namely $\left(\left(\mathbf{C}-\mathbf{C}^0\right)\varepsilon(\omega)\right)$ and $(\mathbf{e}\,\mathbf{H}(\varrho))$.

Taking a closer look at the first product for example, such a coefficient would be computed as the discrete convolution

$$\widehat{\left(\mathbf{C}-\mathbf{C}^0\right)\varepsilon(\omega)}(\mathbf{k}) = \sum_{\mathbf{l}\in\mathbb{Z}_N} \widehat{\left(\mathbf{C}-\mathbf{C}^0\right)}(\mathbf{k}-\mathbf{l})\left(\hat{\varepsilon}(\omega)\right)(\mathbf{l})\,. \tag{5.10}$$

One should note that the summation is finite, since one is only looking for approximate solutions $\varepsilon(\omega) \in \Pi^{\tilde{d}}_N$. This connects back to the initial comment that the majority of the computations done so far could theoretically also be performed for solution fields with infinite Fourier series. If it were not already for a limited number of voxels from rasterized image data, one would now have to restrict oneself to a finite number of frequencies at the latest anyway, due to this discrete convolution. Even so, the current situation still leads to an unsatisfying observation, which is that with both frequency vectors $\mathbf{k}$ and $\mathbf{l}$ being in $\mathbb{Z}_N$ one would need the stiffness tensor's Fourier coefficients for all frequencies in $\mathbb{Z}_{2N}$, doubling the amount of required frequencies per each spatial dimension. This would result in a highly impractical algorithm as even an approximation of the solutions field's true Fourier series with only a few low-frequency coefficients could only be achieved with a much larger number of data points and therefore only with comparatively highly resolved image data.

That is however, only if one were to work solely within the Fourier domain. One of the truly beneficial concepts of the Basic Scheme is not the usage of truncated trigonometric polynomials alone but the constant switching between the spatial and the frequency domain through FFTs. Different operations might thus be performed within the domain more advantageous to them. For example with (5.10), instead of performing the discrete convolution in the frequency domain, it is certainly preferable to multiply the stiffness tensor with the strain field pointwise in the spatial domain before transforming the product back. Not only does the first step of this procedure work on all data points independently from each other and is therefore easy to parallelize when implemented, but above all it resolves the

problem of requiring additional frequencies, as a discretization of the stiffness tensor according to the vector N is now sufficient to gain all frequencies in $\mathbb{Z}_N$.

Thanks to this trick, one is eventually able to rewrite (5.9) based on the actual input data available in practice and to solve for the strain field on one side of the equation. Given a discretization vector $N \in \mathbb{N}^d$, each entry being an odd number, the total number ρ of discretization points is given by the product of all its entries. Deciding on a certain ordering of the grid points, vectors $\boldsymbol{\varepsilon}_N \in \mathbb{R}^{\rho\tilde{d}}, \mathbf{H}_N \in \mathbb{R}^{\rho d}, \tau_N^{\mathrm{mech}} \in \mathbb{R}^{\rho\tilde{d}}$ and $\mathbf{g}_N^{\mathrm{mech}} \in \mathbb{R}^{\rho d}$ can be set up, collecting the pointwise evaluation of the quantities $\boldsymbol{\varepsilon}(\omega), \mathbf{H}(\varrho), \tau^{\mathrm{mech}}$ and $\mathbf{g}^{\mathrm{mech}}$ respectively in the according order. In the same manner, the block diagonal matrices $\mathbf{C}_N, \mathbf{C}_N^0 \in \mathbb{R}^{\rho\tilde{d}\times\rho\tilde{d}}$ and $\mathbf{e}_N \in \mathbb{R}^{\rho\tilde{d}\times\rho d}$ can be defined. Of course, these matrices would never be fully defined in an actual algorithm but would be applied pointwise directly. They are more so just a necessary formalization to represent the linear system in its entirety on paper.

As with the grid points in the spatial domain, one also has to choose an ordering of the frequencies in the Fourier domain so that block diagonal matrices $\mathbf{G}^{\boldsymbol{\varepsilon}}_{\tau^{\mathrm{mech}}} \in \mathbb{C}^{\rho\tilde{d}\times\rho\tilde{d}}$ and $\mathbf{G}^{\boldsymbol{\varepsilon}}_{\mathbf{g}^{\mathrm{mech}}} \in \mathbb{C}^{\rho\tilde{d}\times\rho d}$ collecting the Green operators $\hat{\Gamma}^{\boldsymbol{\varepsilon}}_{\tau^{\mathrm{mech}}}$ and $\hat{\Gamma}^{\boldsymbol{\varepsilon}}_{\mathbf{g}^{\mathrm{mech}}}$ of all frequencies $\mathbf{k} \in \mathbb{Z}_N$ can be defined. Remember that up to this point the frequency vector equal to zero was of no interest, as the solutions to any cell problem (5.1) are only unique up to a constant term. For the FFT to work however, such a zero frequency is needed, which leads to the often before mentioned convention of choosing the spatial mean value to be explicitly set to zero. To stay in line with the formula of Theorem 5.2.5, one therefore defines the Green operators to have all entries set to zero for $\mathbf{k}$ being the zero frequency. These zero matrices then also have to be included in the block diagonal matrices.

Speaking about the FFT, what is numerically achieved by this highly optimized algorithm can be formally expressed as the application of properly sized DFT and permutation matrices. Leaving out the details on how to exactly define the entries of such a matrix — as this not only strongly depends on the orderings chosen in the spatial and frequency domain but is also again just a formalization not needed in actual implementations — this means that given the ordering of both domains, for any quantity $\mathbf{a}_N \in \mathbb{R}^{\rho m}$ with $m \in \mathbb{N}$ there exists an invertible matrix $\mathcal{F}_m \in \mathbb{C}^{\rho m\times\rho m}$, such that $\hat{\mathbf{a}}_N = \mathcal{F}_m\,\mathbf{a}_N$ holds true where $\hat{\mathbf{a}}_N$ is now the vector containing the DFT of $\mathbf{a}_N$ in the order chosen for the Fourier domain. In fact, $\mathcal{F}_m$ is up to a scaling factor even an orthogonal matrix, meaning that $\mathcal{F}_m\,\mathcal{F}_m^{\mathrm{T}} = \mathcal{F}_m^{\mathrm{T}}\,\mathcal{F}_m$ is a diagonal matrix with a repeating entry along the main diagonal.

With all new notations and quantities at hand, following the idea to work in the spatial domain as well, equation (5.9) finally translates to

$$\mathcal{F}_{\tilde{d}}\,\boldsymbol{\varepsilon}_N = \mathbf{G}^{\boldsymbol{\varepsilon}}_{\tau^{\mathrm{mech}}}\,\mathcal{F}_{\tilde{d}}\left(\left(\mathbf{C}_N - \mathbf{C}_N^0\right)\boldsymbol{\varepsilon}_N - \mathbf{e}_N\,\mathbf{H}_N + \tau_N^{\mathrm{mech}}\right) + \mathbf{G}^{\boldsymbol{\varepsilon}}_{\mathbf{g}^{\mathrm{mech}}}\,\mathcal{F}_d\,\mathbf{g}_N^{\mathrm{mech}} \tag{5.11}$$

or equivalently after rearranging the terms

$$\left(\mathrm{Id}_{\tilde{d}} - \mathcal{F}_{\tilde{d}}^{-1}\,\mathbf{G}^{\boldsymbol{\varepsilon}}_{\tau^{\mathrm{mech}}}\,\mathcal{F}_{\tilde{d}}\left(\mathbf{C}_N - \mathbf{C}_N^0\right)\right)\boldsymbol{\varepsilon}_N = \mathcal{F}_{\tilde{d}}^{-1}\,\mathbf{G}^{\boldsymbol{\varepsilon}}_{\tau^{\mathrm{mech}}}\,\mathcal{F}_{\tilde{d}}\left(-\mathbf{e}_N\,\mathbf{H}_N + \tau_N^{\mathrm{mech}}\right) + \mathcal{F}_{\tilde{d}}^{-1}\,\mathbf{G}^{\boldsymbol{\varepsilon}}_{\mathbf{g}^{\mathrm{mech}}}\,\mathcal{F}_d\,\mathbf{g}_N^{\mathrm{mech}} \tag{5.12}$$

where $\mathrm{Id}_{\tilde{d}}$ is supposed to denote the $\rho\tilde{d}$-dimensional identity matrix. While it proves difficult to show invertibility of the left-hand side matrix directly, the existence of the unique solution vector $\boldsymbol{\varepsilon}_N \in \mathbb{R}^{\rho\tilde{d}}$ is ensured through the application of the Lax–Milgram theorem to the corresponding weak form of the approximate discrete problem. The original Basic Scheme solves this system iteratively through a Neumann series approach but the usage of *conjugate gradient methods* has also been proven to work despite the matrix not being symmetric positive definite [57, 121].

5.2.2 The Magnetic Problem

Having worked through the mechanical equation already, the uncoupled magnetic equation is objectively easier to handle in comparison, thanks to its overall lower dimensionality, as the same steps will be gone through with all possibly arising concerns being already taken care of.

Constant Case

This time a constant permeability tensor $\boldsymbol{\mu}^0 \in \mathbb{R}^{d\times d}$ is chosen to set up the equation

$$\operatorname{div}\left(\boldsymbol{\mu}^0\,\mathbf{H}(\varrho) + \tau^{\mathrm{mag}}\right) + \mathbf{g}^{\mathrm{mag}} = 0\,.$$

With the definitions from the previous subsection one can state the approximate problem for the magnetic equation in its weak form. Since the magnetic field is traditionally defined as the negative gradient of the scalar potential, some attention has to be paid to the occurring signs which differ from the purely mechanical equation.

Problem 8 (Magnetic auxiliary problem)**.** *For $N \in \mathbb{N}^d$, with N being odd in each entry, find $\varrho \in \Pi^1_N$, such that*

$$\int_{\mathbb{T}^d} (\mathbf{H}(\phi))^{\mathrm{T}}\left(\boldsymbol{\mu}^0\,\mathbf{H}(\varrho) + \tau^{\mathrm{mag}}\right) + \phi\,\mathbf{g}^{\mathrm{mag}}\,\mathrm{d}\,\mathbf{y} = 0$$

holds true for all test functions $\phi \in \Pi^1_N$.

Following the same arguments from before, one then chooses the test function $\phi = \mathrm{e}^{2\pi\,\mathrm{i}\langle -\mathbf{k},\mathbf{y}\rangle}$ for some $\mathbf{k} \in \mathbb{Z}_N$ and expresses the weak form in terms of Fourier series as

$$\begin{aligned}
&\int_{\mathbb{T}^d} \left(-2\pi\,\mathrm{i}\,\mathbf{k}_m\,\mathrm{e}^{2\pi\,\mathrm{i}\langle -\mathbf{k},\mathbf{y}\rangle}\right)\left(\boldsymbol{\mu}^0_{mn}\left(\sum_{\mathbf{l}\in\mathbb{Z}_N} -2\pi\,\mathrm{i}\,\mathbf{l}_n\,\hat{\varrho}(\mathbf{l})\,\mathrm{e}^{2\pi\,\mathrm{i}\langle \mathbf{l},\mathbf{y}\rangle}\right) + \left(\sum_{\mathbf{l}\in\mathbb{Z}^d} \hat{\tau}^{\mathrm{mag}}_m(\mathbf{l})\,\mathrm{e}^{2\pi\,\mathrm{i}\langle \mathbf{l},\mathbf{y}\rangle}\right)\right)\mathrm{d}\,\mathbf{y} \\
= &\int_{\mathbb{T}^d} \mathrm{e}^{2\pi\,\mathrm{i}\langle -\mathbf{k},\mathbf{y}\rangle}\left(\sum_{\mathbf{l}\in\mathbb{Z}^d_\star} \hat{\mathbf{g}}^{\mathrm{mag}}(\mathbf{l})\,\mathrm{e}^{2\pi\,\mathrm{i}\langle \mathbf{l},\mathbf{y}\rangle}\right)\mathrm{d}\,\mathbf{y} \qquad (5.13)
\end{aligned}$$

which simplifies again due to the orthogonality property (5.3) to the single-frequency equation

$$-4\pi^2\mu^0_{mn}\mathbf{k}_m\mathbf{k}_n\hat{\varrho} - 2\pi\,\mathrm{i}\,\mathbf{k}_m\hat{\tau}^{\mathrm{mag}}_m = \hat{\mathbf{g}}^{\mathrm{mag}}\,.$$

Rearranging the terms gives

$$\mu^0_{mn}\mathbf{k}_m\mathbf{k}_n\hat{\varrho} = -\frac{\mathrm{i}}{2\pi}\mathbf{k}_m\hat{\tau}^{\mathrm{mag}}_m - \frac{1}{4\pi^2}\hat{\mathbf{g}}^{\mathrm{mag}} \qquad (5.14)$$

whose structure is apart from the change in sign identical to (5.4) in the mechanical case.

In analogy to the acoustic algebraic tensor $\mathbf{A}$, one defines for each frequency $\mathbf{k} \in \mathbb{Z}_N$ the scalar

$$B \coloneqq \boldsymbol{\mu}^0_{mn}\,\mathbf{k}_m\mathbf{k}_n\,. \qquad (5.15)$$

Because of their strong resemblance, $\mathbf{A}$ and B will also be referred to as the *mechanical acoustic tensor* and the *magnetic acoustic tensor* within this thesis (even though B is actually just a scalar). Whereas it was not obvious at first glance that the former one is invertible, the ellipticity condition of $\boldsymbol{\mu}^0$ immediately guarantees B to be positive and therefore invertible, leading to the following theorems

without any additional effort. The first theorem is formulated again in terms of the scalar magnetic potential being the classic solution field. The second one is then a reformulation in terms of the gradient field $\mathbf{H}(\varrho)$.

Theorem 5.2.6. *For every $\mathbf{k} \in \mathbb{Z}_N$, the $\mathbf{k}$-th Fourier coefficient of the magnetic scalar potential field ϱ of Problem 8 can be computed in matrix–vector notation as*

$$\hat{\varrho} = \hat{\Gamma}^{\varrho}_{\tau^{\mathrm{mag}}} \hat{\tau}^{\mathrm{mag}} + \hat{\Gamma}^{\varrho}_{\mathbf{g}^{\mathrm{mag}}} \hat{\mathbf{g}}^{\mathrm{mag}}$$

with the Green operators

$$\begin{aligned} \hat{\Gamma}^{\varrho}_{\tau^{\mathrm{mag}}} &\in \mathbb{C}^{1\times d} \quad \textit{with} \quad \left(\hat{\Gamma}^{\varrho}_{\tau^{\mathrm{mag}}}\right)_m = -\frac{\mathrm{i}}{2\pi B}\mathbf{k}_m \,, \\ \hat{\Gamma}^{\varrho}_{\mathbf{g}^{\mathrm{mag}}} &\in \mathbb{C} \quad \textit{with} \quad \hat{\Gamma}^{\varrho}_{\mathbf{g}^{\mathrm{mag}}} = -\frac{1}{4\pi^2 B} \end{aligned}$$

where the magnetic acoustic tensor B is defined according to (5.15).

Theorem 5.2.7. *For every $\mathbf{k} \in \mathbb{Z}_N$, the $\mathbf{k}$-th Fourier coefficient of the magnetic field $\mathbf{H}(\varrho)$ of Problem 8 can be computed in matrix–vector notation as*

$$\hat{\mathbf{H}}(\varrho) = \hat{\Gamma}^{\mathbf{H}}_{\tau^{\mathrm{mag}}} \hat{\tau}^{\mathrm{mag}} + \hat{\Gamma}^{\mathbf{H}}_{\mathbf{g}^{\mathrm{mag}}} \hat{\mathbf{g}}^{\mathrm{mag}}$$

with the Green operators

$$\begin{aligned} \hat{\Gamma}^{\mathbf{H}}_{\tau^{\mathrm{mag}}} &\in \mathbb{C}^{d\times d} \quad \textit{with} \quad \left(\hat{\Gamma}^{\varrho}_{\tau^{\mathrm{mag}}}\right)_{mn} = -\frac{1}{B}\mathbf{k}_m\mathbf{k}_n \,, \\ \hat{\Gamma}^{\mathbf{H}}_{\mathbf{g}^{\mathrm{mag}}} &\in \mathbb{C}^{d} \quad \textit{with} \quad \left(\hat{\Gamma}^{\varrho}_{\mathbf{g}^{\mathrm{mag}}}\right)_n = \frac{\mathrm{i}}{2\pi B}\mathbf{k}_n \end{aligned}$$

where the magnetic acoustic tensor B is defined according to (5.15).

Non-Constant Case

Now looking at the magnetic equation

$$\operatorname{div}\left(\mathbf{e}^{\mathrm{T}}\,\boldsymbol{\varepsilon}\,(\omega) + \boldsymbol{\mu}\,\mathbf{H}\,(\varrho) + \tau^{\mathrm{mag}}\right) + \mathbf{g}^{\mathrm{mag}} = 0$$

of (5.1), selecting a suitable reference permeability tensor $\boldsymbol{\mu}^0 \in \mathbb{R}^{d\times d}$ and defining

$$\tau^{\mathrm{mag}}_{\mathrm{new}} \coloneqq \left(\boldsymbol{\mu} - \boldsymbol{\mu}^0\right)\mathbf{H}(\varrho) + \mathbf{e}^{\mathrm{T}}\,\boldsymbol{\varepsilon}(\omega) + \tau^{\mathrm{mag}} \in L^2\left(\mathbb{T}^d, \mathbb{R}^d\right)$$

results in the altered equation

$$\operatorname{div}\left(\boldsymbol{\mu}^0\,\mathbf{H}\,(\varrho) + \tau^{\mathrm{mag}}_{\mathrm{new}}\right) + \mathbf{g}^{\mathrm{mag}} = 0\,.$$

The solution in terms of Fourier expressions for each $\mathbf{k} \in \mathbb{Z}_N$ is then given by Theorem 5.2.7 as

$$\begin{aligned} \hat{\mathbf{H}}(\varrho) &= \hat{\Gamma}^{\mathbf{H}}_{\tau^{\mathrm{mag}}} \hat{\tau}^{\mathrm{mag}}_{\mathrm{new}} + \hat{\Gamma}^{\mathbf{H}}_{\mathbf{g}^{\mathrm{mag}}} \hat{\mathbf{g}}^{\mathrm{mag}} \\ &= \hat{\Gamma}^{\mathbf{H}}_{\tau^{\mathrm{mag}}} \left(\widehat{\left(\boldsymbol{\mu} - \boldsymbol{\mu}^0\right)\mathbf{H}\,(\varrho)} + \widehat{\mathbf{e}^{\mathrm{T}}\,\boldsymbol{\varepsilon}\,(\omega)} + \hat{\tau}^{\mathrm{mag}}\right) + \hat{\Gamma}^{\mathbf{H}}_{\mathbf{g}^{\mathrm{mag}}} \hat{\mathbf{g}}^{\mathrm{mag}}\,. \end{aligned} \tag{5.16}$$

Going along with the previous discussion for the mechanical equation, according to the discretization vector $N \in \mathbb{N}^d$, the number of discretization points ρ and the orderings for the discrete input data and frequencies, one can set up the data-point vectors and block diagonal matrices to transfer (5.16)

into the discretized spatial domain. Additionally to the quantities introduced before, this includes $\tau_N^{\mathrm{mag}} \in \mathbb{R}^{\rho d}$ and $\mathbf{g}_N^{\mathrm{mag}} \in \mathbb{R}^{\rho}$ for the inner and outer forces, block diagonal matrices $\boldsymbol{\mu}_N, \boldsymbol{\mu}_N^0 \in \mathbb{R}^{\rho d \times \rho d}$ collecting the pointwise permeability tensors, as well as $\mathbf{G}^{\mathbf{H}}_{\tau^{\mathrm{mag}}} \in \mathbb{C}^{\rho d \times \rho d}$ and $\mathbf{G}^{\mathbf{H}}_{\mathbf{g}^{\mathrm{mag}}} \in \mathbb{C}^{\rho d \times \rho}$ containing the Green operators for different frequencies.

With that the resulting pLS–equation can be written as

$$\mathcal{F}_d \, \mathbf{H}_N = \mathbf{G}^{\mathbf{H}}_{\tau^{\mathrm{mag}}} \, \mathcal{F}_d \left(\left(\boldsymbol{\mu}_N - \boldsymbol{\mu}_N^0 \right) \mathbf{H}_N + \mathbf{e}_N^{\mathrm{T}} \, \boldsymbol{\varepsilon}_N + \tau_N^{\mathrm{mag}} \right) + \mathbf{G}^{\mathbf{H}}_{\mathbf{g}^{\mathrm{mag}}} \, \mathcal{F}_1 \, \mathbf{g}_N^{\mathrm{mag}} \tag{5.17}$$

and can be rearranged to solve for $\mathbf{H}_N$ as the linear system

$$\left(\mathrm{Id}_d - \mathcal{F}_d^{-1} \, \mathbf{G}^{\mathbf{H}}_{\tau^{\mathrm{mag}}} \, \mathcal{F}_d \left(\boldsymbol{\mu}_N - \boldsymbol{\mu}_N^0 \right) \right) \mathbf{H}_N = \mathcal{F}_d^{-1} \, \mathbf{G}^{\mathbf{H}}_{\tau^{\mathrm{mag}}} \, \mathcal{F}_d \left(\mathbf{e}_N^{\mathrm{T}} \, \boldsymbol{\varepsilon}_N + \tau_N^{\mathrm{mag}} \right) + \mathcal{F}_d^{-1} \, \mathbf{G}^{\mathbf{H}}_{\mathbf{g}^{\mathrm{mag}}} \, \mathcal{F}_1 \, \mathbf{g}_N^{\mathrm{mag}} \ . \tag{5.18}$$

The statements about solvability of the system and feasible numerical methods from (5.12) hold true for (5.18) as well.

5.2.3 Recoupling Strategies

With the separately derived pLS–equations (5.12) and (5.18) at hand, it is now time to talk about how they can be combined to solve the coupled problem (5.1). Following two different schools of thought, one may either try to use a *staggered algorithm* or a *monolithic approach* instead.

Staggered Approach

Staggered methods for coupled systems generally aim to split the problem into smaller subproblems which are hopefully easier to analyze. One then attempts to find a solution of the whole system by alternately solving the involved subproblems [109]. The coupling is usually achieved by incorporating the solution of one subroutine as input data for the other one, for example in the form of a right-hand side vector. Such methods, although very simple in their idea, can often already give some satisfying results, while having the great advantage that solvers for the extracted subproblems are often already implemented and optimized, so that only little effort is needed to set up a routine for the coupled problem. This is what makes staggered methods interesting from a practical viewpoint. However, even if the involved subroutines are already proven to converge in each step, the convergence of these approaches in their entirety does not follow immediately. For this reason and because the focus in this thesis is set more on the upcoming alternative of a monolithic approach whose convergence follows directly, the staggered scheme will not be discussed in more detail here, despite it seemingly working well for some of the later discussed numerical examples. For the sake of completeness however, the basic routine of a staggered method for linear magneto-elastic problems is stated below.

Algorithm 1 Staggered Algorithm

Require: Initial values $\boldsymbol{\varepsilon}_N^{(0)}, \mathbf{H}_N^{(0)}$
  while criterion not met **do**
    $\mathbf{H}_N^{(k)} \rightarrow$ rhs of (5.12)
    $\boldsymbol{\varepsilon}_N^{(k+1)} \leftarrow$ solve (5.12)
    $\boldsymbol{\varepsilon}_N^{(k+1)} \rightarrow$ rhs of (5.18)
    $\mathbf{H}_N^{(k+1)} \leftarrow$ solve (5.18)
    increase k
  end while

Alternatively to the order listed here, one could also solve the magnetic equation first and then use the new approximation for the magnetic field in the right-hand side of the mechanical one. Depending on how the pLS–equations are solved, different stopping criteria may be used within the subroutines such as a Cauchy-type criterion for the iterative Neumann series ansatz [57] or a comparison of the residual norm against a set tolerance when using CG-based solvers. Another Cauchy-type criterion may be used for the outer loop as well.

Monolithic Approach

Whereas the staggered approach solves the mechanical and magnetic equations successively, a monolithic method solves the whole system at once. As the coupling terms were already separated from the remaining inner force vectors, the combination of (5.12) and (5.18) into a common linear system happens straightforward by rearranging the terms and defining a common solution vector. Contrary to the staggered approach, the solvability of the linear system in its entirety follows again directly from its derivation from the weak forms and the Lax–Milgram theorem.

Theorem 5.2.8. *For a given discretization vector $N \in \mathbb{N}^d$ and chosen reference tensors $\mathbf{C}^0 \in \mathbb{R}^{\tilde{d}\times\tilde{d}}$ and $\boldsymbol{\mu}^0 \in \mathbb{R}^{d\times d}$, the system $\mathbf{M}\mathbf{x} = \mathbf{b}_\tau + \mathbf{b}_\mathbf{g}$ with the matrix*

$$\mathbf{M} \coloneqq \left(\begin{array}{c|c} \mathrm{Id}_{\tilde{d}} & 0 \\ \hline 0 & \mathrm{Id}_d \end{array}\right) - \left(\begin{array}{c|c} \mathcal{F}_{\tilde{d}}^{-1} & 0 \\ \hline 0 & \mathcal{F}_d^{-1} \end{array}\right)\left(\begin{array}{c|c} \mathbf{G}^{\boldsymbol{\varepsilon}}_{\tau^{\mathrm{mech}}} & 0 \\ \hline 0 & \mathbf{G}^{\mathbf{H}}_{\tau^{\mathrm{mag}}} \end{array}\right)\left(\begin{array}{c|c} \mathcal{F}_{\tilde{d}} & 0 \\ \hline 0 & \mathcal{F}_d \end{array}\right)\left(\begin{array}{c|c} \mathbf{C}_N - \mathbf{C}_N^0 & -\mathbf{e}_N \\ \hline \mathbf{e}_N^{\mathrm{T}} & \boldsymbol{\mu}_N - \boldsymbol{\mu}_N^0 \end{array}\right)$$

and right-hand side vectors

$$\begin{aligned} \mathbf{b}_\tau &\coloneqq \left(\begin{array}{c|c} \mathcal{F}_{\tilde{d}}^{-1} & 0 \\ \hline 0 & \mathcal{F}_d^{-1} \end{array}\right)\left(\begin{array}{c|c} \mathbf{G}^{\boldsymbol{\varepsilon}}_{\tau^{\mathrm{mech}}} & 0 \\ \hline 0 & \mathbf{G}^{\mathbf{H}}_{\tau^{\mathrm{mag}}} \end{array}\right)\left(\begin{array}{c|c} \mathcal{F}_{\tilde{d}} & 0 \\ \hline 0 & \mathcal{F}_d \end{array}\right)\left(\begin{array}{c} \tau_N^{\mathrm{mech}} \\ \hline \tau_N^{\mathrm{mag}} \end{array}\right), \\ \mathbf{b}_\mathbf{g} &\coloneqq \left(\begin{array}{c|c} \mathcal{F}_{\tilde{d}}^{-1} & 0 \\ \hline 0 & \mathcal{F}_d^{-1} \end{array}\right)\left(\begin{array}{c|c} \mathbf{G}^{\boldsymbol{\varepsilon}}_{\mathbf{g}^{\mathrm{mech}}} & 0 \\ \hline 0 & \mathbf{G}^{\mathbf{H}}_{\mathbf{g}^{\mathrm{mag}}} \end{array}\right)\left(\begin{array}{c|c} \mathcal{F}_d & 0 \\ \hline 0 & \mathcal{F}_1 \end{array}\right)\left(\begin{array}{c} \mathbf{g}_N^{\mathrm{mech}} \\ \hline \mathbf{g}_N^{\mathrm{mag}} \end{array}\right) \end{aligned}$$

has a unique solution $\mathbf{x} = (\boldsymbol{\varepsilon}_N \mid \mathbf{H}_N)$. Furthermore, the transformed vectors $\mathcal{F}_{\tilde{d}}\boldsymbol{\varepsilon}_N$ and $\mathcal{F}_d\mathbf{H}_N$ then store the coefficients for uniquely determined trigonometric polynomials $\boldsymbol{\varepsilon} \in \Pi_N^{\tilde{d}}$ and $\mathbf{H} \in \Pi_N^d$ that solve the approximate weak form of the generalized linear magneto-elastic cell problem (5.1).

5.3 Pre-pLS Coupling

Whereas in the previous section mechanical and magnetic effects were only coupled after their pLS–equations were set up, this section will now follow a *pre-pLS coupling*, meaning that the concepts used in the derivation of pLS–equations seen before will be applied to the entire, already coupled system at once, hoping to develop a scheme that might prove advantageous to the post-pLS coupling ones [15]. To achieve this goal one should again start from an auxiliary problem in which only material tensors with constant entries appear.

Constant Case

As with both separated equations before, one needs to define a reference stiffness tensor $\mathbf{C}^0 \in \mathbb{R}^{\tilde{d}\times\tilde{d}}$ and a reference permeability tensor $\boldsymbol{\mu}^0 \in \mathbb{R}^{d\times d}$ fulfilling their respective ellipticity condition. Additionally, $\mathbf{e}^0 \in \mathbb{R}^{\tilde{d}\times d}$ is chosen as a constant coupling tensor. The auxiliary problem takes the following form.

Problem 9 (Combined auxiliary problem)**.** *For $N \in \mathbb{N}^d$, with N being odd in each entry, find $\omega \in \Pi_N^d$ and $\varrho \in \Pi_N^1$ such that*

$$\begin{aligned}\int_{\mathbb{T}^d} (\boldsymbol{\varepsilon}(\mathbf{v}))^{\mathrm{T}} \left(\mathbf{C}^0\, \boldsymbol{\varepsilon}(\omega) - \mathbf{e}^0\, \mathbf{H}(\varrho) + \tau^{\mathrm{mech}}\right) - \mathbf{v}^{\mathrm{T}}\, \mathbf{g}^{\mathrm{mech}}\, \mathrm{d}\,\mathbf{y} &= 0\,,\\ \int_{\mathbb{T}^d} (\mathbf{H}(\phi))^{\mathrm{T}} \left(\left(\mathbf{e}^0\right)^{\mathrm{T}} \boldsymbol{\varepsilon}(\omega) + \boldsymbol{\mu}^0\, \mathbf{H}(\varrho) + \tau^{\mathrm{mag}}\right) + \phi\, \mathbf{g}^{\mathrm{mag}}\, \mathrm{d}\,\mathbf{y} &= 0\end{aligned}$$

hold true for all test functions $\mathbf{v} \in \Pi_N^d$ and $\phi \in \Pi_N^1$.

Choosing test functions $\mathbf{v}$ and ϕ as in the separated problems, the Fourier series representation yields after simplification

$$\begin{aligned}\underline{\mathbf{C}}^0_{mnop}\mathbf{k}_n\mathbf{k}_o\hat{\omega}_p + \underline{\mathbf{e}}^0_{mno}\mathbf{k}_n\mathbf{k}_o\hat{\varrho} &= \frac{\mathrm{i}}{2\pi}\mathbf{k}_n\hat{\underline{\tau}}^{\mathrm{mech}}_{mn} + \frac{1}{4\pi^2}\hat{\mathbf{g}}^{\mathrm{mech}}_m \qquad \text{for all } m \in \{1,\dots,d\}\,,\\ \underline{\mathbf{e}}^0_{opr}\mathbf{k}_o\mathbf{k}_r\hat{\omega}_p - \mu^0_{rs}\mathbf{k}_r\mathbf{k}_s\hat{\varrho} &= \frac{\mathrm{i}}{2\pi}\mathbf{k}_r\hat{\tau}^{\mathrm{mag}}_r + \frac{1}{4\pi^2}\hat{\mathbf{g}}^{\mathrm{mag}}\,.\end{aligned} \tag{5.19}$$

It is important to remember that the coupling tensor is symmetric with respect to its two leading indices. Therefore, the expressions $\underline{\mathbf{e}}^0_{mno}\mathbf{k}_n\mathbf{k}_o = \underline{\mathbf{e}}^0_{nmo}\mathbf{k}_n\mathbf{k}_o$ in the first line and $\underline{\mathbf{e}}^0_{opr}\mathbf{k}_o\mathbf{k}_r$ in the second line actually describe the same operator in the Einstein notation after relabeling the indices accordingly. This leads to the definition of another acoustic-type tensor $\mathbf{D} \in \mathbb{R}^d$ with entries

$$\mathbf{D}_m \coloneqq \underline{\mathbf{e}}^0_{mno}\mathbf{k}_n\mathbf{k}_o \tag{5.20}$$

for each frequency $\mathbf{k} \in \mathbb{Z}_N$. Together with the mechanical acoustic tensor $\mathbf{A}$ and the magnetic acoustic tensor B, this allows to write (5.19) as linear systems

$$\begin{aligned}\mathbf{A}\hat{\omega} + \mathbf{D}\hat{\varrho} &= \frac{\mathrm{i}}{2\pi}\left(\hat{\underline{\tau}}^{\mathrm{mech}}\right)^{\mathrm{T}}\mathbf{k} + \frac{1}{4\pi^2}\hat{\mathbf{g}}^{\mathrm{mech}}\,,\\ \mathbf{D}^{\mathrm{T}}\hat{\omega} - B\hat{\varrho} &= \frac{\mathrm{i}}{2\pi}\left(\hat{\tau}^{\mathrm{mag}}\right)^{\mathrm{T}}\mathbf{k} + \frac{1}{4\pi^2}\hat{\mathbf{g}}^{\mathrm{mag}}\,,\end{aligned}$$

or combined together as

$$\left(\begin{array}{c|c}\mathbf{A} & \mathbf{D}\\ \hline \mathbf{D}^{\mathrm{T}} & -B\end{array}\right)\left(\begin{array}{c}\hat{\omega}\\ \hline \hat{\varrho}\end{array}\right) = \frac{\mathrm{i}}{2\pi}\left(\begin{array}{c}\left(\hat{\underline{\tau}}^{\mathrm{mech}}\right)^{\mathrm{T}}\\ \hline \left(\hat{\tau}^{\mathrm{mag}}\right)^{\mathrm{T}}\end{array}\right)\mathbf{k} + \frac{1}{4\pi^2}\left(\begin{array}{c}\hat{\mathbf{g}}^{\mathrm{mech}}\\ \hline \hat{\mathbf{g}}^{\mathrm{mag}}\end{array}\right)\,. \tag{5.21}$$

Although $\hat{\underline{\tau}}^{\mathrm{mech}}$ would not be transposed in the matrix–vector notation initially as it was done here, its symmetric nature allows to do so to achieve a more standardized structure.

To check whether or not the block matrix of this system can be inverted, it is sufficient to know about the regularity of either $\mathbf{A}$ or B and of their corresponding *Schur complement*, as seen in the next lemma.

Lemma 5.3.1 (Inversion of block matrices; Proof in [122, Ch. 3])**.** *Let the block matrix*

$$\mathbf{M} = \left(\begin{array}{c|c}\mathbf{M}_{11} & \mathbf{M}_{12}\\ \hline \mathbf{M}_{21} & \mathbf{M}_{22}\end{array}\right)$$

have blocks $\mathbf{M}_{11} \in \mathbb{R}^{m\times m}, \mathbf{M}_{12} \in \mathbb{R}^{m\times n}, \mathbf{M}_{21} \in \mathbb{R}^{n\times m}$ and $\mathbf{M}_{22} \in \mathbb{R}^{n\times n}$.
If $\mathbf{M}_{11}$ is invertible, as well as its Schur complement $\mathbf{S}_1 \coloneqq \mathbf{M}_{22} - \mathbf{M}_{21}\mathbf{M}_{11}^{-1}\mathbf{M}_{12}$, the matrix $\mathbf{M}$ is regular with the inverse

$$\mathbf{M}^{-1} = \left(\begin{array}{c|c}\mathbf{M}_{11}^{-1} + \mathbf{M}_{11}^{-1}\mathbf{M}_{12}\mathbf{S}_1^{-1}\mathbf{M}_{21}\mathbf{M}_{11}^{-1} & -\mathbf{M}_{11}^{-1}\mathbf{M}_{12}\mathbf{S}_1^{-1}\\ \hline -\mathbf{S}_1^{-1}\mathbf{M}_{21}\mathbf{M}_{11}^{-1} & \mathbf{S}_1^{-1}\end{array}\right)\,.$$

Alternatively, if $\mathbf{M}_{22}$ *is invertible, as well as its Schur complement* $\mathbf{S}_2 \coloneqq \mathbf{M}_{11} - \mathbf{M}_{12}\mathbf{M}_{22}^{-1}\mathbf{M}_{21}$*, the inverse also exists and can be written as*

$$\mathbf{M}^{-1} = \left(\begin{array}{c|c} \mathbf{S}_2^{-1} & -\mathbf{S}_2^{-1}\mathbf{M}_{12}\mathbf{M}_{22}^{-1} \\ \hline -\mathbf{M}_{22}^{-1}\mathbf{M}_{21}\mathbf{S}_2^{-1} & \mathbf{M}_{22}^{-1} + \mathbf{M}_{22}^{-1}\mathbf{M}_{21}\mathbf{S}_2^{-1}\mathbf{M}_{12}\mathbf{M}_{22}^{-1} \end{array}\right) .$$

For the problem at hand, the first equation appears to be the smarter choice, as the inverse of $\mathbf{A}$ can be computed explicitly in the isotropic case with Lemma 5.2.3. The Schur complement of $\mathbf{A}$ then turns out to be a scalar whose inversion is trivial, as long as it is unequal to zero. Fortunately, this is always the case, as it was already argued that B is a positive quantity and that $\mathbf{A}$ is positive definite. The Schur complement which is computed as $\mathbf{S}_1 = \left(-B - \mathbf{D}^{\mathrm{T}}\mathbf{A}^{-1}\mathbf{D}\right)$ in this case thus has to be negative, therefore non-zero. The inverse then reads

$$\left(\begin{array}{c|c} \mathbf{A} & \mathbf{D} \\ \hline \mathbf{D}^{\mathrm{T}} & -B \end{array}\right)^{-1} =: \left(\begin{array}{c|c} \mathbf{Z}_{11} & \mathbf{Z}_{12} \\ \hline \mathbf{Z}_{12}^{\mathrm{T}} & \mathbf{Z}_{22} \end{array}\right) \tag{5.22}$$

where $\mathbf{Z}_{22} = \mathbf{S}_1^{-1}$ is defined as the inverse of the aforementioned Schur complement and the remaining two blocks can be computed as

$$\begin{aligned} \mathbf{Z}_{11} &= \mathbf{A}^{-1} + \mathbf{A}^{-1}\mathbf{D}\mathbf{Z}_{22}\mathbf{D}^{\mathrm{T}}\mathbf{A}^{-1} , \\ \mathbf{Z}_{12} &= -\mathbf{A}^{-1}\mathbf{D}\mathbf{Z}_{22} . \end{aligned}$$

Based on the resulting equation

$$\left(\begin{array}{c} \hat{\omega} \\ \hline \hat{\varrho} \end{array}\right) = \frac{\mathrm{i}}{2\pi}\left(\begin{array}{c|c} \mathbf{Z}_{11} & \mathbf{Z}_{12} \\ \hline \mathbf{Z}_{12}^{\mathrm{T}} & \mathbf{Z}_{22} \end{array}\right)\left(\begin{array}{c} \left(\hat{\underline{\tau}}^{\mathrm{mech}}\right)^{\mathrm{T}} \\ \hline \left(\hat{\tau}^{\mathrm{mag}}\right)^{\mathrm{T}} \end{array}\right)\mathbf{k} + \frac{1}{4\pi^2}\left(\begin{array}{c|c} \mathbf{Z}_{11} & \mathbf{Z}_{12} \\ \hline \mathbf{Z}_{12}^{\mathrm{T}} & \mathbf{Z}_{22} \end{array}\right)\left(\begin{array}{c} \hat{\mathbf{g}}^{\mathrm{mech}} \\ \hline \hat{\mathbf{g}}^{\mathrm{mag}} \end{array}\right) , \tag{5.23}$$

one is once more able to define consistent operators in the Mandel notation thanks to the symmetrization trick discussed at the end of Subsect. 5.2.1.

Theorem 5.3.2. *For every* $\mathbf{k} \in \mathbb{Z}_N$*, the* $\mathbf{k}$*-th Fourier coefficient of the displacement field* ω *and of the magnetic scalar potential field* ϱ *of Problem 9 can be computed in matrix–vector notation as*

$$\left(\begin{array}{c} \hat{\omega} \\ \hline \hat{\varrho} \end{array}\right) = \left(\begin{array}{c|c} \hat{\Gamma}^{\omega}_{\tau^{\mathrm{mech}}} & \hat{\Gamma}^{\omega}_{\tau^{\mathrm{mag}}} \\ \hline \hat{\Gamma}^{\varrho}_{\tau^{\mathrm{mech}}} & \hat{\Gamma}^{\varrho}_{\tau^{\mathrm{mag}}} \end{array}\right)\left(\begin{array}{c} \hat{\tau}^{\mathrm{mech}} \\ \hline \hat{\tau}^{\mathrm{mag}} \end{array}\right) + \left(\begin{array}{c|c} \hat{\Gamma}^{\omega}_{\mathbf{g}^{\mathrm{mech}}} & \hat{\Gamma}^{\omega}_{\mathbf{g}^{\mathrm{mag}}} \\ \hline \hat{\Gamma}^{\varrho}_{\mathbf{g}^{\mathrm{mech}}} & \hat{\Gamma}^{\varrho}_{\mathbf{g}^{\mathrm{mag}}} \end{array}\right)\left(\begin{array}{c} \hat{\mathbf{g}}^{\mathrm{mech}} \\ \hline \hat{\mathbf{g}}^{\mathrm{mag}} \end{array}\right)$$

with the Green operators

$$\begin{aligned}
\hat{\Gamma}^{\omega}_{\tau^{\mathrm{mech}}} &\in \mathbb{C}^{d\times\bar{d}} \quad \textit{with} \quad \left(\hat{\underline{\Gamma}}^{\omega}_{\tau^{\mathrm{mech}}}\right)_{mop} &&= \frac{\mathrm{i}}{4\pi}\left(\left(\mathbf{Z}_{11}\right)_{mo}\mathbf{k}_p + \left(\mathbf{Z}_{11}\right)_{mp}\mathbf{k}_o\right) , \\
\hat{\Gamma}^{\omega}_{\tau^{\mathrm{mag}}} &\in \mathbb{C}^{d\times d} \quad \textit{with} \quad \left(\hat{\Gamma}^{\omega}_{\tau^{\mathrm{mag}}}\right)_{mo} &&= \frac{\mathrm{i}}{2\pi}\left(\mathbf{Z}_{12}\right)_m\mathbf{k}_o , \\
\hat{\Gamma}^{\varrho}_{\tau^{\mathrm{mech}}} &\in \mathbb{C}^{1\times\bar{d}} \quad \textit{with} \quad \left(\hat{\underline{\Gamma}}^{\varrho}_{\tau^{\mathrm{mech}}}\right)_{mn} &&= \frac{\mathrm{i}}{4\pi}\left(\left(\mathbf{Z}_{12}\right)_m\mathbf{k}_n + \left(\mathbf{Z}_{12}\right)_n\mathbf{k}_m\right) , \\
\hat{\Gamma}^{\varrho}_{\tau^{\mathrm{mag}}} &\in \mathbb{C}^{1\times d} \quad \textit{with} \quad \left(\hat{\Gamma}^{\varrho}_{\tau^{\mathrm{mag}}}\right)_m &&= \frac{\mathrm{i}}{2\pi}\mathbf{Z}_{22}\mathbf{k}_m , \\
\hat{\Gamma}^{\omega}_{\mathbf{g}^{\mathrm{mech}}} &\in \mathbb{C}^{d\times d} \quad \textit{with} \quad \left(\hat{\Gamma}^{\omega}_{\mathbf{g}^{\mathrm{mech}}}\right)_{mo} &&= \frac{1}{4\pi^2}\left(\mathbf{Z}_{11}\right)_{mo} , \\
\hat{\Gamma}^{\omega}_{\mathbf{g}^{\mathrm{mag}}} &\in \mathbb{C}^{d} \quad \textit{with} \quad \left(\hat{\Gamma}^{\omega}_{\mathbf{g}^{\mathrm{mag}}}\right)_{m} &&= \frac{1}{4\pi^2}\left(\mathbf{Z}_{12}\right)_m , \\
\hat{\Gamma}^{\varrho}_{\mathbf{g}^{\mathrm{mech}}} &\in \mathbb{C}^{1\times d} \quad \textit{with} \quad \left(\hat{\Gamma}^{\varrho}_{\mathbf{g}^{\mathrm{mech}}}\right)_{m} &&= \frac{1}{4\pi^2}\left(\mathbf{Z}_{12}\right)_m , \\
\hat{\Gamma}^{\varrho}_{\mathbf{g}^{\mathrm{mag}}} &\in \mathbb{C} \quad \textit{with} \quad \left(\hat{\Gamma}^{\varrho}_{\mathbf{g}^{\mathrm{mag}}}\right) &&= \frac{1}{4\pi^2}\mathbf{Z}_{22}
\end{aligned}$$

where matrices $\mathbf{Z}_{11}, \mathbf{Z}_{12}$ *and* $\mathbf{Z}_{22}$ *are defined according to* (5.22).

Applying the symmetric gradient for the upper part of the system and the negative gradient for the lower one leads to the alternate formulation.

Theorem 5.3.3. *For every $\mathbf{k} \in \mathbb{Z}_N$, the $\mathbf{k}$-th Fourier coefficient of the strain field $\boldsymbol{\varepsilon}(\omega)$ and of the magnetic field $\mathbf{H}(\varrho)$ of Problem 9 can be computed in matrix–vector notation as*

$$\left(\begin{array}{c|c} \hat{\boldsymbol{\varepsilon}}(\omega) \\ \hline \hat{\mathbf{H}}(\varrho) \end{array}\right) = \left(\begin{array}{c|c} \hat{\Gamma}^{\boldsymbol{\varepsilon}}_{\tau^{\mathrm{mech}}} & \hat{\Gamma}^{\boldsymbol{\varepsilon}}_{\tau^{\mathrm{mag}}} \\ \hline \hat{\Gamma}^{\mathbf{H}}_{\tau^{\mathrm{mech}}} & \hat{\Gamma}^{\mathbf{H}}_{\tau^{\mathrm{mag}}} \end{array}\right) \left(\begin{array}{c} \hat{\tau}^{\mathrm{mech}} \\ \hline \hat{\tau}^{\mathrm{mag}} \end{array}\right) + \left(\begin{array}{c|c} \hat{\Gamma}^{\boldsymbol{\varepsilon}}_{\mathbf{g}^{\mathrm{mech}}} & \hat{\Gamma}^{\boldsymbol{\varepsilon}}_{\mathbf{g}^{\mathrm{mag}}} \\ \hline \hat{\Gamma}^{\mathbf{H}}_{\mathbf{g}^{\mathrm{mech}}} & \hat{\Gamma}^{\mathbf{H}}_{\mathbf{g}^{\mathrm{mag}}} \end{array}\right) \left(\begin{array}{c} \hat{\mathbf{g}}^{\mathrm{mech}} \\ \hline \hat{\mathbf{g}}^{\mathrm{mag}} \end{array}\right)$$

with the Green operators

$$\begin{aligned}
\hat{\Gamma}^{\boldsymbol{\varepsilon}}_{\tau^{\mathrm{mech}}} &\in \mathbb{C}^{\tilde{d}\times\tilde{d}} \quad \text{with} \quad \left(\hat{\underline{\Gamma}}^{\boldsymbol{\varepsilon}}_{\tau^{\mathrm{mech}}}\right)_{mnop} &&= -\frac{1}{4}\left((\mathbf{Z}_{11})_{mo}\,\mathbf{k}_n\mathbf{k}_p + (\mathbf{Z}_{11})_{mp}\,\mathbf{k}_n\mathbf{k}_o + (\mathbf{Z}_{11})_{no}\,\mathbf{k}_m\mathbf{k}_p + (\mathbf{Z}_{11})_{np}\,\mathbf{k}_m\mathbf{k}_o\right), \\
\hat{\Gamma}^{\boldsymbol{\varepsilon}}_{\tau^{\mathrm{mag}}} &\in \mathbb{C}^{\tilde{d}\times d} \quad \text{with} \quad \left(\hat{\underline{\Gamma}}^{\boldsymbol{\varepsilon}}_{\tau^{\mathrm{mag}}}\right)_{mno} &&= -\frac{1}{2}\left((\mathbf{Z}_{12})_{m}\,\mathbf{k}_n\mathbf{k}_o + (\mathbf{Z}_{12})_{n}\,\mathbf{k}_m\mathbf{k}_o\right), \\
\hat{\Gamma}^{\mathbf{H}}_{\tau^{\mathrm{mech}}} &\in \mathbb{C}^{d\times\tilde{d}} \quad \text{with} \quad \left(\hat{\underline{\Gamma}}^{\mathbf{H}}_{\tau^{\mathrm{mech}}}\right)_{mop} &&= \frac{1}{2}\left((\mathbf{Z}_{12})_{o}\,\mathbf{k}_p\mathbf{k}_m + (\mathbf{Z}_{12})_{p}\,\mathbf{k}_o\mathbf{k}_m\right), \\
\hat{\Gamma}^{\mathbf{H}}_{\tau^{\mathrm{mag}}} &\in \mathbb{C}^{d\times d} \quad \text{with} \quad \left(\hat{\Gamma}^{\mathbf{H}}_{\tau^{\mathrm{mag}}}\right)_{mo} &&= \mathbf{Z}_{22}\mathbf{k}_m\mathbf{k}_o, \\
\hat{\Gamma}^{\boldsymbol{\varepsilon}}_{\mathbf{g}^{\mathrm{mech}}} &\in \mathbb{C}^{\tilde{d}\times d} \quad \text{with} \quad \left(\hat{\underline{\Gamma}}^{\boldsymbol{\varepsilon}}_{\mathbf{g}^{\mathrm{mech}}}\right)_{mno} &&= \frac{\mathrm{i}}{4\pi}\left((\mathbf{Z}_{11})_{mo}\,\mathbf{k}_n + (\mathbf{Z}_{11})_{no}\,\mathbf{k}_m\right), \\
\hat{\Gamma}^{\boldsymbol{\varepsilon}}_{\mathbf{g}^{\mathrm{mag}}} &\in \mathbb{C}^{\tilde{d}} \quad \text{with} \quad \left(\hat{\underline{\Gamma}}^{\boldsymbol{\varepsilon}}_{\mathbf{g}^{\mathrm{mag}}}\right)_{mn} &&= \frac{\mathrm{i}}{4\pi}\left((\mathbf{Z}_{12})_{m}\,\mathbf{k}_n + (\mathbf{Z}_{12})_{n}\,\mathbf{k}_m\right), \\
\hat{\Gamma}^{\mathbf{H}}_{\mathbf{g}^{\mathrm{mech}}} &\in \mathbb{C}^{d\times d} \quad \text{with} \quad \left(\hat{\Gamma}^{\mathbf{H}}_{\mathbf{g}^{\mathrm{mech}}}\right)_{mo} &&= -\frac{\mathrm{i}}{2\pi}(\mathbf{Z}_{12})_{m}\,\mathbf{k}_o, \\
\hat{\Gamma}^{\mathbf{H}}_{\mathbf{g}^{\mathrm{mag}}} &\in \mathbb{C}^{d} \quad \text{with} \quad \left(\hat{\Gamma}^{\mathbf{H}}_{\mathbf{g}^{\mathrm{mag}}}\right)_{m} &&= -\frac{\mathrm{i}}{2\pi}\mathbf{Z}_{22}\mathbf{k}_m
\end{aligned}$$

where matrices $\mathbf{Z}_{11}, \mathbf{Z}_{12}$ and $\mathbf{Z}_{22}$ are defined according to (5.22).

Remark. *It should be noted that some of the Green operators appearing within these theorems are named the same way as for the mechanical and magnetic cases. One might think that this leads to confusion over which definition is referred to when such an operator is used later on. As it turns out though, the definitions in Theorem 5.3.2 and 5.3.3 coincide with the ones given in 5.2.4, 5.2.5, 5.2.6 and 5.2.7 in the case that the reference coupling tensor $\mathbf{e}^0$ was chosen equal to zero. Then $\mathbf{Z}_{11} = \mathbf{A}^{-1}$ and $\mathbf{Z}_{22} = -B^{-1}$, while $\mathbf{Z}_{12} = 0$, meaning that the definitions in the pre-pLS coupling are a generalization of what was seen before, justifying the naming scheme.*

Non-Constant Case

With the constant case being taken care of, one proceeds to solve the non-constant case

$$\begin{aligned}
\mathbf{div}\left(\mathbf{C}\,\boldsymbol{\varepsilon}(\omega) - \mathbf{e}\,\mathbf{H}(\varrho) + \tau^{\mathrm{mech}}\right) + \mathbf{g}^{\mathrm{mech}} &= 0, \\
\mathrm{div}\left(\mathbf{e}^{\mathrm{T}}\,\boldsymbol{\varepsilon}(\omega) + \boldsymbol{\mu}\,\mathbf{H}(\varrho) + \tau^{\mathrm{mag}}\right) + \mathbf{g}^{\mathrm{mag}} &= 0
\end{aligned}$$

by artificially including appropriate reference tensors $\mathbf{C}^0 \in \mathbb{R}^{\tilde{d}\times\tilde{d}}, \boldsymbol{\mu}^0 \in \mathbb{R}^{d\times d}$ and $\mathbf{e}^0 \in \mathbb{R}^{\tilde{d}\times d}$ and then collecting all non-constant quantities within new inner force vectors. This is similar to what was seen before, the difference this time being that an additional reference tensor in the form of $\mathbf{e}^0$ is involved which was not present during earlier derivations. One defines

$$\begin{aligned}
\tau^{\mathrm{mech}}_{\mathrm{new}} &:= \left(\mathbf{C} - \mathbf{C}^0\right)\boldsymbol{\varepsilon}(\omega) - \left(\mathbf{e} - \mathbf{e}^0\right)\mathbf{H}(\varrho) + \tau^{\mathrm{mech}} &&\in L^2\left(\mathbb{T}^d, \mathbb{R}^{\tilde{d}}\right), \\
\tau^{\mathrm{mag}}_{\mathrm{new}} &:= \left(\boldsymbol{\mu} - \boldsymbol{\mu}^0\right)\mathbf{H}(\varrho) + \left(\mathbf{e} - \mathbf{e}^0\right)^{\mathrm{T}}\boldsymbol{\varepsilon}(\omega) + \tau^{\mathrm{mag}} &&\in L^2\left(\mathbb{T}^d, \mathbb{R}^{d}\right),
\end{aligned}$$

yielding the system

$$\begin{aligned}\mathbf{div}\left(\mathbf{C}^0\,\boldsymbol{\varepsilon}(\omega) - \mathbf{e}^0\,\mathbf{H}(\varrho) + \tau_{\text{new}}^{\text{mech}}\right) + \mathbf{g}^{\text{mech}} &= 0\,,\\ \operatorname{div}\left(\left(\mathbf{e}^0\right)^{\mathrm{T}}\boldsymbol{\varepsilon}(\omega) + \boldsymbol{\mu}^0\,\mathbf{H}(\varrho) + \tau_{\text{new}}^{\text{mag}}\right) + \mathbf{g}^{\text{mag}} &= 0\end{aligned}$$

that is now solvable by Theorem 5.3.3. For every $\mathbf{k} \in \mathbb{Z}_N$, this gives

$$\left(\begin{array}{c}\hat{\boldsymbol{\varepsilon}}(\omega)\\ \hat{\mathbf{H}}(\varrho)\end{array}\right) = \left(\begin{array}{c|c}\hat{\Gamma}^{\boldsymbol{\varepsilon}}_{\tau^{\text{mech}}} & \hat{\Gamma}^{\boldsymbol{\varepsilon}}_{\tau^{\text{mag}}}\\ \hat{\Gamma}^{\mathbf{H}}_{\tau^{\text{mech}}} & \hat{\Gamma}^{\mathbf{H}}_{\tau^{\text{mag}}}\end{array}\right)\left(\begin{array}{c}\hat{\tau}^{\text{mech}}_{\text{new}}\\ \hat{\tau}^{\text{mag}}_{\text{new}}\end{array}\right) + \left(\begin{array}{c|c}\hat{\Gamma}^{\boldsymbol{\varepsilon}}_{\mathbf{g}^{\text{mech}}} & \hat{\Gamma}^{\boldsymbol{\varepsilon}}_{\mathbf{g}^{\text{mag}}}\\ \hat{\Gamma}^{\mathbf{H}}_{\mathbf{g}^{\text{mech}}} & \hat{\Gamma}^{\mathbf{H}}_{\mathbf{g}^{\text{mag}}}\end{array}\right)\left(\begin{array}{c}\hat{\mathbf{g}}^{\text{mech}}\\ \hat{\mathbf{g}}^{\text{mag}}\end{array}\right) \tag{5.24}$$

with

$$\left(\begin{array}{c}\hat{\tau}^{\text{mech}}_{\text{new}}\\ \hat{\tau}^{\text{mag}}_{\text{new}}\end{array}\right) = \overbrace{\left(\begin{array}{c|c}\mathbf{C}-\mathbf{C}^0 & -\left(\mathbf{e}-\mathbf{e}^0\right)\\ \left(\mathbf{e}-\mathbf{e}^0\right)^{\mathrm{T}} & \boldsymbol{\mu}-\boldsymbol{\mu}^0\end{array}\right)\left(\begin{array}{c}\boldsymbol{\varepsilon}(\omega)\\ \mathbf{H}(\varrho)\end{array}\right)} + \left(\begin{array}{c}\hat{\tau}^{\text{mech}}\\ \hat{\tau}^{\text{mag}}\end{array}\right). \tag{5.25}$$

All that is left to do is to set up new block diagonal matrices according to the ordering of the frequencies for the Green operators not present before, namely $\mathbf{G}^{\boldsymbol{\varepsilon}}_{\tau^{\text{mag}}} \in \mathbb{C}^{\rho\tilde{d}\times\rho d}$, $\mathbf{G}^{\mathbf{H}}_{\tau^{\text{mech}}} \in \mathbb{C}^{\rho d\times\rho\tilde{d}}$, $\mathbf{G}^{\boldsymbol{\varepsilon}}_{\mathbf{g}^{\text{mag}}} \in \mathbb{C}^{\rho\tilde{d}}$ and $\mathbf{G}^{\mathbf{H}}_{\mathbf{g}^{\text{mech}}} \in \mathbb{C}^{\rho d\times\rho d}$ before one is able to set up the complete system with the incorporated DFT matrices.

Theorem 5.3.4. *For a given discretization vector $N \in \mathbb{N}^d$ and chosen reference tensors $\mathbf{C}^0 \in \mathbb{R}^{\tilde{d}\times\tilde{d}}$, $\boldsymbol{\mu}^0 \in \mathbb{R}^{d\times d}$ and $\mathbf{e}^0 \in \mathbb{R}^{\tilde{d}\times d}$, the system $\mathbf{M}\mathbf{x} = \mathbf{b}_\tau + \mathbf{b}_\mathbf{g}$ with the matrix*

$$\mathbf{M} \coloneqq \left(\begin{array}{c|c}\mathrm{Id}_{\tilde{d}} & 0\\ 0 & \mathrm{Id}_d\end{array}\right) - \left(\begin{array}{c|c}\mathcal{F}_{\tilde{d}}^{-1} & 0\\ 0 & \mathcal{F}_d^{-1}\end{array}\right)\left(\begin{array}{c|c}\mathbf{G}^{\boldsymbol{\varepsilon}}_{\tau^{\text{mech}}} & \mathbf{G}^{\boldsymbol{\varepsilon}}_{\tau^{\text{mag}}}\\ \mathbf{G}^{\mathbf{H}}_{\tau^{\text{mech}}} & \mathbf{G}^{\mathbf{H}}_{\tau^{\text{mag}}}\end{array}\right)\left(\begin{array}{c|c}\mathcal{F}_{\tilde{d}} & 0\\ 0 & \mathcal{F}_d\end{array}\right)\left(\begin{array}{c|c}\mathbf{C}_N-\mathbf{C}^0_N & -\left(\mathbf{e}_N-\mathbf{e}^0_N\right)\\ \left(\mathbf{e}_N-\mathbf{e}^0_N\right)^{\mathrm{T}} & \boldsymbol{\mu}_N-\boldsymbol{\mu}^0_N\end{array}\right)$$

and right-hand side vectors

$$\begin{aligned}\mathbf{b}_\tau &\coloneqq \left(\begin{array}{c|c}\mathcal{F}_{\tilde{d}}^{-1} & 0\\ 0 & \mathcal{F}_d^{-1}\end{array}\right)\left(\begin{array}{c|c}\mathbf{G}^{\boldsymbol{\varepsilon}}_{\tau^{\text{mech}}} & \mathbf{G}^{\boldsymbol{\varepsilon}}_{\tau^{\text{mag}}}\\ \mathbf{G}^{\mathbf{H}}_{\tau^{\text{mech}}} & \mathbf{G}^{\mathbf{H}}_{\tau^{\text{mag}}}\end{array}\right)\left(\begin{array}{c|c}\mathcal{F}_{\tilde{d}} & 0\\ 0 & \mathcal{F}_d\end{array}\right)\left(\begin{array}{c}\tau^{\text{mech}}_N\\ \tau^{\text{mag}}_N\end{array}\right),\\ \mathbf{b}_\mathbf{g} &\coloneqq \left(\begin{array}{c|c}\mathcal{F}_{\tilde{d}}^{-1} & 0\\ 0 & \mathcal{F}_d^{-1}\end{array}\right)\left(\begin{array}{c|c}\mathbf{G}^{\boldsymbol{\varepsilon}}_{\mathbf{g}^{\text{mech}}} & \mathbf{G}^{\boldsymbol{\varepsilon}}_{\mathbf{g}^{\text{mag}}}\\ \mathbf{G}^{\mathbf{H}}_{\mathbf{g}^{\text{mech}}} & \mathbf{G}^{\mathbf{H}}_{\mathbf{g}^{\text{mag}}}\end{array}\right)\left(\begin{array}{c|c}\mathcal{F}_d & 0\\ 0 & \mathcal{F}_1\end{array}\right)\left(\begin{array}{c}\mathbf{g}^{\text{mech}}_N\\ \mathbf{g}^{\text{mag}}_N\end{array}\right)\end{aligned}$$

has a unique solution $\mathbf{x} = (\boldsymbol{\varepsilon}_N \mid \mathbf{H}_N)$. Furthermore, the transformed vectors $\mathcal{F}_{\tilde{d}}\,\boldsymbol{\varepsilon}_N$ and $\mathcal{F}_d\,\mathbf{H}_N$ then store the coefficients for uniquely determined trigonometric polynomials $\boldsymbol{\varepsilon} \in \Pi_N^{\tilde{d}}$ and $\mathbf{H} \in \Pi_N^d$ that solve the approximate weak form of the generalized linear magneto-elastic cell problem (5.1).

As was already remarked at the end of the previous paragraph, pre-pLS coupling results in a generalization of the post-pLS coupling. The following corollary summarizes this connection.

Corollary 5.3.5. *The pre-pLS coupling system of Theorem 5.3.4 and the monolithic post-pLS coupling system of Theorem 5.2.8 coincide for $\mathbf{e}^0$ being equal to the zero matrix.*

Naturally, this gives rise to the question whether or not the pre-pLS coupling is actually worth the extra effort of choosing one more reference tensor and defining four additional operators in the Fourier domain for each frequency. This comparison is to be kept in mind for the upcoming chapter in which both methods are tested for different unit cell geometries. It is also important to stay aware of the fact that these systems are only given for a theoretical purpose, as all formal matrix applications are more efficiently implemented as either optimized FFT subroutines or parallelizable matrix–vector products in each grid point or frequency.

Before wrapping up the current chapter, there are two topics worth mentioning. First, regarding the structure of the system matrix $\mathbf{M}$. As was explained early on, the magnetic field $\mathbf{H}(\varrho)$ is traditionally defined as the negative gradient of the scalar potential. However, it might be worthwhile to define the solution vector as $\mathbf{x} = (\varepsilon_N \mid -\mathbf{H}_N)$ instead. If that were the case, the signs within the material tensors matrix and the two Green operator matrices were to change accordingly to

$$\left(\begin{array}{c|c} \mathbf{C}_N - \mathbf{C}_N^0 & \mathbf{e}_N - \mathbf{e}_N^0 \\ \hline \left(\mathbf{e}_N - \mathbf{e}_N^0\right)^{\mathrm{T}} & -\left(\boldsymbol{\mu}_N - \boldsymbol{\mu}_N^0\right) \end{array}\right), \quad \left(\begin{array}{c|c} \mathbf{G}^{\boldsymbol{\varepsilon}}_{\tau^{\mathrm{mech}}} & \mathbf{G}^{\boldsymbol{\varepsilon}}_{\tau^{\mathrm{mag}}} \\ \hline -\mathbf{G}^{\mathbf{H}}_{\tau^{\mathrm{mech}}} & -\mathbf{G}^{\mathbf{H}}_{\tau^{\mathrm{mag}}} \end{array}\right) \quad \text{and} \quad \left(\begin{array}{c|c} \mathbf{G}^{\boldsymbol{\varepsilon}}_{\mathbf{g}^{\mathrm{mech}}} & \mathbf{G}^{\boldsymbol{\varepsilon}}_{\mathbf{g}^{\mathrm{mag}}} \\ \hline -\mathbf{G}^{\mathbf{H}}_{\mathbf{g}^{\mathrm{mech}}} & -\mathbf{G}^{\mathbf{H}}_{\mathbf{g}^{\mathrm{mag}}} \end{array}\right).$$

Looking back at the definitions of the Green operators given in Theorem 5.3.3, it can be seen that $\mathbf{G}^{\boldsymbol{\varepsilon}}_{\tau^{\mathrm{mag}}}$ is actually the transpose of $-\mathbf{G}^{\mathbf{H}}_{\tau^{\mathrm{mech}}}$. Therefore, the first two of the three matrices would then take the form of generalized saddle point matrices with perturbation terms; a problem class often found for coupled problems that was already shortly mentioned in the concluding remark of Chap. 3. The third matrix shares a similar structure but does not have the right dimensionalities to be considered a saddle point matrix. The system matrix $\mathbf{M}$ in its entirety however seemingly looses this structure completely. Exploiting this connection might grant access to a rich theory for numerical solvers [10], so it is interesting to keep this in mind. Lastly, the question how to choose the reference tensors and how they will affect the rate of convergence remains. For the original Basic Scheme based on a Neumann iteration, this is discussed for example in [82] and [86].

6 Numerical examples

After having understood the core concepts behind FFT-based schemes for linear magneto-elastic problems, it is now time to put the previously derived methods to the test. In Sect. 6.1 a first simple and analytically solvable problem will be presented to not only validate the monolithic approaches but also to discuss some potential shortcomings of them as well. Afterwards, Sect. 6.2 will revolve around a more practical two-dimensional example with more realistic values for its tensor quantities. On top of taking a second look at the convergence properties of the spectral ansatz itself, it is tested how the contrast between material phases or the choice between pre-pLS and post-pLS systems effect the linear system solver in terms of total number of iterations needed or numerical stability. Finally, Sect. 6.3 will conclude the numerical tests by showing off a three-dimensional example.

6.1 Analytic Problem for Validation

An easy but nonetheless very effective way to construct analytically solvable problems for validation purposes is to start with the solution one wishes for, to insert them into the problem equations and to define the computed terms with opposite signs as source terms. While not always being applicable straight-forward depending on the problem, this *Method of Manufactured Solutions* [93, p. 219 sqq.] is going to be sufficient for the cause of this thesis.

When coming up with a first test case to validate the presented spectral schemes, it would certainly be appropriate to keep it comparatively simple, without getting rid of the characterizing features that are typical for these problems. As the interaction of different material phases within a composite is the leading inspiration, it appears reasonable to consider a two-dimensional unit cell with only two different phases — labeled A and B respectively — whose parameters stay constant within each phase as such a ‘simple’ case. For further simplification, the stiffness tensors should be isotropic, permeabilities only have entries on the main diagonal and the entries of the coupling tensor’s last row, so $\mathbf{e}_{31}$ and $\mathbf{e}_{32}$, are set to zero to reduce the number of parameters for each phase to eight (two stiffness parameters, two permeability entries, four coupling tensor entries).

Given a scalar frequency $k \neq 0$, an interesting type of solution to wish for could be

$$\boldsymbol{\varepsilon} = \begin{pmatrix} \sin(2\pi k \mathbf{y}_1) \\ \sin(2\pi k \mathbf{y}_2) \\ 0 \end{pmatrix} \quad \text{and} \quad \mathbf{H} = \begin{pmatrix} \sin(2\pi k \mathbf{y}_1) \\ \sin(2\pi k \mathbf{y}_2) \end{pmatrix}$$

which would be the symmetric, respectively negative gradient field of

$$\omega = -\frac{1}{2\pi} \begin{pmatrix} \cos(2\pi k \mathbf{y}_1) \\ \cos(2\pi k \mathbf{y}_2) \end{pmatrix} \quad \text{and} \quad \varrho = \frac{1}{2\pi} \left(\cos(2\pi k \mathbf{y}_1) + \cos(2\pi k \mathbf{y}_2) \right) .$$

To be able to easily compute the divergence fields, the idea now is to enforce equality of the divergences' arguments, which means

$$\begin{aligned} \mathbf{C}^{\mathrm{A}}\boldsymbol{\varepsilon} - \mathbf{e}^{\mathrm{A}}\mathbf{H} &\stackrel{!}{=} \mathbf{C}^{\mathrm{B}}\boldsymbol{\varepsilon} - \mathbf{e}^{\mathrm{B}}\mathbf{H}\,, \\ \left(\mathbf{e}^{\mathrm{A}}\right)^{\mathrm{T}}\boldsymbol{\varepsilon} - \boldsymbol{\mu}^{\mathrm{A}}\mathbf{H} &\stackrel{!}{=} \left(\mathbf{e}^{\mathrm{B}}\right)^{\mathrm{T}}\boldsymbol{\varepsilon} - \boldsymbol{\mu}^{\mathrm{B}}\mathbf{H} \end{aligned}$$

where superscripts A and B are indicative of the respective phases. This leads eventually to the following necessary conditions that have to be met:

$$\begin{aligned} &\tilde{\lambda}^{\mathrm{A}} = \tilde{\lambda}^{\mathrm{B}}\,, \quad \mathbf{e}^{\mathrm{A}}_{12} = \mathbf{e}^{\mathrm{B}}_{12}\,, \quad \mathbf{e}^{\mathrm{A}}_{21} = \mathbf{e}^{\mathrm{B}}_{21}\,, \\ &\mathbf{e}^{\mathrm{A}}_{11} - \mathbf{e}^{\mathrm{B}}_{11} = \mathbf{e}^{\mathrm{A}}_{22} - \mathbf{e}^{\mathrm{B}}_{22} = \boldsymbol{\mu}^{\mathrm{B}}_{11} - \boldsymbol{\mu}^{\mathrm{A}}_{11} = \boldsymbol{\mu}^{\mathrm{B}}_{22} - \boldsymbol{\mu}^{\mathrm{A}}_{22} = 2\left(\tilde{\mu}^{\mathrm{A}} - \tilde{\mu}^{\mathrm{B}}\right) = \text{const.} \end{aligned}$$

The parameters $\tilde{\lambda}$ and $\tilde{\mu}$ refer here to the 'fake' Lamé parameters in the plane stress setting introduced in (3.24) at the very end of Subsect. 3.1.2.

While this seems incredibly restrictive at first, there is still a certain amount of freedom given when choosing these parameters, as the second line only dictates equality in differences between two phases, potentially allowing for very different ranges of values for each one. Much more important though is the fact that the solution is completely independent of the way the two phases are distributed within the unit cell. This can be quite useful for validation, as any kind of phase border should not influence the result of the monolithic schemes, no matter how complex the geometry might be, while the Green operators in the frequency domain differ greatly between each chosen distribution. The outer force terms that need to be prescribed are computed as

$$\begin{aligned} \mathbf{g}^{\mathrm{mech}} &= -2\pi k \begin{pmatrix} \left(2\tilde{\mu}^{\mathrm{A}} + \tilde{\lambda}^{\mathrm{A}} - \mathbf{e}^{\mathrm{A}}_{11}\right)\cos\left(2\pi k\,\mathbf{y}_1\right) \\ \left(2\tilde{\mu}^{\mathrm{A}} + \tilde{\lambda}^{\mathrm{A}} - \mathbf{e}^{\mathrm{A}}_{22}\right)\cos\left(2\pi k\,\mathbf{y}_2\right) \end{pmatrix}, \\ \mathbf{g}^{\mathrm{mag}} &= -2\pi k \left(\left(\mathbf{e}^{\mathrm{A}}_{11} + \boldsymbol{\mu}^{\mathrm{A}}_{11}\right)\cos\left(2\pi k\,\mathbf{y}_1\right) + \left(\mathbf{e}^{\mathrm{A}}_{22} + \boldsymbol{\mu}^{\mathrm{A}}_{22}\right)\cos\left(2\pi k\,\mathbf{y}_2\right)\right). \end{aligned}$$

The frequency $k = 512$ for the validation test was now chosen to obtain highly oscillating sine curves. The validation example was then solved with the parameters given in Table 6.1 for increasing odd numbers of grid points in each direction, denoted by N. These parameters are far from being close to values occurring in practice and are only used to test the mathematical soundness of the algorithms before moving to more realistic examples next. Also, it is actually possible to run all previously shown routines with even numbers as well, but it was decided to stick to only odd discretization vectors to stay consistent with the original idea behind the derivation of the schemes. While the results shown here were computed with the post-pLS system, choosing the pre-pLS system instead results in the exact same curve, as the differences between post-pLS and pre-pLS systems primarily influence the performance of the linear system solver but not the solution to the problem itself. The solver used for all upcoming linear systems is MATLAB's integrated `bicgstab` routine with a tolerance of 10^{-6}. All reference tensors are chosen as the spatial mean over the unit cell.

The test was run on a diamond geometry, with the four corners of the unit cell consisting of phase A, while the diamond in the center consists of phase B. For each N, the L^2-error on the unit cell was computed as the ℓ^2-error between the Fourier coefficients of the strain field's analytical solution and the FFT values of the numerical one using Parseval's equation (2.34). Additionally, the maximal error between the (approximate) Fourier coefficients as well as the maximal error between the values on the discretized grid in the spatial domain were determined. These errors are plotted against the step size $h = 1/N$ in Fig. 6.1. The error curves for the magnetic field coincide with the ones depicted, since the third component of $\boldsymbol{\varepsilon}$ was set to zero, resulting in equal norms of both solution fields.

parameters	$\tilde{\lambda}$[Pa]	$\tilde{\mu}$[Pa]	$\boldsymbol{\mu}_{11}[\mathrm{H\,m^{-1}}]$	$\boldsymbol{\mu}_{22}[\mathrm{H\,m^{-1}}]$	$\mathbf{e}_{11}[\mathrm{Vs/m^2}]$	$\mathbf{e}_{12}[\mathrm{Vs/m^2}]$	$\mathbf{e}_{21}[\mathrm{Vs/m^2}]$	$\mathbf{e}_{22}[\mathrm{Vs/m^2}]$
phase A	1000	50	200	300	50	80	80	100
phase B	1000	35	230	330	20	80	80	70

Tab. 6.1: Parameters for the validation example. Parameters not listed are set to zero.

There are quite a few things to notice about these error curves. It is seen that all three errors follow similar courses, with the L^2- and the spatial max-error being almost identical for the most part and the max-error in the Fourier domain usually being lower. The error values themselves are unfortunately rather high, even for smaller step sizes. This is a general problem with the sampling of periodic signals where badly chosen sample rates can result in large aliasing effects. For certain sample rates — in the case at hand for example ones where $N = 2^i + 1$ among others — these effects are especially strong and form distinguishable peaks in the graphic. This is of course only true, until the *Nyquist frequency* is passed. The statement is that for any given sample rate only frequencies below half of that rate can be reconstructed exactly. On the other hand, this means that for a certain frequency to be detected one would need to have a sample rate with at least the doubled frequency. These effects and bounds already played a role before in Definition 5.2.1 and when discussing the discrete convolution in (5.10). As $k = 512$ was chosen for this series of computations, an exact representation of the solution can only be expected for values of N greater than 1024. This expectation is met, as all errors immediately drop down to numerical zero (values in the range of 10^{-12}; not depicted in the graphic anymore) as soon as the step size gets smaller than $1/1024$, observable as the flank to the left side of the plot. Until then, it can be seen that at least the local minima of the error curves follow a first order convergence slope. Peak errors however don't decrease along them, but only stay bounded from above.

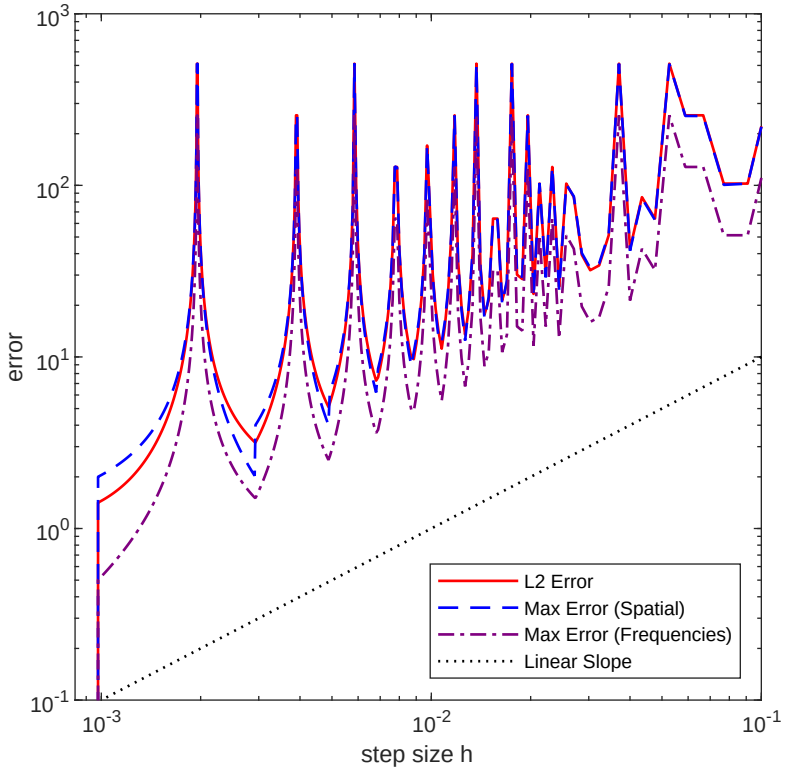

Fig. 6.1: L^2-error, maximum error in the Fourier domain and maximum error in the spatial domain between numerical and analytical solutions of the strain field ε of the validation example plotted against the step size $h = 1/N$.

6.2 Coated Sphere under Plane Stress

One stereotypical geometry that has become an important benchmark in the analysis of composite structures is that of a coated sphere. An analytical solution for the equations of linear elasticity on this structure was first discussed by Zvi Hashin and Shmuel Shtrikman in [51]. Since then further investigations around this geometry have surfaced, as it became the basis for an entire family of problems [83, ch. 7]. As such, the coated sphere in a plane stress setting, sometimes also referred to as *Hashin's structure*, is used for the studies of this section. Its geometry for the radii $r_1 = 0.25$ and $r_2 = 0.4$ is depicted in Fig. 6.2 and consists of three different phases in total: the inner core, the surrounding coating and the outside matrix material. The elastic parameters for the different phases used in the following are taken from [59] which also features an analytical solution for the purely elastic problem of the coated sphere. The entries of the permeability and the coupling tensor are inspired by the values given in [49, p. 110] for polycrystalline Terfenol-D, originally found in [23]. For right now, the coating was chosen to have the magnetic permeability of free space and coupling effects are only occurring within the core material. All parameters for the three phases can be found in Table 6.2. Note however that while the values chosen this time are more realistic than in the example before, they were not actually measured from experiments, but just combined from different sources, which means that neither materials with these combinations of elastic and magnetic parameters have to exists in reality nor that their coupling parameters would be the same as the ones chosen here. Nonetheless, it is hoped for these choices to yield more meaningful mathematical results without demanding to be physically accurate to reality.

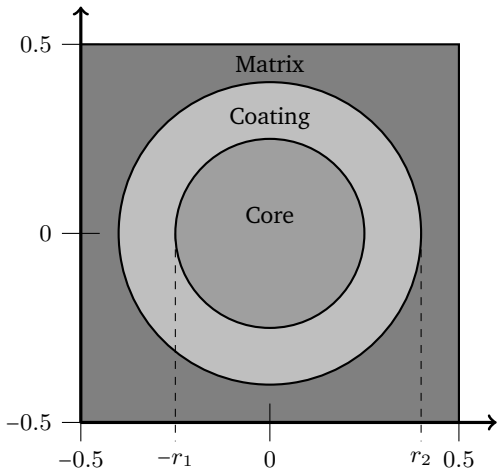

Fig. 6.2: Geometry of a coated sphere, reduced to the two-dimensional plane stress setting.

Inner forces were chosen as

$$\tau^{\text{mech}} = \sum_{i=1}^{2} \mathbf{C}\,\mathbf{z}_i^{\text{mech}} - \sum_{j=1}^{2} \mathbf{e}\,\mathbf{z}_j^{\text{mag}} \quad \text{and} \quad \tau^{\text{mag}} = \sum_{i=1}^{2} \mathbf{e}^{\mathrm{T}}\,\mathbf{z}_i^{\text{mech}} + \sum_{j=1}^{2} \boldsymbol{\mu}\,\mathbf{z}_j^{\text{mag}},$$

while the outer forces were set to zero. The numerical solution for Hashin's structure with these quantities on a 1025×1025 grid is shown in Fig. 6.3. It was computed using the pre-pLS scheme. Most notable here are the different magnitudes of the strain and magnetic fields as well as the, albeit expected, discontinuous changes between phase borders.

parameters	E[Pa]	ν[−]	$\boldsymbol{\mu}_{11}$[H m^{-1}]	$\boldsymbol{\mu}_{22}$[H m^{-1}]	$\mathbf{e}_{11}$[Vs/m^2]	$\mathbf{e}_{21}$[Vs/m^2]	$\mathbf{e}_{31}$[Vs/m^2]
core	10^8	0.3	$3.77 * 10^{-6}$	$10.12 * 10^{-6}$	213.30	−17.66	150.00
coating	10^9	0.3	$4\pi * 10^{-7}$	$4\pi * 10^{-7}$	0	0	0
matrix	$4.5368 * 10^8$	0.3	$3.77 * 10^{-6}$	$10.12 * 10^{-6}$	0	0	0

Tab. 6.2: Parameters for the coated sphere. Parameters not listed are set to zero.

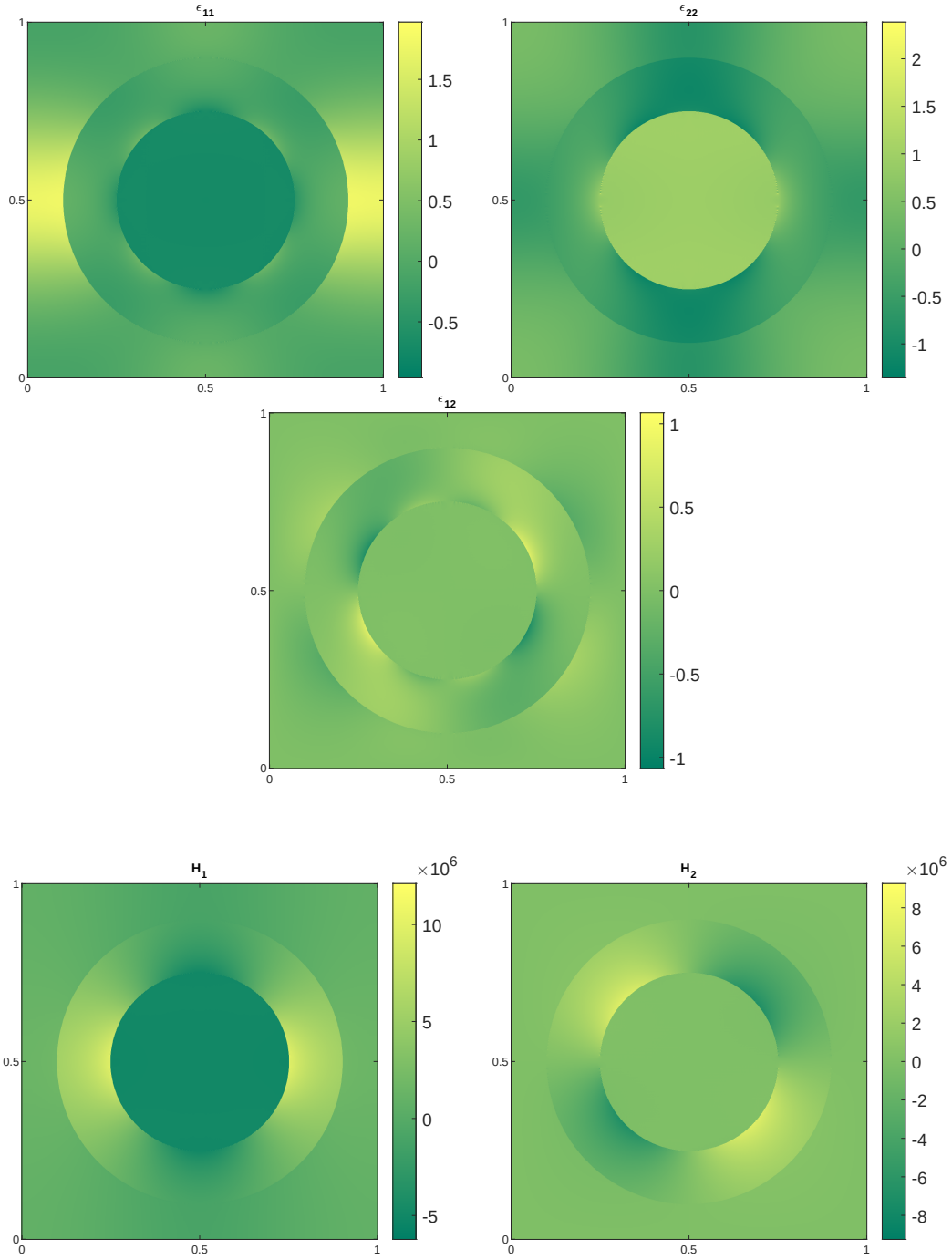

Fig. 6.3: Componentwise solution fields for the Hashin's structure solved with pre-pLS coupling. The component ε_{12} was scaled accordingly to not include factors from the Mandel notation.

To match discontinuities with a Fourier series exactly though, one would need an infinite series. This is obviously not achievable for practical reasons and leads to errors around the phase borders in form of Gibbs phenomenon [46]. While much more noticeable for lower grid resolutions, these overshoots are always present as seen in Fig. 6.4.

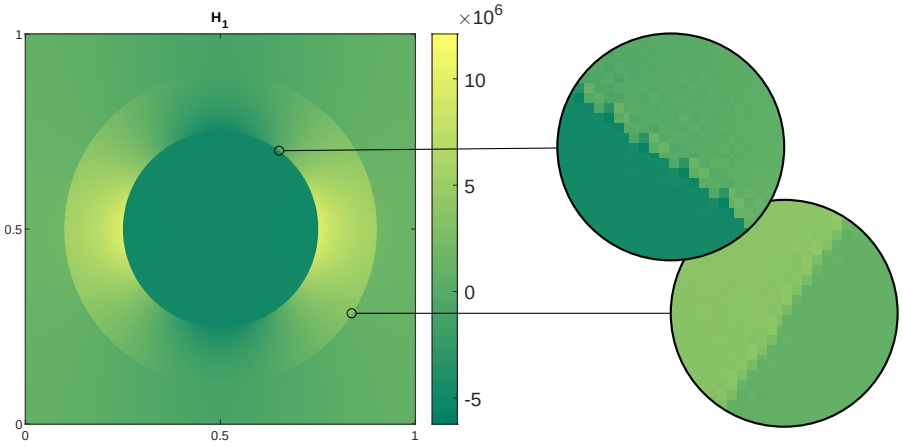

Fig. 6.4: Zoom-in on phase borders in the first component of the magnetic field with occurring Gibbs phenomenon.

Without an analytical solution for the coupled problem, no convergence curves like the ones for the validation example before can be plotted. Instead, what can still be done is to check how well solutions on a low resolution grid compare against high resolution ones. These pseudo-convergence curves are plotted in Fig. 6.5 where once again the L^2-error and the maximal error between Fourier coefficients are computed. The high-res solution that the low-res ones are compared against is the one on the 1025×1025 grid from Fig. 6.3. These pseudo-error curves behave differently from the previous ones, as they don't exhibit distinguishable peaks. The L^2-pseudo-errors are not only overall higher than the maximal ones, but also follow only a $\sqrt{h}$-slope instead of a linear one. One can also observe that the difference in norms between two solutions with almost the same resolution can be rather significant as the depicted pseudo-errors don't go towards zero when the step size is nearing $1/1025$. This is best seen in the plot for the magnetic field pseudo-errors where the max pseudo-error for step sizes around 10^{-3} are still at around 10^3 — which seems ridiculously large at first, but appears more reasonable when compared against the magnitude of 10^6 that the values of the magnetic field have. It may very well be possible that these errors are just the result of minor differences adding up over the entirety of the unit cell. Additionally however, it might be possible that more significant aliasing effects may occur in between the observable grid points that increase these pseudo-errors.

Interestingly, while the post-pLS scheme should also converge in theory for this example, the `bicgstab` method wasn't able to achieve the desired tolerance of 10^{-6} in this case, as the solver stagnated at two consecutive iterations. Trying out different resolutions of the unit cell, it appears that the linear system of the post-pLS method is less suited for this kind of solver, as it sometimes drastically increases the number of iterations needed for the relative residual to fall below the tolerance when compared to the pre-pLS system or even stagnates before. For odd $N \leq 1025$, it reaches its tolerance goal in only 168 out of 512 cases which is equal to 33%. When plotting the number of iterations against the number N of discretization points per spatial direction as in Fig. 6.6 where values of non-convergent runs were omitted, one can see that its iteration count is several times higher than in the pre-pLS cases which remain stable at around 50 iterations. However, the stagnating cases don't cluster around any specific value of N or get more frequent for higher resolutions but are instead evenly distributed, indicating that these instabilities are not tied to the grid resolution but either to the geometry itself or to the values of the material parameters.

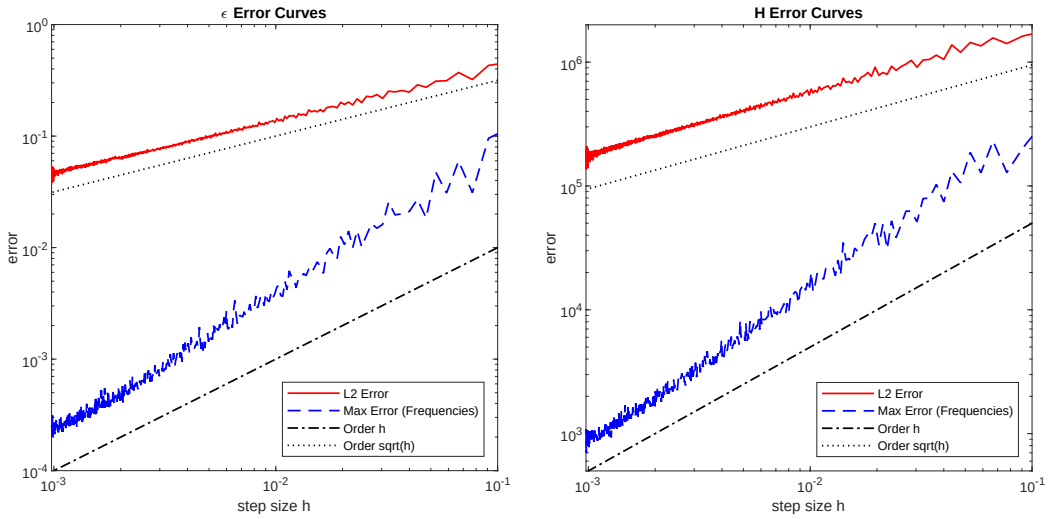

Fig. 6.5: L^2-error and maximum error in the Fourier domain between the numerical solutions on the 1025×1025 grid and lower resolution ones for the strain field $\boldsymbol{\varepsilon}$ (left) and the magnetic field $\mathbf{H}$ (right) of Hashin's structure plotted against the step size $h = 1/N$.

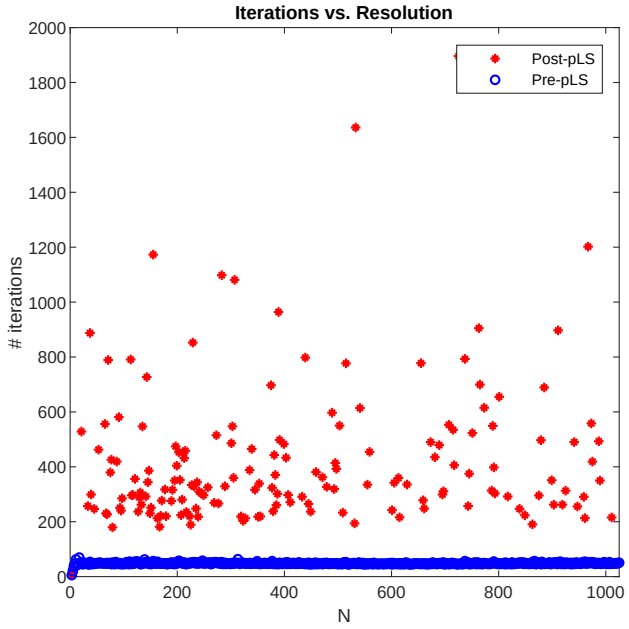

Fig. 6.6: Number of iterations at convergence for different grid resolutions for the coated sphere example. Values of non-converging post-pLS computations are omitted.

The following test strongly suggests that these occurrences are in fact dependent on the different material tensors, more precisely what is referred to as *phase contrast*. As was studied in the purely elastic problem case before, composites with a high phase contrast require more iterations for the original Basic Scheme or the accelerated `bicgstab` compatible system to converge which gave way to more sophisticated methods like augmented Lagrangians or Uzawa's algorithm in these settings [82]. The elastic contrast there was defined as the ratio of the Young's moduli within a two-phase composite. Even though Hashin's structure has three instead of two phases, the elastic contrast for this example shall be defined in a similar attempt as the ratio between the Young's modulus of the core phase and the one of the coating. With that, the next test plots the number of iterations of both monolithic schemes against the phase contrast within the coated sphere. The phase contrast was varied by increasing or decreasing Young's modulus of the coating in Table 6.2 while keeping the other parameters constant. Additionally, the same was done where now the elastic moduli remained unchanged but the permeability tensor of the coating was chosen as a multiple of the core's permeability, as this can be regarded as a magnetic contrast. Both plots, for the elastic and the magnetic contrasts, are depicted in Fig. 6.7. These studies used only a 65×65 grid to reduce computation time.

The number of iterations behave similar to the separated elastic or magnetic problem cases in that it is more or less proportional to the square root of the contrast as it was shown in [82] (if the contrast is larger than one; otherwise one would have to take the reciprocal). In the elastic contrast study, the valley formed around the contrast of one even prolongs towards the right side of higher contrasts and only starts to significantly increase again around a contrast of 10^4. The more obvious observation is that the post-pLS scheme only runs through without stagnating for contrasts larger than 10^2 in the elastic contrast study and contrasts larger than 10^0 in the magnetic contrast study, with just a few exceptions being present. The pre-pLS scheme instead runs through for almost all tested contrasts and only fails in the magnetic contrast study for contrasts around 10^{-5} or lower. Once again, only taking tests into account where both methods converge, the pre-pLS scheme needs less iterations than the post-pLS one on average.

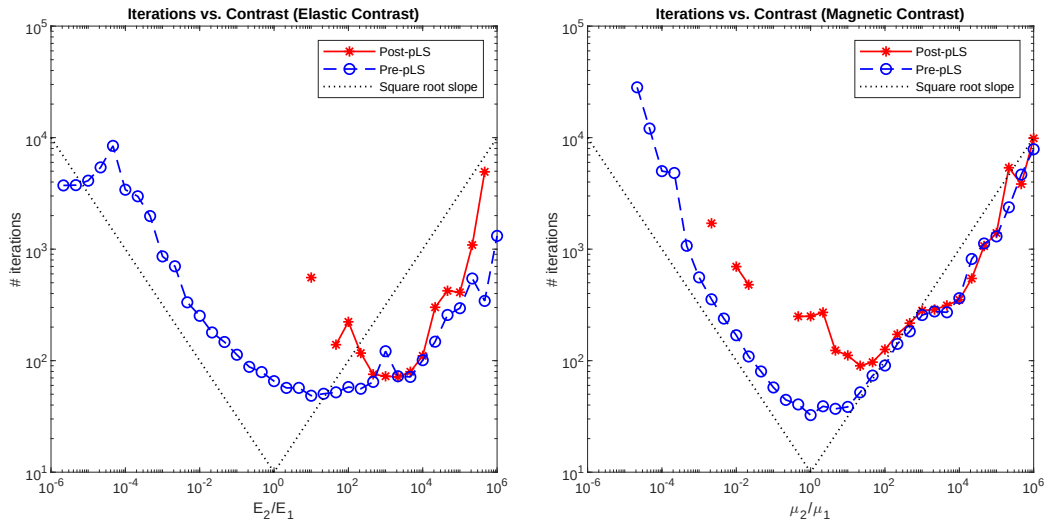

Fig. 6.7: Number of iterations at convergence against different elastic (left) and magnetic (right) contrasts for the coated sphere example. Values of non-converging computations are omitted.

Why is it that the monolithic methods sometimes have vastly different iteration counts and therefore run times? For $E_2/E_1 = 10^1$ as an example where this number differs by an entire order of magnitude, taking a look at how the relative residual changes over the course of the iteration in Fig. 6.8, it turns out that the post-pLS method does not simply converge slower than the pre-pLS method but even increases initially and stays at a high level for most of the time before starting to near the tolerance. For comparison, the relative residuals for $E_2/E_1 = 10^4$, where the number of iterations is roughly the same for both methods, is given as well.

The time needed to solve the linear systems obviously increases with the number of iterations, which means that the pre-pLS approach is generally faster. As it requires more Green operators to be defined, one might wonder though how the times needed to set up the linear systems compare against each other. While these times are indeed slightly lower for the post-pLS system on average, as listed in Table 6.3, their difference is negligibly small compared to the overall computation time which can take over a hundred seconds in the critical high contrast cases if no iteration cap is set. At least that's the case for computations on comparatively coarse grids. Looking back at the simulation on the 1025×1025 grid used for Fig. 6.3, the system setup alone takes already a few seconds, while the actual solver takes well over a minute to reach the tolerance of 10^{-6}. With the additional Green operators also comes the need for more storage memory which is clearly a big disadvantage of the pre-pLS coupling. Focusing on the storage needed for all Green operators, all material tensors and inner and outer forces — as these are the essential quantities needed within an iterative solver and to define the right-hand sides which might differ for each point or frequency — the pre-pLS coupling needs around 1.64 times more memory just to store the data. The time and memory data for both schemes in the high-resolution simulation can be found in Table 6.4.

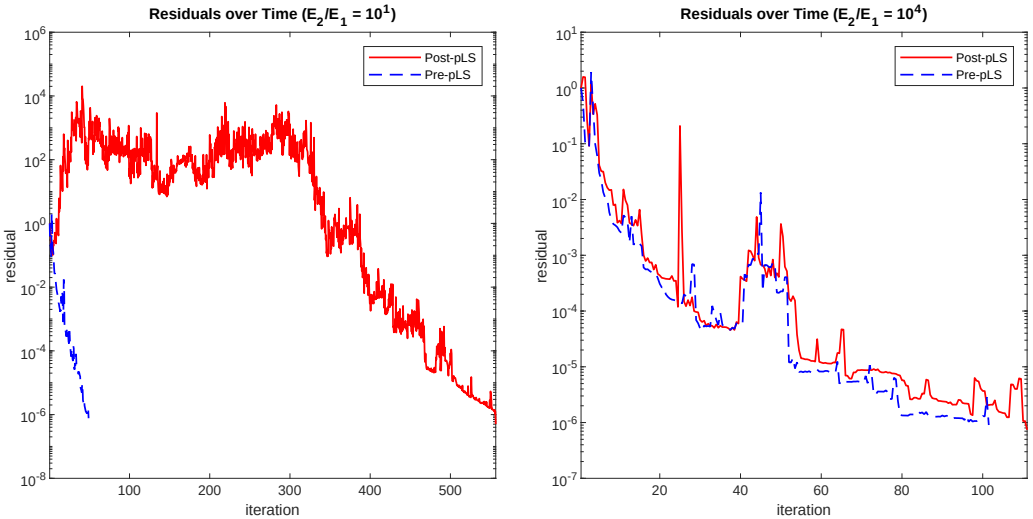

Fig. 6.8: Relative residual over the course of the iteration for elastic contrasts of 10^1 (left) and 10^4 (right). In the left case, the pre-pLS schemes converges faster than the post-pLS scheme that increases the relative residual at first, resulting in a way larger number of iterations. In the right case, where both schemes perform equally good, their residual curves also follow a similar pattern.

System Setup Times [s]	Max	Min	Average
Post-pLS	0.3034	0.0239	0.0290
Pre-pLS	0.0881	0.0274	0.0299

Tab. 6.3: Maximal, minimal and average times needed in the contrast studies to setup the linear system for each monolithic method.

	Setup Time [s]	Solver Time [s]	Memory Storage [MB]
Post-pLS	6.7030	*(stagnates)*	≈ 50
Pre-pLS	7.8856	71.6739	≈ 82

Tab. 6.4: Computation times for the system setup and the solver routine, as well as the memory used to store Green operators, material tensors and force vectors for the high-resolution coated sphere example.

6.3 A Three-Dimensional Geometry

More for the sake of completeness than for gaining new information, a three-dimensional geometry is presented lastly. It is shown in Fig. 6.9 and was created by randomly placing a total number of thirty ellipsoidal inclusions within the unit cube, some of which get cut off by the sides of the cube. The inclusions are assumed to be iron, while the matrix material is given the parameters of copper. The respective elastic moduli and the permeability values were taken from [107]. As no values for the coupling tensor were available to the author at the writing of this thesis, the same values as for the coated sphere example before, now adjusted to 3D, will be used again. An overview of all values can be found in Table 6.5. The inner forces are similarly chosen as

$$\tau^{\mathrm{mech}} = \sum_{i=1}^{3} \mathbf{C}\,\mathbf{z}_i^{\mathrm{mech}} - \sum_{j=1}^{3} \mathbf{e}\,\mathbf{z}_j^{\mathrm{mag}} \quad \text{and} \quad \tau^{\mathrm{mag}} = \sum_{i=1}^{3} \mathbf{e}^{\mathrm{T}}\,\mathbf{z}_i^{\mathrm{mech}} + \sum_{j=1}^{3} \boldsymbol{\mu}\,\mathbf{z}_j^{\mathrm{mag}} ,$$

while the outer forces are set again to zero. The computation was run on a 129^3 grid (≈ 2.1 million grid points). The solution fields were exported as vtk-files with the `vtkwrite` script written by MATLAB user CY Y [119] for further visualization. The three separate columns of the strain tensor $\boldsymbol{\varepsilon}$ are shown alongside the magnetic field $\mathbf{H}$ as vector field plots in Fig. 6.10 and 6.11. It can be seen that the strongest effects occur around the inclusions in a radiating manner. Something else to note is that extraordinarily large values can be measured at some cut-off ellipsoids when these lead to abrupt phase changes over a larger area in the periodically continued unit cube (most noticeable near the bottom left corner). Such effects should be kept in mind as they might only be artificially created when choosing an RVE, whereas the original heterogeneous micro-structure in the case presented would actually consist of whole inclusions with the domain border being the only exception, thus probably not exhibiting effects of the same magnitude.

Table 6.6 lists as before the computation times and the memory needed for storage of both schemes. It comes as no surprise that the memory needed by the pre-pLS scheme is again way higher than what the post-pLS one needs (1.58 times more). In contrast to the coated sphere however does the post-pLS coupling not only converge this time, but also does it at around two thirds of the time the pre-pLS one needed. It is not clear yet whether this is just an exceptional case or if this indicates that the post-pLS scheme can sometimes be favorable over the pre-pLS scheme for certain geometrical configurations, even if memory storage is not limited.

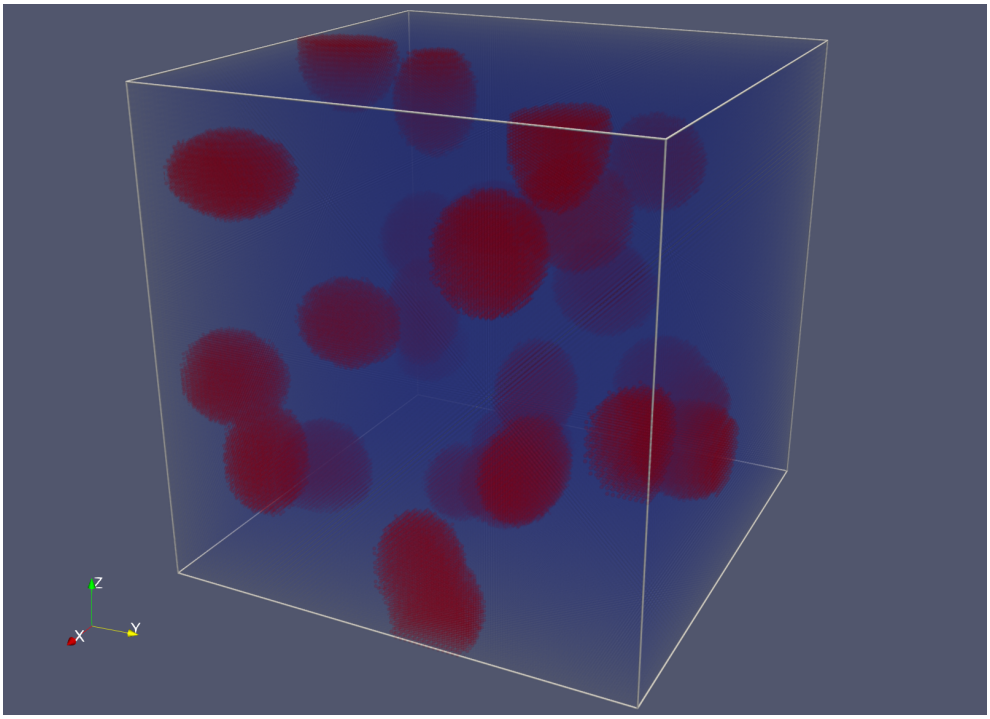

Fig. 6.9: Geometry used for the 3D simulations that consists of 30 ellipsoidal inclusions.

parameters	E[Pa]	ν[−]	$\boldsymbol{\mu}_{11} = \boldsymbol{\mu}_{22} = \boldsymbol{\mu}_{33}$[H m^{-1}]	$\mathbf{e}_{11}$[Vs/m^2]	$\mathbf{e}_{21}$[Vs/m^2]	$\mathbf{e}_{62}$[Vs/m^2]
inclusions	$210 * 10^9$	0.25	$2.5 * 10^{-1}$	213.30	−17.66	150.00
matrix	$117 * 10^9$	0.355	$1.256629 * 10^{-6}$	0	0	0

Tab. 6.5: Parameters for the 3D geometry. Parameters not listed are set to zero.

	Setup Time [s]	Solver Time [s]	Memory Storage [MB]
Post-pLS	27.3022	≈ 2833	≈ 297
Pre-pLS	33.5047	≈ 4274	≈ 469

Tab. 6.6: Computation times for the system setup and the solver routine, as well as the memory used to store Green operators, material tensors and force vectors for the high-resolution 3D example.

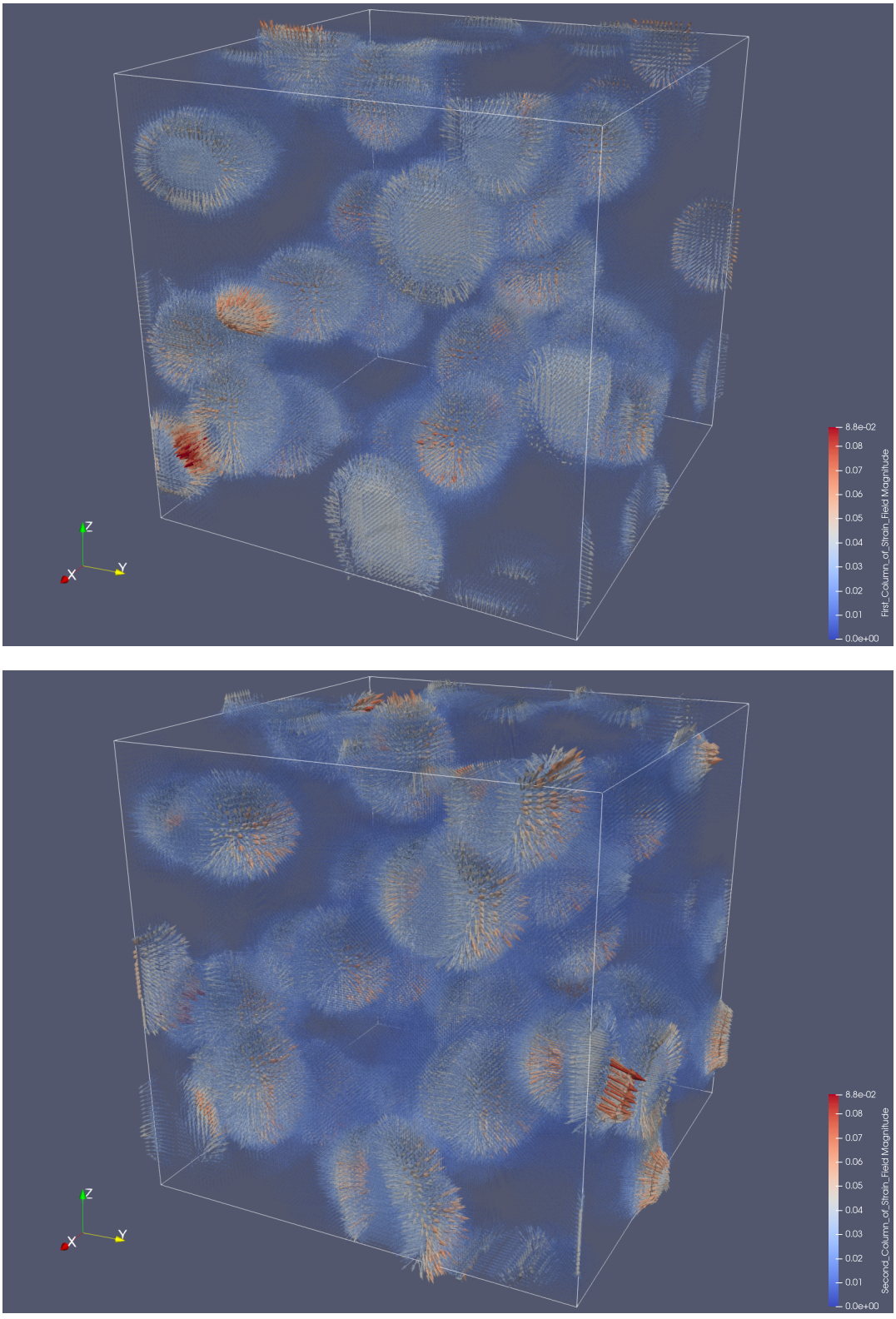

Fig. 6.10: First (top) and second (bottom) column of the strain tensor ε depicted as vector fields computed for the 3D geometry with pre-pLS coupling on a 129^3 grid.

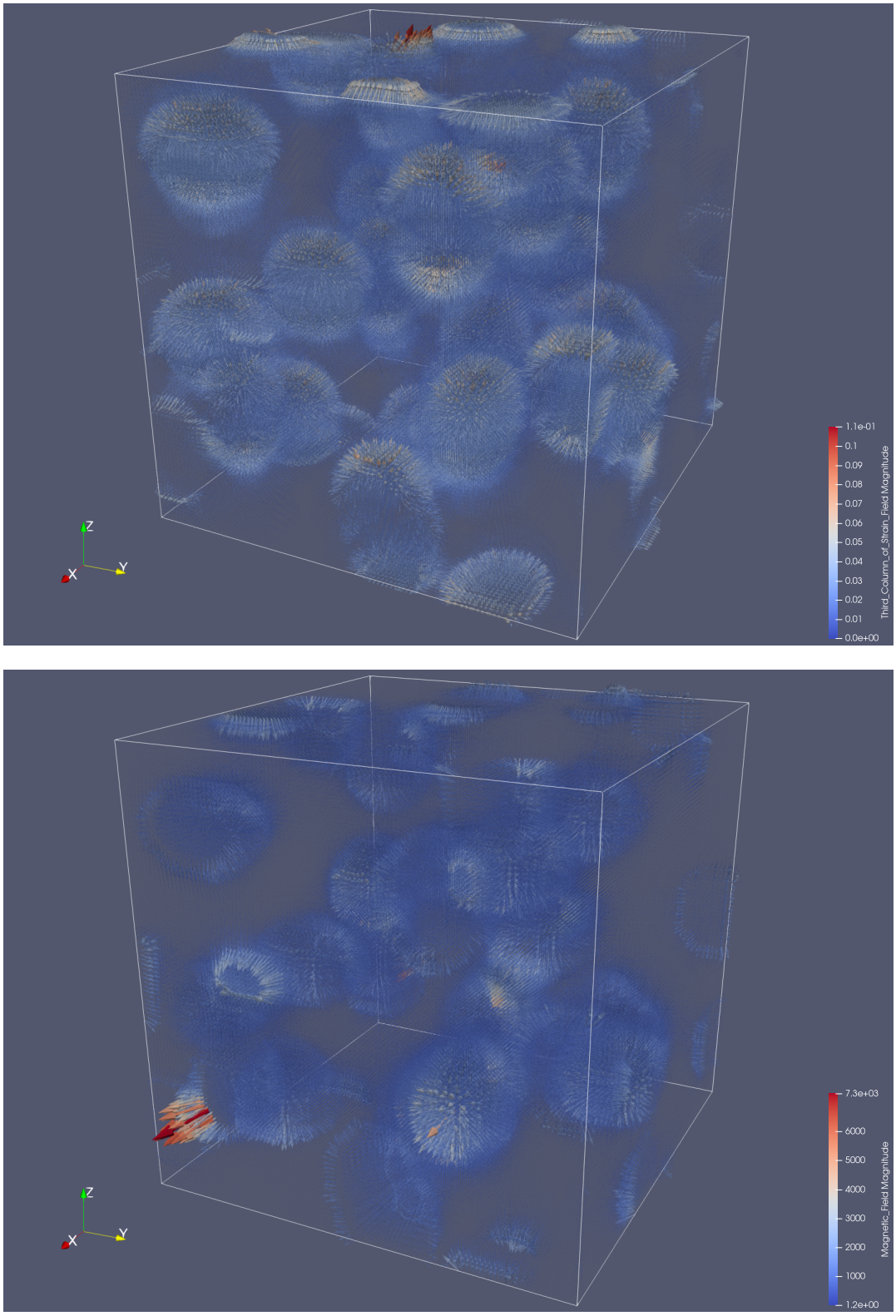

Fig. 6.11: Third column of the strain tensor ε depicted as a vector field (top) and the magnetic vector field $\mathbf{H}$ (bottom) computed for the 3D geometry with pre-pLS coupling on a 129^3 grid.

7 Conclusion

In this thesis, the periodic homogenization procedure was applied to a magneto-elastic system to separate it into a homogenized and a unit cell problem which were shown to have unique weak solutions within properly chosen function spaces and — exploiting its periodic nature — spectral numerical schemes were derived, discussed and tested in different scenarios to solve the latter one.

The coupled system which was based on the constitutive equations from linear elasticity and magnetism was rewritten in a weak form following an energy minimization principle. Classical Lax–Milgram theory guaranteed a unique solution within appropriate Sobolev spaces under the assumption of essentially bounded material tensors, where the stiffness and permeability furthermore need to fulfill an ellipticity condition. To include the effects of the underlying micro-structure into the effective behavior of a composite without drastically increasing the resolution of classic PDE methods, the originally heterogeneous material was then replaced by a homogeneous substitute that supposedly exhibits the same macroscopic properties. The material tensors of this substitute were obtained through a scale separating limit process in which the length of a periodically continued representative volume element went towards zero. This lead to the homogenized problem on the observed domain and the cell problem on the RVE which itself can be interpreted as a linear combination of corrector problems that are independently solvable from the homogenized one. It was shown how two-scale limits provide a mathematical concept to back up more intuitive approaches like the asymptotic expansion.

After repeating the ideas behind the Basic Scheme — a spectral matrix-free algorithm based on trigonometric collocation introduced by Moulinec and Suquet [87] that makes use of the unit cells periodic boundary conditions by transferring the equations to the frequency domain — different possibilities to adapt these concepts to the coupled problem were presented. The idea of a staggered scheme was shortly outlined, but was not further discussed in this work due to the lack of a definitive convergence result. Recombining the periodic Lippmann–Schwinger equations of the separated elastic and magnetic problems into a common linear system, referred to as post-pLS coupling, resulted in a method that was easy to set up and yielded promising results in first numerical tests but proved to abet instabilities within linear system solvers for more complex geometries at certain resolutions or high phase contrasts. An alternative approach was given in the form of pre-pLS coupling where a new auxiliary problem with constant tensors was defined for the already coupled system, leading to a linear system with an additional reference tensor $\mathbf{e}^0$ to be chosen. It was pointed out that the pre-pLS approach equals the post-pLS method if $\mathbf{e}^0$ is chosen as the zero tensor and can therefore be seen as a generalization of the latter. Numerical tests did not only validate both monolithic approaches and their equivalence to each other, but have shown that the pre-pLS method favors numerical stability of the system matrix. In cases where both monolithic methods converge, the pre-pLS coupling was seen to usually need fewer at best or around the same amount of iterations at worst than the post-pLS coupling, as such being less time consuming. The additional time needed to compute the more complex Green operators turns out to be negligibly small, giving the pre-pLS an advantage in comparison as the post-pLS scheme also often fails to converge due to numerical instability. On the other hand, instances might occur where the pre-pLS coupling indeed takes significantly longer than the post-pLS scheme, as it was the case with the 3D geometry presented. Memory usage is also a limiting factor when deciding for one method over the other, as more Green operators need to be stored.

There are several options how the presented works can be extended in the future. For once, the full derivation of the two-scale variational form as well as the pre-pLS coupling can be extended to larger systems such as electro-magneto-elastic ones, for example found in [68]. Then, larger studies regarding the performance of the pre-pLS coupled system need to be conducted. For this, the three following questions should be of particular interest. How does the choice of $\mathbf{e}^0$ influence the stability and convergence rate of the system? What kind of pre-conditioners could be chosen to better the condition number of the coupled system in general? In which cases does the post-pLS coupling outperform the pre-pLS one? More precise convergence results together with error estimates, a priori as well as a posteriori, are also obviously something to study in more detail. Lastly, a full simulation that computes the effective tensors and studies how the errors of the unit cell problem affect the homogenized problem would be a great addition to this work.

Bibliography

[1] J. Aboudi. „Micromechanical analysis of fully coupled electro-magneto-thermo-elastic multiphase composites“. In: *Smart materials and sctructures* 10.5 (2001), pp. 867–877 (cit. on p. 45).

[2] G. Allaire. „Homogenization and Two-Scale Convergence“. In: *SIAM Journal on Mathematical Analysis* 23.6 (1992), pp. 1482–1518 (cit. on pp. 45, 46).

[3] F. Alouges. „Introduction to Periodic Homogenization“. In: *Interdisciplinary Information Sciences* 22.2 (2016), pp. 147–186 (cit. on p. 31).

[4] B. S. Anglin, R. A. Lebensohn, and A. D. Rollett. „Validation of a numerical method based on Fast Fourier Transforms for heterogeneous thermoelastic materials by comparison with analytical solutions“. In: *Computational Materials Science* 87 (2014), pp. 209–217 (cit. on p. 2).

[5] D. N. Arnold, R. S. Falk, and R. Winther. *Finite element exterior calculus, homological techniques. and applications*. Vol. 15. Cambridge University Press, 2006 (cit. on p. 29).

[6] J. L. Auriault. „Heterogeneous medium. Is an equivalent macroscopic description possible?“ In: *International journal of engineering science* 29.7 (1991), pp. 785–795 (cit. on p. 1).

[7] C. E. Bakis, L. C. Bank, V. Brown, et al. „Fiber-reinforced polymer composites for construction—State-of-the-art review“. In: *Journal of composites for construction* 6.2 (2002), pp. 73–87 (cit. on p. 1).

[8] A. H. Barr. „The Einstein Summation Notation“. In: *An Introduction to Physically Based Modeling (Course Notes 19), pages E* 1 (1991) (cit. on p. 57).

[9] A. Bensoussan, J.-L. Lions, and G. Papanicolaou. *Asymptotic analysis for periodic structures*. Vol. 374. American Methematical Society, 2011 (cit. on p. 31).

[10] M. Benzi, G. H. Golub, and J. Liesen. „Numerical solution of saddle point problems“. In: *Acta numerica* 14 (2005), pp. 1–137 (cit. on p. 71).

[11] R. Bergmann and D. Merkert. „FFT-based homogenization on periodic anisotropic translation invariant spaces“. In: *Applied and Computational Harmonic Analysis* 48.1 (2020), pp. 266–292 (cit. on p. 2).

[12] D. Braess. *Finite Elemente: Theorie, schnelle Löser und Anwendungen in der Elastizitätstheorie*. Springer Verlag, 2013 (cit. on pp. 23, 25).

[13]J. Bravo-Castillero, R. Rodríguez-Ramos, H. Mechkour, J. A. Otero, and F. J. Sabina. „Homogenization of magneto-electro-elastic multilaminated materials“. In: *The Quarterly Journal of Mechanics & Applied Mathematics* 61.3 (2008), pp. 311–332 (cit. on p. 45).

[14]R. Brenner. „Computational approach for composite materials with coupled constitutive laws“. In: *Zeitschrift für angewandte Mathematik und Physik* 61.5 (2010), pp. 919–927 (cit. on p. 54).

[15]R. Brenner. „Numerical computation of the response of piezoelectric composites using Fourier transform“. In: *Physical Review B* 79.18 (2009) (cit. on p. 66).

[16]S. C. Brenner and L. R. Scott. *The Mathematical Theory of Finite Element Methods*. Vol. 15. Springer Science & Business Media, 2007 (cit. on pp. 24, 25).

[17]F. Brezzi. „On the existence, uniqueness and approximation of saddle-point problems arising from Lagrangian multipliers“. In: *Publications mathématiques et informatiques de Rennes* S4 (1974), pp. 1–26 (cit. on p. 29).

[18]S. Brisard. „Reconstructing displacements from the solution to the periodic Lippmann–Schwinger equation discretized on a uniform grid“. In: *International Journal for Numerical Methods in Engineering* 109.4 (2017), pp. 459–486 (cit. on p. 2).

[19]S. Brisard and L. Dormieux. „FFT-based methods for the mechanics of composites: A general variational framework“. In: *Computational Materials Science* 49.3 (2010), pp. 663–671 (cit. on p. 2).

[20]W. F. Brown. *Magnetoelastic interactions*. Vol. 9. Springer, 1966 (cit. on p. 2).

[21]P. S. Bullen. *Handbook of means and their inequalities*. Vol. 560. Springer Science & Business Media, 2013 (cit. on p. 27).

[22]D. Cioranescu and P. Donato. *An Introduction to Homogenization*. Vol. 17. Oxford University Press, United Kingdom, 1999 (cit. on pp. 1, 31, 36, 46).

[23]F. Claeyssen, N. Lhermet, F. Barillot, and R. L. Letty. „Giant dynamic strains in magnetostrictive actuators and transducers“. In: *ISAGMM, Guiyang, China* (2006) (cit. on p. 76).

[24]J. M. D. Coey. *Magnetism and Magnetic Materials*. Cambridge University Press, 2010 (cit. on p. 11).

[25]S. Coleman. „The magnetic monopole fifty years later“. In: *The unity of the fundamental interactions* (1983), pp. 21–117 (cit. on p. 20).

[26]*Convocation of the General Conference on Weights and Measures (26th meeting)*. Comité international des poids et mesures (cit. on p. 18).

[27]P. Di Barba, A. Savini, and S. Wiak. *Field models in electricity and magnetism*. Springer Science & Business Media, 2008 (cit. on p. 21).

[28]F. Dietrich and D. Merkert. „Homogenization of periodic micro-structures with FFT-based higher order schemes“. In: *PAMM* 17.1 (2017), pp. 583–584 (cit. on p. 2).

[29]F. Dietrich, D. Merkert, and B. Simeon. „Derivation of higher-order terms in FFT-based numerical homogenization“. In: *European Conference on Numerical Mathematics and Advanced Applications*. Springer. 2017, pp. 289–297 (cit. on p. 2).

[30]E. H. Dill. *Continuum Mechanics: Elasticity, Plasticity, Viscoelasticity*. 1st. CRC Press, 2006 (cit. on p. 11).

[31]W. J. Drugan and J. R. Willis. „A micromechanics-based nonlocal constitutive equation and estimates of representative volume element size for elastic composites“. In: *Journal of the Mechanics and Physics of Solids* 44.4 (1996), pp. 497–524 (cit. on p. 33).

[32]P. Eisenlohr, M. Diehl, R. A. Lebensohn, and F. Roters. „A spectral method solution to crystal elasto-viscoplasticity at finite strains“. In: *International Journal of Plasticity* 46 (2013), pp. 37–53 (cit. on p. 2).

[33]A. Erdélyi. *Asymptotic Expansions*. 3. Courier Corporation, 1956 (cit. on p. 34).

[34]D. J. Eyre and G. W. Milton. „A fast numerical scheme for computing the response of composites using grid refinement“. In: *The European Physical Journal Applied Physics* 6.1 (1999), pp. 41–47 (cit. on p. 2).

[35]G. Fang, B. Wang, and J. Liang. „A coupled FE-FFT multiscale method for progressive damage analysis of 3D braided composite beam under bending load“. In: *Composites Science and Technology* 181 (2019) (cit. on p. 2).

[36]M. Frigo and S. G. Johnson. „FFTW: An adaptive software architecture for the FFT“. In: *Proceedings of the 1998 IEEE International Conference on Acoustics, Speech and Signal Processing, ICASSP'98 (Cat. No. 98CH36181)* 3 (1998), pp. 1381–1384 (cit. on p. 54).

[37]D. Gay. *Composite materials: design and applications*. CRC Press, 2014 (cit. on p. 1).

[38]M. G. D. Geers, V. G. Kouznetsova, and W. A. M. Brekelmans. „Multi-scale computational homogenization: Trends and challenges“. In: *Journal of computational and applied mathematics* 234.7 (2010), pp. 2175–2182 (cit. on pp. 1, 31).

[39]L. Gélébart. „A modified FFT-based solver for the mechanical simulation of heterogeneous materials with Dirichlet boundary conditions“. In: *Comptes Rendus. Mécanique* 348.8-9 (2020), pp. 693–704 (cit. on p. 2).

[40]L. Gélébart. „A simple extension of FFT-based methods to strain gradient loadings-Application to the homogenization of beams and plates“.
Preprint available at https://hal.archives-ouvertes.fr/hal-02942202v2. 2020 (cit. on p. 2).

[41]L. Gélébart and R. Mondon-Cancel. „Non-linear extension of FFT-based methods accelerated by conjugate gradients to evaluate the mechanical behavior of composite materials“. In: *Computational Materials Science* 77 (2013), pp. 430–439 (cit. on p. 2).

[42]I. M. Gelfand and S. W. Fomin. *Calculus of variations*. Ed. by R. A. Silverman. Courier Corporation, 2000 (cit. on p. 22).

[43]F. S. Göküzüm and M.-A. Keip. „An algorithmically consistent macroscopic tangent operator for FFT-based computational homogenization“. In: *International Journal for Numerical Methods in Engineering* 113.4 (2018), pp. 581–600 (cit. on p. 2).

[44]F. S. Göküzüm, L. T. K. Nguyen, and M.-A. Keip. „A multiscale FE-FFT framework for electro-active materials at finite strains“. In: *Computational mechanics* 64.1 (2019), pp. 63–84 (cit. on p. 2).

[45]D. Gottlieb and S. A. Orszag. *Numerical analysis of spectral methods: theory and applications*. SIAM, 1977 (cit. on p. 54).

[46]D. Gottlieb and C.-W. Shu. „On the Gibbs phenomenon and its resolution“. In: *SIAM review* 39.4 (1997), pp. 644–668 (cit. on pp. 54, 78).

[47]H. Grimm-Strele and M. Kabel. „Runtime optimization of a memory efficient CG solver for FFT-based homogenization: implementation details and scaling results for linear elasticity“. In: *Computational Mechanics* 64.5 (2019), pp. 1339–1345 (cit. on p. 2).

[48]A. A. Gusev. „Representative volume element size for elastic composites: A numerical study“. In: *Journal of the Mechanics and Physics of Solids* 45.9 (1997), pp. 1449–1459 (cit. on p. 33).

[49]M. Harutyunyan. „Mathematical Modeling and Numerical Simulation of Magnetoelastic Coupling“. Dissertation. Technische Universität Kaiserslautern, 2019 (cit. on pp. 2, 19, 21, 29, 76).

[50]M. Harutyunyan and B. Simeon. „On a saddle point problem from magneto-elastic coupling“. In: *Appl. Math. Lett.* 83 (2018), pp. 156–163 (cit. on pp. 2, 19).

[51]Z. Hashin and S. Shtrikman. „A variational approach to the theory of the elastic behaviour of multiphase materials“. In: *Journal of the Mechanics and Physics of Solids* 11.2 (1963), pp. 127–140 (cit. on p. 76).

[52]J. H. Huang and W.-S. Kuo. „The analysis of piezoelectric/piezomagnetic composite materials containing ellipsoidal inclusions“. In: *Journal of Applied Physics* 81.3 (1997), pp. 1378–1386 (cit. on p. 2).

[53]„IEEE Standard on Magnetostrictive Materials: Piezomagnetic Nomenclature“. In: *IEEE Transactions on Sonics and Ultrasonics* 20.1 (1973), pp. 67–77 (cit. on p. 21).

[54]V. V. Jikov, S. M. Kozlov, and O. A. Oleinik. *Homogenization of Differential Operators and Integral Functionals*. Springer Science & Business Media, 2012 (cit. on p. 31).

[55]D. Jiles. *Introduction to magnetism and magnetic materials*. 3rd ed. CRC Press, 2015 (cit. on p. 11).

[56]D. C. Jiles and D. l. Atherton. „Theory of ferromagnetic hysteresis“. In: *J. Magn. Magn. Mater.* 61.1–2 (1986), pp. 48–60 (cit. on p. 19).

[57]M. Kabel and H. Andrä. „Fast numerical computation of precise bounds of effective elastic moduli“. In: *Berichte des Fraunhofer ITWM* 224 (2012) (cit. on pp. 62, 66).

[58]M. Kabel, T. Böhlke, and M. Schneider. „Efficient fixed point and Newton–Krylov solvers for FFT-based homogenization of elasticity at large deformations“. In: *Computational Mechanics* 54.6 (2014), pp. 1497–1514 (cit. on p. 2).

[59]M. Kabel, D. Merkert, and M. Schneider. „Use of composite voxels in FFT-based homogenization“. In: *Computer Methods in Applied Mechanics and Engineering* 294 (2015), pp. 168–188 (cit. on pp. 2, 76).

[60]J. Kochmann. „Efficient FE-and FFT-based Two-scale Methods for Micro-heterogeneous Media“. PhD thesis. Universitätsbibliothek der RWTH Aachen, 2019 (cit. on p. 2).

[61]J. Kochmann, K. Manjunatha, C. Gierden, et al. „A simple and flexible model order reduction method for FFT-based homogenization problems using a sparse sampling technique“. In: *Computer Methods in Applied Mechanics and Engineering* 347 (2019), pp. 622–638 (cit. on p. 2).

[62]E. Kröner. *Statistical continuum mechanics*. Springer, 1972 (cit. on p. 54).

[63]A. Kulkarni, F. Franchetti, and J. Kovačević. „Large-scale algorithm design for parallel FFT-based simulations on GPUs“. In: *2018 IEEE Global Conference on Signal and Information Processing (GlobalSIP)*. IEEE. 2018, pp. 301–305 (cit. on p. 2).

[64]M. Ladecký, I. Pultarová, J. Zeman, and J. Vondřejc. „Reference material preconditioning for FFT-based solvers“. In: *PAMM* 19.1 (2019) (cit. on p. 2).

[65]L. D. Landau, E. M. Lifshitz, A. M. Kosevich, and L. P. Pitaevskii. *Theory of Elasticity*. 3rd. Course of theoretical physics. Oxford:Butterworth, 1986 (cit. on p. 11).

[66]L. Lanotte, G. Ausanio, C. Hison, V. Iannotti, and C. Luponio. „The potentiality of composite elastic magnets as novel materials for sensors and actuators“. In: *Sensors and Actuators A: Physical* 106.1-3 (2003), pp. 56–60 (cit. on p. 2).

[67]M. Lapine, I. V. Shadrivov, D. A. Powell, and Y. S. Kivshar. „Magnetoelastic metamaterials“. In: *Nature materials* 11.1 (2012), pp. 30–33 (cit. on p. 2).

[68]J. Lee, J. G. Boyd IV, and D. C. Lagoudas. „Effective properties of three-phase electro-magneto-elastic composites“. In: *Internation Journal of Engineering Science* 43.10 (2005), pp. 790–825 (cit. on pp. 45, 88).

[69]G. Leoni. *A First Course in Sobolev Spaces*. American Methematical Society, 2017 (cit. on p. 39).

[70]W.-D. Lian, G. Legrain, and P. Cartraud. „Image-based computational homogenization and localization: comparison between X-FEM/levelset and voxel-based approaches“. In: *Computational Mechanics* 51.3 (2013), pp. 279–293 (cit. on p. 1).

[71]S. H. Lim, S. R. Kim, S. Y. Kang, et al. „Magnetostrictive properties of polymer-bonded Terfenol-D composites“. In: *Journal of magnetism and magnetic materials* 191.1-2 (1999), pp. 113–121 (cit. on p. 2).

[72]K. Linnemann, S. Klinkel, and W. Wagner. „A constitutive model for magnetostrictive and piezoelectric materials“. In: *International Journal of Solids and Structures* 46.5 (2009), pp. 1149–1166 (cit. on p. 2).

[73]B. A. Lippmann and J. Schwinger. „Variational principles for scattering processes. I“. In: *Physical Review* 79.3 (1950), p. 469 (cit. on p. 54).

[74]S. Lucarini and J. Segurado. „DBFFT: A displacement based FFT approach for non-linear homogenization of the mechanical behavior“. In: *International Journal of Engineering Science* 144 (2019), pp. 103–131 (cit. on p. 2).

[75]D. Lukkassen, G. Nguetseng, and P. Wall. „Two-scale convergence“. In: *International Journal of Pure and Applied Mathematics* 2.1 (2002), pp. 35–86 (cit. on pp. 45, 46).

[76]R. Ma and T. J. Truster. „FFT-based homogenization of hypoelastic plasticity at finite strains“. In: *Computer Methods in Applied Mechanics and Engineering* 349 (2019), pp. 499–521 (cit. on p. 2).

[77]J. Mandel. „Généralisation de la théorie de la plasticité de WT Koiter“. In: *Int. J. Solids Struct.* 1.3 (1965), pp. 273–295 (cit. on p. 11).

[78]P. D. Mangalgiri. „Composite materials for aerospace applications“. In: *Bulletin of Materials Science* 22.3 (1999), pp. 657–664 (cit. on p. 1).

[79]O. B. Mawardi. „On the concept of coenergy“. In: *Journal of the Franklin Institute* 264.4 (1957), pp. 313–332 (cit. on p. 21).

[80]J. C. Maxwell. *A Treatise on Electricity and Magnetism*. Clarendon press, 1881 (cit. on p. 17).

[81]D. Merkert. „Numerical Homogenization for Linear Elasticity in Translation Invariant Spaces“. PhD thesis. TUK, 2018 (cit. on p. 2).

[82]J. C. Michel, H. Moulinec, and P. Suquet. „A computational scheme for linear and non-linear composites with arbitrary phase contrast“. In: *International Journal for Numerical Methods in Engineering* 52.1-2 (2001), pp. 139–160 (cit. on pp. 2, 71, 80).

[83]G. W. Milton and A. T. Sawicki. „Theory of composites. Cambridge monographs on applied and computational mathematics“. In: *Appl. Mech. Rev.* 56.2 (2003), B27–B28 (cit. on p. 76).

[84]V. Monchiet and G. Bonnet. „A polarization-based FFT iterative scheme for computing the effective properties of elastic composites with arbitrary contrast“. In: *International Journal for Numerical Methods in Engineering* 89.11 (2012), pp. 1419–1436 (cit. on p. 2).

[85]L. Morin, R. Brenner, K. Derrien, and K. Dorhmi. „Periodic smoothing splines for FFT-based solvers“. In: *Computer Methods in Applied Mechanics and Engineering* 373 (2021) (cit. on p. 2).

[86]H. Moulinec and F. Silva. „Comparison of three accelerated FFT-based schemes for computing the mechanical response of composite materials“. In: *International Journal for Numerical Methods in Engineering* 97.13 (2014), pp. 960–985 (cit. on p. 71).

[87]H. Moulinec and P. Suquet. „A fast numerical method for computing the linear and nonlinear mechanical properties of composites“. In: *Comptes rendus de l'Académie des sciences. Série II, Mécanique, physique, chimie, astronomie* 318.11 (1994), pp. 1417–1423 (cit. on pp. 1, 54, 87).

[88]H. Moulinec and P. Suquet. „A numerical method for computing the overall response of nonlinear composites with complex microstructure“. In: *Computer methods in applied mechanics and engineering* 157.1 - 2 (1998), pp. 69–94 (cit. on pp. 1, 54).

[89]J. S. Nagra, A. Brahme, R. A. Lebensohn, and K. Inal. „Efficient fast Fourier transform-based numerical implementation to simulate large strain behavior of polycrystalline materials“. In: *International Journal of Plasticity* 98 (2017), pp. 65–82 (cit. on p. 2).

[90]G. Nguetseng. „A general convergence result for a functional related to the theory of homogenization“. In: *SIAM Journal on Mathematical Analysis* 20.3 (1989), pp. 608–623 (cit. on p. 45).

[91]P. Nordeen. „High Frequency Dynamics of Magnetoelastic Composites and Their Application in Radio Frequency Sensors“. PhD thesis. UCLA, 2016 (cit. on p. 2).

[92]J. F. Nye. *Physical Properties of Crystals: Their Representation by Tensors and Matrices*. Paperback Edition. Oxford University Press, United Kingdom, 1985 (cit. on p. 11).

[93]W. L. Oberkampf and C. J. Roy. *Verification and validation in scientific computing*. Cambridge University Press, 2010 (cit. on p. 73).

[94]O. A. Oleinik, A. S. Shamaev, and G. A. Yosifian. *Mathematical problems in elasticity and homogenization*. Vol. 2. Elsevier, 2009 (cit. on p. 37).

[95]F. Ospald. „“fibergen“: An introductory tool for FFT-based material homogenization“. In: *Journal of Open Source Software* 4.34 (2019) (cit. on p. 2).

[96]M. Ostoja-Starzewski. „Material spatial randomness: From statistical to representative volume element“. In: *Probabilistic engineering mechanics* 21.2 (2006), pp. 112–132 (cit. on p. 33).

[97]J. C. Pati and A. Salam. „Lepton number as the fourth “color”“. In: *World Scientific Series in 20th Century Physics: Selected Papers of Abdus Salam* (1994), pp. 343–357 (cit. on p. 20).

[98]S. Ramakrishna, J. Mayer, E. Wintermantel, and K. W. Leong. „Biomedical applications of polymer-composite materials: a review“. In: *Composites science and technology* 61.9 (2001), pp. 1189–1224 (cit. on p. 1).

[99]M. H. Sadd. *Elasticity: Theory, Applications, and Numerics*. Academic Press, 2009 (cit. on p. 11).

[100]M. Schneider. „Convergence of FFT-based homogenization for strongly heterogeneous media“. In: *Mathematical Methods in the Applied Sciences* 38.13 (2015), pp. 2761–2778 (cit. on p. 2).

[101]M. Schneider, F. Ospald, and M. Kabel. „Computational homogenization of elasticity on a staggered grid“. In: *International Journal for Numerical Methods in Engineering* 105.9 (2016), pp. 693–720 (cit. on p. 2).

[102]J. Schröder. „A numerical two-scale homogenization scheme: the FE 2-method“. In: *Plasticity and beyond*. Springer, 2014, pp. 1–64 (cit. on p. 1).

[103]Z. Shen. *Periodic homogenization of elliptic systems*. 2018 (cit. on p. 1).

[104]B. Simeon. *Computational Flexible Multibody Dynamics: A Differential-Algebraic Approach*. Springer, 2013 (cit. on p. 29).

[105]J. Spahn, H. Andrä, M. Kabel, and R. Müller. „A multiscale approach for modeling progressive damage of composite materials using fast Fourier transforms“. In: *Computer Methods in Applied Mechanics and Engineering* 268 (2014), pp. 871–883 (cit. on p. 2).

[106]Q.-D. To and G: Bonnet. „FFT based numerical homogenization method for porous conductive materials“. In: *Computer Methods in Applied Mechanics and Engineering* 368 (2020) (cit. on p. 2).

[107]The Engineering ToolBox. https://www.engineeringtoolbox.com. Retrieved March, 2021 (cit. on p. 82).

[108]T.-H. Tran, V. Monchiet, and G. Bonnet. „A micromechanics-based approach for the derivation of constitutive elastic coefficients of strain-gradient media“. In: *International Journal of Solids and Structures* (2012) (cit. on p. 2).

[109]A. Vidyasagar, W. L. Tan, and D. M. Kochmann. „Predicting the effective response of bulk polycrystalline ferroelectric ceramics via improved spectral phase field methods“. In: *Journal of the Mechanics and Physics of Solids* 106 (2017), pp. 133–151 (cit. on p. 65).

[110]W. Voigt. *Lehrbuch der Kristallphysik (mit Ausschluss der Kristalloptik)*. Vieweg+Teubner Verlag, 1966 (cit. on p. 11).

[111]J. Vondřejc, D. Liu, M. Ladecký, and H. G. Matthies. „FFT-based homogenisation accelerated by low-rank tensor approximations“. In: *Computer Methods in Applied Mechanics and Engineering* 364 (2020) (cit. on p. 2).

[112]J. Vondřejc, J. Zeman, and I. Marek. „An FFT-based Galerkin method for homogenization of periodic media“. In: *Computers & Mathematics with Applications* 68.3 (2014), pp. 156–173 (cit. on p. 55).

[113]H. Weber and H. Ulrich. *Laplace-, Fourier-und z-Transformation*. Springer, 2012 (cit. on pp. 5, 55).

[114]E. Weinan and B. Engquist. „The heterogeneous multiscale methods“. In: *Communications in Mathematical Sciences* 1.1 (2003), pp. 87–132 (cit. on p. 32).

[115]D. Werner. *Funktionalanalysis (8. Auflage)*. Springer, 2018 (cit. on pp. 5, 25, 26, 46).

[116]D. Wicht, M. Schneider, and T. Böhlke. „Anderson-accelerated polarization schemes for FFT-based computational homogenization“. In: *International Journal for Numerical Methods in Engineering* (2021) (cit. on p. 2).

[117]D. Wicht, M. Schneider, and T. Böhlke. „On Quasi-Newton methods in fast Fourier transform-based micromechanics“. In: *International Journal for Numerical Methods in Engineering* 121.8 (2020), pp. 1665–1694 (cit. on p. 2).

[118]F. Willot, B. Abdallah, and Y.-P. Pellegrini. „Fourier-based schemes with modified Green operator for computing the electrical response of heterogeneous media with accurate local fields“. In: *International Journal for Numerical Methods in Engineering* 98.7 (2014), pp. 518–533 (cit. on p. 2).

[119]CY Y. *vtkwrite : Exports various 2D/3D data to ParaView in VTK file format*. (https://github.com/joe-of-all-trades/vtkwrite), GitHub. Retrieved March 7, 2021. (Cit. on p. 82).

[120]J. Yvonnet. „A fast method for solving microstructural problems defined by digital images: a space Lippmann–Schwinger scheme“. In: *International Journal for Numerical Methods in Engineering* 92.2 (2012), pp. 178–205 (cit. on p. 2).

[121]J. Zeman, J. Vondřejc, J. Novák, and I. Marek. „Accelerating a FFT-based solver for numerical homogenization of periodic media by conjugate gradients“. In: *Journal of Computational Physics* 229.21 (2010), pp. 8065–8071 (cit. on pp. 2, 62).

[122]F. Zhang. *The Schur complement and its applications*. Vol. 4. Springer Science & Business Media, 2006 (cit. on p. 67).

List of Figures

List of Tables

Colophon

This thesis was typeset with LaTeX 2$_\varepsilon$. It uses the *Clean Thesis* style developed by Ricardo Langner. The design of the *Clean Thesis* style is inspired by user guide documents from Apple Inc.
Download the *Clean Thesis* style at `http://cleanthesis.der-ric.de/`.

The numerical simulations and their plots were computed with MATLAB 9.8 by The MathWorks, Inc. A license for usage of the software was issued by Technische Universität Kaiserslautern.
Download the MATLAB test version at `https://de.mathworks.com/products/matlab.html`.

The 3D simulations were visualized in the open source software Paraview.
Download the Paraview software at `https://www.paraview.org/`.

All other graphics within this thesis were created using either the PGF/Ti*k*Z package developed by Till Tantau or the open source vector graphics editor Inkscape.
Download the PGF and Ti*k*Z releases at `https://texample.net/tikz/builds/`.
Download the Inkscape software at `https://inkscape.org/release/inkscape-1.0.2/`.

Academic Curriculum Vitae

2011 **Abitur**, *Eleonoren–Gymnasium*, Worms.

2011–2014 **Study of Mathematics**, *Bachelor of Science*, TUK.

- **Bachelor Thesis:** "*Modellierung und numerische Simulation elektrischer Schaltkreise*", supervised by **Prof. Dr. Bernd Simeon**

2014–2016 **Study of Technomathematics**, *Master of Science*, TUK.

- **Master Thesis:** "*FFT-based homogenization of higher order for periodic microstructures*", supervised by **Prof. Dr. Bernd Simeon**

2016–2021 **Research and Teaching Assistant & PhD student**, *Department of Mathematics*, TUK.

- **PhD Thesis:** "*Periodic homogenization and FFT-based methods for resolving microstructures of linear magneto-elastic problems*", supervised by **Prof. Dr. Bernd Simeon**

Publications

- Dietrich, Felix and Merkert, Dennis, "Homogenization of periodic micro-structures with FFT-based higher order schemes", *PAMM Vol. 17, No. 1, pp. 583–584*, 2017, Wiley Online Library. *https://doi.org/10.1002/pamm.201710261*
- Dietrich, Felix and Merkert, Dennis and Simeon, Bernd, "Derivation of higher-order terms in FFT-based numerical homogenization", *European Conference on Numerical Mathematics and Advanced Applications, pp. 289–297*, 2017, Springer. *https://doi.org/10.1007/978-3-319-96415-7_25*
- Dietrich, Felix, "FFT-Based Solution Schemes for the Unit Cell Problem in Periodic Homogenization of Magneto-Elastic Coupling", *submitted and accepted for "Numerical Mathematics and Advanced Applications ENUMATH 2019".*

Wissenschaftlicher Lebenslauf

2011 **Abitur**, *Eleonoren–Gymnasium*, Worms.

2011–2014 **Studium der Mathematik**, *Bachelor of Science*, TUK.

- **Bachelorarbeit:** "*Modellierung und numerische Simulation elektrischer Schaltkreise*", betreut von **Prof. Dr. Bernd Simeon**

2014–2016 **Studium der Technomathematik**, *Master of Science*, TUK.

- **Masterarbeit:** "*FFT-based homogenization of higher order for periodic microstructures*", betreut von **Prof. Dr. Bernd Simeon**

2016–2021 **Wissenschaftlicher Mitarbeiter & Doktorand**, *Fachbereich Mathematik*, TUK.

- **Doktorarbeit:** "*Periodic homogenization and FFT-based methods for resolving microstructures of linear magneto-elastic problems*", betreut von **Prof. Dr. Bernd Simeon**

Veröffentlichungen

- Dietrich, Felix und Merkert, Dennis, "Homogenization of periodic micro-structures with FFT-based higher order schemes", *PAMM Vol. 17, No. 1, pp. 583–584*, 2017, Wiley Online Library. *https://doi.org/10.1002/pamm.201710261*
- Dietrich, Felix und Merkert, Dennis und Simeon, Bernd, "Derivation of higher-order terms in FFT-based numerical homogenization", *European Conference on Numerical Mathematics and Advanced Applications, pp. 289–297*, 2017, Springer. *https://doi.org/10.1007/978-3-319-96415-7_25*
- Dietrich, Felix, "FFT-Based Solution Schemes for the Unit Cell Problem in Periodic Homogenization of Magneto-Elastic Coupling", *eingereicht und akzeptiert für "Numerical Mathematics and Advanced Applications ENUMATH 2019".*